Turbulence modelling of mixed and natural convection regimes in the context of the underhood-space of automobiles.

Syed Mohd Saad Jameel

THÈSE

Pour l'obtention du grade de

DOCTORAT DE L'UNIVERSITE DE PAU

Délivré par l'Université de Pau et des Pays de l'Adour (UPPA-E2S)

Présentation envisagée le 08 Décembre 2020 par :

Syed Mohd Saad JAMEEL

Turbulence modelling of mixed and natural convection regimes in the context of the underhood-space of automobiles

---

JURY

Prof. Lars Davidson	Professor, Chalmers University of Technology, Sweden	Rapporteur
Prof. Didier Saury	Professor, ENSMA, Institut Pprime	Rapporteur
Prof. Eric Lamballais	Professor, Université de Poitiers, Institut Pprime	Examinateur
Dr. Jean Francois Wald	Researcher-EDF	Examinateur
Dr. Rémi MANCEAU	Directeur de recherche, CNRS, Université de Pau	Directeur de thése
Dr. Vincent Herbert	Science of fluids, Thermal and Aeroacoustics team manager, PSA Group	Co-encadrant de thése

---

École doctorale et spécialité :

Ecole Doctorale 211 - Sciences Exactes et Applications

Unité de Recherche :

Universite de Pau et des Pays de l'Adour, E2S UPPA, CNRS, INRIA, équipe CAGIRE, LMAP, Pau, France

À Syed Jameel Ahmad,

Acknowledgement

This thesis is the outcome of 3 years of research, which I started at the Laboratory of Mathematics (LMAP), Inria Cagire, the University of Pau in collaboration with research center at Centre technique Velizy, PSA Group in the framework of the CIFRE program.
First of all, I would like to give thanks to Almighty who gives me courage, patience and passion to pursue research.
A sincere thanks to the PSA Group and the ANRT for the funding of this thesis. I would like to give sincere thanks to all the members of the jury, and especially to Prof. Lars Davidson and Prof. Didier Saury, for taking the time to read the report and for their enriching remarks.
I am grateful to Dr. Herwig for providing the DNS statistics of the vertical channel flow.
Thanks to the MCIA (Meso centre de Calcul Intesif Aquitain) at Bordeaux for granting the computing facilities.
I acknowledge fruitful discussions with Didier Bessette at Ansys Fluent and his support for implementing the buoyancy sensitised models in ANSYS Fluent.
Thanks to the members of the laboratory, most of whom knew me since my internship at the lab for a long time already. Thanks to Mr. Bruno Demoisy at LMAP and Madame Sandrine Loze at PSA Groupe for facilitating the administrative work.
Thanks to all the students I have met during my last 3 years at UPPA and PSA Group. A special thanks to Id Moulay with whom we form a team of proud warriors, a bit skeptical sometimes but still holding. And thanks to Puneet, Adrien, and Salah for their support.
Thank you to the friends, who are near and far especially Rashid and Francois who have shown their support through their thought-provoking messages.
Thank you to the one with whom I have shared many years of my life and to those who followed me in every aspect of life with patience and dedication.
More importantly thanks to my parents, my brother, my sister, my wife, my son and all the members of my beautiful family who act as the powerful propeller during my research time.
I would like to express my deepest gratitude to Dr. Rémi Manceau who introduced me to the intriguing world of turbulence in my second year of Master at ENSMA, Poitiers and since then, his continuous guidance, motivation, constant supervision, and support are greatly appreciated. Working with such an involved researcher is an honour.
Special thanks to Dr. Vincent Herbert (co-supervisor of thesis), who improved my understanding of the flows in the underhood space of automobiles at PSA Group.

Résumé

Le sujet de cette thèse concerne la modélisation de la turbulence des écoulements influencés par la flottabilité, qui émanent de l'interaction de la force gravitationnelle avec une différence de densité. Cette étude est motivée par des problématiques rencontrées par le groupe PSA dans la simulation des écoulements à convection naturelle dans le compartiment moteur des véhicules.
L'objectif principal de ce travail est de tester plusieurs modéles pour prendre en compte la flottabilité et de proposer des améliorations efficaces qui pourraient fournir un modèle applicable aux écoulements engendrés par la flottabilité. En outre, ces modifications doivent pouvoir être mises en œuvre dans le code Ansys Fluent pour le calcul des écoulements de convection naturelle dans les problèmes typiques cités ci-dessus.
Dans le cadre de cet objectif, nous avons adapté trois modèles à viscosité turbulente aux effets de la flottabilité. La première approche qui offre le meilleur cadre physique implique l'extension des lois de comportement pour le tenseur de Reynolds et le flux thermique turbulent de manière linéaire, pour tenir compte de l'influence anisotrope de la flottabilité. Cette approche, appliquée à trois modèles différents, permet d'améliorer considérablement les résultats en reproduisant l'écoulement moyen et les quantités turbulentes. Dès lors, on se rend compte que cette approche conduit à des améliorations significatives en terme de physique.
De plus, on observe que l'utilisation d'une approche simple d'hypothèse de diffusion par simple gradient "SGDH" pour modéliser le terme source de flottabilité conduit à une sous-estimation de l'effet de la flottabilité sur la turbulence. En outre, la comparaison avec les données de la simulation numérique directe (DNS) montre que l'hypothèse de diffusion par gradient généralisé "GGDH" donne de meilleures prédictions de l'écoulement moyen et du champ de température.
Un autre aspect abordé dans ce travail concerne la sensibilité au modéle du terme de production par flottabilité dans l'equation de ε ou ω. Après une analyse détaillée, on constate que les résultats sont tré s sensibles à ce terme et que la valeur optimale du coefficient est liée au choix du modèle de turbulence. Pour éviter cette sensibilité, on utilise une autre expression du terme source pour la modélisation de la flottabilité dans les équations ε ou ω qui tient compte du nombre de Richardson de flux et on observe une amélioration de la prédiction des profils moyens.
Trois régimes différents d'écoulement convectif sont étudiés, à savoir les régimes de convection forcée, mixte et naturelle. Parmi ceux-ci, la configuration de canal vertical différentiellement chauffé est considérée pour développer le modèle adapté à la flottabilité. C'est celle qui pose le plus grand défi pour les modèles à viscosité turbulente. Ces études ont abouti à la proposition d'une forme plus physique et simplifiée de modèles adaptés à la flottabilité, qui est considérée comme le meilleur compromis entre la précision physique et la stabilité numérique pour des écoulements induits par la flottabilité.

Ces modèles sensiblisés à la flottabilité offrent des perspectives pour étudier d'autres configurations d'écoulements de convection mixte et naturelle et ouvrent la voie à l'utilisation de ces modèles dans les simulations dans le compartiment moteur des véhicules.

Abstract

The subject of this thesis is the turbulence modeling of buoyancy-driven flows, which emanate through the interaction of the gravitational force with a density difference. The motivation of this investigation comes from the problem faced by the PSA group in simulating natural convection flows in the underhood-space of cars.
The main goal of the present investigation is to test several models to account for buoyancy and to propose effective improvements which could provide a model applicable in buoyancy-driven flows and in addition to that, can be easily implemented in the software Ansys Fluent for the computation of natural convection flows in the Underhood-space of cars.
In the context of this goal, three eddy-viscosity turbulence models are sensitized to the effects of buoyancy. The first approach which offers the better physical framework involves the extension of the constitutive relations for the Reynolds stress and turbulent heat flux in a linear way, to account for the anisotropic influence of buoyancy. This approach is applied to three different models and brings in drastic improvement of the results in reproducing the mean flow and the turbulent quantities and thus it is realized that this approach leads to physically based improvements.
Furthermore, it is observed that, using a simple gradient diffusion hypothesis (SGDH) approach to model the buoyancy source terms leads to underestimate the effect of buoyancy on turbulence and the comparison with the DNS data shows that the generalized gradient diffusion hypothesis (GGDH) give improved predictions of the mean flow and temperature field. Another issue addressed in this work involves the sensitiveness to buoyancy production term in ε or ω equations and after the detailed analysis, it is realized that the results are very sensitive to this term and the optimal value of the coefficient ($C_{\varepsilon 3}$) is linked to the choice of turbulence model. To avoid this limitation, another expression for the model of the buoyancy source term in the ε or ω equations is tried which considers the flux Richardson number and it is observed that there is an improvement in the prediction of mean flow profiles.
Three different regimes of convective flows are studied namely, forced, mixed and natural convection and the more challenging differentially heated vertical channel flow configuration which poses a major challenge to the eddy-viscosity models is considered to develop the buoyancy sensitized model. As an outcome of these studies, the more physical and simplified forms of buoyancy sensitized model are proposed which is considered as the best compromise between the physical accuracy and numerical stability for buoyancy-driven flows. These buoyancy-sensitized models provide an opportunity to investigate

other buoyancy-driven flows and paves the way for these models to be applied in the under hood space simulation.

Contents

Nomenclature

Mathematical operators

$\underline{u}.\underline{v}$ Scalar product of vectors u and v

$\frac{Df}{Dx_i}$ Total derivate of f with respect to distance x_i

$\frac{Df}{Dt}$ Total derivate of f with respect to time

$\frac{\partial f}{\partial x_i}$ Partial derivate of f with respect to distance x_i

$\frac{\partial f}{\partial t}$ Partial derivate of f with respect to time

∇f Gradient of f

$\nabla . f$ Divergence of f

$\nabla^2 f$ Laplacien of f

$\frac{\partial^2 f}{\partial x_i \partial x_i}$ Second partial derivate of f with respect to distance x_i

Latin symbols

a_{ij} Anisotropy tensor

$\mathbf{a}$ non-dimensional symmetric tensor

b_{ij} Anisotropy tensor

a_1, a_2, a_3, b_1, b_2, b_3 Coefficients of fluctuation of velocity in Taylor series expansion

$A_{\theta 2}$ Scalar flux invariant

A^+, B^+ Coefficients of Taylor series expansion of turbulent kinetic energy

C_{BV1}, C_{BV2} Coefficients of model function f_{BV}

$C_{B\theta 1}$, $C_{B\theta 2}$ Coefficients of model function $f_{B\theta}$

C_L Constant of length scale BL-$\overline{v^2}/k$ model

C_T Constant of time scale BL-$\overline{v^2}/k$ model

Pr Prandtl number

p Pressure

$p^{'}$ Fluctuating Pressure

Pr_t Turbulent Prandtl number

$R = \frac{\overline{\theta^2}}{\varepsilon_\theta}\frac{\varepsilon}{k}$ Thermal-to-mechanical time scale ratio

R^h Thermal-to-mechanical time scale ratio in homogenous zone

Ra Rayleigh number

Ra_t Turbulent Rayleigh number

Re Reynolds number

$Re_{critical}$ Critical Reynolds number

C_η Constant of time scale BL-$\overline{v^2}/k$ model

Re_{tr} Transition Reynolds number

Re_T Turbulent Reynolds number

R_f Flux Richardson number

Ri_g Gradient Richardson number

T_{ref} Reference temperature

T_τ Friction temperature

T_b Bulk mean temperature

Re_τ Friction Reynolds number

S_ε Source term in ε equation

$\mathbf{s}$ Symmetric tensor

$C^*_{\varepsilon 2}$ Constant in dissipation rate of BL-$\overline{v^2}/k$ model

S_{ij} Strain rate

u_i i^{th} component of velocity

$u_i^{'}$ i^{th} component of fluctuating velocity

$\overline{u_i{}'\theta'}$ i^{th} component of thermal heat flux

u_τ Friction velocity

$u_{\tau,h}$ Friction velocity at hot wall

$u_{\tau,c}$ Friction velocity at cold wall

N_g Number of grid cells

U_b Bulk mean velocity

$\overline{v^2}$ Wall-normal energetic scale

$C_{\varepsilon 4}$ Constant in dissipation rate of BL-$\overline{v^2}/k$ model

$\mathbf{x} = (x, y, z)$ Vector position

$\mathbf{w}$ Non-dimensional antisymmetric tensor

C_μ Constant of model k-ε

$C_\theta{}^*$ Constant of Buoyancy extension

$c_{1\theta w}$ Coefficient of wall reflection term $\phi_{i\theta w}$

C_θ Constants of models GGDH, AFM

$C_{\varepsilon 1}$, $C_{\varepsilon 2}$ Constants of dissipation equation

$C_{\varepsilon 3}$ Constant of dissipation equation for buoyancy

C_p Specific heat at constant pressure

C_s Constant of turbulent diffusion

C_v Specific heat at constant volume

C_1 Constant of slow-term of pressure-strain tensor

$C_{\varepsilon 1}$ Constant of dynamic production of ε

$C_{\varepsilon 2}$ Constant of dissipation of ε

C_2 Constant of rapid-term of pressure-strain tensor

C_3 Constant of buoyancy-term of pressure-strain tensor

$C_{\theta 1}$ Constant of slow-term of pressure-scrambling

$C_{\theta 1}^{'}$ Constant of slow-term of pressure-scrambling of Kenjeres model

$C_{\theta 2}$ Constant of rapid-term of pressure-scrambling

$C_{\theta 2}^{'}$ Constant of additional contribution of rapid-term of pressure-scrambling

$C_{\theta 3}$ Constant of buoyancy-term of pressure-scrambling

$C_{\theta\theta}$ Constant of turbulent diffusion of thermal variance

$CD_{k\omega}$ Positive portion of cross-diffusion term

$2-D$ Two-dimensional

$3-D$ Three-dimensional

D Extra source term in k for Launder-Sharma model

D_{ij} Diffusion tensor of Reynolds stress

D_{ij}^t Turbulent diffusion tensor of Reynolds stress

D_k^t Transport of k by turbulent diffusion

D_ε^t Transport of ε by turbulent diffusion

D_ε^p Transport of ε by pressure diffusion

D_ε^ν Transport of ε by molecular diffusion

D_k^ν Transport of k by viscous diffusion

D_{ij}^ν Molecular diffusion tensor of Reynolds stress

D_k^p Transport of k by pressure diffusion

D_{ij}^p Pressure diffusion tensor of Reynolds stress

D_θ^ν Molecular diffusion of thermal variance

$D_{i\theta}$ Diffusion vector of thermal heat flux

D_θ^t Turbulent diffusion of thermal variance

$D_{i\theta}^t$ Turbulent diffusion vector of thermal heat flux

$D_{i\theta}^\nu$ Molecular diffusion vector of thermal heat flux

$D_{i\theta}^p$ Pressure diffusion vector of thermal heat flux

E Extra source term in ε equation for Launder-Sharma model

f_μ Damping function of turbulent viscosity in Launder-Sharma model

f_1 Damping function in Launder-Sharma model

f_2 Damping function in Launder-Sharma model

f_h Elliptic relaxation factor in BL-$\overline{v^2}/k$ model

F_1, F_2 Blending functions of k-ω-SST model

f_{BV}, $f_{B\theta}$ Model functions

g Acceleration due to gravity

G_{ij} Buoyancy production tensor of Reynolds stress

$G_{i\theta}$ Buoyancy production vector of turbulent heat flux

$G_k = \frac{1}{2}G_{jj}$ Buoyancy production of k

G_ε Buoyancy production of dissipation

$G_{\overline{v^2}}$ Buoyancy production of cross-stream component of the Reynolds stress

Gr Grashof number

Gr_L Grashof based on width

Gr_H Grashof based on height

$k = \frac{1}{2}\overline{u_i' u_i'}$ Turbulent kinetic energy

L unit Length

M unit Mass

n_i Unit vector normal to the wall

P_{ij} Dynamic production tensor of Reynolds stress

$P_k = \frac{1}{2}P_{ii}$ Production of k

$P_{\varepsilon 1} + P_{\varepsilon 2}$ Mixed production of ε

$P_{\varepsilon 3}$ Production by the Hessian of velocity

$P_{\varepsilon 4}$ Turbulent production of ε

Y_ε Major destruction of ε

P_θ Thermal production of thermal variance

$P_{\theta i}^{th}$ Thermal production vector of turbulent heat flux

$P_{\theta i}^m$ Mechanical production vector of turbulent heat flux

ϕ_{ij} Pressure-strain tensor of Reynolds stress

ϕ_{ijw} Wall reflection term of pressure-strain tensor of Reynolds stress

ϕ_{ij}^1 Slow term of pressure-strain tensor of Reynolds stress

ϕ_{ij}^2 Rapid term of pressure-strain tensor of Reynolds stress

ϕ_{ij}^3 Buoyancy term of pressure-strain tensor of Reynolds stress

$\phi_{\theta i}$ Pressure-scrambling term of turbulent heat flux

$\phi_{\theta iw}$ Wall reflection term of pressure-scrambling term of turbulent heat flux

$\phi_{\theta i}^1$ Slow term of pressure-scrambling of turbulent heat flux

$\phi_{\theta i}^2$ Rapid term of pressure-scrambling of turbulent heat flux

$\phi_{\theta i}^{2'}$ Additional contribution to rapid term of pressure-scrambling of turbulent heat flux

$\phi_{\theta i}^3$ Buoyancy term of pressure-scrambling of turbulent heat flux

P Hydrostatic pressure

q_w Heat flux

$\mathbf{I}$ Identity tensor

T Mean temperature

U_i i^{th} component of mean velocity

Nu Nusselt number

Greek Symbols

α Elliptic relaxation factor

κ Thermal diffusivity

ℓ Length scale

α_θ Thermal elliptic relaxation factor

β Thermal expansion coefficient

β' Constant in k-ω model

β^* Constant in k-ω model

δ Channel half width

δ_{ij} Kronecker symbol

Θ Temperature

ϑ Linear contribution of temperature

θ Fluctuation of temperature

$\overline{\theta^2}$ Variance of temperature

ΔT Temperature difference

ρ Density

ρ_0 Reference constant density

$\Delta\rho$ Density difference

$\widetilde{\varepsilon}$ Modified dissipation rate in Launder-Sharma model

ε_{ij} Dissipation tensor of Reynolds stress

$\varepsilon_{\theta i}$ Dissipation vector of turbulent heat flux

ε_θ Dissipation rate of thermal variance

$\varepsilon = \frac{1}{2}\varepsilon_{kk}$ Turbulent dissipation

η Constant of AFM model

η^* Kolmogorov scale

η Coefficient of Algebraic heat flux model

ξ Coefficient of Algebraic heat flux model

e internal energy

ν Kinematic viscosity

ν_t Turbulent viscosity

ω Specific dissipation rate

μ Molecular viscosity

$\overline{\phi}$ Mean value of variable ϕ

$\overline{\phi'}$ Fluctuating value of variable ϕ

ϕ_{rms} Root mean square of variable ϕ

σ_k Diffusion coefficient of turbulent kinetic energy

σ_ε Diffusion coefficient of dissipation rate of turbulent kinetic energy

σ_ω Diffusion coefficient of specific dissipation rate of turbulent kinetic energy

φ Wall-normal energetic scale in BL-$\overline{v^2}/k$ model

λ Thermal conductivity

τ_{ij} Viscous stress tensor

τ Dynamic time scale

τ_θ Thermal time scale

υ Velocity scale

ε Dissipation rate of turbulent kinetic energy

ζ_i Anisotropy vector of turbulent heat flux

Acronyms

AFM Algebraic Flux Model

CAC Charge air cooler

CFD Computational Fluid Dynamics

DNS Direct Numerical Simulation

GGDH Generalized Gradient Diffusion Hypothesis

LES Large Eddy Simulation

PSA Peugeot Société Anonyme

RANS Reynolds-Averaged Navier-Stokes

rms Root mean square

RSM Reynolds Stress Model

SGDH Simple Gradient Diffusion Hypothesis

Chapter 1

Introduction

Contents

1.1 Introduction

Heat transfer flows are of great importance to many industrial applications of interest, particularly in the designing of the underhood-space of automobiles. One of the important phases during the development process of a passenger car is to ensure that the components in the engine compartment do not overheat. Underhood aerothermal management is an important phase in the vehicle design and manufacturers spend considerable engineering resources and research activities in the early development phase of new cars [Gu et al., 2013, Kaushik, 2007, Mansor and Passmore, 2013].

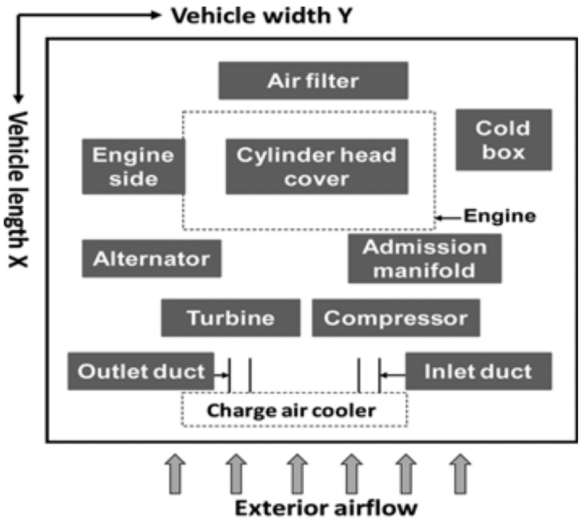

(a) Top view

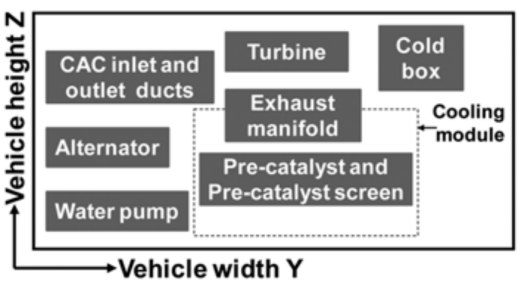

(b) Side view from front of vehicle

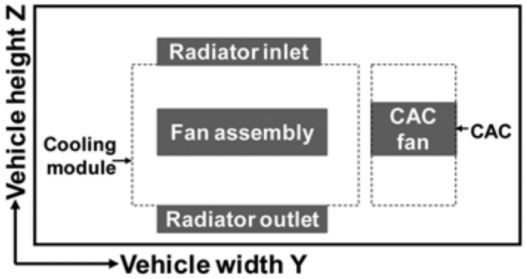

(c) Side view from back of vehicle

Figure 1.1 – Different components housed in the underhood space of a vehicle [Figures are taken from Khaled et al., 2015]

The heat transfer from the engine greatly affects the components placed in the underhood space. E.g., turbine, compressor, cold box (zone comprising battery), apron, cylinder head insulation, alternator, inlet and outlet pipes of charge air cooler (CAC) and the engine right side, screen shield, turbo screen, air conditioning compressor, gearbox, catalyseur.

The different components housed in the underhood space in schematic representation are shown in Fig. 1.1 with different views. The important air zones are those near the cold box, apron, air filter, cylinder head cover, the CAC inlet, and outlet pipes, engine right side and downstream of the engine, CAC, and the fan [Khaled et al., 2015]. In addition to the engine performance, geometry restrictions due to the compactness and sealing of the car underhood compartment are required from the style constraint point of view. Thus, a restricted space must be imposed on the underhood space of cars that restrains the airflow. Moreover, a large number of components need to be housed in the compartment, and owing to this, heat transfer phenomena become complex.

Experimental analyses of aerothermal phenomena are few [Fournier and Bayne, 2007, 2004, 2006]. For instance, Fournier and Bayne [2004] measured the underhood temperature of four different vehicles in order to identify the range of temperatures reached in under hood that the spilled fluids may be exposed to. Comparisons were made against the auto ignition temperatures of various automotive fluids. The measurements of temperature were conducted for both level road and uphill driving conditions where the vehicles were loaded to their rated capacity. The temperatures were recorded when the vehicles pulled off to the side of the road and engine turned off. This condition corresponds to the collision in which the vehicle may come to a sudden stop. For both the driving conditions that is when the vehicle is running on level road and uphill, the estimated temperatures initially increased with the maximum temperatures being reached within 1 to 2 minutes after the vehicle was stopped and engine turned off. For both driving conditions, increased temperatures were observed which was sufficient to ignite most of the engine compartment fluids, particularly for coolant which shows the highest auto ignition temperature.

Another study related to the efficiency of thermocouples and its attachment methods was conducted by Fournier and Bayne [2006]. The tests were conducted on only one vehicle at one speed (96 km/h) during level road and uphill driving conditions. Five different K-type thermocouple and attachment methods were selected for the surface temperature measurements. Brazed on, welded on, clamped on and cemented on thermocouple attachment methods were selected to measure the surface temperatures at two different locations along the exhaust system. For the two measurement locations and under both the driving conditions, the brazed on thermocouple bead registered the highest surface temperature and the clamp on surface temperature thermocouple measured the lowest temperature. It was interpreted that the difference in the temperature range between the two measured locations may be due to the turbulence of the exhaust gas flow which travelled different distances. Furthermore, the increase in temperature after the engine was turned off was a phenomenon which is likely related to the specific thermocouple and its attachment method. The brazed-on thermocouple bead was recommended for the further measurements under similar conditions.

Temperatures in the underhood compartment are sensitive to all three modes of heat trans-

fer namely conduction, convection, and radiation. Furthermore, multi-mode heat transfer calculation has been performed [Bendell, 2005, Reister and Maihöfer, 2003, Schuster, 2003]. Numerical studies mainly focus on temperature analyses [Franchetta et al., 2005, 2006, Khaled et al., 2008, 2009, Kumar et al., 2009, Weidmann et al., 2009]. Most of the studies deal with a vehicle driving at maximum speed or traveling uphill at 35 km/h. In both cases, the temperature of components is dominated by forced convection owing to the high velocities in the engine compartment.

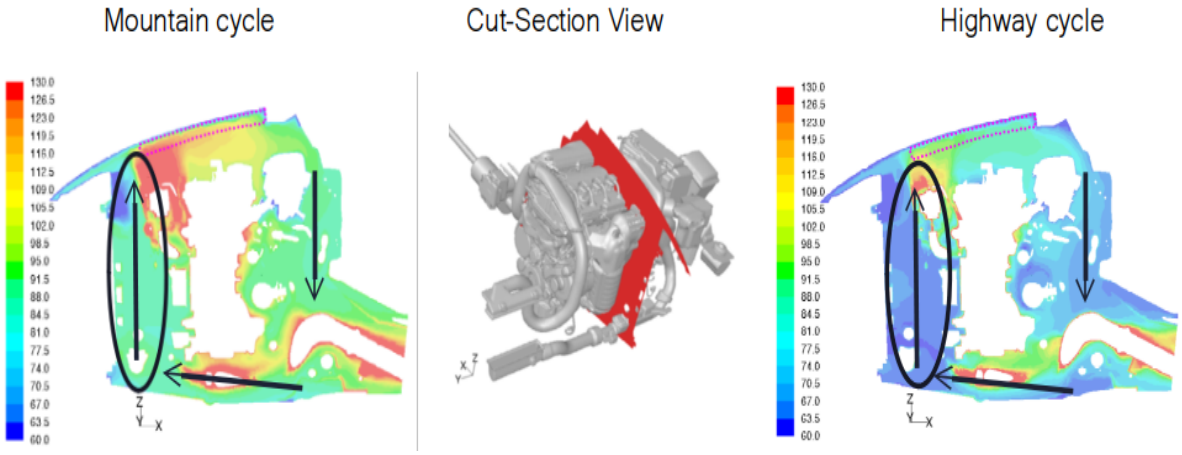

Figure 1.2 – Cut section view of the simulation after stabilising of forced convection phase [Plots are taken from simulation performed at PSA Group, Courtsey (V. Herbert)]

Steady forced flow simulation has proven to be reliable [Alajbegovic et al., 2006, Juan, 2008, Kini and Thoms, 2009]. Also in PSA Group, computations have been performed in cruising stages by categorizing the flow into three cycles based on load, speed, and temperature, and the cycles are named as Mountain, Highway, and City cycle respectively. The situation after the stabilizing of forced convection phase is shown in Fig. 1.2, where it is observed that temperature levels are high, particularly close to the turbo and exhaust manifold for both the Mountain and Highway cycle and the results were found to be reliable in this phase dominated by forced convection. However, when the vehicle is driven at high load and then shut down, phase known as a thermal soak appears. In this situation, underhood cooling through airflow circulation is provided only by fan rotation and natural convection. Simulating such a phase is challenging due to the lack of validated studies [Chen et al., 2006, Franchetta et al., 2005, 2006, Weidmann et al., 2005]. Recently, experiments were performed at PSA group to realize this phase where natural convection is a dominant phenomenon.
From the study of Khaled et al. [2015], it has been infered that during the first phase of thermal soak, the flow is maintained by a fan which runs for a short time about 1-5 minutes and then stops. In the second phase of thermal soak, the flow is completely governed by natural convection such that the thermal inertia allows the temperature to

rise even though the engine has stopped. In the second phase of thermal soak, Khaled et al. [2015] have categorized the flow into two categories namely 'Category 1' and 'Category 2'. In the flow of 'Category 1', it has been observed that the temperature drops with time, however in 'Category 2', the temperatures reach peak values and the components affected are screens of the turbine, pre-catalyst, steering junction, compressor oil pump, and water outlet plenum respectively. In this case, the components heat up after stopping the engine for 3 to 24 minutes depending upon the position in the underhood space. The temperature of some components increases by almost 80°C (pre-catalyst) and by 40°C in the air zones (crawl area) [Khaled et al., 2015].
The dimensionless numbers which describe natural convection flow are the Grashof and Rayleigh numbers relating buoyancy forces to viscous forces, are expressed as follows:

$$\begin{aligned} Gr &= \frac{\beta g \Delta T \delta^3}{\nu^2} \\ Ra &= \frac{\beta g \Delta T \delta^3}{\nu \alpha} \end{aligned} \tag{1.1}$$

where, β, ΔT, ν and α are the thermal expansion coefficient, temperature difference, kinematic viscosity and thermal diffusivity, respectively.
The order of magnitude of Grashof and Rayleigh numbers based on the width and height of underhood-space of car is reported in the experiments performed in PSA Group

— based on width:

$$Gr_L = [5.0 \times 10^5 - 1.7 \times 10^7]; \;\; Ra_L = [3.0 \times 10^5 - 1.0 \times 10^7] \tag{1.2}$$

— based on height:

$$Gr_H = [6.0 \times 10^7 - 6.0 \times 10^8]; \;\; Ra_H = [4.0 \times 10^7 - 4.0 \times 10^8] \tag{1.3}$$

These orders of magnitude suggest that the flow becomes turbulent in the natural convection regime and therefore it is crucial to better understand the natural convection phenomena occurring in the underhood space of automobiles. In the context of underhood space thermal design, researchers have tried to use Computational Fluid Dynamics (CFD) as a tool by importing CFD calculations into thermal analysis code [Bendell, 2005, Reister and Maihöfer, 2003]. In view of this context, a discussion on the rationale of the CFD and turbulence model is discussed briefly in the next section of this chapter.

1.2 Computational Fluid Dynamics

Computational fluid dynamics is the method of doing analysis of fluid flow, heat transfer, and related phenomena by means of computer-based simulation. The CFD technique is very vigorous and encompasses a wide range of industrial and academic applications. In the mid-nineties, the aerospace industry had integrated CFD in the design of air-

craft. Moreover, this technique has been applied consistently in the automotive industry to predict drag forces and underhood space design which is our concern. Owing to the availability of high computing resources, CFD concept is the mainstay of the wider industrial community. The advancement of turbulence theory is slow owing to the robustness of experimental instruments and also due to the fact that many turbulent flows are too expensive to be investigated by existing experimental techniques. Indeed, CFD reduces some expensive phases of physical tests and gives better insight into the effective design of the cars. Recent developments in the computational technique, such as supercomputers have significantly improved the way turbulence is analyzed.

1.2.1 Why CFD is important

Highly precise types of equipment are very expensive and difficult to modify as per the requirement, for instance changing the Rayleigh number, requires great effort. Nonetheless experimental data are always useful for the validation of computational results owing to the direct measurement of situations which are a reflection of real-life problems. However, using experiments could hardly provide all the information to the engineers or researchers and therefore CFD attracted the attention.

1.2.2 Importance of RANS

There are mainly three different approaches in the computational fluid dynamics study of turbulent flows: Direct numerical simulation (DNS), Large-eddy simulation (LES), and Reynolds averaged Navier-Stokes equation (RANS) and, in addition, Hybrid RANS-LES strategies have been developed to couple RANS and LES in the same computation. There are pros and cons of each approach over the others and therefore it is difficult to predict which approach is the more appropriate one in computing turbulent flows as one approach is suitable in a few cases while the other is suitable for other cases.
The DNS approach involves the calculation of instantaneous turbulent variables, such an approach uses no approximation, and the results represent the real characteristics of turbulence. Indeed, with DNS, it is possible to calculate the complete budget of turbulent quantities that cannot be accessed by experimental studies. However, it is not possible to perform DNS for turbulent flows in most engineering applications owing to a large number of scales to be solved, which range from large scale of the size of the geometry to the smallest scale that must be resolved. As the smallest scale is of the order of the Kolmogorov scale, ($\eta^* = \nu^3/\varepsilon^{1/4}$), such a simulation requires refined meshes with cell sizes of the order of η^*. Consequently, the number of cells (N_g) far from the wall depends on the Reynolds number such that N_g is proportional to $Re^{9/4}$. For the computation of natural convection flows, it is crucial to predict the behavior close to the wall which requires even a large number of grid cells. Therefore, the development of computational resources is not at the pace with which the DNS of most of the flows is possible.

To overcome the limitation of DNS, an alternative way is to use the Large Eddy Simulation (LES) approach. This approach resolves the large scales, while the small scales are modeled. The rationale behind the LES approach is that most of the transport of momentum or energy is carried out by large scales while small scales do not significantly contribute to the transport process but rather to dissipation processes. Therefore, the LES approach needs coarser mesh relatively and thus requires less computational resources. In the case of buoyancy-driven flows, most of the important heat transfer process occurs close to the wall and woefully large scale eddies in the near-wall regions are of the same size as small scale ones. And undoubtedly, buoyancy-driven flows require much attention to the treatment of the near-wall region which requires refined meshes which is indeed too expensive for most of the industrial applications.
The Reynolds-Averaged Navier-Stokes Equation (RANS) approach has been widely used by most of the researchers and engineers due to the available computational resources. However, the turbulence variables calculated using models based on the RANS approach are only the approximation of turbulence due to the fact that the RANS approach is based on statistical averaging in a manner that the variables are decomposed into mean and fluctuating variables instead of solving instantaneous quantities. For the engineers, the mean flow field is of major interest and that is why the RANS approach has been widely used in the industrial community.

1.2.3 Turbulence model

In the last decades, modeling of turbulence had received a great deal of attention among the industrial and academic research community. A lot of attention has been focussed on the improvement of models. Despite substantial progress in the turbulence modeling, there is still a need to formulate a more fundamental approach so that the general behavior of turbulence can be predicted with adequate accuracy. Turbulence modeling is a procedure to close the system of Reynolds averaged mean flow equations. The Reynolds averaging introduce two unknown quantities in the conservation equations, namely Reynolds stresses and turbulent heat fluxes and to close the system of equations, these two unknown quantities need to be modeled.
One of the first known turbulence models is the mixing length model based on turbulent viscosity hypothesis which considers the relation of Reynolds stress to the velocity gradients and a prescribed length scale. This approach is relatively successful in simple flows. However, there are serious discrepancies in this approach that limit its applicability. Further improvement is made by proposing two-equation models. For instance, k-ε models which solve the transport equation of turbulent kinetic energy and its dissipation rate. An important feature of two-equation models is that it is independent of any prior details of the flow parameters and owing to this the range of application is wider. However, it has been revealed that the two-equation models show numbers of deficiencies, for instance, the

anisotropy of normal stress is not correctly represented in the models. To overcome the limitations of two-equation models, it is required to move to a higher level of modeling Reynolds stresses and turbulent heat fluxes by introducing differential equations for these two quantities. The modeling approach at this level is known as second-moment closure. For the turbulence model to be reliable, it should possess a few characteristics, like physical relevance, and more importantly, it should reproduces the physical phenomenon. Besides, the model ought to be primarily based on physical phenomena, and also it has to be simple without skipping the critical features. However, these crucial requirements are very tough to be fulfilled via the available turbulence models. As we know that the turbulence takes place almost everywhere ranging from simple to complicated configurations. It is very difficult to have one version of model which can correctly compute turbulent flows with the desired accuracy. Since the eddy-viscosity based models are nevertheless the mainstay for industrial computations particularly models used in PSA Group, so the goal of the present work is to recommend models in such a way that there may be a compromise between robustness and accuracy. The precedence is given to introduce buoyancy effects in the eddy-viscosity based turbulence models.

1.3 Objective of the work

The main objective of the work is to improve and expand eddy-viscosity based turbulence models for thermal buoyancy-driven flows, which would be applicable to a span of buoyancy-affected flows encountered in industry, particularly in the underhood space of automobiles.

At the earlier step, three new buoyancy-extended models are developed, in such a way that the weak equilibrium hypothesis is introduced into the k-ω-SST, BL-$\overline{v^2}/k$ and Launder-Sharma models. The buoyancy contribution is introduced in the Boussinesq relation for the Reynolds stress and in thermal heat flux relation using the generalized gradient diffusion hypothesis (GGDH). The main purpose of this modification is to propose a simple and linear buoyancy extension to the Reynolds stress relation by keeping the first part of Reynolds stress that corresponds to Boussinesq relation and including the buoyancy contribution that comes from the exact Reynolds stress equation. The models are then applied to the buoyancy modified flows namely natural and mixed convection in a differentially heated vertical channel and differentially heated cavities. Despite the success of the buoyancy extended model, it is diagnosed that the modeling of tensorial diffusivity is difficult in commercial codes specifically in ANSYS Fluent utilized by PSA Group. So it is for the practical purpose that simple buoyancy-extended models is also proposed. In this approach, the effect of buoyancy on the Reynolds stress is accounted for via adding buoyancy extension as is done within the previous model. However, the simple gradient diffusion hypothesis (SGDH) instead of the generalized gradient diffusion hypothesis (GGDH) is considered to model heat fluxes appeared in temperature equation.

For completion, the detailed evaluation of introducing only buoyancy production terms in the transport equation of turbulent kinetic energy and its dissipation rate are also analyzed with three turbulence models, namely k-ω-SST, BL-$\overline{v^2}/k$, and low-Reynolds number Launder-Sharma models. These model modifications are also related to buoyancy parameter known as flux Richardson number which is integrated into the dissipation or specific dissipation of k-ω-SST and BL-$\overline{v^2}/k$.
The open source code "Code Saturne" is utilised to develop these models owing to the flexibility of modifying the turbulence models and also due to the open access to the source code.

1.4 Thesis outline

The present work consists of six chapters namely Introduction, RANS modeling of turbulent flows, Influence of buoyancy on turbulent channel flows, Development of buoyancy extended models, Rectangular cavity, and conclusion and perspectives respectively.
After the introduction chapter (Chapter 1), Chapter 2 summarises the mathematical description of the governing equations. A brief description of the transport equation of Reynolds stress and turbulent heat flux equations are given, accompanied by the discussion of the modeling of the various terms. Attention is given to the buoyancy sensitized models by means of looking into the effect of introducing buoyancy production terms, the impact of turbulent Prandtl number and subsequently a detailed discussion on the simplification of Reynolds stress and heat flux models which take into account of buoyancy effects.
Chapter 3 presents the description of test cases which covers the span of turbulent convection regimes. A short discussion on the choice of turbulence models is given accompanied with the aid of the description of their overall performance through simulating the different convection regimes.
Chapter 4 presents the proposed buoyancy extended models. In the Reynolds stress relation, attention is paid to the enhancement of Boussinesq relation while maintaining the linearity of the relation. In the thermal part, improvement of generalized gradient diffusion hypothesis (GGDH) is made with the aid of introducing the buoyancy extension. Owing to the impossibility of modeling tensorial diffusivity in ANSYS Fluent, simple versions of buoyancy-extended models are proposed in which the simplicity is coming from the modeling of turbulent heat fluxes using the simple gradient diffusion hypothesis (SGDH). In addition to that, the effect of only including buoyancy production terms is analyzed along with the sensitivity of the coefficient ($C_{\varepsilon 3}$) in the ε or ω equations.
Chapter 5 describes the differentially heated cavity case and reviews the utility of buoyancy-extended k-ω-SST and BL-$\overline{v^2}/k$ models. In order to validate the proposed modified model, the comparison is made with DNS data of Trias [Trias et al., 2007, 2010].
Chapter 6 provides the overall conclusion and perspective of the study.

Chapter 2

RANS Modeling of turbulent flows

Contents

2.1 Introduction

This chapter provides an overview of the fundamental concepts that govern the basis for studying turbulent convective regimes that can be affected or driven with the aid of buoyancy. The chapter starts with the description of differential form for the conservation of mass, momentum, and energy equation that govern fluid flows and also their time-averaged form is discussed. This is followed by the discussion of turbulence models of various levels, starting from the Reynolds stress models to eddy-viscosity based models. The simplified form of turbulent kinetic energy and its dissipation equation of its exact form is also discussed. In addition to that, a brief evaluation of the turbulence closure is presented. Consequently, the issue of modeling the transport equation for Reynolds stress, heat flux, and temperature variance is also discussed. To shed light on the influence of including the buoyancy source terms in eddy-viscosity models, a detailed discussion of various proposals is made. Finally, this chapter discusses the weak and strong equilibrium hypotheses for the truncation of the transport equations for Reynolds stress and turbulent heat flux which results in the formulation of algebraic stress or algebraic heat flux models.

2.1.1 Navier Stokes equations

Continuity equation

The differential form of the continuity equation writes:

$$\frac{1}{\rho}\frac{D\rho}{Dt} + \nabla.\mathbf{u} = 0 \tag{2.1}$$

Where $\rho = \rho(x, y, z, t)$ is the density and $\mathbf{u}$ is the velocity vector.

Momentum equation

The momentum relation in differential form is expressed as follows :

$$\rho\left(\frac{\partial u_i}{\partial t} + u_j\frac{\partial u_i}{\partial x_j}\right) = -\frac{\partial p}{\partial x_i} + \frac{\partial \tau_{ij}}{\partial x_i} + \rho g_i \tag{2.2}$$

Where p, τ_{ij} and g_i are pressure, viscous stress and acceleration due to gravity respectively. Viscous stresses are proportional to strain rates and coefficient of viscosity and expressed as follows:

$$\tau_{ij} = 2\mu\left(S_{ij} - \frac{1}{3}S_{kk}\delta_{ij}\right) \tag{2.3}$$

where S_{ij} is the strain rate, $S_{ij} = \frac{1}{2}\left(\frac{\partial u_i}{\partial x_j} + \frac{\partial u_j}{\partial x_i}\right)$

Substituting Eq. 2.3 into Eq. 2.2 yields

$$\rho\left(\frac{\partial \mathbf{u}}{\partial t} + \nabla \mathbf{u}.\mathbf{u}\right) = -\nabla p + \nabla.(\mu(\nabla u + (\nabla u)^T) - \frac{2}{3}\mu(\nabla.u)\mathbf{I}) + \rho\mathbf{g} \tag{2.4}$$

Eq. 2.4 is the differential momentum equation for newtonian fluid.

Energy equation

The simplified form of energy equation in terms of temperature (T) is expressed as follows:

$$\rho C_p \frac{DT}{Dt} = \lambda \nabla^2 T \tag{2.5}$$

where C_p and λ are specific heat at constant pressure and thermal conductivity respectively.

Boussinesq approximation

The Boussinesq approximation states that the density variation is only considered in the buoyancy term, $\rho\mathbf{g}$, of the momentum equation and can be neglected in the rest of equation Eq. 2.4. Assuming this Eq. 2.4 becomes:

$$\rho_0\left(\frac{\partial \mathbf{u}}{\partial t} + \nabla \mathbf{u}.\mathbf{u}\right) = -\nabla p + \nabla.(\mu(\nabla \mathbf{u} + (\nabla \mathbf{u})^T) - \frac{2}{3}\mu(\nabla.\mathbf{u})\mathbf{I}) + \rho\mathbf{g} \tag{2.6}$$

With $\rho = \rho_0 =$ constant, the Eq. 2.1 becomes

$$\nabla.\mathbf{u} = 0 \tag{2.7}$$

and that makes $-\frac{2}{3}\mu(\nabla.\mathbf{u})\mathbf{I}$ to be zero in the Eq. 2.6. It is also assumed that the viscosity, μ, is constant which makes Eq. 2.6 to yield:

$$\rho_0\left(\frac{\partial \mathbf{u}}{\partial t} + \nabla \mathbf{u}.\mathbf{u}\right) = -\nabla p + \mu\nabla^2\mathbf{u} + \rho\mathbf{g} \tag{2.8}$$

The buoyancy term ($\rho\mathbf{g}$) can be written as $(\rho_0 + \Delta\rho)\mathbf{g}$ such that the Eq. 2.8 becomes:

$$\rho_0\left(\frac{\partial \mathbf{u}}{\partial t} + \nabla \mathbf{u}.\mathbf{u}\right) = -\nabla p + \mu\nabla^2\mathbf{u} + (\rho_0 + \Delta\rho)\mathbf{g} \tag{2.9}$$

In order to avoid the evaluation of the fluid density based on the local temperature, for small temperature differences, it is usual to assume a linear variation of density with

temperature, such that the buoyancy source term ($\Delta\rho\mathbf{g} = (\rho - \rho_0)\mathbf{g}$) can be written as:

$$(\rho - \rho_0)\mathbf{g} = -\beta\rho_0(T - T_{ref})\mathbf{g} \tag{2.10}$$

where β is the thermal expansion coefficient and T_{ref} is the reference temperature.
With this approximation, Eq. 2.9 becomes:

$$\rho_0\left(\frac{\partial\mathbf{u}}{\partial t} + \nabla\mathbf{u}.\mathbf{u}\right) = -\nabla p + \mu\nabla^2\mathbf{u} + \rho_0\mathbf{g} - \rho_0\mathbf{g}\beta(T - T_{ref}) \tag{2.11}$$

Taking into account of hydrostatic pressure,

$$P = p + \rho_0 gh \tag{2.12}$$

Eq. 2.11 becomes:

$$\rho_0\left(\frac{\partial\mathbf{u}}{\partial t} + \nabla\mathbf{u}.\mathbf{u}\right) = -\nabla P + \mu\nabla^2\mathbf{u} - \rho_0\mathbf{g}\beta(T - T_{ref}) \tag{2.13}$$

In the next section, we discuss the turbulence phenomena and how they change the behavior of the flow by inducing mixing and other effects.

2.1.2 Turbulence

There are many engineering applications to observe turbulent flows such as flows in compressors, pumps, flow around vehicles, mixing of air and fuel in engines and in many other applications. One of the important characteristics of turbulence is the mixing of fluid and more effective transport than laminar flow. Because of this effective mixing of fluids and transport, turbulence phenomena are of vital importance to many industrial applications. The Reynolds number of the flow determines the relative importance of the inertial forces and the viscous forces. From experiments on fluid flows, it is observed that below the threshold value of Reynolds number ($Re_{critical}$), adjacent layers of fluid past each other in an orderly manner and the flow is smooth. This part of the flow regime is known as laminar flow. However, above the value of $Re_{critical}$, a series of complex events takes place which gradually leads to significant changes in the flow behaviour and the flow becomes random and chaotic. The flow properties vary in a very random way and such type of chaotic regime of flow is called turbulent flow. This agitated nature of turbulent flow needs complete description of the motion of all the fluid particles. Statistical study of turbulent flows involves the decomposition of instantaneous quantities into its mean and fluctuating components. Turbulent fluctuations are **three-dimensional** in character which is varied in space. In addition to that, there are rotational flow structures which is known as turbulent eddies and these eddies have a wide span of length scales. Moreover, length scales of these eddies can be comparable to the dimensions of the flow configuration

as well as there are intermediate and small size scales. Fluid particles are brought close to each other by the motion of eddies in turbulent flows. The consequence of this is the significant exchange of mass, momentum and heat. This leads to the mixing of fluid which amplifies the diffusion for mass, momentum and heat.
In the next section of this chapter, a brief discussion of the Reynolds averaging of the conservation of mass, momentum and energy equation is done.

2.1.3 Reynolds averaged Navier Stokes Equation

In order to avoid very high computational cost of simulating turbulent structures, the standard method for industrial simulations is the RANS method, based on the Reynolds decomposition, which consists of calculating only certain statistical moments of the variables. Reynolds average is a statistical average and the Reynolds averaged equations provide the basis for analysing and calculating the transport phenomena in engineering application problems. In this approach, the variable ϕ is decomposed into the mean part $\overline{\phi}$ and the fluctuating part $\phi^{'}$ such that:

$$\phi(t) = \overline{\phi(t)} + \phi^{'}(t) \tag{2.14}$$

For stationary flows, $\overline{\phi}$ can be computed as:

$$\overline{\phi} = \lim_{\tau \to \infty} \frac{1}{\tau} \int_{t_0}^{t_0+\tau} \widetilde{\phi(t)} dt \tag{2.15}$$

where τ represents a time interval which is large enough to average the unsteadiness of the flow. The time average of the fluctuations $\phi^{'}$ is zero:

$$\overline{\phi^{'}} = 0 \tag{2.16}$$

Some information related to the intensity of the fluctuations can be obtained from the root-mean-square, which is expressed as follows:

$$\phi_{rms} = \sqrt{\overline{(\phi^{'})^2}} \tag{2.17}$$

To investigate the effect of turbulent fluctuations on averaged equations, we need to replace the flow variable u, v, w and p in Eq. 2.1, Eq. 2.4 and in Eq.2.5 by the sum of mean and fluctuating components such that

$$u_i = U_i + u_i^{'}; p = P + p^{'}; \Theta = T + \theta \tag{2.18}$$

Also by assuming the Boussinesq hypothesis, the averaged equations become

$$\frac{\partial U_i}{\partial x_i} = 0 \tag{2.19}$$

$$\frac{DU_i}{Dt} = -\frac{\partial P}{\partial x_i} + \frac{\partial}{\partial x_j}\left[\nu\left(\frac{\partial U_i}{\partial x_j} - \overline{u_i' u_j'}\right)\right] - g_i\beta(T - T_{ref}) \tag{2.20}$$

$$\frac{DT}{Dt} = \frac{\partial}{\partial x_i}\left(\frac{\nu}{Pr}\frac{\partial T}{\partial x_i} - \overline{\theta u_i'}\right) \tag{2.21}$$

The time averaging of the equations introduces the second moments $\overline{u_i' u_j'}$ in the momentum equation and $\overline{\theta u_i'}$ in energy equation. To close the system of equations, information is required on turbulent momentum fluxes and turbulent heat fluxes. The most detailed and natural way to have these fluxes is to solve their transport equations and the process of closing this system of equations is known as second moment closure. Moreover, the goal of most commercial CFD code is to provide simple, applicable and economical turbulence model to compute wide variety of flows. Next section of this chapter deals with the discussion of turbulence closure of Reynolds stress and heat flux models.

2.1.4 Reynolds Stress Models

This part of the chapter involves the discussion of the Reynolds stress equation and its closure. The Reynolds stress and turbulent heat flux terms that comes out due to the averaging in the momentum and energy equations is the second moments for the exact differential transport equations. These differential equations consist of number of terms that cannot be calculated exactly, but these terms need modeling for the closure of the equations. Since the second moments are obtained by solving the modeled transport equations, closure at this level provides more accurate predictions of the turbulent quantities as compared to the standard eddy-viscosity/eddy-diffusivity based models. Simplest linear models mainly for pressure-strain and pressure-temperature-gradient correlation are discussed for both the Reynolds stress and heat flux equations.
The partial differential equation for Reynolds stress under the Boussinesq hypothesis writes:

$$\frac{D\overline{u_i' u_j'}}{Dt} = \boxed{\underbrace{-\frac{\partial}{\partial x_k}\overline{(u_i' u_j' u_k')}}_{D_{ij}^t}} + \underbrace{\frac{\partial}{\partial x_k}(\nu\frac{\partial \overline{u_i' u_j'}}{\partial x_k})}_{D_{ij}^\nu} - \boxed{\underbrace{\frac{\partial}{\partial x_k}\left(\overline{\frac{p'}{\rho}(u_i'\delta_{jk} + u_j'\delta_{ik})}\right)}_{D_{ij}^p}} - \underbrace{\left(\overline{u_i' u_k'}\frac{\partial U_j}{\partial x_k} + \overline{u_j' u_k'}\frac{\partial U_i}{\partial x_k}\right)}_{P_{ij}} - \underbrace{\beta(g_j\overline{\theta u_i'} + g_i\overline{\theta u_j'})}_{G_{ij}} - \boxed{\underbrace{\overline{\frac{p'}{\rho}\left(\frac{\partial u_i'}{\partial x_j} + \frac{\partial u_j'}{\partial x_i}\right)}}_{\phi_{ij}}} - \boxed{\underbrace{2\nu\overline{\frac{\partial u_i'}{\partial x_k}\frac{\partial u_j'}{\partial x_k}}}_{\varepsilon_{ij}}} \tag{2.22}$$

$D_{ij}^t \equiv$ Turbulent diffusion; $D_{ij}^\nu \equiv$ Viscous diffusion; $D_{ij}^p \equiv$ Pressure diffusion
$P_{ij} \equiv$ Dynamic Production; $G_{ij} \equiv$ Buoyancy production
$\phi_{ij} \equiv$ Pressure velocity correlation; $\varepsilon_{ij} \equiv$ dissipation tensor

${D^t}_{ij}$, ${D^p}_{ij}$, ϕ_{ij} and ε_{ij} needs modelling. The function of pressure-strain correlation is merely to redistribute the energy between normal components of the Reynolds stress and this term is modeled as a sum of three contributions

$$\phi^*_{ij} = \underbrace{\phi^1_{ij}}_{Slow-term} + \underbrace{\phi^2_{ij}}_{Rapid-term} + \underbrace{\phi^3_{ij}}_{Buoyancy-term} \tag{2.23}$$

Since Reynolds stress models (RSM) are not the focus of this work, a very short description is given here. The reader is requested to refer Hanjalić and Launder [2011] for a complete introduction.

Modeling of pressure-strain correlation terms

For modeling the slow-term, Rotta [1951] have proposed the return-to-isotropy model which is expressed as follows:

$$\phi^1_{ij} = -C_1 \frac{\varepsilon}{k}\left(\overline{u'_i u'_i} - \frac{2}{3}k\delta_{ij}\right) \tag{2.24}$$

The Isotropization-of-production model by Naot [1970] is used to model the rapid-term of the pressure-strain term:

$$\phi^2_{ij} = -C_2\left(P_{ij} - \frac{2}{3}\delta_{ij}P_k\right) \qquad with \qquad C_2 = 0.6 \tag{2.25}$$

Buoyancy effects play an important role on the pressure-strain correlation and the role of buoyancy is to reduce the anisotropy of buoyancy production. The buoyancy contribution to pressure-strain can be modeled by using the isotropization-of-model proposed by Launder [1975, 1976] or by Gibson and Launder [1976] which is expressed as:

$$\phi^3_{ij} = -C_3\left(G_{ij} - \frac{2}{3}G_k\delta_{ij}\right) \qquad with \qquad C_3 = 0.6 \tag{2.26}$$

Modeling of the dissipation tensor

Small scale motions are isotropic for high Reynolds number and assuming this to model dissipation tensor leads to

$$\varepsilon_{ij} = 2\nu\overline{\frac{\partial u'_i}{\partial x_k}\frac{\partial u'_i}{\partial x_k}} = \frac{2}{3}\varepsilon\delta_{ij} \tag{2.27}$$

Modeling diffusion terms

One of the way of modeling the turbulent diffusion is by using generalized gradient diffusion hypothesis (GGDH) of Daly and Harlow [1970], the pressure diffusion is generally

modeled along with turbulent diffusion as it participates in the overall diffusion.

$$D^p_{ij} + D^t_{ij} = \frac{\partial}{\partial x_k}\left[C_s \frac{k}{\varepsilon}\overline{u_k' u_l'}\frac{\partial \overline{u_i' u_j'}}{\partial x_l}\right] \tag{2.28}$$

2.1.5 Turbulent heat flux equation

The exact equation of the turbulent heat flux writes:

$$\frac{D\overline{\theta u_i}}{Dt} = \underbrace{\left[\boxed{\underbrace{\frac{\partial}{\partial x_k}\left(\nu\overline{\frac{\partial u_i'}{\partial x_k}\theta} + \alpha\overline{u_i'\frac{\partial \theta}{\partial x_k}}\right)}_{D^\nu_{\theta i}}} - \boxed{\underbrace{\frac{\partial}{\partial x_k}\overline{(u_i' u_k' \theta)}}_{D^t_{\theta i}}} + \underbrace{\frac{\partial}{\partial x_k}\left(\frac{\partial}{\partial x_j}\left(\overline{\frac{\theta p}{\rho}}\delta_{ij}\right)\right)}_{D^p_{\theta i}}\right]}_{D_{\theta i}}$$
$$\underbrace{-\overline{u_i' u_j'}\frac{\partial T}{\partial x_k}}_{P^{th}_{\theta i}} \underbrace{-\overline{\theta u_k'}\frac{\partial U_i}{\partial x_k}}_{P^m_{\theta i}} - \boxed{\underbrace{g_i\beta\overline{\theta^2}}_{G_{\theta i}}} - \boxed{\underbrace{\overline{\frac{\partial p}{\partial x_i}\frac{\theta}{\rho}}}_{\phi_{\theta i}}} - \boxed{\underbrace{(\nu+\alpha)\overline{\frac{\partial u_i'}{\partial x_k}\frac{\partial \theta}{\partial x_k}}}_{\varepsilon_{\theta i}}} \tag{2.29}$$

where,
$D^t_{\theta i} \equiv$ Turbulent diffusion; $D^\nu_{\theta i} \equiv$ Molecular diffusion; $D^p_{\theta i} \equiv$ Pressure diffusion
$P^{th}_{\theta i} \equiv$ Thermal production; $P^m_{\theta i} \equiv$ Mechanical production; $G_{\theta i} \equiv$ Buoyancy production
$\phi_{\theta i} \equiv$ Pressure scrambling; $\varepsilon_{\theta i} \equiv$ Molecular dissipation
The terms showed in boxes need to be modeled. It is worth noting that molecular diffusion also needs to be modeled. The terms involve gradients of mean velocity and mean temperature which shows that turbulent heat fluxes depend on thermal as well as velocity field. Pressure-scrambling has a significant effect on turbulent heat fluxes and so the precise prediction of this term is vital. Pressure-scrambling is composed of three terms.

$$\phi_{\theta i} = \underbrace{\phi^1_{\theta i}}_{Slow-term} + \underbrace{\phi^2_{\theta i}}_{Rapid-term} + \underbrace{\phi^3_{\theta i}}_{Buoyancy-term} \tag{2.30}$$

The simplest model for the slow term ($\phi^1_{\theta i}$) was proposed by Monin [1965] which is based on a linear return to isotropy approximation.

$$\phi^1_{\theta i} = -C_{\theta 1}\overline{\theta u_i'}\frac{1}{\tau} \tag{2.31}$$

The model for the rapid term ($\phi^2_{\theta i}$) proposed by Owen [1974] is based on the isotropization of production due to velocity gradient.

$$\phi^2_{\theta i} = C_{\theta 2}\overline{\theta u_k'}\frac{\partial U_i}{\partial x_k} \tag{2.32}$$

Although the temperature gradient does not appear in the exact expression of $\phi^2_{\theta i}$ [Launder, 1975]. Durbin [1993] proposed an additional contribution for $\phi^2_{\theta i}$ which is based on the

isotropization due to gradient of temperature.

$$\phi_{\theta i}^{2'} = C'_{\theta 2}\overline{u'_i u'_j}\frac{\partial \theta}{\partial x_j} \tag{2.33}$$

However, this appears artificial since the temperature gradient does not appear in the exact expression of $\phi_{\theta i}^{2}$. The effect of buoyancy on pressure-scrambling is denoted by $\phi_{\theta i}^{3}$ and the modeling of this term is done analogous to ϕ_{ij}^{3} part based on the isotropization of production due to buoyancy of Owen [1974].

$$\phi_{\theta i}^{3} = C_{\theta 3}\beta g_i \overline{\theta^2} \tag{2.34}$$

Finally, the pressure scrambling term by assembling all the proposals reads:

$$\phi_{\theta i} = -C_{\theta 1}\frac{1}{\tau}\overline{u'_i\theta} + C_{\theta 2}\overline{u'_j\theta}\frac{\partial U_i}{\partial x_j} + C_{\theta 3}\beta g_i\overline{\theta^2} + C'_{\theta 2}\overline{u'_i u'_j}\frac{\partial \theta}{\partial x_j} \tag{2.35}$$

The coefficients used by different authors are listed in Table 2.1.

Researchers	$C_{\theta 1}$	$C_{\theta 2}$	$C_{\theta 3}$	$C_{\theta 2}{}'$
Launder [1975]	3.2	0.5	0.5	–
Gibson and Launder [1978]	3.0	0.33	0.33	–
Launder [1988]	3.0	0.4	0.33	–
Lai and So [1990]	3.0	0.4	–	–
Peeters and Henkes [1992]	3.75	0.5	0.5	–
Durbin [1993]	2.5	0	–	0.45
Dol et al. [1997]	3.75	0.5	0.5	–
Kenjeres [1998]	5.0	0.4	0.4	–
Dol et al. [1999]	3.75	0.5	0.5	–
Dol and Hanjalić [2001]	3.75	0.5	0.5	–
Shin et al. [2005]	2.5	0	–	0.45
Shin et al. [2008]	3.0	0.4	0.33	0
Choi and Kim [2008]	3.75	0.5	0.5	–

Table 2.1 – Different values of constants for $\phi_{\theta i}$

Using the analogy of Daly and Harlow [1970], the turbulent diffusion term can be modeled using the model of Wyngaard and Coté [1974].

$$D_{\theta i}^{t} = \frac{\partial}{\partial x_k}\left[C_\theta \tau \overline{u'_k u'_l}\frac{\partial \overline{\theta u'_i}}{\partial x_l}\right] \tag{2.36}$$

Peeters and Henkes [1992] proposed the model for molecular diffusion which is as follows:

$$D_{\theta i}^{\nu} = \nu\frac{\partial^2 \overline{u'_i\theta}}{\partial {x_k}^2} + (\alpha - \nu)\overline{u'_i\frac{\partial^2\theta}{\partial {x_k}^2}} + (\alpha - \nu)\overline{\frac{\partial u'_i}{\partial x_k}\frac{\partial \theta}{\partial x_k}} \tag{2.37}$$

Rearranging this leads to:

$$D^{\nu}_{\theta i} = \frac{\partial}{\partial x_k}\left(\frac{\nu+\alpha}{2}\frac{\partial \overline{u_i^{'}\theta}}{\partial x_k}\right) - \frac{1}{2}\overline{\theta\frac{\partial^2 u_i^{'}}{\partial {x_k}^2}} + \frac{1}{2}(\alpha-\nu)\overline{u_i^{'}\frac{\partial^2\theta}{\partial {x_k}^2}} \tag{2.38}$$

2.1.6 Temperature variance equation

The Reynolds-averaged transport equation for the temperature variance writes

$$\frac{D\overline{\theta^2}}{Dt} = \Bigg[\underbrace{\frac{\partial}{\partial x_k}\left(\alpha\frac{\partial\overline{\theta^2}}{\partial x_k}\right)}_{D^{\nu}_{\theta}} - \boxed{\underbrace{\frac{\partial}{\partial x_k}\left(\overline{\theta^2 u_k^{'}}\right)}_{D^{t}_{\theta}}}\Bigg] - \underbrace{2\overline{\theta u_k^{'}}\frac{\partial T}{\partial x_k}}_{P_{\theta}} - \boxed{\underbrace{2\alpha\overline{\frac{\partial\theta}{\partial x_k}\frac{\partial\theta}{\partial x_k}}}_{\varepsilon_{\theta}}} \tag{2.39}$$

where,
$D^{\nu}_{\theta} \equiv$ Molecular diffusion; $D^{t}_{\theta} \equiv$ Turbulent diffusion
$P_{\theta} \equiv$ Thermal production; $\varepsilon_{\theta} \equiv$ Dissipation rate
Turbulent diffusion and dissipation rate in the boxes needs modeling. D^{t}_{θ} can be modeled using Wyngaard and Coté [1974] model expressed as follows:

$$D^{t}_{\theta} = \frac{\partial}{\partial x_j}\left(C_{\theta\theta}\frac{k}{\varepsilon}\overline{u_i^{'}u_j^{'}}\frac{\partial\overline{\theta^2}}{\partial x_j}\right); \qquad with \qquad C_{\theta\theta} = 0.22 \tag{2.40}$$

However, thermal production and molecular diffusion can be computed exactly. Eq. (2.39) is similar to the turbulent kinetic energy equation. In order to close the temperature variance equation, one has to either solve the dissipation rate of temperature variance or model it. It can be simply expressed from the definition of the time-scale ratio, R, which represents the ratio between the thermal (τ_{θ}) and the mechanical time scale, τ_m:

$$R = \frac{\tau_{\theta}}{\tau_m} = \frac{\frac{\overline{\theta^2}}{2\varepsilon_{\theta}}}{\frac{k}{\varepsilon}} \tag{2.41}$$

Where R is considered as constant, generally taken as 0.5.
However, for inhomogeneous flows, R cannot be constant and there are several proposals to model R. For instance, Ince and Launder [1989] suggested a correlation of the time scale which is expressed in terms of a scalar flux invariant, $A_{\theta 2}$, which is defined as follows:

$$A_{\theta 2} = \frac{\overline{\theta u_k^{'}\theta u_k^{'}}}{k\overline{\theta^2}} \tag{2.42}$$

The definition of R by using Eq. (2.42) yields:

$$R = \frac{1}{1.5(1+A_{\theta 2})} \tag{2.43}$$

2.1.7 Eddy viscosity based models

The simplest method to model the Reynolds stresses and heat fluxes is based on eddy-viscosity and diffusivity model, where Reynolds stresses and heat fluxes are expressed in terms of velocity and temperature gradients respectively.
The Boussinesq constitutive relation for Reynolds stresses writes:

$$\overline{u_i^{'}u_j^{'}} = \frac{2}{3}k\delta_{ij} - \nu_t\left(\frac{\partial U_i}{\partial x_j} + \frac{\partial U_j}{\partial x_i}\right) \tag{2.44}$$

and the simple gradient diffusion hypothesis (SGDH) is expressed as follows:

$$\overline{\theta u_i^{'}} = -\frac{\nu_t}{Pr_t}\frac{\partial T}{\partial x_i} \tag{2.45}$$

Where Pr_t is the turbulent Prandtl number which is considered constant in many flows and most of the CFD codes assume the values of Pr_t close to 1.0.

k-ε model

Based on dimensional grounds, the eddy-viscosity can be defined based on a velocity scale υ and a length scale ℓ which are representative of large-scale turbulence

$$\nu_t \propto \upsilon\ell \tag{2.46}$$

It is very common to relate eddy-viscosity with quantities that have a clear physical meaning. The square root of turbulent kinetic energy has been used as a velocity scale and the length scale of energy containing eddies has been used as length scale. Using Kolmogorov assumptions, [Kolmogorov, 1941], the length scale ℓ can be related to the dissipation rate by $l = \frac{k^{3/2}}{\varepsilon}$, such that

$$\nu_t = C_\mu\frac{k^2}{\varepsilon} \tag{2.47}$$

Where the coefficient C_μ is equal to 0.09.

Turbulent kinetic energy and dissipation rate equations

In this part of the section, exact equations of the turbulent kinetic energy and its dissipation rate is discussed along with modeling different terms in the exact equations so that the more simplified form of equation can be achieved and this makes possible to solve

the equation computationally. The exact equation of turbulent kinetic energy writes:

$$\underbrace{\frac{\partial k}{\partial t}}_{L_k} + \underbrace{U_k \frac{\partial k}{\partial x_k}}_{C_k} = \underbrace{\left[\boxed{\underbrace{\frac{\partial}{\partial x_k}\left(-\overline{u_k' u_l' u_l'} \right)}_{D_k^t}} - \boxed{\underbrace{\frac{\partial}{\partial x_k}\left(\frac{1}{\rho}\overline{u_k' p'} \right)}_{D_k^p}} + \underbrace{\frac{\partial}{\partial x_k}\left(\nu \frac{\partial k}{\partial x_k} \right)}_{D_k^\nu} \right]}_{D_k} - \underbrace{\overline{u_i' u_k'} \frac{\partial U_i}{\partial x_k}}_{P_k} - \underbrace{\beta g_i \overline{\theta u_i'}}_{G_k} - \boxed{\underbrace{\nu \overline{\frac{\partial u_i' \partial u_i'}{\partial x_k \partial x_k}}}_{\varepsilon}} \tag{2.48}$$

where,
$L_k \equiv$ Rate of change of k, $\quad C_k \equiv$ Transport of k by convection
$D_k^t \equiv$ Transport of k by turbulent diffusion, $\quad D_k^p \equiv$ Transport of k by pressure diffusion
$D_k^\nu \equiv$ Transport of k by viscous diffusion, $\quad P_k \equiv$ Production rate of k
$G_k \equiv$ Production of k due to buoyancy $\quad \varepsilon \equiv$ Dissipation
The terms in boxes need modeling. Pressure diffusion is modeled with turbulent diffusion using the simple gradient diffusion hypothesis (SGDH):

$$D_k^t = \frac{\partial}{\partial x_k}\left(\frac{\nu_t}{\sigma_k} \frac{\partial k}{\partial x_k} \right) \tag{2.49}$$

So the final modeled form of turbulent kinetic energy is as follows:

$$\frac{\partial k}{\partial t} + U_k \frac{\partial k}{\partial x_k} = \frac{\partial}{\partial x_k}\left[\left(\nu + \frac{\nu_t}{\sigma_k} \frac{\partial k}{\partial x_k} \right) \right] - \overline{u_i' u_k'} \frac{\partial U_i}{\partial x_k} - \beta g_i \overline{\theta u_i'} - \varepsilon \tag{2.50}$$

The exact transport equation for the dissipation rate of turbulent kinetic energy can be written as:

$$\underbrace{\frac{\partial \varepsilon}{\partial t}}_{L_\varepsilon} + \underbrace{U_k \frac{\partial \varepsilon}{\partial x_k}}_{C_\varepsilon} = \underbrace{\left[\boxed{\underbrace{\frac{\partial}{\partial x_k}\left(-2\frac{\nu}{\rho}\overline{\frac{\partial p'}{\partial x_l}\frac{\partial u_k'}{\partial x_l}} \right)}_{D_\varepsilon^p}} - \boxed{\underbrace{\frac{\partial}{\partial x_k}\left(\nu \overline{u_k{}' \left(\frac{\partial u_i{}'}{\partial x_l} \right)^2} \right)}_{D_\varepsilon^t}} + \underbrace{\frac{\partial}{\partial x_k}\left(\nu \frac{\partial \varepsilon}{\partial x_k} \right)}_{D_\varepsilon^\nu} \right]}_{D_\varepsilon}$$
$$\boxed{\underbrace{-2\nu \frac{\partial U_i}{\partial x_k}\left(\overline{\frac{\partial u_i{}'}{\partial x_l}\frac{\partial u_k{}'}{\partial x_l}} + \overline{\frac{\partial u_l{}'}{\partial x_i}\frac{\partial u_l{}'}{\partial x_k}} \right)}_{P_{\varepsilon 1}+P_{\varepsilon 2}}} \boxed{\underbrace{-2\nu \overline{u_k{}'\frac{\partial u_i{}'}{\partial x_l}\frac{\partial^2 U_i}{\partial x_k \partial x_l}}}_{P_{\varepsilon 3}}} \boxed{\underbrace{-2\nu \overline{\frac{\partial u_i{}'}{\partial x_l}\frac{\partial u_k{}'}{\partial x_l}\frac{\partial u_i{}'}{\partial x_l}}}_{P_{\varepsilon 4}}}$$
$$\boxed{\underbrace{-2\nu \left(\overline{\frac{\partial^2 u_i{}'}{\partial x_k \partial x_l}} \right)^2}_{Y_\varepsilon}} \boxed{\underbrace{-2\beta\nu g_i \overline{\frac{\partial u_i{}'}{\partial x_l}\frac{\partial \theta}{\partial x_l}}}_{G_\varepsilon}} \tag{2.51}$$

where, $L_\varepsilon \equiv$ Rate of change of ε, $\quad C_\varepsilon \equiv$ Transport of ε by convection

$D_\varepsilon^t \equiv$ Transport of ε by turbulent diffusion, $\quad D_\varepsilon^p \equiv$ Transport of ε by pressure diffusion
$D_\varepsilon^\nu \equiv$ Transport of ε by viscous diffusion, $\quad P_{\varepsilon 1} + P_{\varepsilon 2} \equiv$ Mixed Production of ε
$P_{\varepsilon 3} \equiv$ Production by the Hessian of velocity, $\quad P_{\varepsilon 4} \equiv$ Turbulent production of ε
$Y_\varepsilon \equiv$ Major destruction of ε, $\quad G_\varepsilon \equiv$ Buoyancy production term
The terms in boxes need modeling. Turbulent diffusion of ε is modeled using the simple gradient diffusion hypothesis (SGDH),

$$D_\varepsilon^t = \frac{\partial}{\partial x_k}\left(\frac{\nu_t}{\sigma_\varepsilon}\right) \tag{2.52}$$

Far from the walls, the main production of ε is due to $P_{\varepsilon 4}$ which is modeled along with destruction term Y_ε such that:

$$P_{\varepsilon 4} - Y_\varepsilon = \frac{\varepsilon}{k}\left(C_{\varepsilon 1} P_k - C_{\varepsilon 2}\varepsilon\right) \tag{2.53}$$

Terms $P_{\varepsilon 1}$, $P_{\varepsilon 2}$ and $P_{\varepsilon 3}$ can be neglected in regions far from the walls. The modeled transport equation of dissipation rate becomes:

$$\frac{\partial \varepsilon}{\partial t} + U_k \frac{\partial \varepsilon}{\partial x_k} = \frac{\partial}{\partial x_k}\left[\left(\nu + \frac{\nu_t}{\sigma_\varepsilon}\frac{\partial \varepsilon}{\partial x_k}\right)\right] + C_{\varepsilon 1}\frac{\varepsilon}{k}(-\overline{u_i' u_k'}\frac{\partial U_i}{\partial x_k}) + C_{\varepsilon 3}\frac{\varepsilon}{k}G - C_{\varepsilon 2}\varepsilon\frac{\varepsilon}{k} \tag{2.54}$$

The standard $k-\varepsilon$ model uses following values of the constants:

$$\boxed{C_\mu = 0.09; \sigma_k = 1.0; \sigma_\varepsilon = 1.30; C_{\varepsilon 1} = 1.44; C_{\varepsilon 2} = 1.92} \tag{2.55}$$

2.1.8 Low-Reynolds number models

In the industrial applications, the success of the turbulence models for the prediction of wall-bounded shear flows is dependent to a large extent on the use of wall functions which relates the surface boundary conditions to the point in the flow far away from the surface and so avoids the problem of modeling the viscous effects. However, there are several flows in which this approach has to be stranded. For instance, in turbulent boundary layers at transitional Reynolds numbers and in seperated flows. An alternative approach to avoid the use of wall functions is the use of low-Reynolds number models, where the equations are solved right up to the wall. Over the last few decades, many proposals have been made for turbulence closures to enable their use to describe the flow close to a wall. Most of the models use either a wall damping effect on the empirical coefficients and on functions in the turbulence equations. These modifications are mainly dependent upon numerical experiments and comparisons of global parameters. The general form of low-Reynolds number $k-\varepsilon$ type model is expressed as follows:

$$\frac{\partial k}{\partial t} + U_j \frac{\partial U_i}{\partial x_j} = \frac{\partial}{\partial x_j}\left[\left(\nu + \frac{\nu_t}{\sigma_k}\right)\frac{\partial k}{\partial y}\right] - \overline{u_i' u_j'}\frac{\partial U_i}{\partial x_j} - \widetilde{\varepsilon} - D \tag{2.56}$$

$$\frac{\partial \widetilde{\varepsilon}}{\partial t} + U_j \frac{\partial \widetilde{\varepsilon}}{\partial x_j} = \frac{\partial}{\partial x_j}\left[\left(\nu + \frac{\nu_t}{\sigma_\varepsilon}\right)\frac{\partial \varepsilon}{\partial y}\right] - C_{\varepsilon 1} f_1 \frac{\widetilde{\varepsilon}}{k}\left(\overline{u_i' u_j'}\frac{\partial U_i}{\partial x_j}\right) - C_{\varepsilon 2} f_2 \frac{\widetilde{\varepsilon}^2}{k} + E \tag{2.57}$$

$$\nu_t = C_\mu f_\mu \frac{k^2}{\widetilde{\varepsilon}}; \quad R_T = \frac{k^2}{\nu \widetilde{\varepsilon}}; \quad R_y = \frac{\sqrt{k} y}{\nu} \tag{2.58}$$

Researchers	Model	$C_{\varepsilon 1}$	$C_{\varepsilon 2}$	C_μ	σ_k	σ_ε
Jones and Launder [1972, 1973]	JL	1.45	2.0	0.09	1.0	1.3
Launder and Sharma [1974]	LS	1.44	1.82	0.09	1.0	1.3
Hoffman [1975]	HO	1.81	2.0	0.09	2.0	3.0
Hassid and Poreh [1978]	HP	1.45	2.0	0.09	1.0	1.3
Lam and Bremhorst [1981]	LB	1.44	1.92	0.09	1.0	1.3
Chien [1982]	CH	1.35	1.8	0.09	1.0	1.3
Lai and So [1990]	LSO	1.35	1.8	0.09	1.0	1.3
So et al. [1991]	SZS	1.5	1.83	0.096	0.75	1.45
Yang and Shih [1993]	YS	1.44	1.92	0.09	1.0	1.3
Fan et al. [1993]	FLB	1.4	1.8	0.09	1.0	1.3
Rodi and Mansour [1993]	RMM	1.44	1.92	0.09	1.3	1.3
Michelassi et al. [1993]	MR	1.44	1.92	0.09	1.3	1.3

Table 2.2 – Numerical values of constants $C_{\varepsilon 1}$, $C_{\varepsilon 2}$, C_μ, σ_k and σ_ε for different models

Table 2.2 summarises the details of the low-Reynolds number functions for the $k-\varepsilon$ group of models. To have better representation of the near-wall behavior, extra terms denoted by D and E were added as listed in Table 2.4. Mainly three different definition of D were used by researchers listed in Table 2.3. Moreover, the models from the $k-\varepsilon$ group are different from the basic version by introducing the viscous diffusion terms and by the inclusion of damping functions (f) to modify constants ($C_{\varepsilon 1}$ and $C_{\varepsilon 2}$). $\widetilde{\varepsilon}$ is defined as :

$$\widetilde{\varepsilon} = \varepsilon + D \tag{2.59}$$

This definition of $\widetilde{\varepsilon}$ is chosen so that it has zero value at the wall which explains the appearance of D. This definition of $\widetilde{\varepsilon}$ has decisive advantages as this condition is numerically stable.

D	Near wall value of ε
$2\nu\left(\frac{k}{y^2}\right)$	$\nu\ (\overline{a_1}^2 + \overline{a_3}^2)$
$\frac{\nu}{y}\frac{\partial k}{\partial y}$	$\nu\ (\overline{a_1}^2 + \overline{a_3}^2)$
$2\nu\left(\frac{\partial \sqrt{k}}{\partial y}\right)^2$	$\nu\ (\overline{a_1}^2 + \overline{a_3}^2)$

Table 2.3 – Near-wall values of D

Model	D	E	Wall boundary condition
JL	$2\nu\left(\frac{d\sqrt{k}}{dy}\right)^2$	$2\nu\nu_t\left(\frac{d^2U}{dy^2}\right)^2$	$k=0;\varepsilon=0$
LS	$2\nu\left(\frac{d\sqrt{k}}{dy}\right)^2$	$2\nu\nu_t\left(\frac{d^2U}{dy^2}\right)^2$	$k=0;\varepsilon=0$
HO	$\frac{\nu}{y}\frac{\partial k}{\partial y}$	0	$k=0;\varepsilon=0$
HP	$2\nu\frac{k}{y^2}$	$-2\nu\left(\frac{\partial\sqrt{\widetilde{\varepsilon}}}{\partial y}\right)^2$	$k=0;\varepsilon=0$
LB	0	0	$\frac{dk}{dy}=0,\varepsilon=\nu\frac{d^2k}{dy^2}$
CH	$2\nu\frac{k}{y^2}$	$(-2\nu\frac{\varepsilon}{y^2})\exp(-0.5y^+)$	$k=0;\varepsilon=0$
LSO	0	$2\nu C_{\varepsilon 2}f_2\frac{\varepsilon}{k}\left(\frac{d\sqrt{k}}{dy}\right)^2+\exp\left[-(\frac{R_T}{64})^2\right][(\frac{7}{9}C_{\varepsilon 2}-2)$ $\frac{\varepsilon}{k}\left(\varepsilon-2\nu\left(\frac{d\sqrt{k}}{dy}\right)^2\right)-\frac{1}{2k}\left(\varepsilon-\frac{2\nu k}{y^2}\right)^2]$	$k=0,\varepsilon=2\nu\left(\frac{d\sqrt{k}}{dy}\right)^2$
SZS	0	$2\nu C_{\varepsilon 2}f_2\frac{\varepsilon}{k}\left(\frac{d\sqrt{k}}{dy}\right)^2+\exp\left[-(\frac{R_T}{64})^2\right]$ $\frac{-2\varepsilon}{k}\left(\varepsilon-2\nu\left(\frac{d\sqrt{k}}{dy}\right)^2\right)+\frac{3}{2k}\left(\varepsilon-\frac{2\nu k}{y^2}\right)^2]$	$k=0,\varepsilon=2\nu\left(\frac{d\sqrt{k}}{dy}\right)^2$
YS	0	$\nu\nu_T\left(\frac{d^2U}{dy^2}\right)^2$	$k=0,\varepsilon=2\nu\left(\frac{d\sqrt{k}}{dy}\right)^2$
FLB	0	0	$k=0,\frac{\partial\varepsilon}{\partial y}=0$
RMM	0	$1.2\nu\nu_t\left(\frac{d^2U}{dy^2}\right)^2$ $+0.0075\nu\frac{k}{\varepsilon}\left(\frac{dk}{dy}\right)\left(\frac{dU}{dy}\right)\left(\frac{d^2U}{dy^2}\right)$	$k=0,\varepsilon=2\nu\left(\frac{d\sqrt{k}}{dy}\right)^2$

Table 2.4 – Summary of D and E terms, and wall boundary conditions for k and ε

The term D should asymptote to the non-zero value of ε at the wall if $\widetilde{\varepsilon}=0$ is specified and also to have the correct balance with the k equation. Using Taylor series expansions in the vicinity of the wall, the fluctuating component of velocity is expressed as follows:

$$\begin{aligned} u' &= a_1 y + b_1 y^2 + ... \\ v' &= b_2 y^2 + ... \\ w' &= a_3 y + b_3 y^2 + ... \end{aligned} \tag{2.60}$$

this leads to

$$k = \frac{1}{2}(\overline{a_1}^2 + \overline{a_3}^2)y^2 + (\overline{a_1 b_1} + \overline{a_3 b_3})y^3 + ... \tag{2.61}$$

The value of ε close to wall writes,

$$\varepsilon = \nu\overline{a_1}^2 + 4\nu(\overline{a_1 b_1} + \overline{a_3 b_3})y + ... \tag{2.62}$$

Near wall values for ε for three different definitions of D are mentioned in Table 2.3. In the fully turbulent regime, $\widetilde{\varepsilon}$ should be equal to ε as the value of D vanishes in this zone. From the Table 2.3, it is observed that all the three different definition of D lead to the correct value of ε at the wall that is ν $(\overline{a_1}^2 + \overline{a_3}^2)$.

Model	f_μ	f_1	f_2
JL	$\exp\left[\frac{-2.5}{(1+R_T/50)}\right]$	1.0	$1.0 - 0.3\exp\left(-{R_T}^2\right)$
LS	$\exp\left[\frac{-3.4}{(1+R_T/50)^2}\right]$	1.0	$1.0 - 0.3\exp\left(-{R_T}^2\right)$
HO	$\exp\left[\frac{-1.75}{(1+R_T/50)}\right]$	1.0	$1.0 - 0.3\exp\left(-{R_T}^2\right)$
HP	$1 - \exp\left(-0.001R_T\right)$	1.0	$1.0 - 0.3\exp\left(-{R_T}^2\right)$
LB	$[1 - \exp\left(-0.0165R_y\right)]^2(1 + \frac{20.5}{R_T})$	$1 + \left(\frac{0.05}{f_\mu}\right)^3$	$1 - \exp\left(-R_T\right)^2$
CH	$1 - \exp\left(-0.0115y^+\right)$	1.0	$1 - 0.22\exp\left[-\left(\frac{R_T}{6}\right)^2\right]$
LSO	$1 - \exp\left(-0.0115y^+\right)$	$1 + [1 - 0.6\exp\left(-\frac{Re}{10^4}\right)]\exp\left[-\left(\frac{R_T}{64}\right)^2\right]$	$1 - 0.22\exp\left[-\left(\frac{R_T}{6}\right)^2\right]$
SZS	$(1 + \frac{3.45}{\sqrt{R_T}})\tanh\left(\frac{y^+}{115}\right)$	1.0	1.0
YS	$(1 + \frac{1}{\sqrt{R_T}})(1 - \exp\left(-1.5\times10^{-4}R_y - 5.0\times10^{-7}{R_y}^3 - 1.0\times10^{-10}{R_y}^5\right))^{0.5}$	$\frac{\sqrt{R_T}}{1+\sqrt{R_T}}$	$\frac{\sqrt{R_T}}{1+\sqrt{R_T}}$
FLB	$0.4\frac{f_w}{\sqrt{R_T}} + (1 - 0.4\frac{f_w}{\sqrt{R_T}}) \times[1 - \exp -\left(\frac{R_y}{42.63}\right)]^3$	1.0	$(1 - 0.22\exp\left[-\left(\frac{R_T}{6}\right)^2\right]){f_w}^2$
RMM	$\frac{{f_\mu}'}{[1-\exp\left(-0.095R_y\right)]}$	1.0	$[1 - 0.22\exp\left(-0.3357\sqrt{R_T}\right)] \times [1 - \exp\left(-0.095R_y\right)] + \exp\left(1.8{R_p}^3\right) - 1$

Table 2.5 – Details of functions f_μ, f_1, f_2

The function f_μ is multiplied to the eddy-viscosity relation and the purpose of this function is to model the influence of the wall on the shear stress. The shear stress near the wall is further reduced by the action of non-viscous effects, although this effect cannot be modeled separately using this kind of damping function and so the f_μ attempts to model both the viscous and pressure strain effects simultaneously. Various proposals for f_μ are listed in Table 2.5. The extra term E is added to represent the effects in the near-wall region of the terms $P_{\varepsilon 1}$, $P_{\varepsilon 2}$ and $P_{\varepsilon 3}$, which are neglected far from the wall. A number of proposals are listed in Table 2.4.

Low-Reynolds Launder-Sharma model [Launder and Sharma, 1974]

The low-Reynolds number Launder-Sharma model is presented in this section which proves to be a robust versions of low-Reynolds number model. The transport equation of turbulent kinetic energy (k) and its dissipation (ε) is expressed as follows:

$$\frac{\partial k}{\partial t} + U_k \frac{\partial k}{\partial x_k} = P_k + \frac{\partial}{\partial x_j}\left[\left(\nu + \frac{\nu_t}{\sigma_k}\right)\frac{\partial k}{\partial x_j}\right] - \left[\widetilde{\varepsilon} + 2\frac{\mu}{\rho}\left(\frac{\partial \sqrt{k}}{\partial x_j}\right)^2\right] \tag{2.63}$$

$$\frac{\partial \widetilde{\varepsilon}}{\partial t} + U_k \frac{\partial \widetilde{\varepsilon}}{\partial x_k} = C_{\varepsilon 1} f_1 \frac{\widetilde{\varepsilon}}{k} P_k + \frac{\partial}{\partial x_j}\left[\left(\nu + \frac{\nu_t}{\sigma_\varepsilon}\right)\frac{\partial \widetilde{\varepsilon}}{\partial x_j}\right] - C_{\varepsilon 2} f_2 \frac{\widetilde{\varepsilon}}{k} + 2\nu\nu_t\left[\left(\frac{\partial^2 U_i}{\partial x_j^2}\right)^2\right] \tag{2.64}$$

The damping functions used in this model are expressed as follows:

$$f_1 = 1.0;\ \ ; f_2 = 1 - 0.3\exp\left(-{Re_t}^2\right);\ \ f_\mu = \exp\left[\frac{-3.4}{\left(1 + \frac{Re_t}{50}\right)^2}\right];\ \ Re_t = \frac{\rho k^2}{\mu \widetilde{\varepsilon}} \tag{2.65}$$

2.1.9 $\overline{v^2}$-f models

Non-homogenous inner region predictions have been performed by using ad hoc damping functions, but the limitations of this damping functions is that they are fitted to experimental or DNS data and so lost its universality. The $k-\varepsilon$ models are based on a single velocity scale, $\sqrt{k}$, although a second important scale is involved in the near-wall region, $\sqrt{\overline{v^2}}$, where $\overline{v^2}$ is the wall-normal component of the Reynolds stress. The correct representation of ν_t near the wall is due to $\overline{v^2}$ scaling [Durbin, 1991]. The inviscid blocking of $\overline{v^2}$ is represented by an elliptic partial differential equation. The rationale of different variants of $\overline{v^2}$-f models is to take into account the kinematic blocking due to solid boundaries. In the next section, the most recent and robust version of $\overline{v^2}$-f model that is BL-$\overline{v^2}/k$ is discussed.

BL-$\overline{v^2}/k$ Billard and Laurence [2012]

In BL-$\overline{v^2}/k$ model, in addition to the transport equation of turbulent kinetic energy (k) and dissipation (ε), two more extra transport equation of wall normal energetic scale

($\overline{v^2}$) and the elliptic equation (f) is solved. The primary objective of BL-$\overline{v^2}/k$ model is to improve the numerical stability of the model by using the variable $\overline{v^2}/k$. The boundary condition is more robust than of $\overline{v^2}$ by replacing the elliptic relaxation of Durbin [1991] with the elliptic blending of Manceau and Hanjalić [2002]. The objective of the BL-$\overline{v^2}/k$ model is to correct the discrepancy observed with previous versions of $\overline{v^2}$-f models, for instance the behaviour of the model to represent buffer layer is enhanced and also near-wall peak of $y^+\frac{dU^+}{dy^+}$ is very well reproduced. Another favourable aspect of this model is weak dependency on Re_τ which allows the improved predictions of $y^+\varepsilon^+$ and $y^+\frac{dU^+}{dy^+}$ in the logarithmic layer. Further the reduction of the $C_{\varepsilon 2}$ coefficient in the defect layer have a great influence in the correct prediction of $\frac{k^+}{y^+\varepsilon^+}$ and hence $\frac{\nu_t{}^+}{y^+}$ is better predicted in the defect layer whereas all the other versions of $\overline{v^2}$-f model over-predict these variables. The equations of this model are:

$$\frac{Dk}{Dt} = P_k - \varepsilon - 2C_{\varepsilon 3}\nu\nu_t(1-\alpha)^3\frac{k}{\varepsilon}\left(\frac{\partial^2 U_i}{\partial x_k \partial x_j}\right)^2 + \frac{\partial}{\partial x_j}\left[\left(\frac{\nu}{2}+\frac{\nu_t}{\sigma_k}\right)\frac{\partial k}{\partial x_j}\right] \tag{2.66}$$

$$\frac{D\varepsilon}{Dt} = \frac{C_{\varepsilon 1}P_k - C_{\varepsilon 2}{}^*\varepsilon}{T} + \frac{\partial}{\partial x_j}\left[\left(\frac{\nu}{2}+\frac{\nu_t}{\sigma_\varepsilon}\right)\frac{\partial \varepsilon}{\partial x_j}\right] \tag{2.67}$$

$$\frac{D\varphi}{Dt} = -(1-\alpha^3)\frac{\varepsilon}{2}\frac{\varphi}{k} + \alpha^3 f_h - P\frac{\varphi}{k} + \frac{2}{k}\frac{\nu_t}{\sigma_k}\frac{\partial k}{\partial x_j}\frac{\partial \varphi}{\partial x_j} + \frac{\partial}{\partial x_j}\left[\left(\frac{\nu}{2}+\frac{\nu_t}{\sigma_\varphi}\right)\frac{\partial \varphi}{\partial x_j}\right] \tag{2.68}$$

$$f_h = -\frac{1}{T}\left(C_1 - 1 + C_2\frac{P}{\varepsilon}\right)\left(\varphi - \frac{2}{3}\right) \tag{2.69}$$

$$\alpha - L^2\Delta\alpha = 1 \tag{2.70}$$

$$k|_{y=0} = 0; \quad \varepsilon|_{y=0} = \lim_{y\to 0}\frac{\nu k}{y^2}; \quad \varphi|_{y=0} = 0; \quad \alpha|_{y=0} = 0 \tag{2.71}$$

$C_{\varepsilon 1}$	$C_{\varepsilon 2}{}^*$	$C_{\varepsilon 2}$	$C_{\varepsilon 3}$	$C_{\varepsilon 4}$	σ_k	σ_ε
1.44	$C_{\varepsilon 2} + \alpha^3(C_{\varepsilon 4} - C_{\varepsilon 2})\tanh\left(\left\lvert\frac{\partial}{\partial x_j}\left(\frac{\nu_t}{\sigma_k}\frac{\partial k}{\partial x_j}\right)/\varepsilon\right\rvert^{3/2}\right)$	1.83	2.3	0.4	1.0	1.5

Table 2.6 – Constants of the BL-v^2/k model

T	C_T	L	C_L	C_η	ν_t	C_μ
$\sqrt{\left(\frac{k}{\varepsilon}\right)^2 + {C_T}^2\left(\frac{\nu}{\varepsilon}\right)}$	4.0	$C_L\sqrt{\frac{k^3}{\varepsilon^2} + {C_\eta}^2\left(\frac{\nu^3}{\varepsilon}\right)}^{1/2}$	0.164	75	$C_\mu\varphi k T$	0.22

Table 2.7 – Related constants, time, length scales and turbulent viscosity

2.1.10 $k-\omega$ model Wilcox [1993]

Another possibility to avoid the use of damping functions was proposed by Wilcox [1993] where the equation for the dissipation (ε) is replaced by an equation for the so-called specific dissipation ($\omega = \varepsilon/k$). The model derived by Wilcox [1993] is integrable down to the solid wall and another reason for its popularity in comparison with $k-\varepsilon$ models is its ability to predict the effect of adverse pressure gradients in boundary layers. The turbulent viscosity is expressed as follows:

$$\nu_t = \frac{k}{\omega} \tag{2.72}$$

The transport equations of k and ω are:

$$\frac{\partial k}{\partial t} + U_k \frac{\partial k}{\partial x_k} = P - \beta' k\omega + \frac{\partial}{\partial x_k}\left[\left(\nu + \frac{\nu_t}{\sigma_k}\right)\frac{\partial k}{\partial x_k}\right] \tag{2.73}$$

$$\frac{\partial \omega}{\partial t} + U_k \frac{\partial \omega}{\partial x_k} = \alpha S^2 - \beta\omega^2 + \frac{\partial}{\partial x_k}\left[\left(\nu + \frac{\nu_t}{\sigma_\omega}\right)\frac{\partial \omega}{\partial x_k}\right] \tag{2.74}$$

Where S is defined as

$$S = \sqrt{2S_{ij}S_{ij}} \tag{2.75}$$

The constants are listed in Table 2.8 respectively.

β'	α	β	σ_k	σ_ω
0.09	5/9	3/40	2.0	2.0

Table 2.8 – Constants of $k-\omega$ model

k-ω-SST model [Menter, 1994]

The main limitation of the $k-\omega$ model of Wilcox [1993] is its sensitivity to the arbitrary values used for k and ω outside of the boundary layer in external aerodynamics. To address this issue, Menter [1994] derived the k-ω-SST model. This is achieved by using a blending function F_1 which is one in the internal region of the boundary layer and logarithmic region and gradually becomes zero in the wake zone. The role of the blending function is to switch to the Wilcox [1993] model near the wall, and to the $k-\varepsilon$ model in the outer wake region. For this purpose, the equations of the $k-\varepsilon$ model are written under the form of a $k-\omega$ model by introducing the change of variable $\omega = \varepsilon/k$. The equations then read:

$$\frac{\partial k}{\partial t} + U_k \frac{\partial k}{\partial x_k} = P_k - \beta^* k\omega + \frac{\partial}{\partial x_k}\left[\left(\nu + \sigma_k \nu_t\right)\frac{\partial k}{\partial x_k}\right] \tag{2.76}$$

$$\frac{\partial \omega}{\partial t} + U_k \frac{\partial \omega}{\partial x_k} = \frac{\gamma}{\nu_t} P - \beta\omega^2 + \frac{\partial}{\partial x_k}\left[\left(\nu + \sigma_\omega \nu_t\right)\frac{\partial \omega}{\partial x_k}\right] + 2(1-F_1)\sigma_{\omega 2}\frac{1}{\omega}\frac{\partial k}{\partial x_k}\frac{\partial \omega}{\partial x_k} \tag{2.77}$$

The last term of Eq. 2.77 is the only term that distinguishes the k-ω model of Wilcox [1993] and the k-ε model written under the form of a k-ω model. Therefore, when the function F_1 goes from one at the wall to zero far from the wall, the system of equations Eq. 2.76 - 2.77 gradually switches from the k-ω model to the k-ε model. The next step will be to modify the eddy-viscosity such that Bradshaw constraint ($\overline{u'v'} < a_1 k$) can be taken into account and turbulent viscosity is expressed as follows:

$$\nu_t = \frac{a_1 k}{max(a_1\omega, SF_2)} \tag{2.78}$$

where S is the strain rate and F_2 is a function that is one for boundary layer flows and zero for free shear layers and it is expressed as follows:

$$F_2 = \tanh\left[{\phi_2}^2\right], \quad \phi_2 = max\left(\frac{2\sqrt{k}}{\beta^*\omega y}, \frac{500\nu}{y^2\omega}\right) \tag{2.79}$$

The dynamic production is:

$$P_k = min(P, 10\beta^* k\omega) \tag{2.80}$$

The constants are defined in Table 2.9, Table 2.10 and Table 2.11

α_1	β_1	σ_{k1}	$\sigma_{\omega 1}$
5/9	3/40	0.85	0.5

Table 2.9 – Constants of k-ω-SST model

α_2	β_2	σ_{k2}	$\sigma_{\omega 2}$
0.44	0.0828	1.0	0.856

Table 2.10 – Constants of k-ω-SST model

β_*	a_1
0.09	0.31

Table 2.11 – Constants of k-ω-SST model

In order for the model to switch from the k-ω to the k-ε model, the constants ϕ of the model are calculated from constants, ϕ_1, ϕ_2 as follows:

$$\phi = \phi_1 F_1 + \phi_2(1 - F_1) \tag{2.81}$$

$$F_1 = \tanh\left(arg_1{}^4\right) \tag{2.82}$$

$$arg_1 = min\left[max\left(\frac{\sqrt{k}}{\beta^*\omega y}, \frac{500\nu}{y^2\omega}\right), \frac{4\sigma_{\omega 2}k}{CD_{k\omega}y^2}\right] \tag{2.83}$$

where y is the distance to the wall and $CD_{k\omega}$ is the positive portion of the cross-diffusion term.
The arg_1 term goes to zero far from the wall. The first argument in Eq. (2.83) is the turbulent length scale divided by y and it is equal to 2.5 in the log layer and becomes zero towards the boundary layer edge. The role of the second argument is to ensure that F_1 is 1.0 in the sublayer and goes to zero in the log region. The third argument is an additional term to make free stream-dependent solution and it also ensure that arg_1 goes to zero near the boundary layer edge.

$$CD_{k\omega} = max\left(2\rho\sigma_{\omega 2}\frac{1}{\omega}\frac{\partial k}{\partial x_i}\frac{\partial \omega}{\partial x_i}, 10^{-20}\right) \tag{2.84}$$

The boundary condition for ω at wall is:

$$\omega = 10\frac{6\nu}{\beta_1(y_1)^2} \quad at \quad y = 0 \tag{2.85}$$

where, y_1 is the distance to the next point away from wall.
The next section of this chapter presents the literature review of various proposals of the buoyancy modifications in the eddy viscosity models.

2.2 Survey of turbulence models for buoyancy-driven flows

This part of the chapter sheds light on the buoyancy sensitized eddy-viscosity models used by several researchers. Buoyancy-driven flows arise in the environment and many industrial applications ranging from nuclear, automotive, solar receivers, indoor air management and in several other applications. Buoyancy forces influences the turbulent mixing and movement of fluid in the enclosure.

2.2.1 Buoyancy sensitized models based on buoyancy production

In flows driven by buoyancy, additional production terms G_k and G_ε appear in the k-equation (Eq. 2.48) and the ε equation (Eq. 2.51), respectively. The effect of buoyancy is to enhance the turbulence level in a unstably stratified flows and to reduce it in a stably stratified flow region. It is usual practice to model buoyancy production terms based on simple gradient diffusion hypothesis (SGDH) Annarumma et al. [1991], Cox and Kumar [1987], Crauford et al. [1985], Fletcher et al. [1994], Markatos et al. [1982], Nam and Bill Jr [1993] which is expressed as follows:

$$\begin{aligned} \overline{u_i'\theta} &= -\frac{\nu_t}{Pr_t}\frac{\partial T}{\partial x_i} \\ G_k &= -\beta g_i \overline{u_i{}'\theta} \end{aligned} \tag{2.86}$$

However, with this simple gradient diffusion hypothesis (SGDH), the effects of buoyancy on turbulence is underestimated [Yan and Holmstedt, 1999]. To overcome this problem, authors [Brescianini and Delichatsios, 2003, Ince and Launder, 1989, Van Maele and Merci, 2006, Worthy et al., 2001, Yan and Holmstedt, 1999] have tried generalized gradient diffusion hypothesis (GGDH) of Daly and Harlow [1970] or algebraic flux model (AFM) of Liu and Wen [2002] to model buoyancy source terms.

$$\begin{aligned} GGDH: \quad & \overline{u_i'\theta} = -C_\theta \frac{k}{\varepsilon} \overline{u_i'u_j'} \frac{\partial T}{\partial x_j} \\ AFM: \quad & \overline{u_i'\theta} = -C_\theta \frac{k}{\varepsilon} \left[\overline{u_i'u_j'} \frac{\partial T}{\partial x_j} + \xi \overline{u_j'\theta} \frac{\partial U_i}{\partial x_j} + \eta \beta g_i \overline{\theta^2} \right] \end{aligned} \tag{2.87}$$

The main difference of Eq. (2.87) with Eq. (2.86) is the inclusion of transverse temperature gradient into the buoyancy source term and this has a strong effect on the predictions, as in weakly stratified flows, the gradient of temperature in the vertical direction is negligible and using the Eq. (2.86) approach will lead to the underestimation of the buoyancy effect on turbulence. In this context, Ince and Launder [1989] have simulated natural convection in infinite cavity, with aspect ratios 5:1 and 30:1 using low-Reynolds number $k-\varepsilon$ model of Jones and Launder [1972]. In this study, buoyancy production terms are modeled using a generalized gradient diffusion hypothesis (GGDH) and the favorable effect of introducing these terms in the transport equation of k and ε is observed. Further, as far as the modeling of G_ε or G_ω is concerned, it is not very established whether it is crucial to include these terms, and different authors consider different formulation for modeling this term. Some authors neglect the effect of this term which is also the default condition in Ansys Fluent. Several authors Bilger [1994], Brescianini and Delichatsios [2003], Cox and Kumar [1987], Crauford et al. [1985], Davidson [1990], Liu and Wen [2002], Shabbir and Taulbee [1990] used the definition mentioned below:

$$G_\varepsilon = C_{\varepsilon 3} \frac{\varepsilon}{k} G_k \tag{2.88}$$

such that the ε-equation reads

$$\frac{\partial \varepsilon}{\partial t} + U_k \frac{\partial \varepsilon}{\partial x_k} = \frac{\partial}{\partial x_k} \left[\left(\nu + \frac{\nu_t}{\sigma_\varepsilon} \frac{\partial \varepsilon}{\partial x_k} \right) \right] + \underbrace{C_{\varepsilon 1} \frac{\varepsilon}{k} P_k + C_{\varepsilon 3} \frac{\varepsilon}{k} G_k - C_{\varepsilon 2} \frac{\varepsilon^2}{k}}_{S_\varepsilon} \tag{2.89}$$

where $C_{\varepsilon 3}$ is considered constant or variable. Based on the Eq. (2.88), a review of the source term in the ε equation used by several researchers is listed in Table. 2.12 where different value of the coefficient $C_{\varepsilon 3}$ is tried by the researchers.

References	$C_{\varepsilon 3}$
$S_\varepsilon = C_{\varepsilon 1}\frac{\varepsilon}{k}P_k + C_{\varepsilon 3}\frac{\varepsilon}{k}G_k - C_{\varepsilon 2}\frac{\varepsilon^2}{k}$	–
Crauford et al. [1985]	$1.4 - 3.4(\frac{k}{\varepsilon}\frac{\partial \overline{u}}{\partial x})^3_c$
Cox and Kumar [1987]	1.44
Shabbir and Taulbee [1990]	1.44
Annarumma et al. [1991]	1.44
Nam and Bill Jr [1993]	1.44
Luo and Beck [1994]	1.44
Bilger [1994]	1.44
Rho and Ryou [1999]	1.44
Murakami et al. [2000]	1.44
Liu and Wen [2002]	0.8
Brescianini and Delichatsios [2003]	1.0

Table 2.12 – Value of Constant for definition of S_ε

Markatos et al. [1982] performed the sensitivity analysis of the coefficient $C_{\varepsilon 3}$ in buoyant smoke flow and found that there were no significant effect of changing the value of this coefficient. Parametric study of the coefficient $C_{\varepsilon 3}$ is also performed by Worthy et al. [2001] in buoyant plume but due to lack of consistent experimental data, optimization of this coefficient was not made. Chung and Devaud [2008] simulated turbulent plume and the modified $k-\varepsilon$ model by introducing buoyancy production terms in the transport equations of turbulent kinetic energy and its dissipation rate. It was observed that the SGDH approach (to model buoyancy source terms) leads to underpredict the influence of buoyancy on turbulence. So in order to overcome this problem, they used the GGDH approach and also performed the sensitivity analysis of coefficient $C_{\varepsilon 3}$. In this study, they observed that the results are sensitive to this coefficient $C_{\varepsilon 3}$ and the best-suited value is 0.23 for GGDH and 0.3 for SGDH.
For mixed flows, Heindel et al. [1994] used another definition of $C_{\varepsilon 3}$ ($C_{\varepsilon 3} = \tanh(\frac{U}{V})$), where U is the local horizontal velocity and V is the local vertical velocity.
Some authors, listed in Table. 2.13, formulate the buoyancy source term as follows:

$$G_\varepsilon = C_{\varepsilon 3}\frac{\varepsilon}{k}max(G_k, 0) \tag{2.90}$$

This buoyancy source term is based on the distinction of stable or unstable stratification in flows. Moreover, this formulation of buoyancy source term is a default option in Ansys Fluent. The expression of S_ε mentioned in Table 2.13 was also tried by some authors Fletcher et al. [1994], Hara and Kato [2004], Novozhilov [2001], Sinai and Owens [1995] and the definition of S_ε is different from other definition (Table. 2.12) in such a way that in a stably stratified flow, buoyancy has a tendency to damp the turbulence and G_k is negative and due to the max in the relation, the influence of buoyancy on the transport equation for ε is 0 in this case. For unstably stratified flows, Eq. (2.90) reduces to Eq.

(2.88).

References	$C_{\varepsilon 3}$
$S_\varepsilon = C_{\varepsilon 1}\frac{\varepsilon}{k}[P_k + C_{\varepsilon 3} max(G_k, 0)] - C_{\varepsilon 2}\rho\frac{\varepsilon^2}{k}$	–
Novozhilov [2001]	1.0
Fletcher et al. [1994]	1.0
Hara and Kato [2004]	1.0
Sinai and Owens [1995]	1.0

Table 2.13 – Value of Constant for definition of S_ε

Markatos et al. [1982] have investigated that the influence of buoyancy on ε equation is very small but removal of buoyancy production terms from k and ε has a appreciable effect on the flow predictions. This prediction was further strengthened by Worthy et al. [2001]. In their study, they observed that the influence of buoyancy on the ε equation is negligible when SGDH approach is used to model buoyancy production term in turbulent kinetic energy equation. Most of the researchers have used the definition of S_ε mentioned in Table. 2.12 for both horizontal and vertical shear layers with the value of $C_{\varepsilon 3} = C_{\varepsilon 1}$. Another definition of buoyancy source term is based on flux Richardson number and this formulation is motivated by the fact that the optimal value of $C_{\varepsilon 3}$ is flow-dependent, so it is interesting to formulate a modification which sensitizes the term to the type of flow. Van Maele and Merci [2006] have sensitized $k-\varepsilon$ and realizable $k-\varepsilon$ models to buoyancy effects by incorporating buoyancy production terms in the turbulent kinetic energy and its dissipation equations, where the buoyancy production terms were modeled using the GGDH approach along with flux Richardson number. Usually the flux Richardson number is defined as the ratio of buoyancy production and shear production,

$$R_f = -\frac{G_k}{P_k} \tag{2.91}$$

Rodi [1984] proposed another definition of flux Richardson number so that the same value of $C_{\varepsilon 3}$ can be used for horizontal and vertical shear layers. The definition of R_f proposed was:

$$R_f = -\frac{G_k}{(P_k + G_k)} \tag{2.92}$$

According to Rodi [1984], $C_{\varepsilon 3} = 0$ for vertical buoyant shear layers and $C_{\varepsilon 3} = 1$ for horizontal shear layers. The authors who considered this definition is listed in Table 2.14. In order to distinguish between the vertical and horizontal buoyant flows, Rodi [1979] proposes to sensitize both the production terms (P and G_k) by a term which is a function of a buoyancy parameter and such a parameter is the modified form of flux Richardson

number as expressed below:

$$R_f = -\frac{1}{2}\frac{G_{\overline{v^2}}}{P_k + G_k} \tag{2.93}$$

where $G_{\overline{v^2}}$ is the buoyancy production of the cross-stream component of $\overline{v^2}$ as can be determined from the Reynolds stress equation. With this definition, the production term in the ε equation becomes:

$$C_{\varepsilon 1}\frac{\varepsilon}{k}(P_k + G_k)(1 + C_{\varepsilon 3}R_f) \tag{2.94}$$

References	$C_{\varepsilon 3}$	R_f
$S_\varepsilon = C_{\varepsilon 1}\frac{\varepsilon}{k}(P_k + G_k)(1 + C_{\varepsilon 3}R_f) - C_{\varepsilon 2}\rho\frac{\varepsilon^2}{k}$	–	–
Worthy et al. [2001]	Different value	$R_f = \frac{-G_k}{P_k+G_k}$
Markatos et al. [1982]	0.9	$R_f = \frac{-G_k}{P_k+G_k}$
Yan and Holmstedt [1999]	0.6	R_f not given
Xue et al. [2001]	0.8	R_f not given

Table 2.14 – Value of Constant for definition of S_ε

In fire simulations, Markatos et al. [1982] observed that the buoyancy production (G_k) term is more important than the coefficient of R_f term, also Bos et al. [1986] and Cox [1995] have concluded that the R_f have little effect in fire simulations. Worthy et al. [2001] did the detailed analysis of introducing the flux Richardson number in the ε equation by considering different modified $k-\varepsilon$ models. It was infered that using GGDH approach to model buoyancy production terms along with R_f term in ε equation yield a significant improvement of results as compared to using SGDH approach to model buoyancy production terms. Liu and Wen [2002] have modified Hanjalic [1994] four equation (k,ε, $\overline{\theta^2}$, ε_θ) model and used the Algebraic flux model to model buoyancy production terms in k and ε equations, which is represented in Eq. 2.95 and Eq. 2.96 respectively.

$$G_k = -\beta g_i \overline{u_i{}'\theta} = \beta g_i C_\theta \frac{k}{\varepsilon}\left[\overline{u_i{}'u_j{}'}\frac{\partial T}{\partial x_j} + \xi\overline{\theta u_j{}'}\frac{\partial U_i}{\partial x_j} + \eta\beta g_i\overline{\theta^2}\right] \tag{2.95}$$

$$G_\varepsilon = -C_{\varepsilon 3}\frac{\varepsilon}{k}\beta g_i \overline{u_i{}'\theta} = C_{\varepsilon 3}\frac{\varepsilon}{k}\beta g_i C_\theta \frac{k}{\varepsilon}\left[\overline{u_i{}'u_j{}'}\frac{\partial T}{\partial x_j} + \xi\overline{\theta u_j{}'}\frac{\partial U_i}{\partial x_j} + \eta\beta g_i\overline{\theta^2}\right] \tag{2.96}$$

C_θ	ξ	η	C_ε
0.28	0.6	0.6	0.8

Table 2.15 – Coefficients and constants in modified Hanjalic model

It has been observed that it is important to include all the three terms of the Algebraic flux model in simulating diffusion flames. Kumar and Dewan [2013] have studied the thermal buoyant plume in self-similar region by modifying three turbulence models, namely standard k-ε, the RNG k-ε and the k-ω respectively. It has been observed in their studies that using the SGDH approach to model buoyancy source terms leads to incorrect predictions of spreading rates, mean flow properties and turbulence quantities. In order to overcome this problem, they have considered the GGDH approach to account for the cross-stream density variation in turbulence models. For the ε equation, they have used the proposal of Rodi [1984] by incorporating flux Richardson number and the expression for source term S_ε mentioned in Table. 2.14 with the coefficient $C_{\varepsilon 3} = 0.8$ is used. It has been concluded that RNG k-ε model along with GGDH approach to model buoyancy source terms lead to capture the mean and turbulent flow properties quite effectively.

2.2.2 Effects of turbulent Prandtl number

The primary objective of this section is to examine critically the effect of turbulent Prandtl number based on the available literature. The origin of turbulent Prandtl number concept dates back from early twentieth century when Taylor [1915] proposed the concept of eddy-diffusivity for describing heat transfer by turbulent wind field in analogy of thermal diffusivity. From the atmospheric modeling point of view, a correct parametrization of the turbulent Prandtl number leads to better predictions of weather and climate related to heat transfer as well as it will have an impact on the estimation of air quality, ecosystem and agricultural management. The limitation of higher level of turbulence models to be utilised is constrained by the modeling of several terms and calibration of many constants. This favored the use of eddy-diffusivity models for momentum along with the eddy-diffusivity for heat transfer using the turbulent Prandtl number which represents the dissimilarity between turbulent transport of momentum and heat. The eddy-diffusivity concept introduces the following definitions:

$$\begin{aligned} \overline{u'v'} &= -\nu_t \left(\frac{\partial U}{\partial y} \right) \\ \overline{v'\theta} &= -\alpha_t \left(\frac{\partial T}{\partial y} \right) \end{aligned} \tag{2.97}$$

where ν_t and α_t are effective diffusivity for momentum and heat respectively.
The turbulent Prandtl number is defined as follows:

$$Pr_t = -\frac{\overline{u'v'}\frac{\partial T}{\partial y}}{-\overline{v'\theta}\frac{\partial U}{\partial y}} \tag{2.98}$$

One of the accepted concept for most boundary layer to model turbulent Prandtl number is Reynolds analogy which states that the transport of heat is taking in the same way as

the transport of momentum and $Pr_t \simeq 1.0$. Garcia-Villalba and Del Alamo [2011] have performed direct numerical simulation (DNS) of channel flow in a stable stratification condition with different levels of stratification achieved by changing the Richardson number. It has been reported that corresponding to the cases with the highest stratification, the turbulent Prandtl number is ill-defined in the center of channel as α_t is undefined. Moreover, it has also been reported that the turbulent Prandtl does not vary substantially with the gradient Richardson number which is defined as:

$$Ri_g = -\frac{g\partial/\partial y(\rho)}{\rho_0(\partial/\partial y(u))^2} \tag{2.99}$$

In the range, $Ri_g \leq 0.2$, $Pr \approx 1$ is a reasonable choice for turbulence models for smaller values of Ri_g.

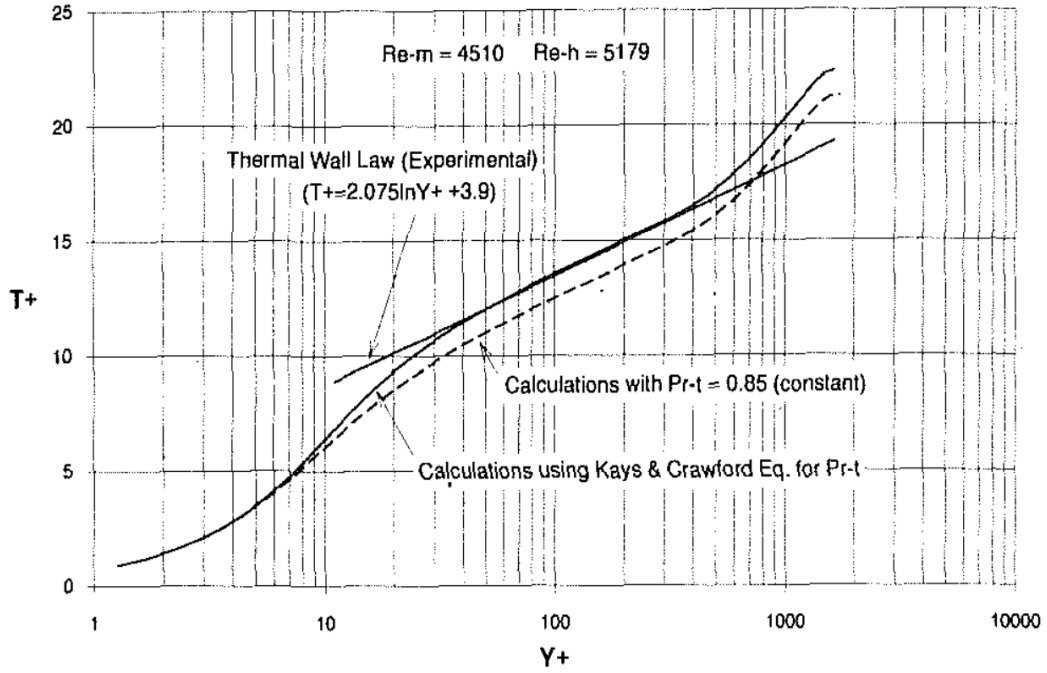

Figure 2.1 – Effect of Pr_t on air temperature distribution [Plots are taken from Kays [1994]]

Kays [1994] has analyzed the effect of turbulent Prandtl number (Pr_t) for air based on the evaluation of temperature profiles in log layer of isothermal flows. In his study, it has been observed that the value of $Pr_t = 0.85$, seems to underpredict the mean temperature profile in log layer as compared to the wall law of temperature which is expressed as follows:

$$T^+ = 2.075 \ln y^+ + 3.9 \tag{2.100}$$

So it has been inferred that the value of the turbulent Prandtl number should be variable with the wall distance and in this context Kays and Crawford [1993] have proposed the

relation to calculate Pr_t which is expressed as follows:

$$Pr_t = \frac{1}{\left[0.5882 + 0.228(\nu_t/\nu) - 0.0441(\nu_t/\nu)^2\left[1 - \exp\left(\frac{-5.165}{(\nu_t/\nu)}\right)\right]\right]} \tag{2.101}$$

This relation lead to a better prediction of the mean temperature in the log region as can be seen in Fig. 2.1. Using the relation of Heskestad [1984], Nam and Bill Jr [1993] tuned the model for buoyant plume by varying the coefficients (C_μ) and turbulent Prandtl number (Pr_t) as these coefficients affect the prediction of mean velocity and temperature.

2.2.3 Thermal to mechanical time scale ratio (R)

In order to close the system of equations involving the momentum, energy and turbulence equations, particularly the temperature variance equation ($\overline{\theta^2}$), the dissipation of the temperature variance (ε_θ) needs to be specified. A consistent approach would be to solve the transport equation of ε_θ, but it requires further modeling of other terms [Hanjalić et al., 1996, Kenjereš and Hanjalić, 2000, Kenjeres, 1998, Peeters and Henkes, 1992]. However, modeling of the ε_θ equation brings in much uncertainty as it involves twice as many free parameters as compared to the dissipation rate of turbulence (ε). Furthermore, determining new coefficients requires more information that is impossible to measure even for simple generic flows and only provided by a very limited number of DNS studies. This fact motivated researchers [Craft, 1991, Dol et al., 1999] to evaluate (ε_θ) from thermal to mechanical time scale ratio as expressed below:

$$R = \frac{\tau_\theta}{\tau_m}, \tag{2.102}$$

where $\tau_\theta = \frac{\overline{\theta^2}}{2\varepsilon_\theta}$ is thermal time scale and $\tau_m = \frac{k}{\varepsilon}$ is mechanical time scale respectively. The assumption of the constant time scale ratio works considerably well in number of flows [Dol et al., 1997, Hanjalić et al., 1996, Kenjereš and Hanjalić, 2000, Kenjeres, 1998]. However an analysis of DNS data shows that the time-scale ratio is not constant everywhere but varies significantly particularly close to wall. This parameter also depend on the flow configurations as well as on Ra and Pr numbers [Dol et al., 1999, Kenjeres, 1998, Versteegh and Nieuwstadt, 1998, Wörner, 1994]. A relation for determining R was proposed by Craft [1991] which is based on local turbulent flux anisotropy as expressed as follows:

$$R = \frac{1}{1.5(1 + A_{2\theta})}, \tag{2.103}$$

where $A_{2\theta} = \frac{\overline{u_i{}'\theta}^2}{\overline{\theta^2}k}$ is the scalar flux invariant. This expression is tested in forced convection in a heated plane and axisymmetric jets. Another proposal was made by Dol et al. [1999] for buoyancy-driven side heated infinitely long channel for a relatively low Rayleigh

number, Ra ($10^5 \leq Ra \leq 5 \times 10^6$) as expressed follows:

$$R = min(2.2{Ra_t}^{-0.13}, 0.75), \tag{2.104}$$

Where $Ra_t = \beta g\sqrt{\overline{\theta^2}k^9}Pr/\nu^2\varepsilon$ is the turbulent Rayleigh number. Kenjereš et al. [2005] proposed a new model which takes into account of flux anisotropy and stress anisotropy and it is expressed as follows:

$$R = max\left(\frac{{A_2}^{1/2}}{1 + A_{2\theta}}, 0.6A\right), \tag{2.105}$$

Where $A_2 = a_{ij}a_{ji}$, $A_3 = a_{ij}a_{jk}a_{ki}$ and $A = 1 - 9/8(A_2 - A_3)$ with $a_{ij} = \overline{u_i{}'u_j{}'}/k - 2/3\delta_{ij}$. In the side heated turbulent natural convection flow, R is almost constant far from the wall region with a strong peak close to the wall. In view of this behaviour, Dehoux et al. [2012] proposed a relation to model the thermal to mechanical time scale ratio, R, which involves the elliptic blending approach:

$$R = {\alpha_\theta}^3 R^h + (1 - {\alpha_\theta}^3)Pr \tag{2.106}$$

where α_θ is the elliptic factor which goes from zero at the wall to unity far from the wall. The value of $R^h = 0.5$ is constant in regions far from the wall.

2.2.4 Buoyancy-extended Reynolds stress and heat flux models

Approximated transport equations proposed by researchers like Donaldson et al. [1972], Lumley [1972] and Dehoux et al. [2017] require a formidable task to solve 17 equations for velocity, pressure, Reynolds stress components, temperature, turbulent heat fluxes, dissipation of turbulent kinetic energy, temperature variance and dissipation of temperature variance respectively. The presence of a rigid surface significantly changes the character of pressure fluctuations in its vicinity which affect the level of stress and heat flux [Bradshaw, 1973, Launder et al., 1975]. Turbulent pressure fluctuations have been affected by the gravitational forces and their influence needs to be included in any second-moment closure. However, these models are too expensive for most practical applications. Motivated by this fact, authors like Launder [1975] have provided a intermediate model by formulating algebraic models for turbulent stresses and turbulent heat fluxes which is connected with the local value of k and ε with the mean velocity and temperature fields. The origin of these algebraic models is mainly based on two hypotheses which are weak equilibrium hypothesis and strong equilibrium hypothesis. According to weak equilibrium hypothesis, the anisotropy tensor is conserved along the streamlines and the diffusion of anisotropy is negligible [Gatski and Speziale, 1993], such that

$$\frac{db_{ij}}{dt} = 0; \quad \frac{D_{ij}}{D_{kk}} = \frac{\overline{u_i'u_j'}}{\overline{u_k'u_k'}} \tag{2.107}$$

where $b_{ij} = \overline{u_i' u_j'}/(2k) - \delta_{ij}/3$ and D_{ij} are the anisotropy tensor and total diffusion of $\overline{u_i' u_j'}$ respectively. Using the chain rule, we get

$$\left(2k\frac{db_{ij}}{dt} = 0 = \frac{d\overline{u_i' u_j'}}{dt} - \frac{\overline{u_i' u_j'}}{k}\frac{dk}{dt}\right) \tag{2.108}$$

such that

$$P_{ij} + G_{ij} + \phi_{ij} - \varepsilon_{ij} = \frac{\overline{u_i' u_j'}}{k}(P_k + G_k - \varepsilon) \tag{2.109}$$

where diffusion terms have canceled out due to Eq. 2.107 and P_{ij}, G_{ij}, ϕ_{ij} and ε_{ij} are production, buoyant production, redistribution and dissipation tensor of the Reynolds stress transport equation respectively.
Using the modeling approach for pressure-strain correlations (slow,rapid and buoyancy terms), for dissipation tensor and for turbulent diffusion as described in equations (2.24), (2.25), (2.26), (2.27) and (2.28) respectively. Eq. 2.109 becomes:

$$\overline{u_i' u_j'} = \frac{2}{3}k\delta_{ij} + \frac{k}{\varepsilon}\left[\frac{1 - C_2}{C_1 + \frac{(P+G)}{\varepsilon} - 1}\left(P_{ij} - \frac{2}{3}P\delta_{ij}\right) + \frac{1 - C_3}{C_1 + \frac{(P+G)}{\varepsilon} - 1}\left(G_{ij} - \frac{2}{3}G\delta_{ij}\right)\right] \tag{2.110}$$

This algebraic relation can be simplified further using the strong equilibrium hypothesis, $P + G = \varepsilon$. Eq. (2.110) becomes

$$\overline{u_i' u_j'} = \frac{2}{3}k\delta_{ij} + \frac{k}{\varepsilon}\left[\frac{1 - C_2}{C_1}\left(P_{ij} - \frac{2}{3}P\delta_{ij}\right) + \frac{1 - C_3}{C_1}\left(G_{ij} - \frac{2}{3}G\delta_{ij}\right)\right] \tag{2.111}$$

In the absence of buoyancy effects ($G_{ij} = 0$), these simplified relations show that the main source of turbulence anisotropy is the deviatoric part of production ($P_{ij} - 2/3P_k\delta_{ij}$). When buoyancy is active, the deviatoric part of buoyancy production ($G_{ij} - 1/3G_{kk}\delta_{ij}$) is also a source of anisotropy, and this effect must be accounted for in turbulence models.

C_1	C_2	C_3
1.8	0.6	0.6

Table 2.16 – Value of Constant for algebraic Reynolds stress model

The values of the coefficients are listed in Table. 2.16 respectively. These two formulation for Reynolds stress have been tested by Hossain [1980] in simulating vertical buoyant jets and observed that more refined model Eq. (2.110) deteriorated the results as compared to simple formulation mentioned in Eq. (2.111). Also Shabbir and Taulbee [1990] have tried both the simple and refined algebraic Reynolds stress models in buoyant plumes and vertical buoyant jets and found good agreement with experimental results.
Similarly to the case of the Reynolds stress, weak equilibrium hypothesis assumes that the

nondimensional heat flux vector is conserved which yields following relation:

$$\begin{aligned} \frac{D\left(\frac{\overline{\theta u_i'}}{\sqrt{\overline{\theta^2}k}}\right)}{Dt} &= 0 \\ \frac{D\overline{\theta u_i'}}{Dt} &= \frac{1}{2}\left(\frac{1}{k}\frac{Dk}{Dt} + \frac{1}{\overline{\theta^2}}\frac{D\overline{\theta^2}}{Dt}\right)\overline{\theta u_i'} \end{aligned} \tag{2.112}$$

and diffusion

$$D_{\theta i} = \frac{1}{2}\left(\frac{1}{k}D_k + \frac{1}{\overline{\theta^2}}D_{\overline{\theta^2}}\right)\overline{\theta u_i'} \tag{2.113}$$

where $D_{\theta i}$, D_k and $D_{\overline{\theta^2}}$ represents the total diffusion of $\overline{\theta u_i'}$, k and $\overline{\theta^2}$, respectively. The turbulent heat flux algebraic equation becomes:

$$P_{\theta i}^{th} + P_{\theta i}^{m} + G_{\theta i} + \phi_{\theta i} - \varepsilon_{\theta i} = \frac{\overline{u_i'\theta}}{2}\left(\frac{P_k + G_k - \varepsilon}{k} + \frac{P_{\overline{\theta^2}} - \varepsilon_{\overline{\theta^2}}}{\overline{\theta^2}}\right) \tag{2.114}$$

If the production and the dissipation terms of k and $\overline{\theta^2}$ are assumed to be locally in balance, i.e., considering strong equilibrium assumption which writes:

$$\begin{aligned} P_k + G_k &= \varepsilon \\ P_{\overline{\theta^2}} &= \varepsilon_{\overline{\theta^2}} \end{aligned} \tag{2.115}$$

where $P_{\overline{\theta^2}}$ and $\varepsilon_{\overline{\theta^2}}$ are the production and dissipation terms in the thermal variance transport equation. Using the strong equilibrium hypothesis (Eq. 2.115), Eq. 2.114 reduces to

$$P_{\theta i}^{th} + P_{\theta i}^{m} + G_{\theta i} + \phi_{\theta i} - \varepsilon_{\theta i} = 0 \tag{2.116}$$

Introducing the model (Eq. 2.31, Eq. 2.32 , Eq. 2.33 and Eq. 2.34) for scrambling term ($\phi_{\theta i}$) and considering that the small scales are isotropic such that dissipation ($\varepsilon_{\theta i}$) is zero. Eq. 2.116 thus reduces to linear algebraic flux model that reads,

$$\overline{\theta u_i'} = -\frac{1}{C_{\theta 1}}\tau\left((1 - C_{\theta 2}')\overline{u_i'u_j'}\frac{\partial T}{\partial x_j} + (1 - C_{\theta 2})\overline{\theta u_j'}\frac{\partial U_i}{\partial x_j} + (1 - C_{\theta 3})\beta g_i\overline{\theta^2}\right) \tag{2.117}$$

In the context of buoyancy-extended models, Davidson [1990] proposed buoyancy sensitized $k-\varepsilon$ model. In his work, he computed two-dimensional cavity of aspect ratio 5 : 1 in which horizontal walls were adiabatic and the vertical walls are isothermal. Low-Reynolds number $k-\varepsilon$ model similar to the model of Jones and Launder [1972] and Lam and Bremhorst [1981] was used. He formulated the algebraic Reynolds stress model which can take into account of anisotropy of turbulence due to buoyancy. In Eq. 2.110 in forced convection, $G_{ij} = 0$ and the third term of the right-hand side is zero. In the framework of eddy-viscosity models, the Boussinesq relation assumes that the second term can be mod-

eled as $-2\nu_t S_{ij}$ and the idea of Davidson [1990] thus consists in sensitizing the Boussinesq relation to buoyancy as

$$\begin{aligned}\overline{u_i' u_j'} &= (\overline{u_i' u_j'})_{Boussinesq} + (\overline{u_i' u_j'})_{Buoyancy-extension} \\ (\overline{u_i' u_j'})_{Boussinesq} &= -2\nu_t S_{ij} + 2/3 k\delta_{ij} \\ (\overline{u_i' u_j'})_{Buoyancy-extension} &= \frac{k}{\varepsilon}\frac{(1-c_3)(G_{ij} - \frac{2}{3}\delta_{ij}G)}{c_1 + (P+G)/\varepsilon - 1}\end{aligned} \tag{2.118}$$

where $G_{ij} = -\beta(g_i\overline{u_j'\theta} + (g_j\overline{u_i'\theta})$ and $G = \frac{1}{2}G_{kk}$, The constants used are: $c_1 = 1.8$ and $c_3 = 0.6$. Further, he used generalized gradient diffusion hypothesis (GGDH) to model the heat flux which is used in the temperature equation. Although the simple gradient diffusion hypothesis (SGDH) is used to model the heat fluxes in buoyancy extension part of Reynolds stress and also to model the buoyancy production terms. He concluded that the buoyancy-extended model is able to take into account the anisotropy of turbulence in such a way that there is a reduction of vertical turbulent velocity fluctuations and an increase of horizontal velocity fluctuation in stably stratified flows. Also the turbulent shear stress is increased significantly by the inclusion of buoyancy extension which is substantially underpredicted by the original $k-\varepsilon$ model. Moreover, the prediction of normal Reynolds stresses is significantly modified by the inclusion of the buoyancy extension.
Murakami et al. [1996] proposed buoyancy sensitized $k-\varepsilon$ model by computing thermally-stratified flow fields. One of the aspects of stably stratified flow is that there is a suppression of turbulence in the vertical direction. The role of buoyancy is crucial as it damps the turbulence and this affects the characteristics of the flow. In order to correct the limitations of the $k-\varepsilon$ model to predict these type of flows, an attempt was made by Murakami et al. [1996] to formulate the model functions f_{BV} and $f_{B\theta}$ which can reflect the buoyancy damping effect in the Reynolds stress and heat flux equations which is expressed as follows:

$$\begin{aligned}-\overline{u_i' u_j'} &= C_\mu f_\mu f_{BV}\frac{k^2}{\varepsilon}\left(\frac{\partial U_i}{\partial x_j} + \frac{\partial U_j}{\partial x_i}\right) - \frac{2}{3}k\delta_{ij} \\ -\overline{u_i'\theta} &= \frac{1}{Pr_t}C_\mu f_\mu f_{B\theta}\frac{k^2}{\varepsilon}\frac{\partial T}{\partial x_i}\end{aligned} \tag{2.119}$$

where the subscript B, V and θ in model functions f_{BV} and $f_{B\theta}$ stands for buoyancy, velocity and temperature, respectively. The model function are expressed as follows:

$$\begin{aligned}f_{BV} &= C_{BV1} - C_{BV2}\frac{P_k}{\varepsilon} + C_{BV3}\frac{G_k}{\varepsilon} \\ f_{B\theta} &= C_{B\theta 1} - C_{B\theta 2}\frac{P_k}{\varepsilon} + C_{B\theta 3}\frac{G_k}{\varepsilon}\end{aligned} \tag{2.120}$$

Where the value of the coefficients are: $C_{BV1} = 1.36$, $C_{BV2} = 0.36$, $C_{BV3} = 0.72$, $C_{B\theta 1} = 1.37$, $C_{B\theta 2} = 0.37$ and $C_{B\theta 3} = 1.6$. The role of the model function f_{BV} is to damp the active turbulent shear stress component and $f_{B\theta}$ damps the active turbulent heat flux

component. Also they proposed a new damping function (f_μ) based on the model of Abe et al. [1993] and they have concluded that the inclusion of these damping functions leads to the better prediction of the results as compared to k-ε model.
Liu and Wen [1999] proposed a buoyancy-modified turbulence model which is based on the four equation k-ε-$\overline{\theta^2}$-ε_θ model of Hanjalić et al. [1996]. They computed natural convection flow in a two-dimensional enclosure in tall rectangular cavity and square cavity at higher Rayleigh numbers. Three turbulence models namely, the model of Ince and Launder [1989], three equation and four equation models of Hanjalić et al. [1996] are compared with the proposed model [Liu and Wen, 1999]. The origin of their model comes from the fact that buoyancy induces anisotropy in Reynolds stresses which influences the vertical boundary layer and they have used return-to-isotropy concept in the pressure-strain correlation. For the Hanjalic model, the reader is requested to refer to [Hanjalić et al., 1996]. However the major modifications are presented here. In Liu and Wen [1999] work, buoyancy extension is added to the Boussinesq relation and expressed as follows:

$$\overline{u_i' u_j'} = \frac{2}{3}k\delta_{ij} - \nu_t\left(\frac{\partial U_i}{\partial x_j} + \frac{\partial U_i}{\partial x_j}\right) + \frac{k}{\varepsilon}\frac{(1-c_3 f_\mu)}{(c_1 f_\mu + f_s)}\left(G_{ij} - \frac{2}{3}\delta_{ij}G\right) + \frac{k}{\varepsilon}\frac{1}{(c_1 f_\mu + f_s)}\phi_{ijw} \quad (2.121)$$

Where $f_\mu = \exp\left(-3.4/(1+Re_t/50)\right)^2$ and $f_s = (1+0.1Re_t)^{-1}$.
Using the Eq. 2.31, Eq. 2.32 and Eq. 2.34 for slow, rapid and buoyancy term of pressure srambling and neglecting $\varepsilon_{\theta i}$ as small eddies are isotropic, Eq. 2.114 become:

$$\overline{\theta u_i'} = \frac{\overline{u_i' u_k'}\frac{\partial T}{\partial x_k} + \xi\overline{\theta u_k'}\frac{\partial U_i}{\partial x_k} + \eta\beta g_i\overline{\theta^2}}{-C_{\theta 1}\frac{\varepsilon}{k} + \frac{1}{\overline{\theta^2}}\left(\overline{\theta u_k'}\frac{\partial T}{\partial x_k} + \varepsilon_\theta\right) + \frac{1}{2k}\left(\overline{u_i' u_k'}\frac{\partial U_i}{\partial x_k} + \beta g_i\overline{\theta u_i'} + \varepsilon\right)} \quad (2.122)$$

Simplified form of turbulent heat flux equation can be formulated by assuming strong equilibrium for dynamic ($P_k + G_k = \varepsilon$) and thermal ($P_{th} = \varepsilon_{th}$) turbulence. The simplified form of turbulent heat flux is expressed as follows:

$$\overline{\theta u_i'} = -\frac{1}{C_{\theta 1}}\frac{k}{\varepsilon}\left[\overline{u_i' u_k'}\frac{\partial T}{\partial x_k} + \xi\overline{\theta u_k'}\frac{\partial U_i}{\partial x_k} + \eta\beta g_i\overline{\theta^2}\right] \quad (2.123)$$

where $\xi = (1 - C_{\theta 2})$ and $\eta = (1 - C_{\theta 3})$ as per Hanjalić [2002].

C_s	$C_{\theta 1}$	$C_{\theta 2}$	$C_{\theta 3}$
0.22	3.0	0.5	0.5

Table 2.17 – Value of constants for heat flux model

In the work of Liu and Wen [1999], the algebraic form of the turbulent heat flux is

derived from the full transport equation and expressed as follows:

$$\overline{u_i'\theta} = -C\frac{k}{\varepsilon}\left(\overline{u_i'u_i}\frac{\partial T}{\partial x_j} + \xi\overline{u_j'\theta}\frac{\partial U_j}{\partial x_j} + \eta\beta g_i\overline{\theta^2} + \phi_{i\theta w}\right) \tag{2.124}$$

where, $\phi_{i\theta w}$ is the wall-reflection term [Gibson and Launder, 1978] and can be expressed as follows:

$$\phi_{i\theta w} = -c_{1\theta w}\frac{\varepsilon}{k}\overline{u_k{}'\theta}n_k n_i\frac{k^{3/2}}{c_1\varepsilon x_n}$$

where, x_n is the distance from the wall and n_i is the unit vector normal to wall. The different values of constants used in the model are listed in Table. 2.18.

C	ξ	η	$C_{1\theta w}$	c_1
0.28	0.6	0.6	0.25	1.8

Table 2.18 – Specification of coefficients and constants

These modifications lead to better prediction of velocity fluctuations for the near wall region. It has been concluded that the predictions of the Reynolds shear stress and the turbulent kinetic energy were well predicted as compared to the experimental data [Tian, 1997, Tian et al., 1998]. However, the predictions in tall cavity, particularly Reynolds shear stresses, by all the considered models were not in agreement with experimental data.
In the context of elliptic relation, Kenjereš et al. [2005] have proposed a buoyancy-extended five equation ($k-\varepsilon-\overline{v^2}-f-\overline{\theta^2}$) model for computing 2D and 3D natural and mixed convection flows in turbulent regime. The motivation comes from the fact that the low-Reynolds number models lacks physical justification and the damping functions used in these models have a non-linear behaviour which requires a strong clustering of grid near the wall, and it is believed that this low-Reynolds number model approach fails in complex flows. So in order to avoid this limitation, Durbin [Durbin, 1991] proposed the elliptic relaxation approach to model non-viscous wall effects in eddy-viscosity models ($\overline{v^2}-f$) or in full Reynolds stress ($\overline{u_i{}'u_j{}'}$ - f_{ij}) model, so that there will be compromise between correct wall treatment and computational robustness. In the Durbin [1991] model, it was proposed to solve a separate equation for the wall-normal Reynolds stress ($\overline{v^2}$) which is reduced significantly close to the wall as compared to k. Kenjeres [Kenjereš et al., 2005] used the same extension as Davidson [1990] which writes:

$$\overline{u_i'u_j'} = \frac{2}{3}k\delta_{ij} - C_\mu\tau\overline{v^2}\left(\frac{\partial U_i}{\partial x_j}+\frac{\partial U_j}{\partial x_i}\right) + C_\theta\tau\beta\left(g_i\overline{u_j'\theta}+g_j\overline{u_i'\theta}-\frac{2}{3}g_k\overline{u_k'\theta}\delta_{ij}\right) \tag{2.125}$$

The model is associated with a nonlinear algebraic heat flux model as expressed below:

$$\overline{u_i'\theta} = -C_\theta\tau\left(\zeta\overline{u_i'u_j}\frac{\partial T}{\partial x_j} + \xi\overline{u_j'\theta}\frac{\partial U_i}{\partial x_j} + \eta\beta g_i\overline{\theta^2}\right) + C_{\theta 1}{}'a_{ij}\overline{u_j'\theta} \tag{2.126}$$

where the model coefficients ζ, ξ and η corresponds to $(1 - C_{\theta 2}{}')$, $(1 - C_{\theta 2})$ and $(1 - C_{\theta 3})$ respectively and $a_{ij} = \frac{\overline{u_i' u_j'}}{k} - \frac{2}{3}\delta_{ij}$ is the stress anisotropy.

$$\nu_t = C_\mu \tau \overline{v^2}; \;\; \tau = max\left[\frac{k}{\varepsilon}, C_T \frac{\nu}{\varepsilon}^{1/2}\right] \tag{2.127}$$

The value of the coefficients are listed in Table. 2.19.

ξ	η	ζ	$C_{\theta 1}{}'$	C_μ
0.6	0.6	0.6	1.5	0.22

Table 2.19 – Model coefficients

Also in this work, a relation for thermal to mechanical time scale ratio expression was proposed which takes into account of stress anisotropy and heat flux anisotropy through its invariants:

$$R = max\left(\frac{A_2{}^{1/2}}{1 + A_{2\theta}}, 0.6A\right) \tag{2.128}$$

Where $A_2 = a_{ij}a_{ji}$, $A_3 = a_{ij}a_{jk}a_{ki}$ and $A = 1 - 9/8(A_2 - A_3)$, with $a_{ij} = \frac{\overline{u_i{}' u_j{}'}}{k} - 2/3\delta_{ij}$. It was observed that the proposed buoyancy-extended $\overline{v^2} - f$ model is able to better predict natural and mixed convection regimes in the differentially heated vertical channel configuration as compared to the two-equation $k - \varepsilon$ type models and this modified model is found to be numerically robust and requires less grid clustering close to the wall.
This Chapter provides meaningful insight into the RANS models and since our goal is to sensitize the eddy-viscosity models to buoyancy effects, attention is given to the models which are commonly used in the industrial computations. Further, in the pursuit of the various buoyancy modifications in these models, a detailed literature survey is conducted. This survey provides several methodologies to develop a range of buoyancy sensitized models and the conclusions of this analysis are used in the next chapters, where new developments are proposed.
The next chapter is dedicated to the selection of the test cases in three different regimes and in addition to that, the performance of the selected turbulence models in these regimes are examined.

Chapter 3

Influence of buoyancy on turbulent channel flows

Contents

3.1 Introduction

In this chapter, an evaluation of the capacity of three different eddy-viscosity based turbulence models is performed by simulating different regimes of thermal convective flows. The first regime corresponds to the forced convection flow with different friction Reynolds number and the heat flux is imposed on the walls. The second case is Kasagi and Nishimura [1997]'s mixed convection flow which corresponds to $Re_\tau = 150$ and $\mathrm{Gr} = 9.6 \times 10^5$. The third one is of natural convection corresponding to the DNS data of Versteegh and Nieuwstadt [1998] at $\mathrm{Ra} = 5.0 \times 10^6$ and Kiš and Herwig [2014] with $\mathrm{Ra} = 1.7 \times 10^7$ respectively. The order of magnitude of Rayleigh number found in the experiments at PSA groupe are close to the one selected for assessing and developing the buoyancy sensitised models. The Boussinesq hypothesis is considered for the variation of density in the gravity term of the Reynolds averaged equations.
In addition to that, the effect of introducing the Yap term [Yap, 1987] in the low-Reynolds number Launder-Sharma model is analyzed.

3.2 Description of the test cases

3.2.1 Forced convection regime

Numerical simulations of the fully developed turbulent flow in a channel at four different Reynolds numbers ($Re_\tau = 180, 395, 640, 1020$) is performed and results are compared with DNS data [Abe et al., 2004]. The flow takes place between two plates which are separated by a distance of 2δ. The heat flux q_w is imposed on the two walls as shown in Fig. 3.1 and periodic boundary conditions are applied in the streamwise (x) and spanwise (z) directions. The Reynolds number (Re_τ) is based on the channel half-width (δ) and the friction velocity (u_τ) and air is considered as the fluid which corresponds to the molecular Prandtl number $Pr = 0.71$. The flow and coordinates are normalized by the friction velocity u_τ, channel half-width δ, density ρ and friction temperature $T_\tau = \frac{q_w}{\rho C_p u_\tau}$.

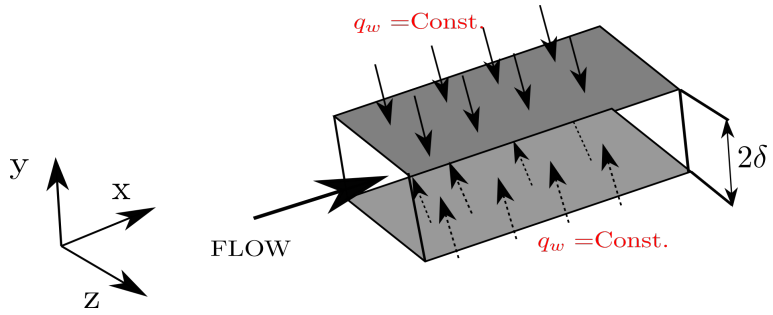

Figure 3.1 – Channel flow configuration for the forced convection regime

To maintain periodicity in pressure, the mean pressure gradient is subtracted and the

modified pressure becomes:

$$P^* = P - \frac{dP}{dx}x; \qquad \frac{\partial P}{\partial x} = -\frac{\tau_w}{\delta} \tag{3.1}$$

Where τ_w is the wall shear stress and δ is the channel half-width.
Defining $\beta^* = \frac{\tau_w}{\delta}$, Eq. 3.1 becomes

$$P = P^* - \beta^* x \tag{3.2}$$

By introducing the decomposition of pressure, the momentum equation becomes:

$$0 = -\frac{\partial P^*}{\partial x} + \beta^* + \nu\frac{\partial^2 U}{\partial y^2} - \frac{\partial \overline{u'v'}}{\partial y} \tag{3.3}$$

Using the system of units defined as follows:

$$M = \rho\delta^3; \qquad L = \delta; \qquad T = \frac{\delta}{u_\tau} \tag{3.4}$$

the non-dimensionalized form of Eq. 3.3 becomes:

$$0 = -\frac{\partial \widetilde{P}^*}{\partial \widetilde{x}} + \widetilde{\beta^*} + \frac{1}{Re_\tau}\frac{\partial^2 \widetilde{U}}{\partial \widetilde{y^2}} - \frac{\partial \widetilde{\overline{u'v'}}}{\partial \widetilde{y}} \tag{3.5}$$

When the heat flux (q_w) is imposed on the walls, the energy equation needs to be solved and expressed as follows:

$$\frac{\partial U\rho C_p T}{\partial x} = \lambda\frac{\partial^2 T}{\partial y^2} - \frac{\partial \rho C_p \overline{v'\theta}}{\partial y} \tag{3.6}$$

where λ and C_p are thermal conductivity and specific heat at constant pressure respectively.
There is a gradient of mean temperature in the streamwise direction that must be subtracted for the periodicity and taking the integral of Eq. 3.6 in the limits of $y = 0$ to $y = 2\delta$ yields

$$\frac{\partial}{\partial x}\left[\rho C_p \int_0^{2\delta} UT dy\right] = \lambda\frac{\partial T}{\partial y}\bigg|_{2\delta} - \lambda\frac{\partial T}{\partial y}\bigg|_0 \tag{3.7}$$

$$U_b = \frac{1}{2\delta}\int_0^{2\delta} U dy \tag{3.8}$$

$$T_b = \frac{1}{2\delta U_b}\int_0^{2\delta} UT dy \tag{3.9}$$

where U_b and T_b are the bulk velocity and bulk temperature.
By substituting the value of T_b in Eq. 3.7 gives:

$$\rho C_p U_b \delta\frac{\partial T_b}{\partial x} = q_w \tag{3.10}$$

By decomposing the mean temperature into two contributions, we have

$$T = T_b + \vartheta \tag{3.11}$$

Eq. 3.6 becomes:

$$0 = \kappa \frac{\partial^2 \vartheta}{\partial y^2} - \frac{\partial \overline{v'\theta}}{\partial y} - \frac{q_w}{\rho C_p \delta} \frac{U}{U_b} \tag{3.12}$$

Where κ is the thermal diffusivity, $\kappa = \frac{\lambda}{\rho C_p}$.
The friction temperature (T_τ) is defined as follows

$$T_\tau = \frac{q_w}{\rho C_p u_\tau} \tag{3.13}$$

where u_τ is the friction velocity.
The non-dimensional temperature equation becomes:

$$0 = \frac{1}{PrRe_\tau} \frac{\partial^2 \widetilde{\vartheta}}{\partial \widetilde{y^2}} - \frac{\partial \widetilde{\overline{v'\theta}}}{\partial \widetilde{y}} - \frac{\widetilde{U}}{\widetilde{U_b}} \tag{3.14}$$

The boundary condition at the walls is defined as follows:

$$\left. \frac{\partial \widetilde{\vartheta}}{\partial \widetilde{y}} \right|_0 = -PrRe_\tau \tag{3.15}$$

3.2.2 Mixed convection regime

Mixed convection is the mode of heat transfer where both pressure and buoyancy forces interact. These type of flows occurs in many engineering applications like nuclear reactors, heat exchanger, turbine blades, solar panels, and in many other applications. These type of convective flows is referred as aiding flows when the buoyancy force is in the same direction as the pressure force and opposing flows when the buoyancy force is in the opposite direction. For the turbulent mixed convection in vertical flow passages, major modifications take place in the turbulence structure and the effects on heat transfer performance is complex. Experimental investigation of ascending mixed convection air flows has been studied [Carr et al., 1973, Polyakov and Shindin, 1988, Shehata and McEligot, 1998, Steiner, 1971, Vilemas et al., 1992]. The experimental studies on turbulent mixed convection has been complemented by the Direct Numerical Simulation (DNS) results. DNS by Kasagi and Nishimura [1997] are among the earliest studies carried out in a vertical differentially heated channel. Moreover, You et al. [2003] performed DNS for the study of turbulent mixed convection in a vertical uniformly-heated pipe where attention was restricted to hydrodynamically and thermally fully-developed flow.
The assessment of turbulence models in mixed convection flows have been reported by Abdelmeguid and Spalding [1979], Cotton and Jackson [1990], Kim et al. [2006], Kirwin [1995], Mikielewicz [1994], Walklate [1976], Yu [1991], where all those authors have tried

many variants of two-equation closure models. Authors have also evaluated the performances of other models, for example, Richards et al. [2004] and Kim et al. [2006] observed some success with the $\overline{v^2}-f$ model of Durbin [1991]. Keshmiri et al. [2008] have compared the performance of four eddy-viscosity models namely Launder and Sharma [1974], Cotton and Ismael [1998], Craft et al. [1996] and $\overline{v^2}-f$ models against the Large-eddy simulation (LES) in ascending turbulent mixed convection flows. In this study, the Launder-Sharma model captures the impairment of heat transfer quite well as compared to other models. For instance, Cotton and Ismael [1998] show the occurrence of impairment of heat transfer at high values of buoyancy parameter and the model by Craft et al. [1996] significantly underestimates the extent of impairment. At maximum impairment, flow and turbulence profiles were accurately resolved by LES, $\overline{v^2}-f$ and Launder-Sharma model.
In this study, attempts are made to evaluate the performance of three very different eddy-viscosity models in reproducing the effect of buoyancy on the statistics of turbulent mixed convection in a vertical channel. The turbulence models considered are the k-ω-SST, BL-$\overline{v^2}/k$ and Launder-Sharma models respectively. The thermal condition on the walls has been chosen to investigate the effect of aiding and opposing flow together. In the mixed convection, turbulence is enhanced or damped by the additional forces acting on the flow, and the velocity and temperature profiles in heated flow are described by the momentum and energy equation together as these equations are coupled. In this work, differentially heated vertical channel flow is computed and the results are compared with the DNS data [Kasagi and Nishimura, 1997]. The pressure gradient acts in the upward direction and buoyancy acts in upward direction (aiding flow) on the hot side of the wall and a downward direction (opposing flow) on the cold side of the wall. This flow configuration is interesting from an application perspective, since it is representative of many heat transfer applications such as flow inside a hollow wall and double glazed windows. All the physical properties are constant except the density which is varying in the buoyancy term only (Boussinesq approximation), where it varies linearly with temperature. The two walls are kept at different but constant temperature. The friction Reynolds number, $Re_\tau = 150$ is based on the mean wall friction velocity u_τ, and the channel-half width δ. The Prandtl number, $Pr = 0.71$ and the Grashof number (based on the temperature difference between two walls and channel width 2δ) are imposed explicitly by the virtue of non-dimensionalisation. The flow configuration and the convention for axes are given in Fig. 3.2. Periodic boundary conditions are imposed in the x-direction and to account the periodicity in pressure, the pressure gradient is subtracted. The momentum equation in the x-direction reads:

$$0 = -\frac{1}{\rho}\frac{\partial P}{\partial x} + \nu\frac{\partial^2 U}{\partial y^2} - \frac{\partial \overline{u'v'}}{\partial y} - g + \beta g(T - T_{ref}) \tag{3.16}$$

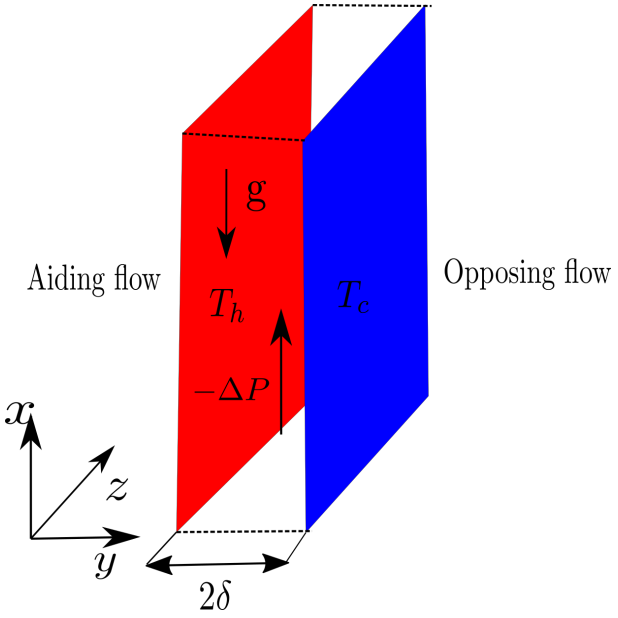

Figure 3.2 – Channel flow configuration for the mixed convection regime

The pressure gradient satisfying the momentum balance can be evaluated by integrating momentum equation between two walls separated by 2δ,

$$0 = \frac{2\delta}{\rho}\frac{\partial P}{\partial x} - ({u_\tau}^h)^2 - ({u_\tau}^c)^2 + \beta g \int_0^{2\delta} (T - T_{ref})dy - 2\delta g \tag{3.17}$$

where ${u_\tau}^h$ and ${u_\tau}^c$ are friction velocity at hot and cold walls respectively. By taking the average of the mean temperature over the channel, the bulk mean temperature is defined as:

$$T_m = \frac{1}{2\delta}\int_0^{2\delta} T dy \tag{3.18}$$

and the friction velocity is expressed as follows:

$${u_\tau}^2 = \frac{1}{2}(({u_\tau}^h)^2 + ({u_\tau}^c)^2) \tag{3.19}$$

Mean pressure is decomposed into two contributions:

$$P = P^* - \rho\Gamma x \tag{3.20}$$

where Γ is defined as:

$$\Gamma = \frac{{u_\tau}^2}{\delta} + g - \beta g(T_m - T_{ref}) \tag{3.21}$$

The pressure gradient becomes:

$$-\frac{1}{\rho}\frac{\partial P}{\partial x} = -\frac{1}{\rho}\frac{\partial P^*}{\partial x} + \Gamma \tag{3.22}$$

Using the Eq. (3.22), the momentum Eq. (3.16) becomes

$$0 = -\frac{1}{\rho}\frac{\partial P^*}{\partial x} + \Gamma + \nu\frac{\partial^2 U}{\partial y^2} - \frac{\partial \overline{u'v'}}{\partial y} - g + \beta g(T - T_{ref}) \tag{3.23}$$

Using the system of units:

$$L = \delta;\ \ T = \frac{\delta}{u_\tau};\ \ M = \rho\delta^3;\ \ \Theta = \Delta T \tag{3.24}$$

The variables become:

$$\widetilde{T} = \frac{T}{\Delta T};\ \ \widetilde{g} = \frac{gh}{{u_\tau}^2};\ \ \widetilde{\beta} = \beta\Delta T;\ \ \widetilde{\beta g} = \frac{Gr}{8Re_\tau^2};\ \ \widetilde{U} = \frac{U}{u_\tau};\ \ \widetilde{P^*} = \frac{P^*}{\rho {u_\tau}^2} \tag{3.25}$$

The non-dimensionalized momentum equation reads:

$$0 = -\frac{\partial \widetilde{P^*}}{\partial \widetilde{x}} + \widetilde{\Gamma} + \frac{1}{Re_\tau}\frac{\partial^2 \widetilde{U}}{\partial \widetilde{y^2}} - \frac{\partial \widetilde{\overline{u'v'}}}{\partial \widetilde{y}} - \widetilde{g} + \frac{Gr}{8{Re_\tau}^2}(\widetilde{T} - \widetilde{T}_{ref}) \tag{3.26}$$

where $\widetilde{T}_{ref}$ is the average of the temperature at hot and cold walls respectively. The source term of momentum equation, Grashof number and friction Reynolds number reads:

$$\widetilde{\Gamma} = 1 + \widetilde{g} - \frac{Gr}{8{Re_\tau}^2}(\widetilde{T_m} - \widetilde{T_{ref}});\ \ Gr = \frac{\beta g \Delta T (2\delta)^3}{\nu^2};\ \ Re_\tau = \frac{u_\tau \delta}{\nu} \tag{3.27}$$

The non-dimensionalized mean temperature equation writes:

$$0 = \frac{1}{Re_\tau Pr}\frac{\partial^2 \widetilde{T}}{\partial \widetilde{y^2}} - \frac{\partial \widetilde{\overline{v'\theta'}}}{\partial \widetilde{y}} \tag{3.28}$$

With these non-dimensional equations, the three independent parameters that characterize the flow are Re_τ, Pr, and Gr respectively, and these parameters are imposed.
Thermal boundary condition on the walls reads:

$$\widetilde{T} = \widetilde{T}_{ref} \pm \frac{1}{2} \tag{3.29}$$

where $\widetilde{T}_{ref}$ is the reference temperature.

3.2.3 Natural convection regime

Now we look at the natural convection case which is purely driven by buoyancy. In flow configurations like the flow between two infinite walls separated by a distance with different temperatures, investigation of turbulence is most effectively made as the influence of various physical processes can be isolated. This flow is important from a fundamental point of view as the production of turbulence by shear and buoyancy takes place in the same direction. Also, homogeneity in two directions makes sure there is no disturbing top/bottom or sidewall effects. In contrast to Section 3.2.2, there is no pressure gradient

in this flow configuration and the flow is computed in a differentially heated vertical channel such a way that the walls are kept at different temperatures. Temperature difference makes the natural convection flow to develop and when the Rayleigh number is sufficiently large, this flow becomes turbulent. The temperature difference (ΔT) and the distance between the two walls (δ) are taken as temperature scale and length scale respectively. The flow is characterized by the Rayleigh number, $Ra = \beta g \Delta T (\delta)^3/(\nu\kappa)$, based on the width ($\delta$) of the channel. The flow is periodic in the vertical x-direction and the flow configuration is shown in Fig. 3.3. The results are compared with the DNS data of Versteegh and Nieuwstadt [1998] at $Ra = 5 \times 10^6$ and Kiš and Herwig [2014] at $Ra = 1.7 \times 10^7$, respectively.

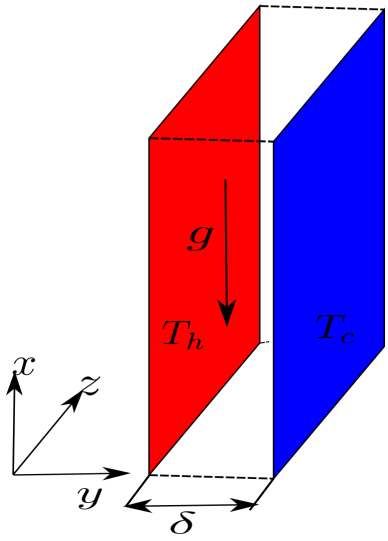

Figure 3.3 – Flow configuration for the differentially heated vertical channel

The properties of the fluid are considered to be constant and density is variable only in the buoyancy force term. With the Boussinesq approximation, Reynolds averaged momentum equation for a vertical channel flow in the x-direction can be expressed as follows:

$$0 = -\frac{\partial P}{\partial x} + \nu \frac{\partial^2 U}{\partial y^2} - \frac{\partial(\overline{u'v'})}{\partial y} - g + \beta g (T - T_{ref}) \tag{3.30}$$

where β is the thermal expansion coefficient, T_{ref} is the reference temperature, the x-direction is the streamwise direction, and y is the wall-normal direction respectively.
By taking the hydrostatic pressure contribution into account, the modified pressure reads

$$P^* = P - \rho g x \tag{3.31}$$

Since the flow is homogenous in the x-direction (that is $\frac{\partial P^*}{\partial x} = 0$), Eq. 3.30 becomes:

$$0 = \beta g (T - T_{ref}) + \nu \frac{\partial^2 U}{\partial y^2} - \frac{\partial(\overline{u'v'})}{\partial y} \tag{3.32}$$

Where ν is the kinematic viscosity and T_{ref} is the reference temperature. The averaged temperature equation writes:

$$0 = \kappa \frac{\partial^2 T}{\partial y^2} - \frac{\partial \overline{v'\theta}}{\partial y} \tag{3.33}$$

Where κ is the thermal diffusivity. Using the system of units,

$$L = \delta; \quad T = \frac{\delta^2}{\kappa}; \quad M = \rho\delta^3; \quad \Theta = \Delta T \tag{3.34}$$

variables become:

$$\widetilde{U} = \frac{U}{U_{ref}}; \quad U_{ref} = \frac{\kappa}{\delta}; \quad \widetilde{T} = \frac{T}{\Delta T}; \quad \widetilde{\beta g} = RaPr; \quad \widetilde{\overline{u'v'}} = \frac{\overline{u'v'}}{(U_{ref})^2}; \quad \widetilde{\nu} = Pr; \quad \widetilde{\kappa} = 1 \tag{3.35}$$

With these variables, the non-dimensional momentum equation becomes:

$$0 = RaPr(\widetilde{T} - \widetilde{T}_{ref}) + Pr\frac{\partial^2 \widetilde{U}}{\partial \widetilde{y^2}} - \frac{\widetilde{\partial \overline{u'v'}}}{\partial \widetilde{y}} \tag{3.36}$$

and non-dimensional temperature equation becomes:

$$0 = \frac{\partial^2 \widetilde{T}}{\partial \widetilde{y^2}} - \frac{\partial \widetilde{\overline{v'\theta}}}{\partial \widetilde{y}} \tag{3.37}$$

The thermal boundary condition on the walls are defined as:

$$\widetilde{T} = \widetilde{T}_{ref} \pm \frac{1}{2} \tag{3.38}$$

where $\widetilde{T}_{ref} = 0.5$.

3.3 Selection of turbulence models

In industrial flow computations, standard wall functions are found to be inadequate for complex flows, specifically in regions where the flow departs from energy equilibrium. Moreover, to be able to evaluate the influence of buoyancy-related terms in the models, it is preferable to get away from the standard wall laws, which are only suitable for forced convection flows and could contaminate all the results. So in this work, the wall-function approach is not considered with the turbulence models.

Several low-Reynolds number versions have been proposed so that the equations can be integrated down to the wall. In most of the near-wall modifications of the turbulence models, non-viscous and molecular effects are modeled using damping functions which are based on the non-dimensional wall distance and the turbulent Reynolds number [Chien, 1982, Jones and Launder, 1972, Launder and Sharma, 1974]. Despite of the fact that such functions are unable to capture non-viscous effects, some of the low-Reynolds number models have proven to be successful in several flows owing to the sagacious tuning of

damping functions to imitate the wall effects.
Given this fact, three very different turbulence models are selected from three families of turbulence models. The reason for choosing models from different families is to ensure that the extensions that will be introduced into the models to take into account buoyancy effects are not only valid for a particular model or type of model. From the k-ω family, the k-ω-SST is considered owing to its wide use in industrial flows and relative success in forced convection. The k-ω-SST model is a blend between the k-ε and the k-ω models such that the model behaves as the k-ω model in the near-wall region and acts as the k-ε model in the outer region and thus this model removes the deficiency of the k-ω model in the computation of the outer region [Menter, 1994].
The selection of BL-$\overline{v^2}/k$ model from $\overline{v^2}$-f family is based on the fact that the BL-$\overline{v^2}/k$ model was able to satisfactorily predict mixed and natural convection flows [Billard and Laurence, 2012]. Also the BL-$\overline{v^2}/k$ model is more robust as compared to other versions of $\overline{v^2}$-f models. For instance in the mixed convection regime, the $\overline{v^2}$-f model by Lien and Kalitzin [2001] has failed to predict the mean flow and turbulent flow profiles as compared to DNS data. Moreover, the BL-$\overline{v^2}/k$ model had given encouraging predictions in other heat transfer flows, e.g., natural convection in a rectangular cavity, impinging jet on a flat plate, flow in a ribbed channel [Billard and Laurence, 2012] respectively and given these studies, BL-$\overline{v^2}/k$ model has been selected in the present study.
The selection of low-Reynolds number Launder and Sharma [1974] model among other low-Reynolds number is based on the ability to prove more accurate in the natural convection boundary layers [Henkes and Hoogendoorn, 1989, Patel et al., 1985]. The Launder-Sharma model had been applied in the ascending and descending turbulent mixed convection flows and found to give reasonable quantitative results with the exception of the descending flow data of Axcell and Hall [1978] at large buoyancy effects [Cotton and Jackson, 1990]. Subsequent computations in the case of ascending mixed convection flow in vertical pipes by Cotton and Kirwin [1993] and Jackson and Mikielewicz [1996] had confirmed that the Launder-Sharma model was superior to other low-Reynolds number $k-\varepsilon$ turbulence models.

3.4 Performance of selected turbulence models

Except in the appendices, where ANSYS FLUENT is applied, all the computations have been performed using *Code_Saturne*, developed by EDF [Archambeau et al., 2004]. It is an open-source code, distributed under a Gnu GPL licence. It is an unstructured, finite volume code, in collocated arrangement, of second order accuracy. Reynolds-averaged incompressible Navier-Stokes equations are solved using a SIMPLEC algorithm with a Rhie and Chow interpolation.

3.4.1 Forced convection flow in a channel

Mean velocity distribution corresponding to $Re_\tau = 180$, 395, 640 & 1020 and $Pr = 0.71$ is shown in Fig. 3.4 and compared with the DNS data [Abe et al., 2004]. Reynolds-number effect on turbulent quantities is significant and that's why four different Reynolds number flows are computed in this study. From Fig. 3.4, it can be observed that the logarithmic region expands with increasing Reynolds number. There is some discrepancy in the prediction of mean velocity by k-ω-SST in the defect layer and there is a good agreement in the apparent log layer. Moreover in the viscous sub-layer, the agreement of the velocity profile is satisfactory due to momentum balance. The BL-v^2/k model gives a better estimate of mean velocity profiles that matches in the whole domain of the channel. Overall prediction of mean velocity by all the three models is in agreement with the DNS data and this can be attributed to the fact that these models are generally calibrated using this test case.

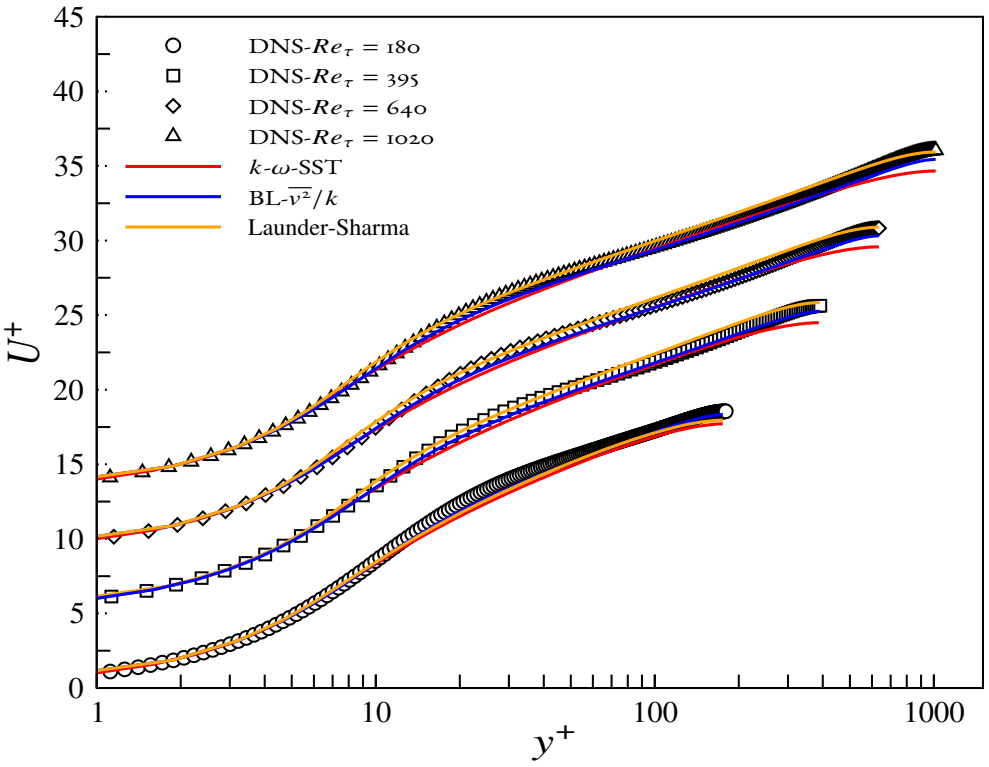

Figure 3.4 – Mean velocity at $Re_\tau = 180, 395, 640, 1020$ [Plots are shifted for clarity]

Further, a closer look at the velocity distribution can be done by scrutinizing the variable $y^+ \frac{dU^+}{dy^+}$ (for assessing the predictions in the log region) shown in Fig 3.5. Appreciable difference between the models can be seen. Near-wall peaks are underpredicted by k-ω-SST model although predictions from BL-v^2/k and Launder-Sharma models seem to be satisfactory in the near-wall region. In the logarithmic region, only the BL-v^2/k model can slightly better predict the von Karman constant (in the logarithmic region, at infinite

Reynolds number, $y^+ \frac{dU^+}{dy^+} = \frac{1}{\kappa}$).

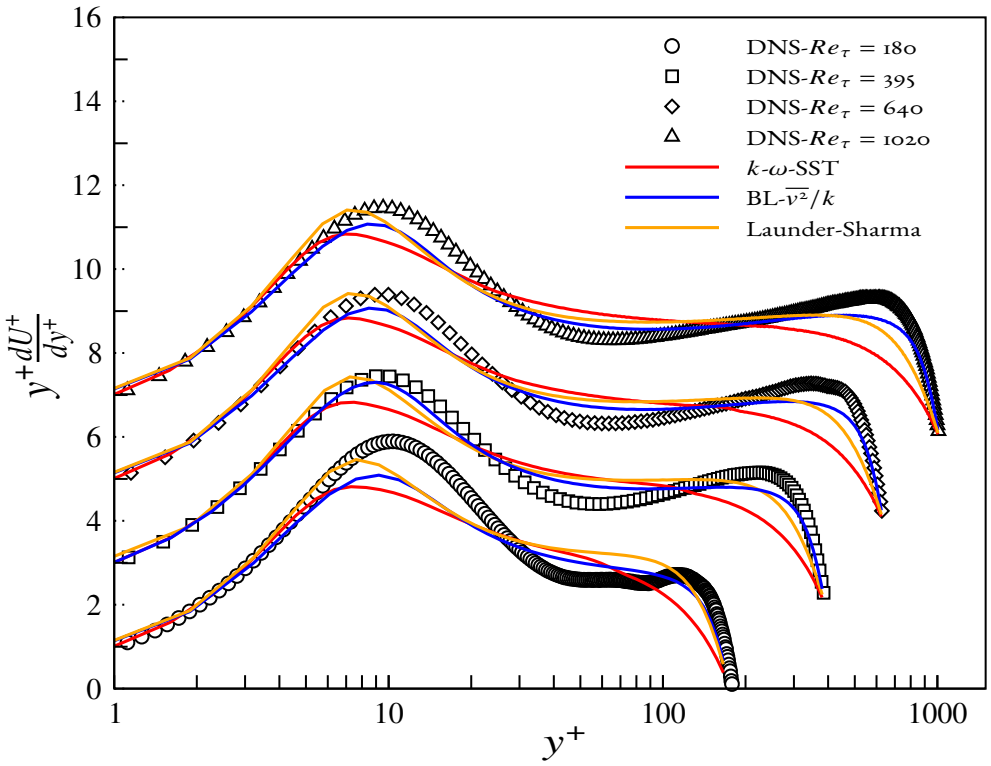

Figure 3.5 – Premultiplied gradient of mean velocity at $Re_\tau = 180, 395, 640, 1020$ [Plots are shifted for clarity]

The distribution of turbulent kinetic energy is shown in Fig. 3.6 and it is observed that the peak value of k is Reynolds number dependent as the peak value is varying from 4.10 at $Re_\tau = 180$ to 5.11 at $Re_\tau = 1020$ as can be seen in DNS data. However, as far as the predictions by models are concerned, it is observed that there is a severe underestimation of the peak value of turbulent kinetic energy by k-ω-SST and Launder-Sharma models, although BL-v^2/k model seems to give relatively better prediction when compared with DNS data. The near-wall behaviour of k is affected by the boundary condition on ε and ω and this is one of the reasons of the differences in the prediction of turbulent kinetic energy. Recalling the turbulent viscosity expression for the models:

$$\begin{aligned} \nu_t &= \frac{a_1 k}{max(a_1\omega, SF_2)} \\ \nu_t &= C_\mu \frac{\overline{v^2}}{k} kT \\ \nu_t &= C_\mu f_\mu \frac{k^2}{\varepsilon} \end{aligned} \tag{3.39}$$

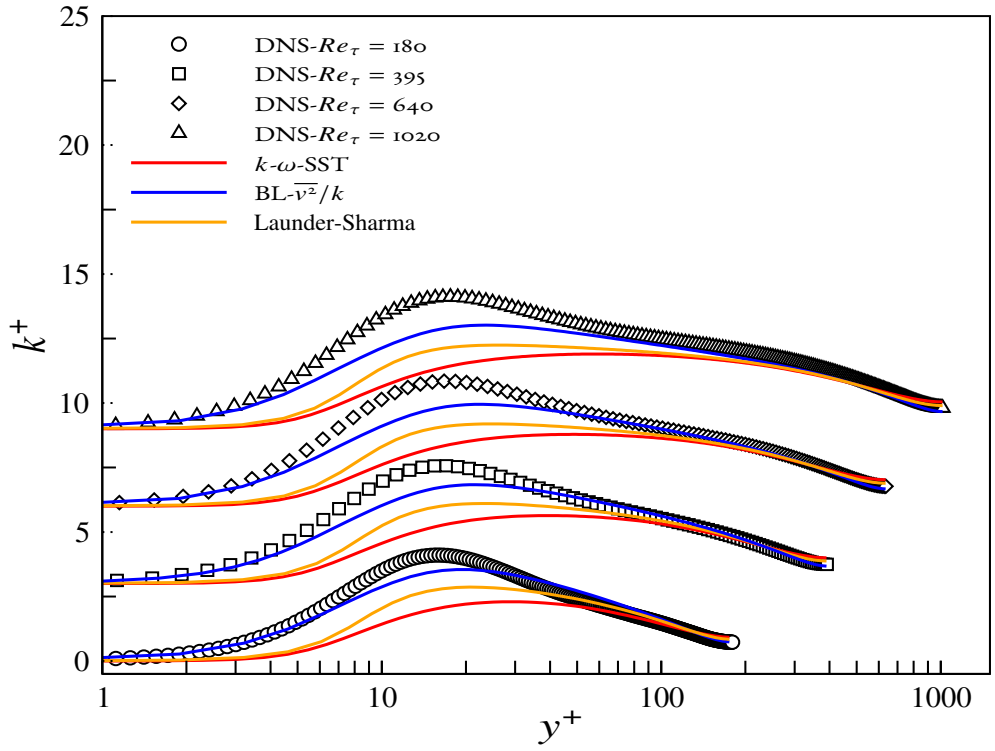

Figure 3.6 – Turbulent kinetic energy at $Re_\tau = 180, 395, 640, 1020$ [Plots are shifted for clarity]

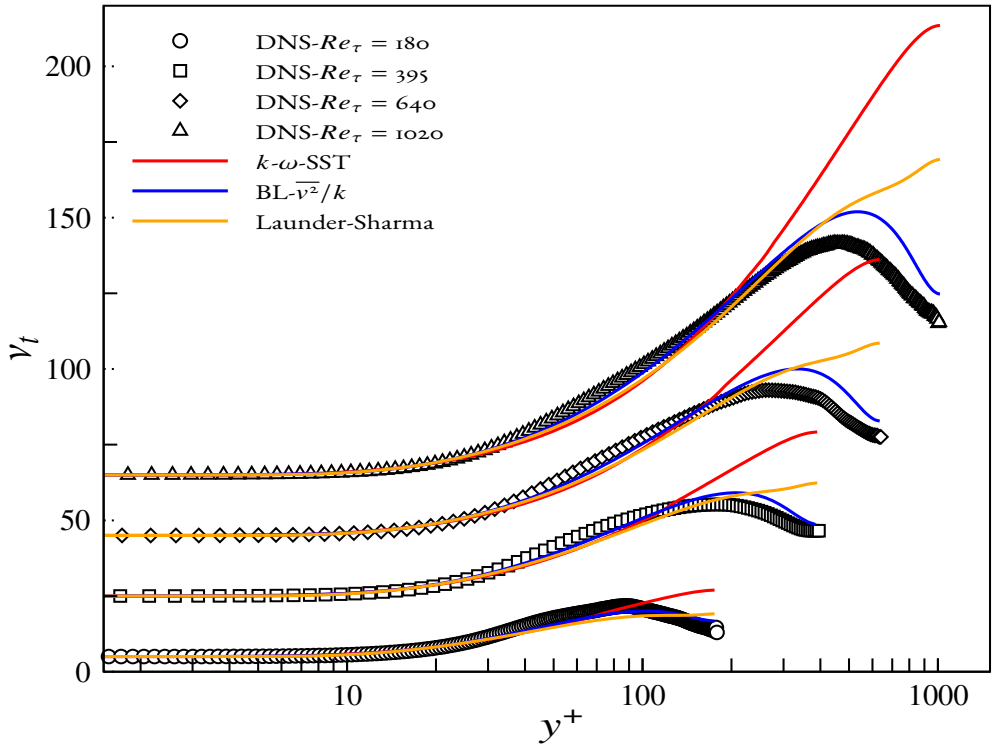

Figure 3.7 – Turbulent viscosity at $Re_\tau = 180, 395, 640, 1020$ [Plots are shifted for clarity]

The turbulent viscosity (ν_t) predictions are shown in Fig. 3.7. In the wake region there is severe overestimation of turbulent viscosity (ν_t) by k-ω-SST and Launder-Sharma model, although BL-$\overline{v^2}/k$ model seems to better predict this quantity. Mean temperature (T^+) distribution is shown in Fig. 3.8. Similar to mean velocity distribution, there is a logarithmic region in the temperature profile also [Kader, 1981].

$$T^+ = \frac{1}{\kappa_T} \ln y^+ + C_T \tag{3.40}$$

where κ_T is the von Karman constant of mean temperature profile and this constant is calculated by the following relation:

$$\kappa_T = \left(y^+ \frac{dT^+}{dy^+} \right)^{-1} \tag{3.41}$$

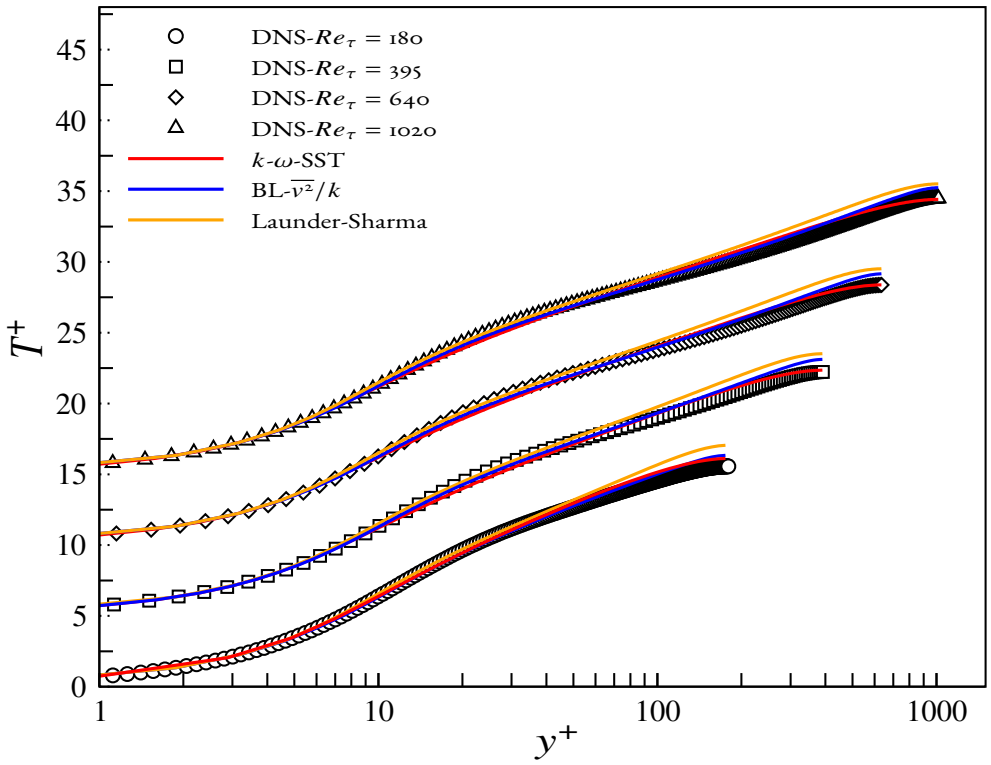

Figure 3.8 – Mean temperature at $Re_\tau = 180, 395, 640, 1020$ [Plots are shifted for clarity]

It has been observed that T^+ is well predicted up to $y^+ = 30$ by all the models as expected since q_w is imposed. Moreover, in the log region, there is an overestimation of the mean temperature by all the models. There are some discrepancy in the prediction of mean temperature by the k-ω-SST and Launder-Sharma model as can be seen in Fig. 3.8.

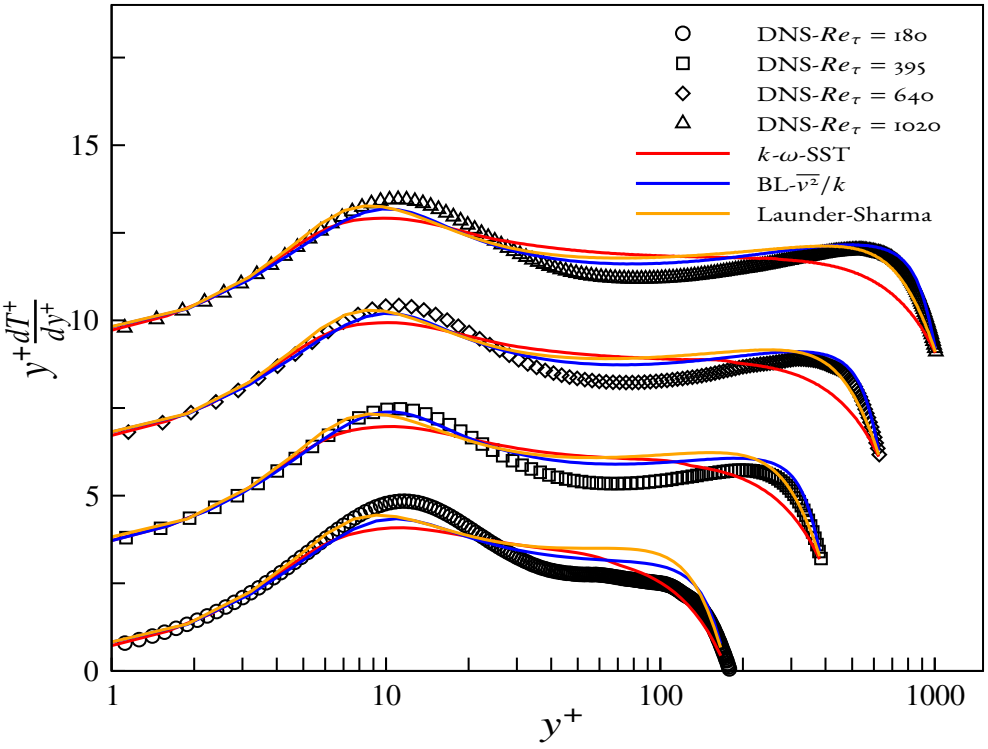

Figure 3.9 – Premultiplied temperature gradient at $Re_\tau = 180, 395, 640, 1020$ [Plots are shifted for clarity]

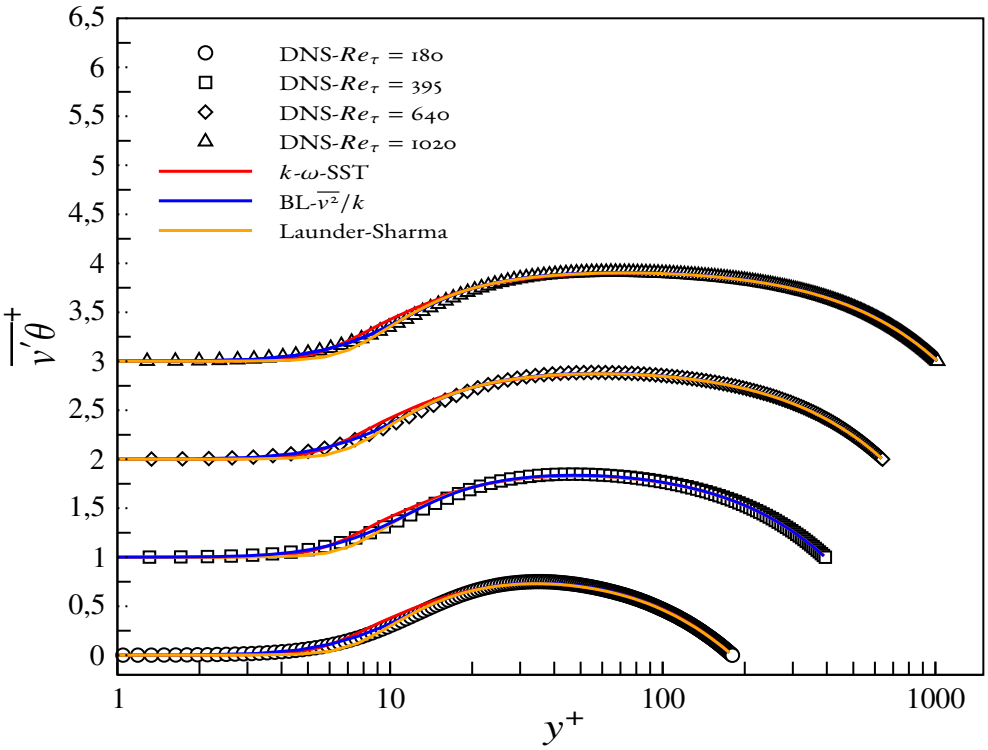

Figure 3.10 – Normal heat flux at $Re_\tau = 180, 395, 640, 1020$ [Plots are shifted for clarity]

To look further in the temperature distribution, the variable $y^+\frac{dT^+}{dy^+}$ is shown in Fig. 3.9, the interest of this quantity is to look at the log layer prediction of models. In the logarithmic region, there is an overestimation of this quantity which yields an underestimation of the von Karman constant (κ_T) by all the three models. However, the BL-$\overline{v^2}/k$ seems to give relatively better prediction of this quantity ($y^+\frac{dT^+}{dy^+}$) as compared to other models.
The wall normal heat flux component observed to be well predicted by all three models as can be seen in Fig. 3.10 and the component $\overline{v'\theta}$ goes to zero (in the central region) because of the term $\frac{U}{U_b}$.

3.4.2 Mixed convection in the vertical channel flow

The mean velocity profile in computational units is shown in Fig. 3.11. It can be seen that buoyancy makes mean velocity profile asymmetric in such a way that the mean velocity increases on aiding side (near the hot wall) and reduces on the opposing side (near the cold wall). For the comparison of model prediction, it is observed that k-ω-SST model underpredicts the mean velocity profile. On the contrary, there is overprediction of mean velocity by the Launder-Sharma model. The prediction by BL-$\overline{v^2}/k$ is observed to be in good agreement with DNS data of Kasagi and Nishimura [1997] as can be seen in Fig. 3.11.

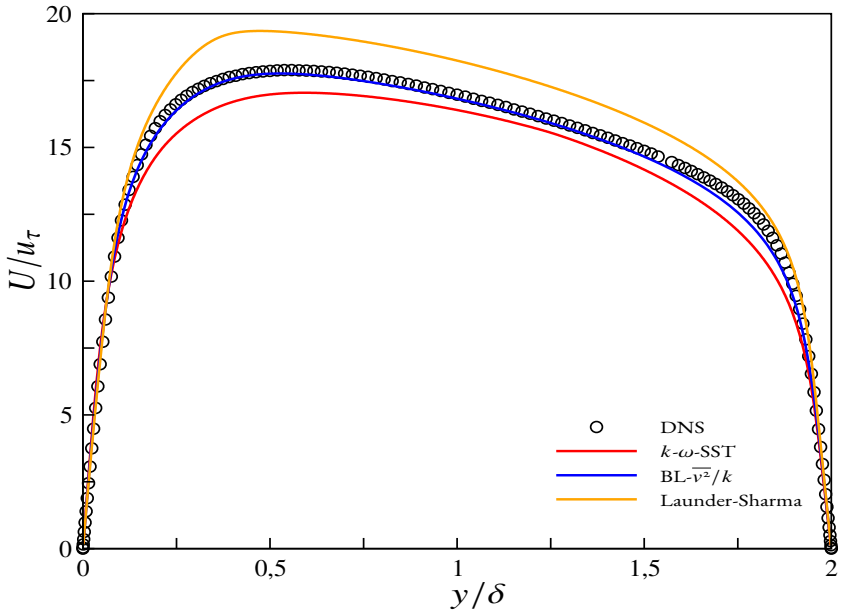

Figure 3.11 – Mean velocity at $Gr = 9.6 \times 10^5$ and $Pr = 0.71$ [Kasagi and Nishimura, 1997]

This behavior can be interpreted by observing the stress balance by integrating the momentum equation from the wall to some distance y.

The momentum equation (Eq. 3.26) becomes:

$$\left[\nu\frac{d\widetilde{U}}{d\widetilde{y}} - \nu\frac{d\widetilde{U}}{d\widetilde{y}}\bigg|_{y=0}\right] - \widetilde{\overline{u'v'}} + \frac{Gr}{8Re_\tau}\int_0^y(\widetilde{T}-\widetilde{T}_m)d\widetilde{y} = -\widetilde{y}\frac{1}{\rho}\frac{\partial\widetilde{P}^*}{\partial\widetilde{x}} \tag{3.42}$$

In Eq. 3.42, the three terms on the left hand side are viscous stresses, the Reynolds shear stress and buoyancy force respectively, and the pressure gradient balances these three forces.

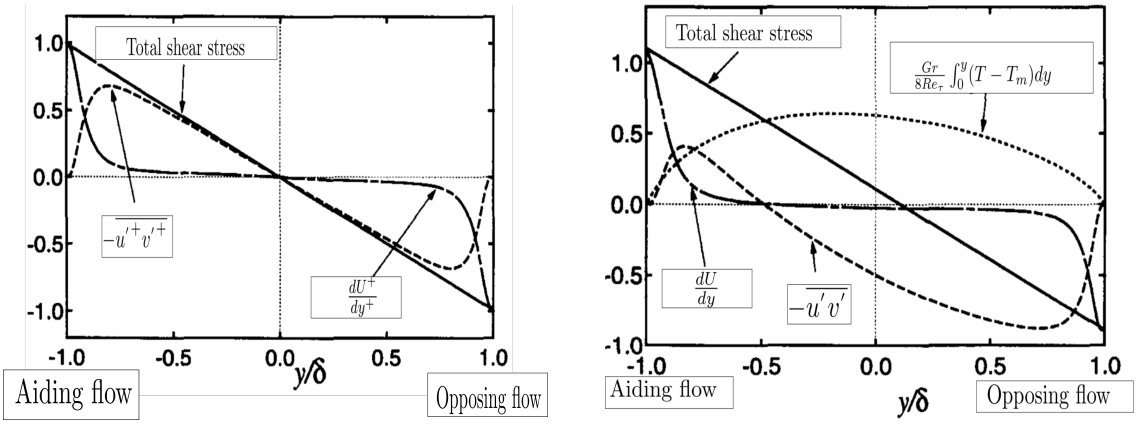

(a) Isothermal flows (b) Mixed convection flows

Figure 3.12 – Stress balance [Plots is taken from Kasagi and Nishimura, 1997]

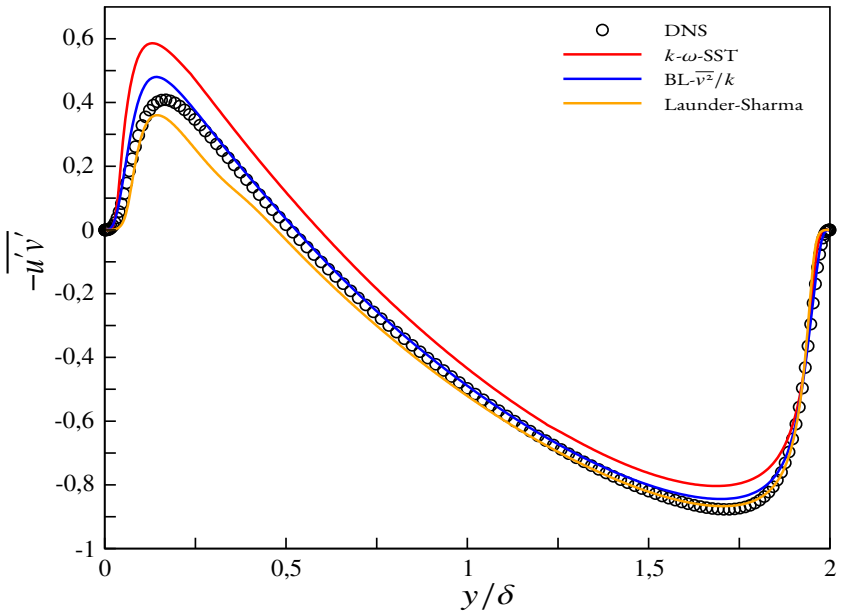

Figure 3.13 – Turbulent shear stress profile at $Gr = 9.6 \times 10^5$ and $Pr = 0.71$ [Kasagi and Nishimura, 1997]

In the isothermal flows, there is a symmetrical distribution of Reynolds stresses and

viscous stresses as can be seen in Fig. 3.12 a. However, when the flows is affected by buoyancy such as mixed convection flow in a vertical channel, the stress distribution is distorted due to the imposed buoyancy and this modifies the shear stress near the wall and thereby causing the turbulence enhancement (on the opposing side) or suppression (on the aiding side) as depicted in Fig. 3.12 b.

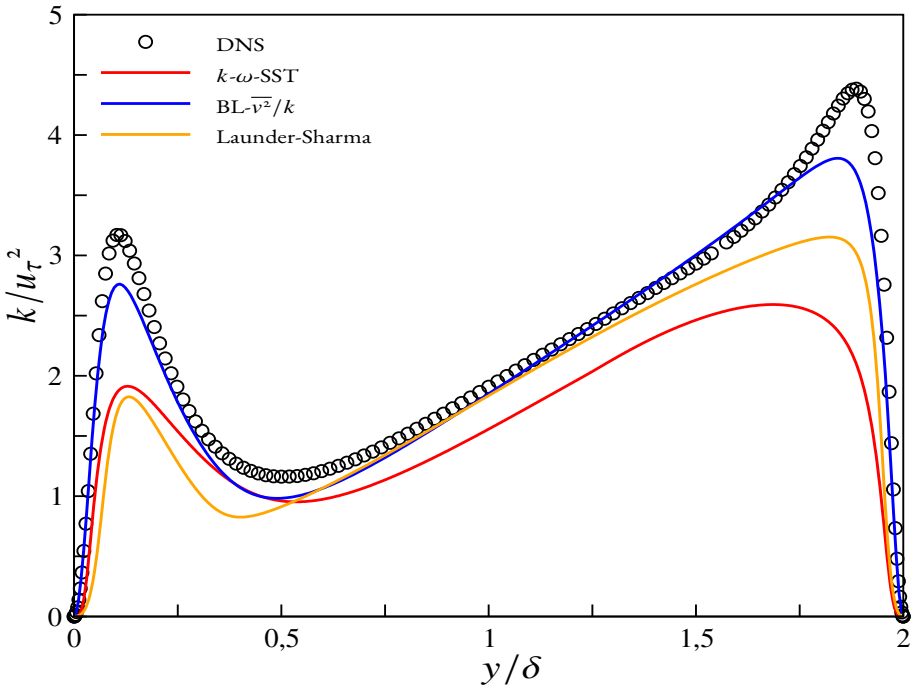

Figure 3.14 – Turbulent kinetic energy profile at $Gr = 9.6 \times 10^5$ and $Pr = 0.71$ [Kasagi and Nishimura, 1997]

Based on this behavior, predictions of mean velocity by turbulence models can be analyzed. Looking into Fig. 3.13, it is realized that the better prediction of turbulent shear stress influences the mean velocity in such a manner that it affects the momentum balance through viscous stress which is imposed at the wall and thereby allows better prediction of mean velocity as observed in the case of BL-$\overline{v^2}/k$ model as shown in Fig. 3.11. If this turbulent shear stress is not properly predicted as observed in the case of k-ω-SST model and Launder-Sharma model, then it affects the momentum balance through viscous stress predictions which allows the mean velocity to be underpredicted with k-ω-SST model and overpredicted with Launder-Sharma model respectively.
The turbulent kinetic energy distribution is shown in Fig. 3.14 and it is observed that the turbulence is modified by the buoyancy such that there is a reduction (on aiding side) and an enhancement (on opposing side) of turbulent kinetic energy. Moreover, it is observed that with k-ω-SST and Launder-Sharma model, there is a severe underestimation of turbulent kinetic energy. However, the predictions are relatively better with BL-$\overline{v^2}/k$ model. Fig. 3.15 shows the mean temperature profile and if we look into the DNS profile for

mean temperature, it is observed that the buoyancy influences the mean temperature predictions such that the profile becomes asymmetric owing to the increase of the temperature gradient in the aiding side (hot wall) while it reduces on the opposing side (cold wall). As far as the prediction of models is concerned, it is observed that the prediction of BL-$\overline{v^2}/k$ model is in good agreement with DNS data [Kasagi and Nishimura, 1997]. However, the mean temperature is overpredicted with k-ω-SST and underpredicted with Launder-Sharma models respectively. Effect of buoyancy on thermal statistics can be better interpreted by integrating the temperature equation from the wall to some distance y towards the center of the channel, which yields

$$0 = \frac{1}{Re_\tau Pr}\frac{d\widetilde{T}}{dy}\bigg|_0 - \int_0^y \widetilde{\overline{v'\theta}} \tag{3.43}$$

Looking at the DNS profile of wall-normal heat flux, it is observed that on the aiding side, wall-normal heat flux is reduced as shown in Fig. 3.16 and to preserve the balance in the temperature equation (Eq. 3.43), the gradient of temperature increases. Now, when we look into the prediction of turbulence models, k-ω-SST model overpredicts the wall-normal heat flux on the aiding side and this makes the gradient of temperature to reduce and as a consequence the mean temperature is overpredicted close to the hot wall.

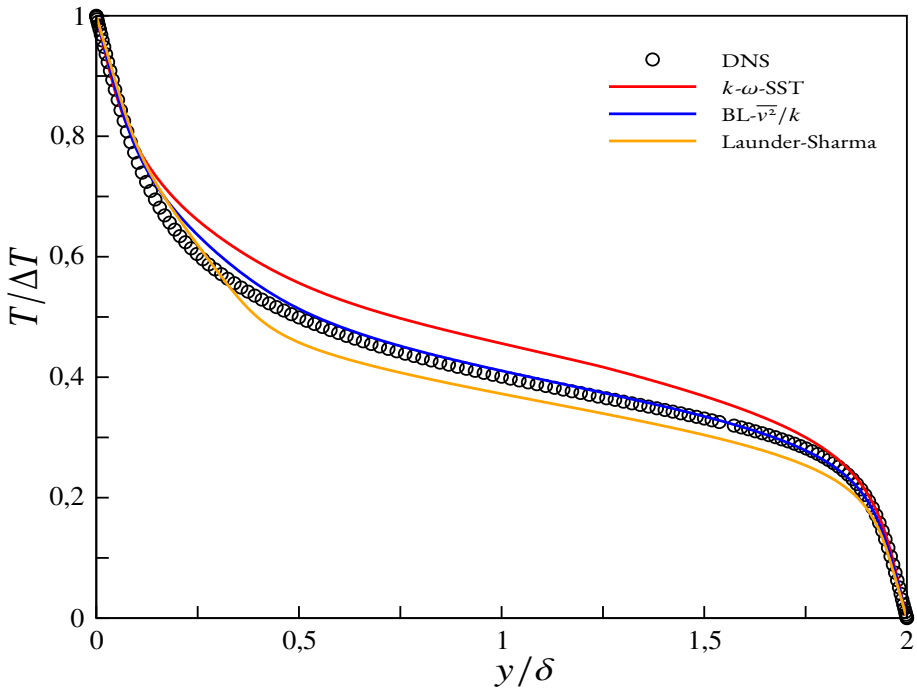

Figure 3.15 – Mean temperature at $Gr = 9.6 \times 10^5$ and $Pr = 0.71$ [Kasagi and Nishimura, 1997]

However, this overprediction of wall-normal heat flux is marginal on the opposing side and lead to less discrepant mean temperature profiles. The wall-normal heat flux

predictions by the BL-$\overline{v^2}/k$ model is found to be in relatively good agreement with DNS data which leads to the better prediction of mean temperature profile as can be seen in Fig. 3.15. For the Launder-Sharma model, there is a severe underprediction of the wall-normal heat flux which allows the gradient of temperature in Eq. 3.43 to increase close to the wall, and thereby the mean temperature is underestimated as can be seen in Fig. 3.15.

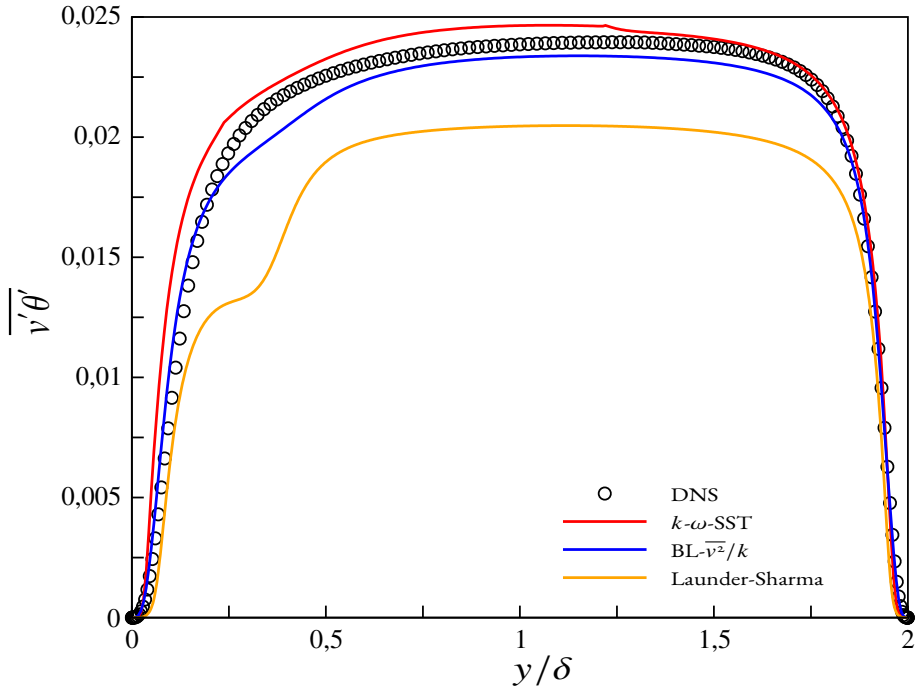

Figure 3.16 – Wall-normal turbulent heat flux profile at $Gr = 9.6 \times 10^5$ and $Pr = 0.71$ [Kasagi and Nishimura, 1997]

3.4.3 Natural convection in the vertical channel flow

The mean velocity profile is shown in Fig. 3.17. DNS data of Versteegh and Nieuwstadt [1996] at $Ra = 5 \times 10^6$ and Kiš and Herwig [2014] at $Ra = 1.7 \times 10^7$ are considered to compare the performance of the turbulence models. To better understand the dynamics of this flow, we need to integrate the momentum equation from the wall to some distance y which is expressed as follows:

$$0 = \int_0^y \widetilde{\beta} g(\widetilde{T} - \widetilde{T}_{ref}) + \widetilde{\nu} \frac{d\widetilde{U}}{d\widetilde{y}}\bigg|_0 - \widetilde{\overline{u'v'}} \tag{3.44}$$

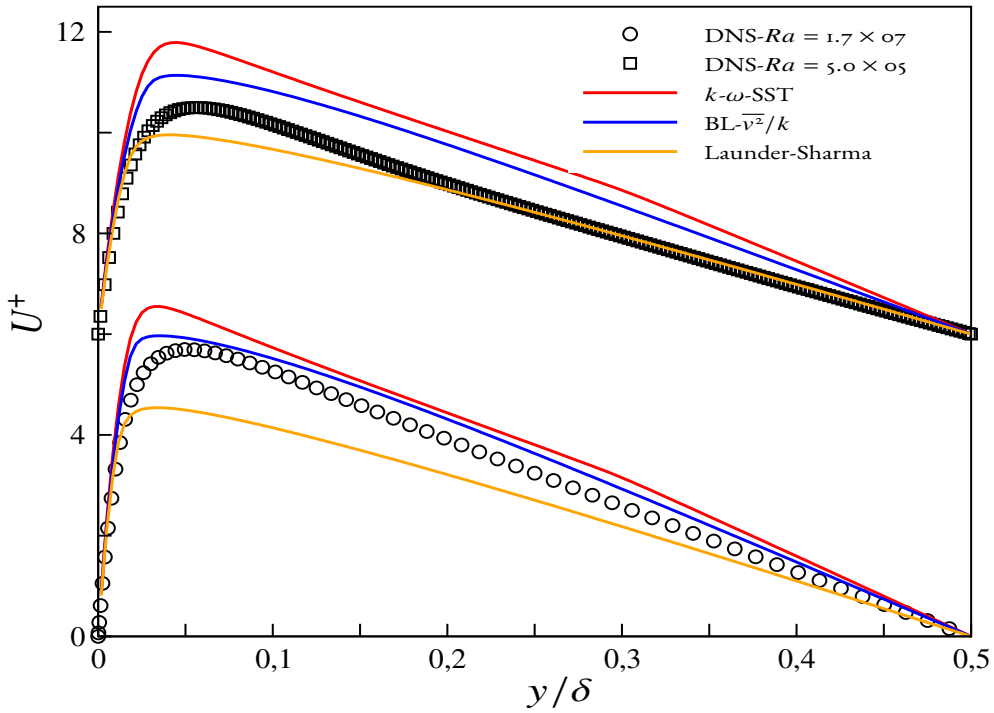

Figure 3.17 – Mean velocity at $Ra = 5 \times 10^6$ [Versteegh and Nieuwstadt, 1996](denoted by □) and $Ra = 1.7 \times 10^7$ [Kiš and Herwig, 2014](denoted by ○) [Plots are shifted for clarity]

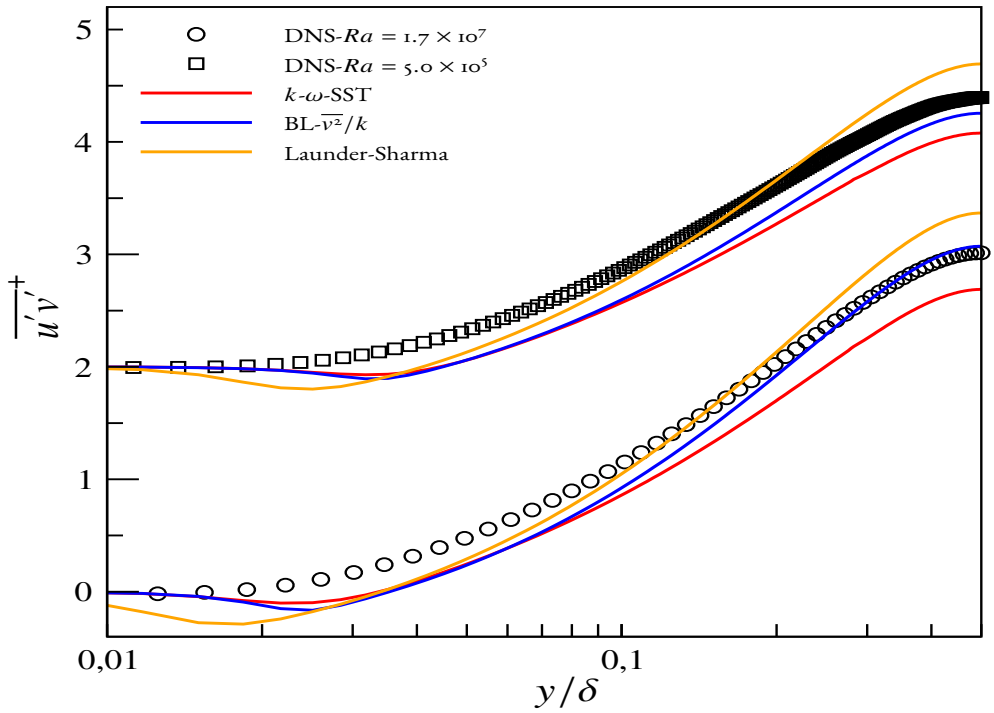

Figure 3.18 – Turbulent shear stress profile at $Ra = 5 \times 10^6$ [Versteegh and Nieuwstadt, 1996](denoted by □) and $Ra = 1.7 \times 10^7$ [Kiš and Herwig, 2014](denoted by ○) [plots are shifted for clarity]

As can be seen from Eq. (3.44) that there is a balance between buoyancy force, viscous stress and turbulent stress. It is observed that there is an overprediction of mean velocity by k-ω-SST and BL-$\overline{v^2}/k$ models owing to the underprediction of the Reynolds shear stress, which is severely underestimated for k-ω-SST model as can be seen in Fig. 3.18, and this is compensated by the increase of velocity gradient to maintain the balance as can be seen in Fig. 3.17. Furthermore, there is a severe underprediction of mean velocity (shown in Fig. 3.17) by the Launder-Sharma model owing to the misprediction of turbulent shear stress as can be seen in Fig. 3.18.

Turbulent viscosity distribution is shown in Fig. 3.19. For the DNS data, the Boussinesq constitutive relation is used to compute the eddy-viscosity which is expressed as follows:

$$\nu_t = \frac{-\overline{u'v'}}{(\frac{dU}{dy})} \tag{3.45}$$

Looking into the Fig. 3.19, it is observed that for both the Rayleigh numbers, the turbulent viscosity is underestimated by k-ω-SST and BL-$\overline{v^2}/k$ models and overestimated by Launder-Sharma model respectively. This prediction of turbulent viscosity is related to the prediction of Reynolds shear stress as Boussinesq relation is used to model Reynolds stress.

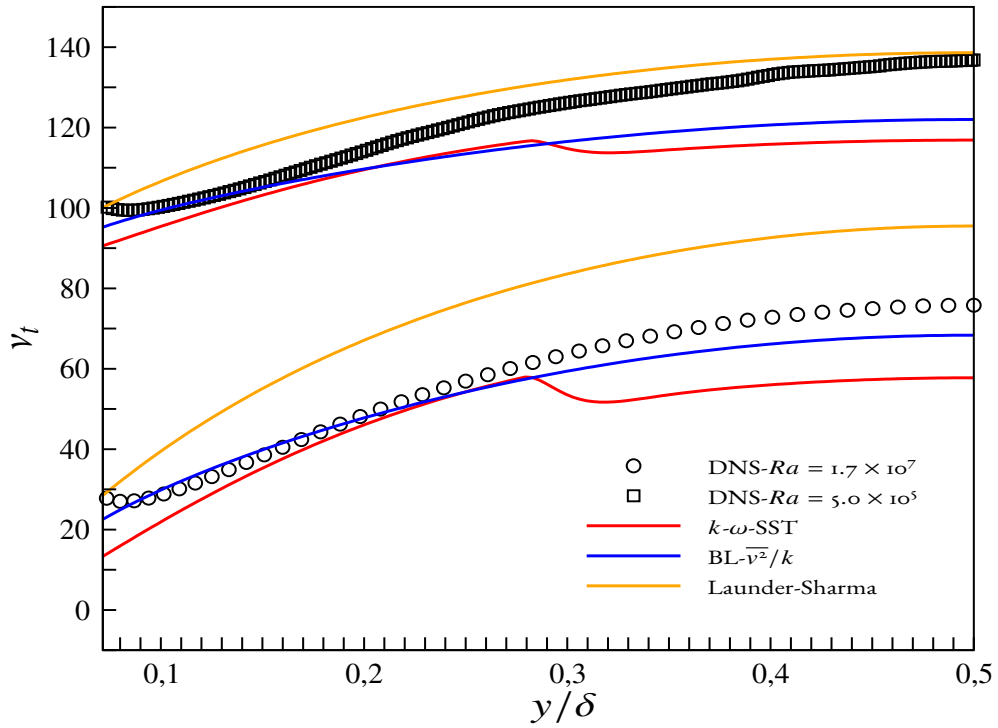

Figure 3.19 – Turbulent viscosity at $Ra = 5 \times 10^6$ [Versteegh and Nieuwstadt, 1996](denoted by □) and $Ra = 1.7 \times 10^7$ [Kiš and Herwig, 2014](denoted by ○) [plots are shifted for clarity]

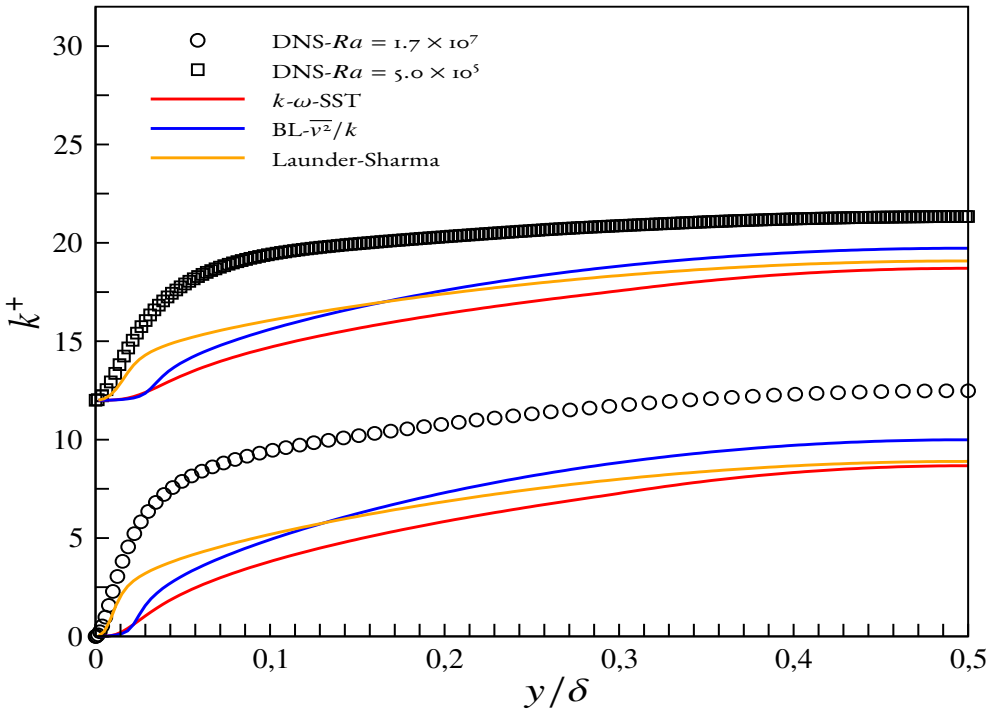

Figure 3.20 – Turbulent kinetic energy at $Ra = 5 \times 10^6$ [Versteegh and Nieuwstadt, 1996](denoted by □) and $Ra = 1.7 \times 10^7$ [Kiš and Herwig, 2014](denoted by ○) [plots are shifted for clarity]

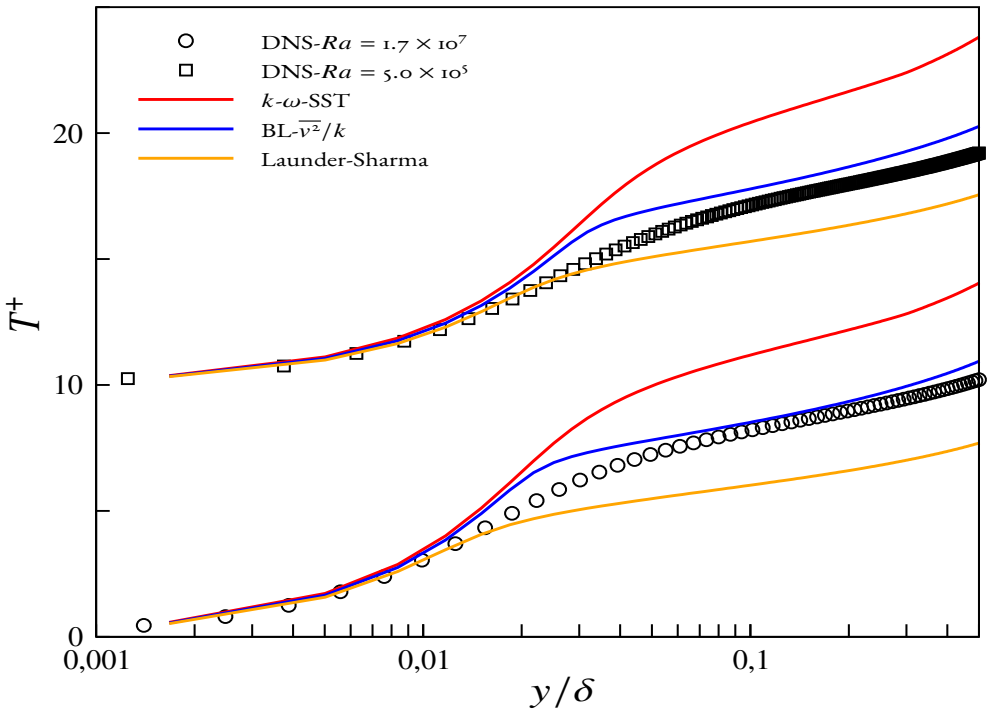

Figure 3.21 – Mean temperature at $Ra = 5 \times 10^6$ [Versteegh and Nieuwstadt, 1996](denoted by □) and $Ra = 1.7 \times 10^7$ [Kiš and Herwig, 2014](denoted by ○) [Plots are shifted for clarity]

Finally, by looking into the turbulent kinetic energy plots shown in Fig. 3.20, it is observed that the turbulent kinetic energy is severely underestimated by all the selected turbulence models far from the wall, however close to the wall Launder-Sharma predictions are relatively better.

The mean temperature distribution is shown in Fig. 3.21. Corresponding to both the Rayleigh numbers, it is observed that both the k-ω-SST and BL-$\overline{v^2}/k$ models overestimate T^+ owing to the underestimation of friction temperature (as shown in Table. 3.1) by at least 26% for k-ω-SST and by 8% for BL-$\overline{v^2}/k$ model respectively. This fact is further reinforced by the predictions of Nusselt number which is also underpredicted by both the models. However, Launder-Sharma model underestimates T^+ (as can be seen in Fig. 3.21) owing to the overprediction of friction temperature. To better understand the prediction of mean temperature by the turbulence models, temperature Eq. (3.37) is integrated twice from the wall to some distance y which yields.

$$\widetilde{T} - \widetilde{T_w} = \int_0^y \widetilde{v'\theta} d\tilde{y} \tag{3.46}$$

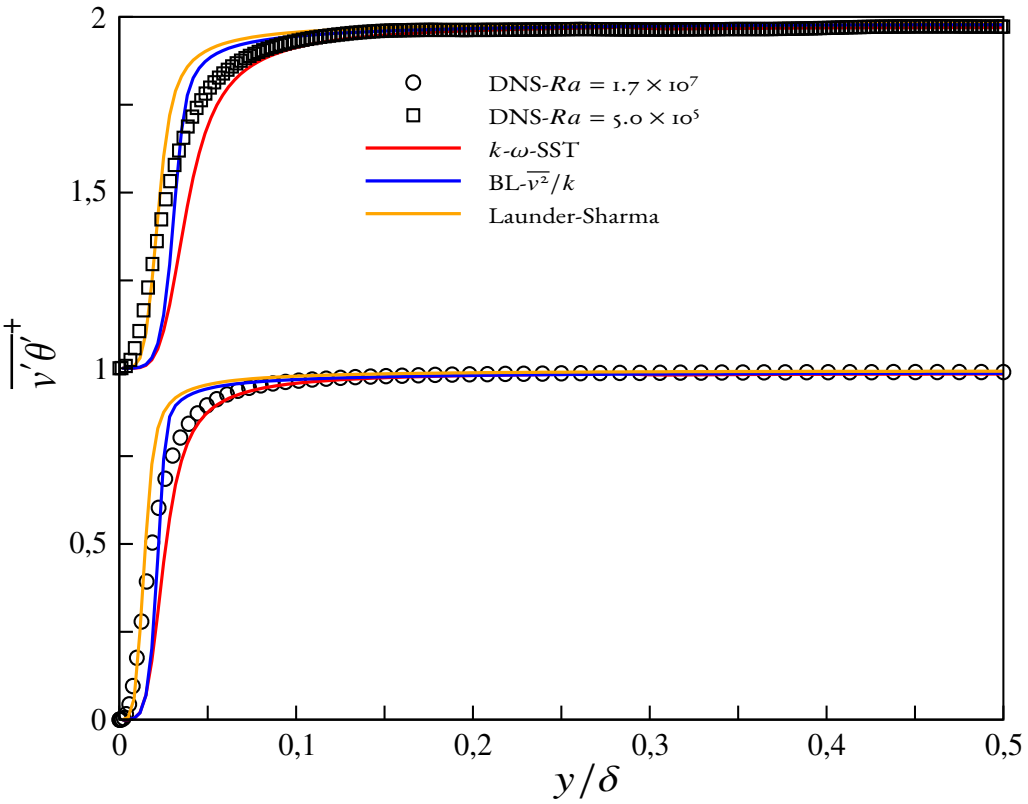

Figure 3.22 – Normal turbulent heat flux at $Ra = 5 \times 10^6$ [Versteegh and Nieuwstadt, 1996](denoted by □) and $Ra = 1.7 \times 10^7$ [Kiš and Herwig, 2014](denoted by ○) [plots are shifted for clarity]

It can be seen from the Eq. (3.46) that the good prediction of wall-normal turbu-

lent heat flux is crucial for a good prediction of mean temperature. For the Launder-Sharma model, $\overline{v'\theta}$ is overestimated virtually everywhere hence the T^+ is underestimated. However, for the k-ω-SST model, this is just the opposite where the Nusselt number is underestimated by 22% as shown in the Table. 3.1. With the BL-$\overline{v^2}/k$ model, there is a compensation in the integral of $\overline{v'\theta}$ due to the underestimation close to the wall and overestimation far from it. This is the reason why the temperature profile is better and as a consequence there is less discrepancy in the prediction of the Nusselt number by only 4%.

Models	u_τ	$Err(\%)$	T_τ	$Err(\%)$	Nu	$Err(\%)$
DNS [Versteegh and Nieuwstadt, 1996]	200.41	-	0.054	-	10.89	-
k-ω-SST	222.68	+11	0.0362	−33	8.047	−26
BL-$\overline{v^2}/k$	210.0	+4	0.0487	−10	10.23	−6
Launder-Sharma	197.11	−1.6	0.066	+21	13.06	+20
Launder-Sharma + Yap term	209.75	+4	0.042	−21	8.9	−17.96
DNS [Kiš and Herwig, 2014]	322	-	0.049	-	15.78	-
k-ω-SST	343.05	+6	0.036	−26	12.24	−22
BL-$\overline{v^2}/k$	328.98	+2	0.045	−8	15.06	−4
Launder-Sharma	312.9	−2	0.065	+32	20.43	+29
Launder-Sharma + Yap term	327.31	+1	0.04	−18	13	−15

Table 3.1 – Comparison of friction velocity, friction temperature and Nusselt number

3.4.4 Effect of Yap term in the Launder-Sharma model

It is well known that when boundary layers are out of equilibrium, the $k-\varepsilon$ model gives large near-wall length scales [Hanjalić and Launder, 1972, Rodi and Scheuerer, 1984]. The problem becomes more severe in separated flows when an equation of ε is solved up to the wall instead of using wall functions. While studying heat transfer in an abrupt pipe enlargement, Yap [1987] noticed that Nusselt number is some five times that of experimental value in the proximity of the reattachment point. To avoid this problem, near-wall modifications were proposed by introducing the source term in the ε equation [Yap, 1987], which is expressed as follows.

$$S_\varepsilon = 0.83\left(\frac{k^{3/2}}{c_l \varepsilon y} - 1\right)\left(\frac{k^{3/2}}{c_l \varepsilon y}\right)^2 \frac{\tilde{\varepsilon}^2}{k} \tag{3.47}$$

Where y is the distance from the wall and $c_l(=2.5)$ represents the slope of the turbulent length scale ($\frac{k^{3/2}}{\varepsilon}$) in the near-wall region. $\frac{k^{3/2}}{\varepsilon}$ becomes large as compared to $c_l y$ in a near-wall separated region. The role of S_ε is to drive the length scale level toward its local equilibrium value.

Considering the extra source term (S_ε), the dissipation equation of the Launder-Sharma

model is expressed as follows:

$$\frac{\partial\widetilde{\varepsilon}}{\partial t}+U_j\frac{\partial\widetilde{\varepsilon}}{\partial x_j}=\frac{\partial}{\partial x_j}\left[\left(\nu+\frac{\nu_t}{\sigma_\varepsilon}\right)\frac{\partial\varepsilon}{\partial x_j}\right]-C_{\varepsilon1}f_1\frac{\widetilde{\varepsilon}}{k}\overline{u_i{}'u_j{}'}\frac{\partial U_i}{\partial x_j}-C_{\varepsilon2}f_2\frac{\widetilde{\varepsilon^2}}{k}+2\nu\nu_t\left(\frac{\partial^2U}{dy^2}\right)+S_\varepsilon \quad (3.48)$$

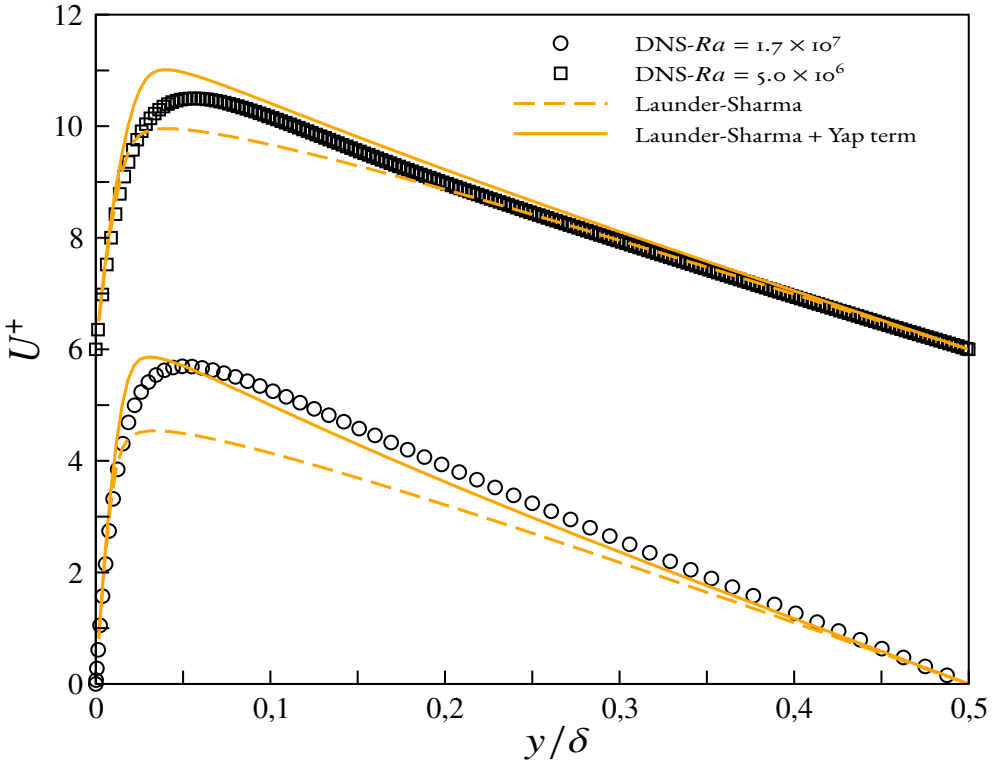

Figure 3.23 – Mean velocity at $Ra = 5 \times 10^6$ [Versteegh and Nieuwstadt, 1996](denoted by □) and $Ra = 1.7 \times 10^7$ [Kiš and Herwig, 2014](denoted by ○) [Plots are shifted for clarity]

Looking into the Fig. 3.23, it is realized that the introduction of the Yap term makes an improvement in the mean velocity. Moreover, the Yap term corrects the Reynolds shear stress distribution, particularly close to the wall as can be seen in Fig. 3.24. To look further into this, turbulent viscosity profile is analyzed which shows drastic improvement in the prediction of turbulent viscosity with the addition of Yap term as shown in Fig. 3.25. Furthermore, by looking into the profile of wall-normal heat flux as shown in Fig. 3.27, it is observed that the introduction of Yap term leads to underestimate $\overline{v'\theta}$ which yields an overestimation of T^+ (as shown in Fig. 3.26) for the compensation in the energy balance. However, the error in Nusselt number prediction is slightly improved by introducing Yap term as can be seen in Table. 3.1.

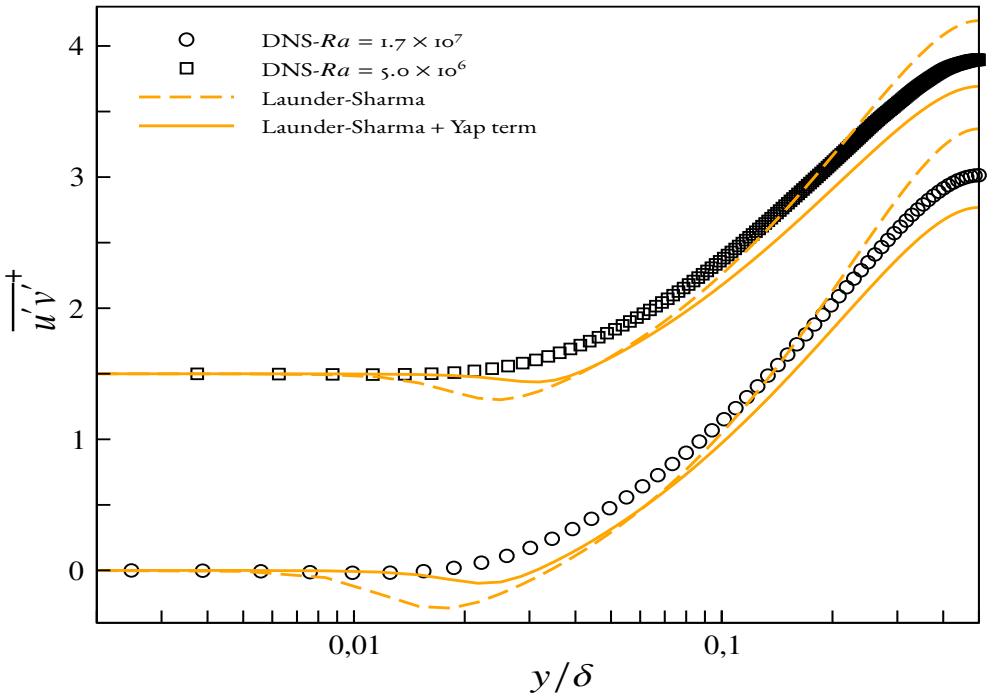

Figure 3.24 – Reynolds shear stress at $Ra = 5 \times 10^6$ [Versteegh and Nieuwstadt, 1996](denoted by □) and $Ra = 1.7 \times 10^7$ [Kiš and Herwig, 2014](denoted by ○) [Plots are shifted for clarity]

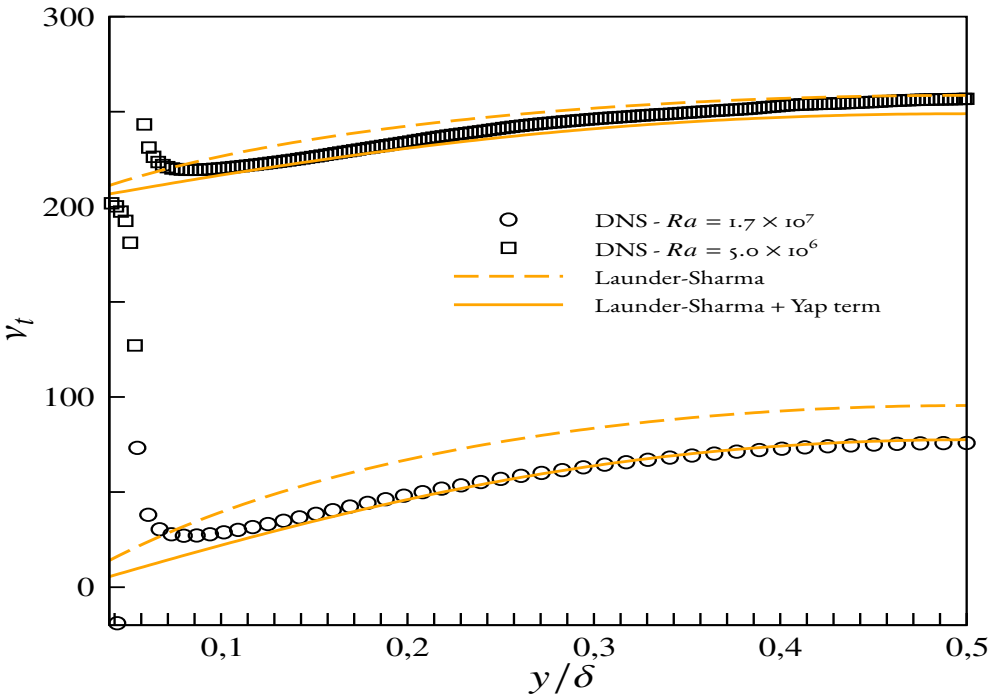

Figure 3.25 – Turbulent viscosity at $Ra = 5 \times 10^6$ [Versteegh and Nieuwstadt, 1996](denoted by □) and $Ra = 1.7 \times 10^7$ [Kiš and Herwig, 2014](denoted by ○) [Plots are shifted for clarity]

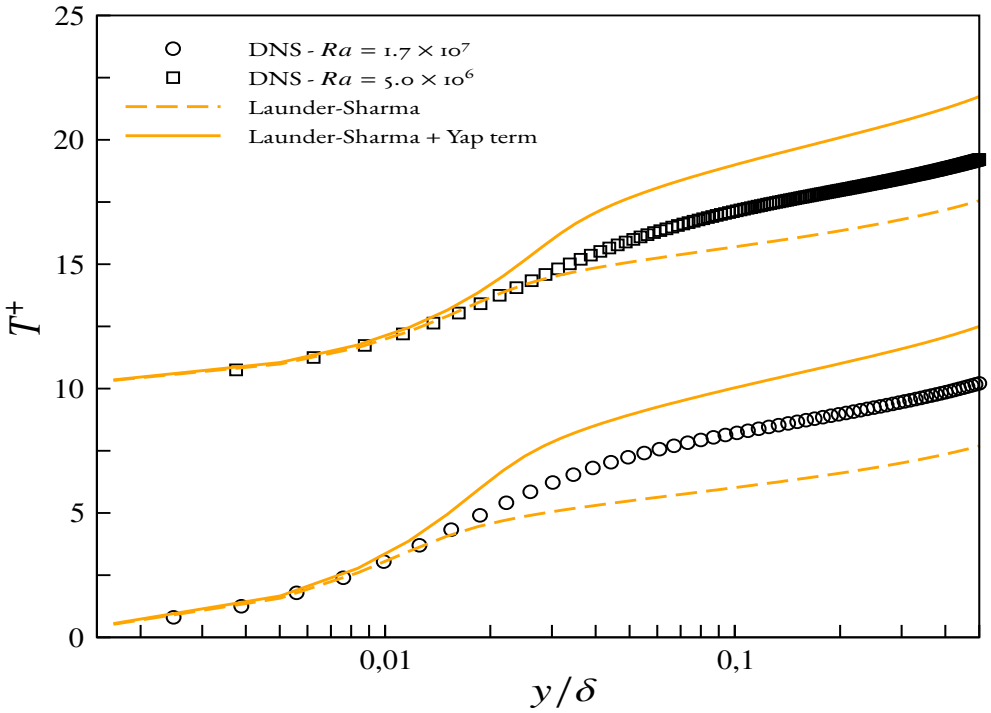

Figure 3.26 – Mean temperature at $Ra = 5 \times 10^6$ [Versteegh and Nieuwstadt, 1996](denoted by □) and $Ra = 1.7 \times 10^7$ [Kiš and Herwig, 2014](denoted by ○) [Plots are shifted for clarity]

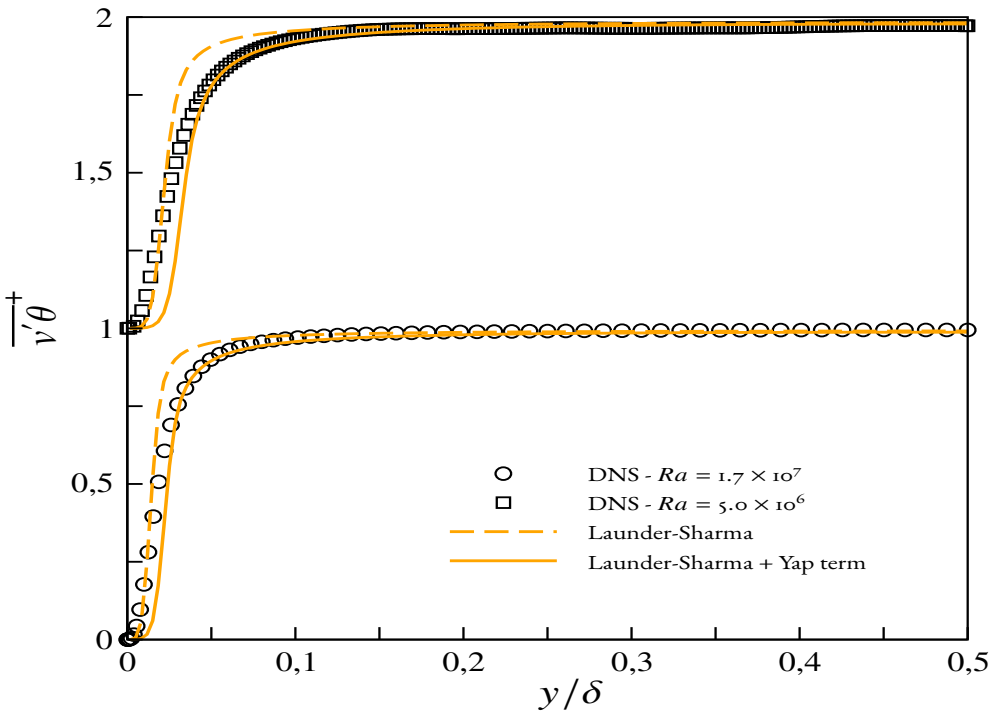

Figure 3.27 – Wall-normal heat flux at $Ra = 5 \times 10^6$ [Versteegh and Nieuwstadt, 1996](denoted by □) and $Ra = 1.7 \times 10^7$ [Kiš and Herwig, 2014](denoted by ○) [Plots are shifted for clarity]

3.5 Conclusion

A detailed comparison of three different turbulence models has been performed by computing three convection regimes namely forced, mixed, and natural convection respectively.

In the forced convection regime, the prediction of mean velocity by all the three turbulence models is in good agreement with the DNS data close to the wall, owing to the momentum balance. However, there are slight discrepancies in the logarithmic region. For the thermal characteristics, it has been observed that the mean temperature distributions are satisfactorily reproduced by all the three models with some discrepancy in the log region. To probe further in the logarithmic region, the von Karman constant (κ) and von Karman temperature constant (κ_t) are also analyzed: it has been inferred that the BL-$\overline{v^2}/k$ leads to the better predictions of these constants. Moreover, it is realized that there are severe underprediction of turbulent kinetic energy by k-ω-SST and Launder-Sharma models, although it is relatively better predicted by BL-$\overline{v^2}/k$ model. So the overall performance of the BL-$\overline{v^2}/k$ model in reproducing mean flow and turbulent quantity is satisfactory in comparison to the other two models.

A mixed convection flow has been computed in a differentially heated vertical channel, it has been observed that the buoyancy force has a considerable effect on the mean flow close to the wall as it drastically changes the near-wall balance of forces, which modify the shear stress distribution and turbulent kinetic energy production rate. All three turbulence models can satisfactorily predict mean velocity close to the wall. However, there is discrepancy in predictions in the center of the channel by the k-ω-SST and Launder-Sharma models. This discrepancy is due to the misprediction of turbulent shear stress, which affects the momentum balance and allows the mean velocity to be underpredicted by the k-ω-SST model and overpredicted by Launder-Sharma model respectively. Although, better prediction of mean velocity is observed with BL-$\overline{v^2}/k$ model. In addition to that, it has been observed that the BL-$\overline{v^2}/k$ model is able to better predict the turbulent kinetic energy. On the contrary, it is severely underpredicted by k-ω-SST and Launder-Sharma models. For the mean temperature predictions by the turbulence models, there is an overprediction of mean temperature by the k-ω-SST model; on the contrary, Launder-Sharma underpredicts it; BL-$\overline{v^2}/k$ comes out to be the model which better predicts the mean temperature. This prediction of the mean temperature is directly linked to the prediction of the wall-normal heat flux which is also modified due to buoyancy and better prediction of this turbulent heat flux component leads to better prediction of mean temperature as observed in the case of BL-$\overline{v^2}/k$ model. So, it is realized that the main effects (viz asymmetry of mean velocity and mean temperature) of buoyancy are reproduced by all the three models.

For the natural convection flow which is completely driven by buoyancy, results are compared against the two available benchmark DNS data bases which correspond to the high Rayleigh number. It has been observed that there is a severe overprediction of the mean

velocity by the k-ω-SST and BL-v^2/k models owing to the underprediction of the Reynolds shear stress. However, for the low-Reynolds number Launder-Sharma model, there is a severe underprediction of the mean velocity close to the wall. This discrepancy can be avoided to a certain extent by introducing an additional source term in the ε equation proposed by Yap [1987]. Moreover, for the predictions of the mean temperature distribution, it has been observed that the underpredictions of the wall-normal heat flux leads to the overprediction of the temperature profile and this behavior is reflected in the predictions by the k-ω-SST and BL-$\overline{v^2}/k$ model. On the contrary, the Launder-Sharma model underestimated the mean temperature and the inclusion of the Yap term leads to an overestimation of mean temperature. However, Nusselt number prediction is improved with the Yap term.

Finally after computing three different regimes it has been observed that the buoyancy has modified the flow significantly and selected baseline models are unable to predict the mean and turbulent quantities satisfactorily which is a major concern for industrial applications particularly in the thermal designing of the under-hood space of automobiles. This motives us to consider the modifications for these eddy-viscosity models in such a way that the effect of buoyancy can be introduced in the turbulence equations. The next chapter of this work is dedicated to the development of buoyancy sensitized turbulence models and to perform the detailed analysis of the several modifications which is affecting the predictions of turbulence models.

Chapter 4

Development of buoyancy extended models

Contents

4.1 Motivation and Objectives

This chapter describes the main contribution of this thesis by outlining the selected models in which various terms in the turbulence equations are modified.
The motivation of the work emanates from the problem faced by PSA Group in simulating natural convection flows in the underhood space of cars. As the available eddy-viscosity models in most of the commercial codes (particularly Ansys Fluent used by PSA group) are not accounting for buoyancy effects with sufficient accuracy, and it is not possible to rely on CFD of natural convection flows in the underhood space of cars. So the main objective of the work is to develop the span of buoyancy sensitized models by testing various modifications available in the literature. The modifications are done in three folds as mentioned below:
(1) Buoyancy extended eddy-viscosity models under algebraic forms.
(2) Simplified buoyancy-sensitized models.
(3) Effect of adding only buoyancy production terms.

4.2 Development of the full buoyancy-extended model

4.2.1 Explicit algebraic models

The explicit algebraic models are derived from the implicit algebraic models and the rationale of the explicit algebraic models involves the use of integrity bases that is the polynomial representations for isotropic tensor functions [Pope, 1975]. These types of models are developed to get an explicit solution and also to avoid the problem that is numerical stiffness occurs in the implicit models. One of the advantages of these models is that the saving of computational time is possible by avoiding the need for successive matrix inversions to formulate the Reynolds stresses for the set of mean velocity gradients [Demuren and Rodi, 1984]. This explicit algebraic methodology was used by many researchers such as Gatski and Speziale [1993], Girimaji [1996], Grundestam et al. [2005], Pope [1975], Rumsey et al. [2000]; among others. Accounting for the effects of buoyancy makes necessary the inclusion of large number of terms and lead to very complex explicit algebraic models [So et al., 2004, Vanpouille et al., 2015], which is not required in our work. Therefore, in the present work, a simpler approach is derived, based on implicit algebraic modeling.

4.2.2 Buoyancy-extended Boussinesq relation

Buoyancy driven flows show markedly different characteristics as compared to isothermal flows due to the influence of buoyancy forces on the internal structure of turbulent motions. Monin [1965] is the first among other workers who modeled buoyant effects on turbulence by using the transport equations for the Reynolds stresses and the heat fluxes.

The rationale behind his modeling approach is to have both the direct and indirect influence of the force field on Reynolds stresses and heat fluxes and it is assumed that the empirical correlations which were used for non-buoyant flows can be extrapolated to estimate the buoyancy effects.
Launder [1975] proposed the approximated set of equations for the turbulent stresses and the turbulent heat fluxes in a buoyancy affected shear flows. The approximation of these turbulent quantities was performed using the exact equation of the Reynolds stress and the heat fluxes and then assuming the model for the pressure-containing correlations which takes into account the buoyancy effects. These types of models were shown to give good results in free stratified shear flow and atmospheric flows [Gibson and Launder, 1978].
In this context, significant progress was recently achieved by using the elliptic blending concept to model the Reynolds stresses [Manceau, 2015] which is extended to turbulent heat flux so that near-wall effects can be taken into account [Choi et al., 2017, Dehoux et al., 2017].
The transport equation of Reynolds stresses is mentioned below:

$$\frac{D\overline{u_i'u_j'}}{Dt} = \mathcal{D}_{ij} - \underbrace{\overline{u_i'u_k'}\frac{\partial U_j}{\partial x_k} - \overline{u_j'u_k'}\frac{\partial U_i}{\partial x_k}}_{P_{ij}} - \underbrace{\beta(g_j\overline{u_i'\theta} + g_i\overline{u_j'\theta})}_{G_{ij}} - \underbrace{\overline{\frac{p'}{\rho}\left(\frac{\partial u_i'}{\partial x_j} + \frac{\partial u_j'}{\partial x_i}\right)}}_{\phi_{ij}} - \varepsilon_{ij} \tag{4.1}$$

where $\mathcal{D}_{ij}$ is the diffusion tensor. Buoyancy directly affects the dynamics of the Reynolds stress due to the buoyancy-production term G_{ij}. However, it also has an indirect influence through the redistribution term ϕ_{ij}. Indeed, ϕ_{ij} contains the contribution of three terms namely the slow-term, the rapid term, and the buoyancy term, respectively. The modeling of the slow-term is made by "the Rotta model" [Rotta, 1951] which is expressed as follows:

$$\phi_{ij}^1 = -C_1\frac{\varepsilon}{k}\left(\overline{u_i'u_j'} - \frac{2}{3}k\delta_{ij}\right) \tag{4.2}$$

For modeling the rapid term, Naot [1970] proposes the isotropization of production model which writes:

$$\phi_{ij}^2 = -C_2\left(P_{ij} - \frac{2}{3}\delta_{ij}P_k\right), \qquad C_2 = 0.6. \tag{4.3}$$

The buoyancy contribution to the pressure-strain can be modeled [Launder, 1975] by the by the isotropization of buoyancy production model.

$$\phi_{ij}^3 = -C_3\left(G_{ij} - \frac{2}{3}\delta_{ij}G_k\right), \qquad C_3 = 0.6. \tag{4.4}$$

The dissipation tensor (ε_{ij}) is modeled with the assumption that the small scale motion is isotropic for high Reynolds number flows, and the expression becomes:

$$\varepsilon_{ij} = \frac{2}{3}\varepsilon\delta_{ij} \tag{4.5}$$

As presented in Section 2.2.4, By assuming weak equilibrium hypothesis in Eq. (4.1), the algebraic relation for the Reynolds stresses become [Rodi, 1972]:

$$\overline{u_i'u_j'} = \frac{2}{3}k\delta_{ij} + \frac{k}{\varepsilon}\frac{1-C_2}{C_1+\frac{P+G}{\varepsilon}-1}\left(P_{ij}-\frac{2}{3}P\delta_{ij}\right) + \frac{k}{\varepsilon}\frac{1-C_2}{C_1+\frac{P+G}{\varepsilon}-1}\left(G_{ij}-\frac{1}{3}G_{kk}\delta_{ij}\right) \tag{4.6}$$

An interesting/favorable feature of this algebraic model as shown in Eq. (4.6) is that the buoyancy (G_{ij}) term is directly taken from the exact equation of the Reynold stress. Further simplification can be obtained using the strong equilibrium hypothesis which is expressed as follow:

$$\frac{P+G}{\varepsilon} = 1 \tag{4.7}$$

Following the proposal made by Davidson [1990], the first part of the relation is modeled by the Boussinesq constitutive relation and second part which represents the anisotropy due to buoyancy and it is directly taken from the Eq. (4.6). Now the buoyancy-extended Boussinesq relation for the Reynolds stress can be expressed as:

$$\begin{aligned}\overline{u_i'u_j'} &= \underbrace{\frac{2}{3}k\delta_{ij} - \nu_t\left(\frac{\partial U_i}{\partial x_j}+\frac{\partial U_j}{\partial x_i}\right)}_{Boussinesq} + \underbrace{C_\theta^*\tau(G_{ij}-\frac{1}{3}\delta_{ij}G_{kk})}_{Buoyancy-extension} \\ G_{ij} &= -\beta(g_j\overline{u_i'\theta} + g_i\overline{u_j'\theta})\end{aligned} \tag{4.8}$$

where the coefficient C_θ^* is to be calibrated.
In the present work, the same approach is adopted with the three very different eddy-viscosity based turbulence models namely k-ω-SST, BL-$\overline{v^2}/k$ and low-Reynolds number Launder-Sharma respectively.

4.2.3 Buoyancy-extended heat flux model

The same algebraic approach as adopted for the Reynolds stress is considered for the formulation of an algebraic turbulent heat flux model and the parent equation for the turbulent heat flux is expressed as follows:

$$\frac{D\overline{u_i'\theta}}{Dt} = \mathcal{D}_{\theta i} - \underbrace{\overline{u_i'u_k'}\frac{\partial T}{\partial x_k}}_{P_{\theta i}^{th}} - \underbrace{\overline{u_k'\theta}\frac{\partial U_i}{\partial x_k}}_{P_{\theta i}^{m}} - \underbrace{g_i\beta\overline{\theta^2}}_{G_{\theta i}} - \underbrace{\overline{\frac{\partial p}{\partial x_i}\frac{\theta}{\rho}}}_{\phi_{\theta i}} - \underbrace{(\nu+\alpha)\overline{\frac{\partial u_i'}{x_k}\frac{\partial\theta}{\partial x_k}}}_{\varepsilon_{\theta i}} \tag{4.9}$$

The pressure scrambling term ($\phi_{\theta i}$) has a significant effect on the turbulent heat fluxes. This term involves the contribution of three terms namely slow, rapid, and buoyant terms,

respectively.

$$\phi_{\theta i} = \underbrace{\phi^1_{\theta i}}_{Slow-term} + \underbrace{\phi^2_{\theta i}}_{Rapid-term} + \underbrace{\phi^3_{\theta i}}_{Buoyancy-term} \tag{4.10}$$

For the slow term, the Monin [1965] model is considered which is based on the return to isotropy approximation and is expressed as follow:

$$\phi^1_{\theta i} = -C_{\theta 1}\overline{\theta u_i'}\frac{1}{\tau} \tag{4.11}$$

The model of the rapid term by Owen [1974] is considered which is based on isotropization of production due to velocity gradient and is given as follow:

$$\phi^2_{\theta i} = C_{\theta 2}\overline{u_k'\theta}\frac{\partial U_i}{\partial x_k} \tag{4.12}$$

The effect of buoyancy on the pressure-scrambling term is denoted by ${\phi_{\theta i}}^3$ and the modeling of this term is based on isotropization of buoyancy production as proposed by Owen [1974] and is expressed as follows:

$$\phi^3_{\theta i} = C_{\theta 3}\beta g_i\overline{\theta^2} \tag{4.13}$$

Under the assumption that the major contribution to $\varepsilon_{\theta i}$ comes from the finest scale eddies and that these eddies are isotropic, the contribution of $\varepsilon_{\theta i}$ to turbulent heat flux can be neglected which yields:

$$\varepsilon_{\theta i} = 0 \tag{4.14}$$

since the only isotropic vector is the zero vector.
As presented in Section 2.2.4, considering the weak equilibrium hypothesis and the proposed models for pressure scrambling and dissipation in the transport equation of heat flux (Eq. 4.9) lead to the algebraic relation for heat flux expressed as follows:

$$\overline{u_i'\theta} = \frac{\overline{u_i'u_k'}\frac{\partial T}{\partial x_k} + \xi\overline{u_k'\theta}\frac{\partial U_i}{\partial x_k} + \eta\beta g_i\overline{\theta^2}}{-C_{\theta 1}\frac{\varepsilon}{k} + \frac{1}{\overline{\theta^2}}\left(\overline{u_k'\theta}\frac{\partial T}{\partial x_k} + \varepsilon_\theta\right) + \frac{1}{2k}\left(\overline{u_i'u_k'}\frac{\partial U_i}{\partial x_k} + \beta g_i\overline{u_i'\theta} + \varepsilon\right)} \tag{4.15}$$

where $\xi = (1 - C_{\theta 2})$ and $\eta = (1 - C_{\theta 3})$, respectively. Simplification of this algebraic heat flux form can be obtained by considering the strong equilibrium hypothesis ($P + G = \varepsilon$ and $P_\theta = \varepsilon_\theta$) in the Eq. 4.15 which yields:

$$\overline{u_i'\theta} = -\frac{1}{C_{\theta 1}}\frac{k}{\varepsilon}\left(\overline{u_i'u_k'}\frac{\partial T}{\partial x_k} + \xi\overline{u_k'\theta}\frac{\partial U_i}{\partial x_k} + \eta\beta g_i\overline{\theta^2}\right) \tag{4.16}$$

This relation for the heat flux model needs the temperature variance equation to be solved. In the present work, the generalized gradient diffusion hypothesis (GGDH) is considered to model heat fluxes, where the anisotropy of turbulence is taken into account from the

first term of the Eq. (4.16). The generalized gradient diffusion hypothesis (GGDH) for turbulent heat fluxes thus writes:

$$\begin{aligned}\overline{u_i'\theta} &= -C_\theta \frac{k}{\varepsilon}\left[(\overline{u_i'u_j'})_{Boussinesq} + (\overline{u_i'u_j'})_{Buoyancy-extension}\right]\frac{\partial T}{\partial x_j} \\ &= -C_\theta \frac{k}{\varepsilon}\left[\underbrace{\left\{\frac{2}{3}k\delta_{ij} - \nu_t\left(\frac{\partial U_i}{\partial x_j} + \frac{\partial U_j}{\partial x_i}\right)\right\}}_{Boussinesq} + \underbrace{\left\{C_\theta^*\tau(G_{ij} - \frac{1}{3}\delta_{ij}G_{kk})\right\}}_{Buoyancy-extension}\right]\frac{\partial T}{\partial x_j}\end{aligned} \tag{4.17}$$

where C_θ^* is to be calibrated.

4.2.4 Constraint and formulation of C_θ

One of the main constraints in our work is that the eddy-viscosity models should be modified in such a way that the buoyancy-extended model will revert back to the original eddy-viscosity model when the effect of buoyancy is negligible (forced convection flows). In forced convection flows, the influence of buoyancy is negligible such that Eq. (4.8) reduce to Boussinesq relation, but the use of the GGDH (Eq. 4.17) instead of SGDH implies to pay a careful attention to the coefficient C_θ. To avoid the modification of the predictions in a thermal boundary layer in the forced convection regime, in which temperature profile is driven by the wall-normal turbulent heat flux (say $\overline{v'\theta}$), the model must revert to the original model, such that

$$\overline{v'\theta} = \underbrace{-\frac{\nu_t}{Pr_t}\frac{\partial T}{\partial y}}_{SGDH} = \underbrace{-C_\theta \tau \overline{v^2}\frac{\partial T}{\partial y}}_{GGDH} \tag{4.18}$$

Since the turbulent viscosity (ν_t) for k-ω-SST and BL-$\overline{v^2}/k$ is expressed as follows:

$$\begin{aligned}\nu_t &= \frac{a_1 k}{max(a_1\omega, SF_2)} \\ \nu_t &= C_\mu \varphi k \tau\end{aligned} \tag{4.19}$$

Using the Eq.(4.18) and Eq.(4.19), and noting that, with the Boussinesq relation, $\overline{v^2} = 2/3k$, the final expression of C_θ for k-ω-SST and BL-$\overline{v^2}/k$ model become:

$$\begin{aligned}C_\theta &= \frac{3}{2}\frac{C_\mu}{Pr_t}\frac{a_1\omega}{max(a_1\omega, SF_2)} \\ C_\theta &= \frac{3}{2}\frac{C_\mu}{Pr_t}\varphi\end{aligned} \tag{4.20}$$

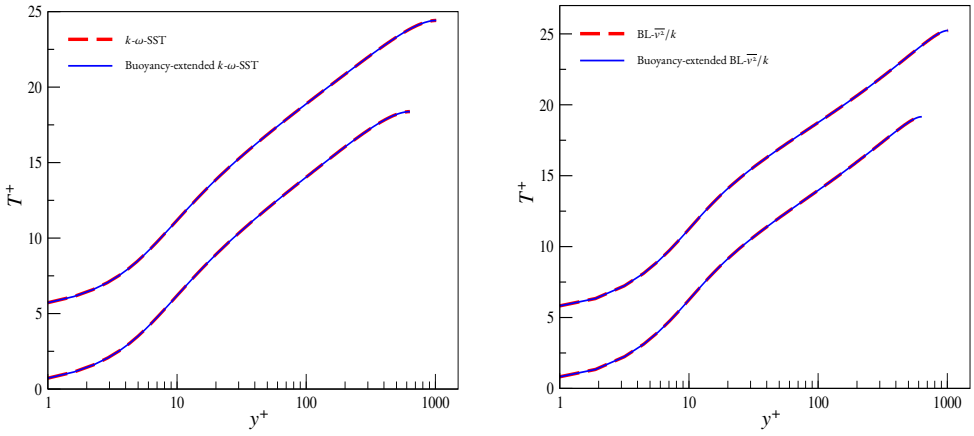

(a) (b)

Figure 4.1 – Effect of the formulation of C_θ on mean temperature profile at $Re_\tau = 640$ & $Re_\tau = 1020$ and $Pr = 0.71$

Simulation of forced convection in a differentially heated channel corresponding to two friction Reynolds number ($Re_\tau = 640$ & $Re_\tau = 1020$) has been performed. Mean temperature distribution is shown in Fig. 4.1, it is realized that the prediction with these buoyancy-extended models remain the same as with the original models and this confirms that the buoyancy-extended model reverts back to the original model when the buoyancy effects are negligible.

4.2.5 Buoyancy-extended k-ω-SST model

In this part of the chapter, a buoyancy-extended k-ω-SST model is formulated and validation is performed in two different convection regimes, namely mixed and natural convection flows in a differentially heated channel. The buoyancy extended Reynolds stress relation for k-ω-SST model is expressed as follows:

$$\overline{u_i' u_j'} = \underbrace{\frac{2}{3}k\delta_{ij} - \nu_t\left(\frac{\partial U_i}{\partial x_j} + \frac{\partial U_j}{\partial x_i}\right)}_{Boussinesq} + \underbrace{C_\theta^* \frac{1}{C_\mu \omega}(G_{ij} - \frac{1}{3}\delta_{ij}G_{kk})}_{Buoyancy-extension} \tag{4.21}$$

where the turbulent time scale for the model writes:

$$\tau = \frac{1}{C_\mu \omega} \tag{4.22}$$

By taking into account the buoyancy contribution, buoyancy extended heat flux relation for the k-ω-SST model is described as follows:

$$\overline{u_i'\theta} = -\frac{3}{2}\frac{1}{Pr_t}\frac{a_1}{max(a_1\omega, SF_2)}\left[(\overline{u_i' u_j'})_{Boussinesq} + (\overline{u_i' u_j'})_{Buoyancy-extension}\right]\frac{\partial T}{\partial x_j} \tag{4.23}$$

where the first term $\left(\frac{3}{2}\frac{1}{Pr_t}\frac{a_1}{max(a_1\omega,SF_2)}\right)$ in Eq. (4.23) comes from Eq. (4.20). This buoyancy-modified Reynolds stress and heat flux relations are used in the momentum and energy equations. The effect of the buoyancy extension should also be considered in the dynamic production of turbulent kinetic energy as expressed by the following equation:

$$P_k = -\left[(\overline{u_i{}' u_j{}'})_{Boussinesq} + (\overline{u_i{}' u_j{}'})_{Buoyancy-extension}\right]\frac{\partial U_i}{\partial x_j} \tag{4.24}$$

Buoyancy production terms in the transport equation of turbulent kinetic energy and dissipation equations become:

$$\begin{aligned} G_k &= -\beta g_i \overline{u_i'\theta} \\ G_\omega &= \frac{\gamma}{\nu_t} max(G_k, 0) \end{aligned} \tag{4.25}$$

where $C_\theta^* = 0.1$ and other coefficients are the same as per original k-ω-SST model [Menter, 1994].
In the next part of this section, the description of the buoyancy-extended BL-$\overline{v^2}/k$ model is presented.

4.2.6 Buoyancy-extended BL-$\overline{v^2}/k$ model

In this part of the chapter, the buoyancy extension is provided in the Reynolds stress and heat flux equation in the framework of the BL-$\overline{v^2}/k$ model. Similar to the formulation as discussed in Section 4.2.5 for the k-ω-SST model, the buoyancy-extended Reynolds stress relation for the BL-$\overline{v^2}/k$ model writes:

$$\overline{u_i' u_j'} = \underbrace{\frac{2}{3}k\delta_{ij} - \nu_t\left(\frac{\partial U_i}{\partial x_j} + \frac{\partial U_i}{\partial x_j}\right)}_{Boussinesq} + \underbrace{C_\theta^*\tau(G_{ij} - \frac{1}{3}\delta_{ij}G_{kk})}_{Buoyancy-extension} \tag{4.26}$$

where $C_\theta^* = 0.1$ and $\tau = \sqrt{\left(\frac{k}{\varepsilon}\right)^2 + {C_T}^2\left(\frac{k}{\varepsilon}\right)}$ respectively.
The buoyancy-extended heat flux relation for the BL-$\overline{v^2}/k$ model is described as follows:

$$\overline{u_i'\theta} = -\frac{3}{2}\frac{C_\mu}{Pr_t}\varphi\tau\left((\overline{u_i'u_j'})_{Boussinesq} + (\overline{u_i'u_j'})_{Buoyancy-extension}\right)\frac{\partial T}{\partial x_j} \tag{4.27}$$

where the first term $\left(\frac{3}{2}\frac{C_\mu}{Pr_t}\varphi\tau\right)$ in Eq. (4.27) comes from Eq. (4.20). Buoyancy-extended Reynolds stress and heat flux relations must be considered in the momentum and energy equation. The buoyancy extension is also considered in dynamic production (P_k) of

turbulent kinetic energy and expressed as follows:

$$P_k = -\left((\overline{u_i' u_j'})_{Boussinesq} + (\overline{u_i' u_j'})_{Buoyancy-extension} \right) \frac{\partial U_i}{\partial x_j} \tag{4.28}$$

Buoyancy production terms in the transport equation of turbulent kinetic energy and dissipation equation are modeled using generalized gradient diffusion hypothesis (GGDH) and expressed as follows:

$$\begin{aligned} G_k &= -\beta g_i \overline{u_i' \theta} \\ G_\varepsilon &= C_{\varepsilon 1} \frac{1}{\tau} max(G_k, 0) \end{aligned} \tag{4.29}$$

Note that the models developed above are called "Full buoyancy-extended" to distinguish them from the simplified version developed in the next section.

4.2.7 Validation in the channel flow in the natural convection regime

In order to investigate the performance of the buoyancy-extended models proposed in the previous section, the well-documented differentially heated channel is considered and shown in Fig. 4.2. The flow in a tall or infinite vertical cavity is considered to be extremely challenging for modeling due to the subtle couplings between dynamic and turbulent thermal fields. The recent DNS data of Kiš and Herwig [2014] is particularly relevant due to the realistic values of the Rayleigh number. The highest Rayleigh number, $Ra = \beta g \Delta T \delta^3/(\nu\kappa)$ available, $Ra = 1.7 \times 10^7$ is based on the width of the channel. Due to the antisymmetry of the configuration, only the hot side of the flow is plotted. In order to help the comparison of the predictions of the models against DNS data, mean and turbulent quantities are plotted in wall units on the ordinate axis. However, the abscissa axis is plotted in computational units.

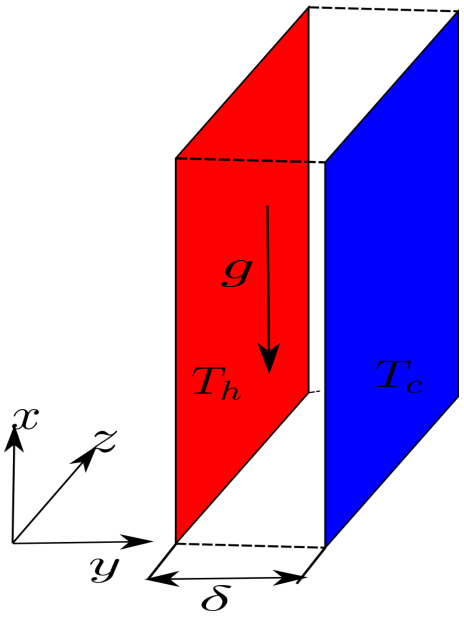

Figure 4.2 – Flow configuration for the differentially heated vertical channel

In general, turbulence models including Reynolds stress models have a tendency to overestimate the mean velocity peak and this is also the case with the original k-ω-SST and BL-$\overline{v^2}/k$ models as shown in Fig. 4.3 and this is supplemented by the overestimation of friction velocity as can be seen in Table. 4.1.

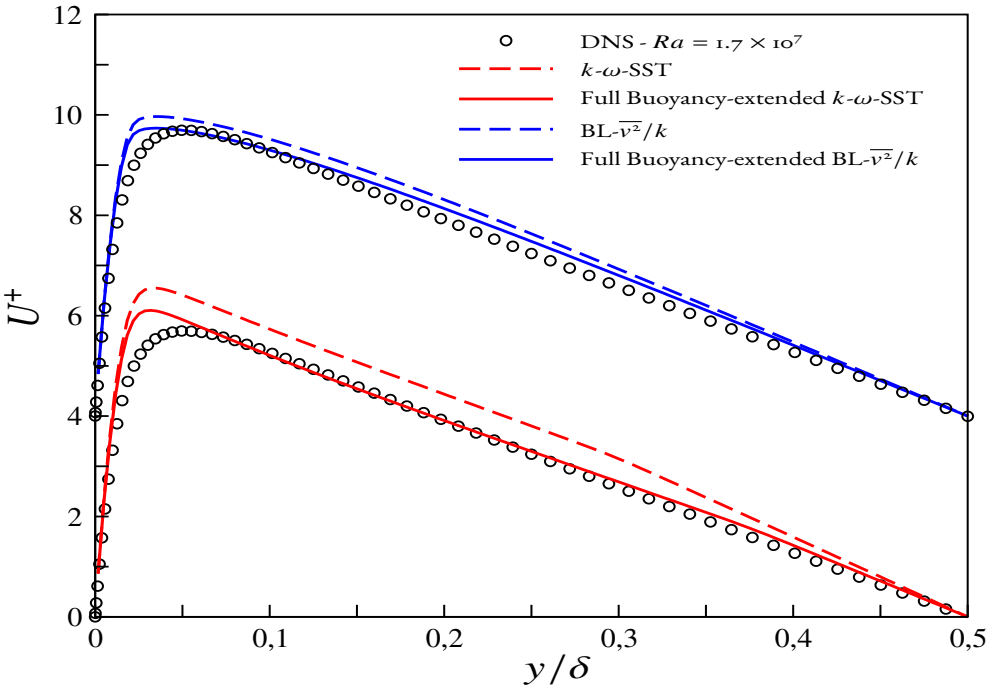

Figure 4.3 – Mean velocity profile at Ra $= 1.7 \times 10^7$ [Kiš and Herwig, 2014] [Plots are shifted for clarity]

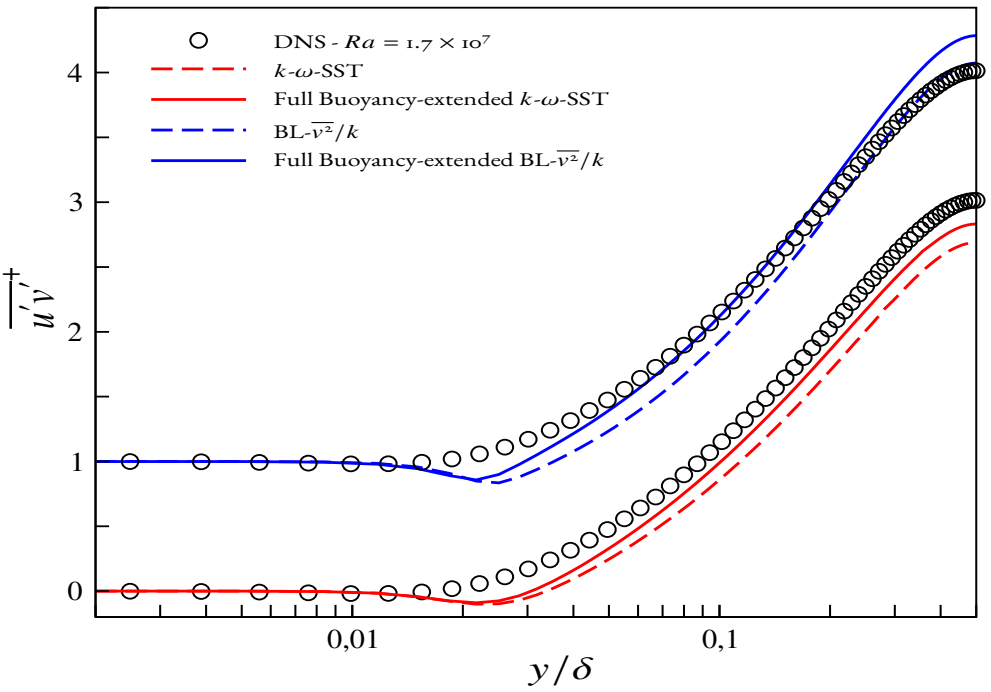

Figure 4.4 – Reynolds shear stress profile at Ra $= 1.7 \times 10^7$ [Kiš and Herwig, 2014] [Plots are shifted for clarity]

This limitation is directly linked to a severe underestimation of Reynolds shear stress

$(\widetilde{u'v'})$ as can be seen in Fig. 4.4. To probe further, integrating the momentum balance in the x-direction between the hot wall and to some distance y yields

$$0 = \int_0^y \nu \frac{\partial^2 \widetilde{U}}{\partial \widetilde{y}^2} d\widetilde{y} - \int_0^y \frac{\partial \widetilde{u'v'}}{\partial \widetilde{y}} d\widetilde{y} + \int_0^y \widetilde{\beta} g(\widetilde{T} - \widetilde{T}_{ref}) d\widetilde{y} \tag{4.30}$$

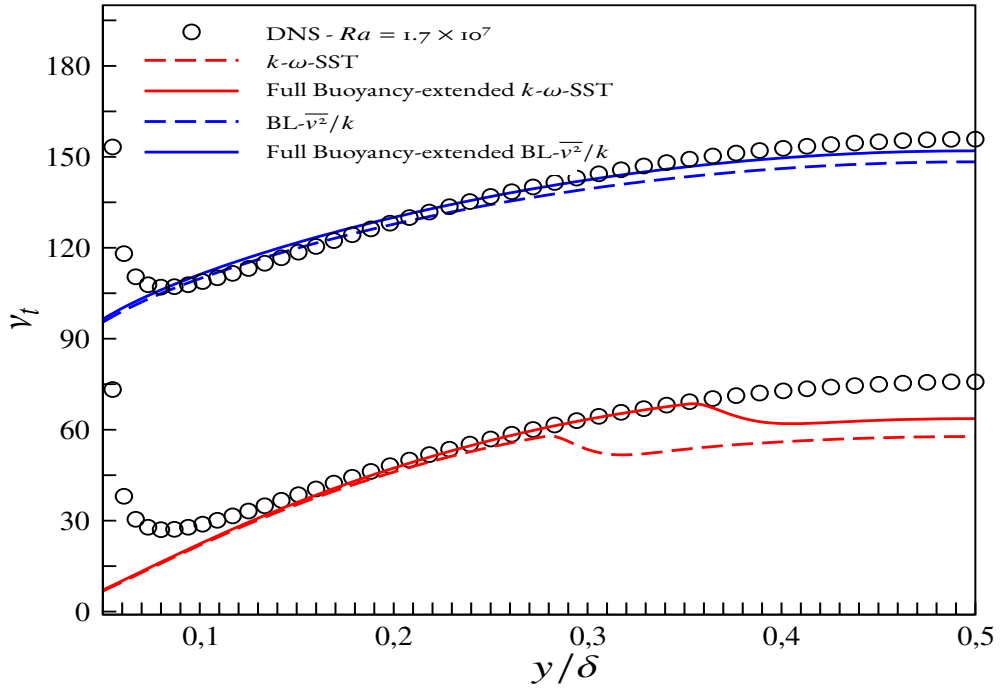

Figure 4.5 – Turbulent viscosity profile Ra $= 1.7 \times 10^7$ [Kiš and Herwig, 2014] [Plots are shifted for clarity]

For y located between the peak of mean velocity and center of the channel, the contribution of buoyancy force must be balanced by the viscous friction at the wall and the sum of viscous friction and turbulent shear stress in y, which is directed downwards such that

$$\int_0^y \widetilde{\beta} g(\widetilde{T} - \widetilde{T}_{ref}) d\widetilde{y} = \rho {u_\tau}^2 - \nu \frac{\partial \widetilde{U}}{\partial \widetilde{y}} + \widetilde{u'v'} \tag{4.31}$$

From Fig. 4.4, it is observed that the turbulent stress is severely underestimated, which is compensated by the viscous stresses in such a manner that the negative slope of mean velocity and friction velocity are both overestimated. This shortcoming of Boussinesq constitutive relation is corrected by the buoyancy extension in Eq. (4.21), which in the present case reads:

$$\widetilde{u'v'} = -\nu_t \frac{\partial \widetilde{U}}{\partial \widetilde{y}} + C_\theta^* \tau \widetilde{\beta} g \widetilde{v'\theta} \tag{4.32}$$

In Fig. 4.8, $\overline{v'\theta}$ is positive such that the buoyancy extension enhances the turbulent shear stress, and owing to this, the balance in Eq. (4.31) is improved. Viscous friction does not

need to be overestimated to compensate for the lack of turbulent stress, and eventually the velocity gradient is corrected.
Looking into the turbulent viscosity distribution, it is observed that the inclusion of this buoyancy extension leads to the improvement in the prediction of turbulent viscosity which is severely underestimated by both the original k-ω-SST and BL-$\overline{v^2}/k$ models over a large part of the channel as shown in Fig. 4.5. This behavior is due to the increase in the total production ($P_k + P_{buo-extension} + G_k$) far from the wall as shown in Fig. 4.6, owing to the inclusion of buoyancy production terms namely G_k and $P_{buo-extension}$ which is missing in the original models.

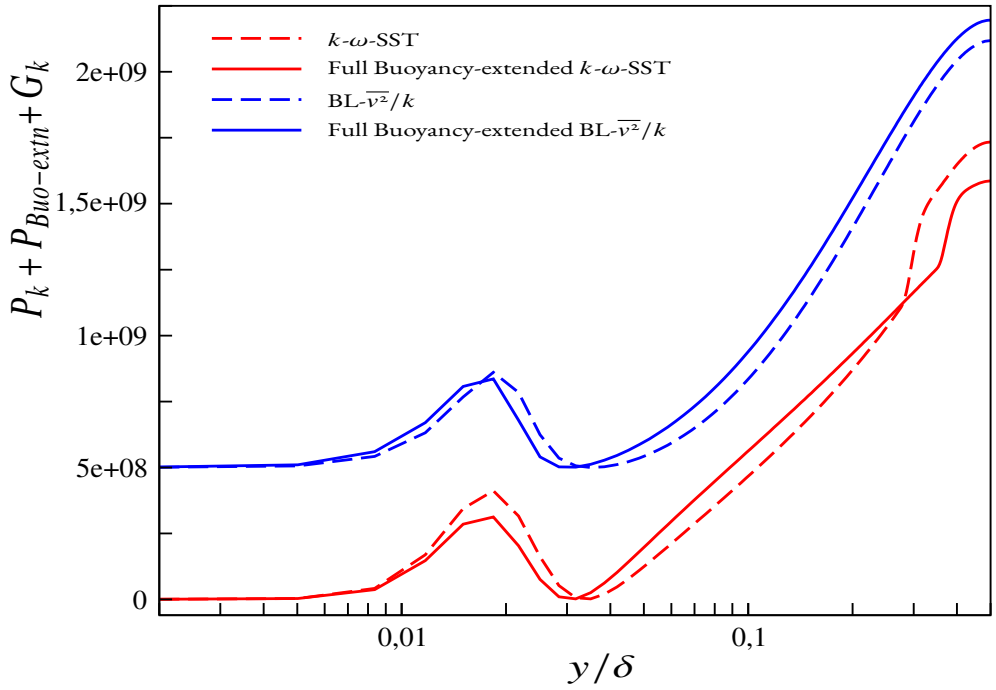

Figure 4.6 – Total production of turbulent kinetic energy profile at Ra = 1.7×10^7 [Kiš and Herwig, 2014] [Plots are shifted for clarity]

In order to understand the effect of buoyancy extension on thermal characteristics, the mean temperature distribution is plotted in wall units and shown in Fig. 4.7. It is observed that the buoyancy extension leads to the improvement of the predictions, although it is not sufficient for the k-ω-SST model.

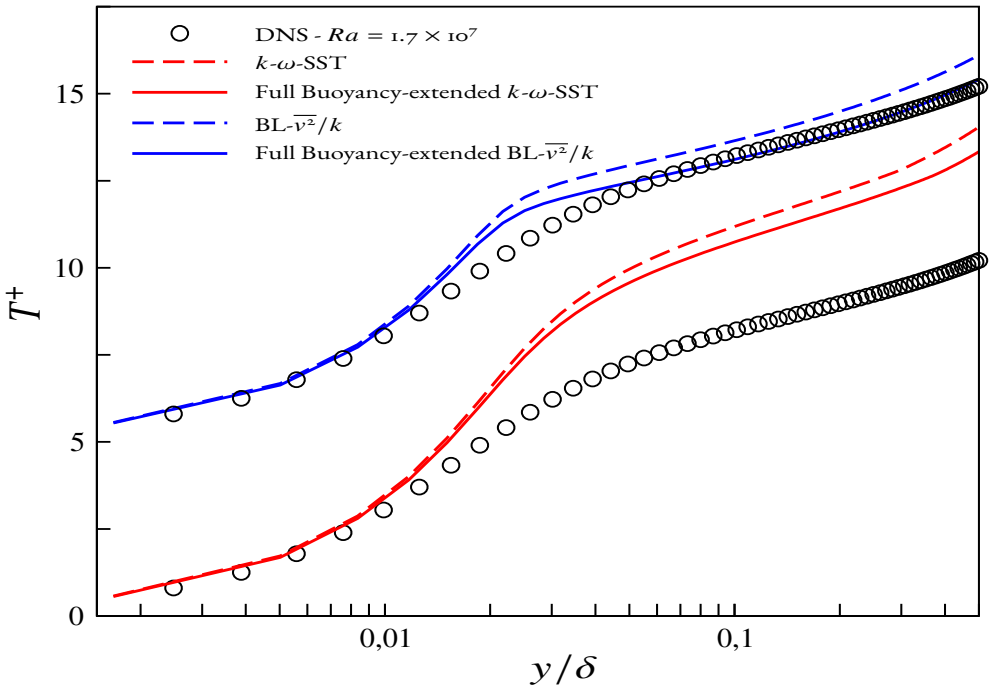

Figure 4.7 – Mean temperature profile at Ra $= 1.7 \times 10^7$ [Kiš and Herwig, 2014] [Plots are shifted for clarity]

To probe the influence of the buoyancy extension on the energy balance, the temperature equation is integrated between the wall and an arbitrary point y, which yields

$$0 = \int_0^y \alpha \frac{\partial^2 \widetilde{T}}{\partial \widetilde{y}^2} d\widetilde{y} - \int_0^y \frac{\partial \widetilde{\overline{v'\theta}}}{\partial \widetilde{y}} d\widetilde{y} \tag{4.33}$$

The heat flux at the wall must be balanced by the sum of the molecular and turbulent heat fluxes. In the wall units, the heat flux at the wall is unity and the balance reduces to

$$1 = -\frac{1}{Pr}\frac{\partial T^+}{\partial \widetilde{y}} + \widetilde{\overline{v'\theta}}^+ \tag{4.34}$$

In order to satisfy this balance, $\overline{v'\theta}^+$ goes to one far from the wall (where molecular heat flux is negligible) as shown in Fig. 4.8 and it does not depend on the heat flux model. Integrating Eq. (4.34) between the wall and arbitrary distance y leads to

$$\frac{T^+}{Pr} = \widetilde{y} - \int_0^y \widetilde{\overline{v'\theta}} d\widetilde{y} \tag{4.35}$$

Eq. (4.35) shows that the departure from the laminar profile is due to the integral of the turbulent heat flux.

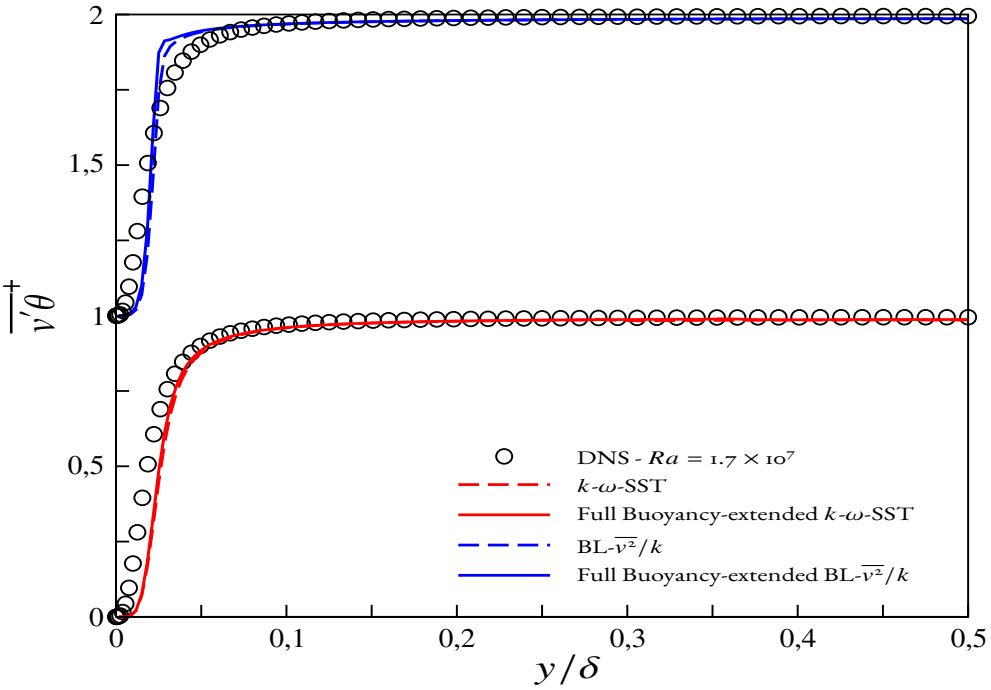

Figure 4.8 – Wall normal heat flux profile at Ra $= 1.7 \times 10^7$ [Kiš and Herwig, 2014] [Plots are shifted for clarity]

The misprediction of the temperature profiles as shown in Fig. 4.7 is specifically related to the fact that $\overline{v'\theta}^+$ is underestimated. By providing the buoyancy contribution which is positive as expressed below,

$$\underbrace{\widetilde{\overline{v'\theta}}}_{Buo} = \frac{1}{3}\frac{C_\theta^*}{C_\mu \omega}\widetilde{\beta g \overline{u'\theta}} \tag{4.36}$$

there is an improvement in the prediction of mean temperature, although the improvement is insufficient.

The buoyancy-extended BL-$\overline{v^2}/k$ model yields satisfactory velocity and temperature profiles. In contrast, for the k-ω-SST model, the buoyancy extension very significantly improve the prediction of velocity, but does not succeed in fully correcting the temperature profile. This behavior is summarised by Table 4.1, where it can be seen that the prediction of u_τ, U_{max} and T_τ are significantly improved by the buoyancy-extension for the two models. It is noticeable, as can be seen in Fig. 4.3, that, although the correction is the same for the two models., with the same coefficient $C_\theta^* = 0.1$, the amplitude of the correction depends upon the initial error. This can be traced to the fact that this extension is not an ad hoc correction, but a physically based term. The absence of this term in the original models leads to a misrepresentation of the balance 4.31, compensated by an overestimation of the velocity gradients which depends on the model. The introduction of the buoyancy extension restores the correct balance. Another favorable aspect of this modification is that it fulfills the forced convection constraint where the modified models revert back to the original model when the buoyancy has negligible influence.

Models	u_τ	$Err(\%)$	U_{max}	$Err(\%)$	T_τ	$Err(\%)$
DNS Kiš and Herwig [2014]	322	-	5.69	-	0.049	-
k-ω-SST	343.05	+6	6.55	+15	0.036	−26
BL-$\overline{v^2}/k$	328.98	+2	5.96	+5	0.045	−8
Buoyancy-extended k-ω-SST	334.44	+4	6.10	+7	0.038	−22
Buoyancy-extended BL-$\overline{v^2}/k$	326.06	+1	5.73	+0.7	0.048	−2

Table 4.1 – Comparison of friction velocity, friction temperature and friction temperature

4.2.8 Validation in the channel flow in the mixed convection regime

In this part of the section, an analysis of buoyancy extended k-ω-SST and BL-$\overline{v^2}/k$ models is performed by simulating differentially heated mixed convection flow and results are compared with DNS data of Kasagi and Nishimura [1997] corresponding to $Gr = 9.6 \times 10^5$ and $Pr = 0.71$. The schematic diagram of the mixed convection in a vertical channel is shown in Fig. 4.9

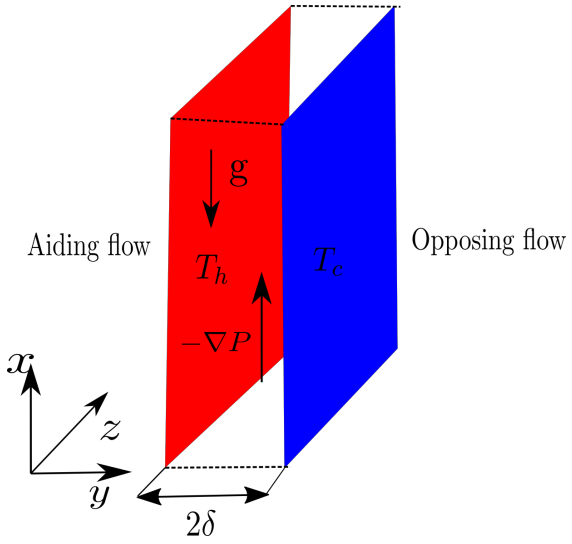

Figure 4.9 – Channel flow configuration for the mixed convection regime

The mean velocity profile for aiding side is shown in Fig. 4.10 and it is observed that there is an improvement in the prediction with the buoyancy-extended models. The amplitude of the improvement is modest owing to the modest influence of buoyancy in this configuration. In order to better understand the influence of the buoyancy extension, we need to consider the predictions of the shear stress ($\overline{u'v'}$) which is playing a crucial role in the momentum balance. On the aiding side, by integrating the momentum equation

from the hot wall to some distance y, the momentum equation becomes:

$$\widetilde{\nu}\frac{d\widetilde{U}}{d\widetilde{y}} - \underbrace{\widetilde{\nu}\frac{d\widetilde{U}}{d\widetilde{y}}\bigg|_{y=0}}_{\rho {u_\tau}^2} - \widetilde{\overline{u'v'}} + \frac{Gr}{8Re_\tau}\int_0^y (\widetilde{T} - \widetilde{T_{ref}}) = \widetilde{y}\frac{1}{\rho}\frac{\partial \widetilde{P^*}}{\partial \widetilde{x}} \tag{4.37}$$

From Eq. (4.37), it can be seen that the pressure gradient is balanced by three forces namely, viscous stress, turbulent shear stress, and buoyancy force. On the aiding side, there is an overprediction of the shear stress ($\overline{u'v'}$) with original models particularly with the k-ω-SST as showed in Fig. 4.11. However, this overprediction is reduced to some extent with the buoyancy extended models. Owing to the limited contribution of Reynolds stresses due to buoyancy, this slight improvement of Reynolds shear stress restricts the underprediction of viscous stress to a certain extent which in turn allows the friction velocity to increase and leads to the marginal improvement in the mean velocity predictions as shown in Fig. 4.10.

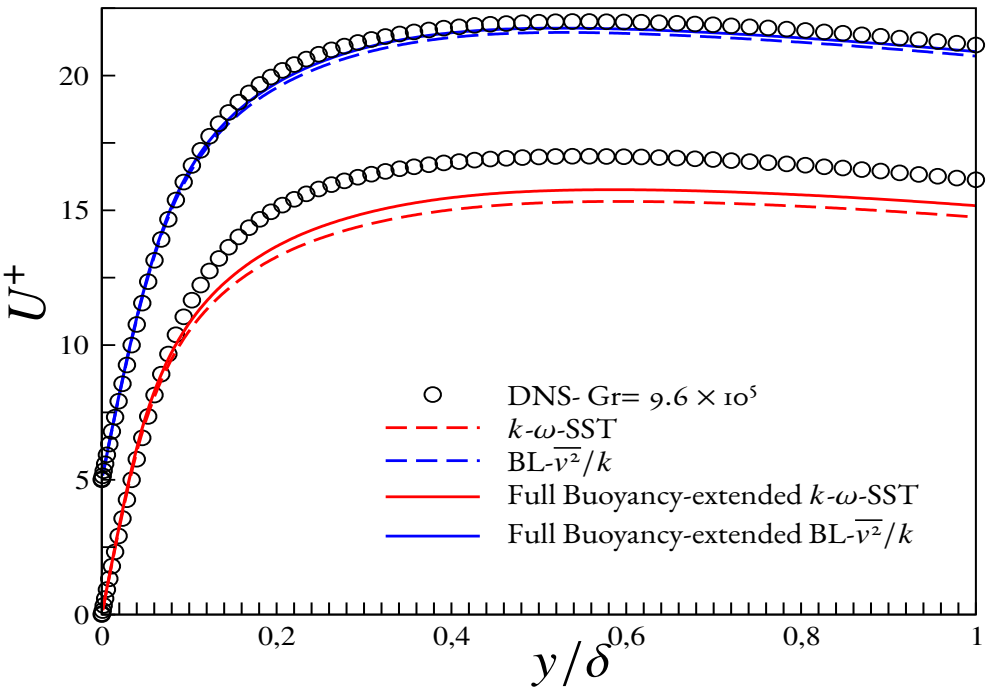

Figure 4.10 – Mean velocity for the aiding side at Gr = 9.6×10^5 [Kasagi and Nishimura, 1997][Plots are shifted for clarity]

However, for the opposing side, there is a very small effect of the buoyancy extension on the turbulent shear stress as can be seen in Fig. 4.13 and thereby there is a slight effect on mean velocity predictions as shown in Fig. 4.12.

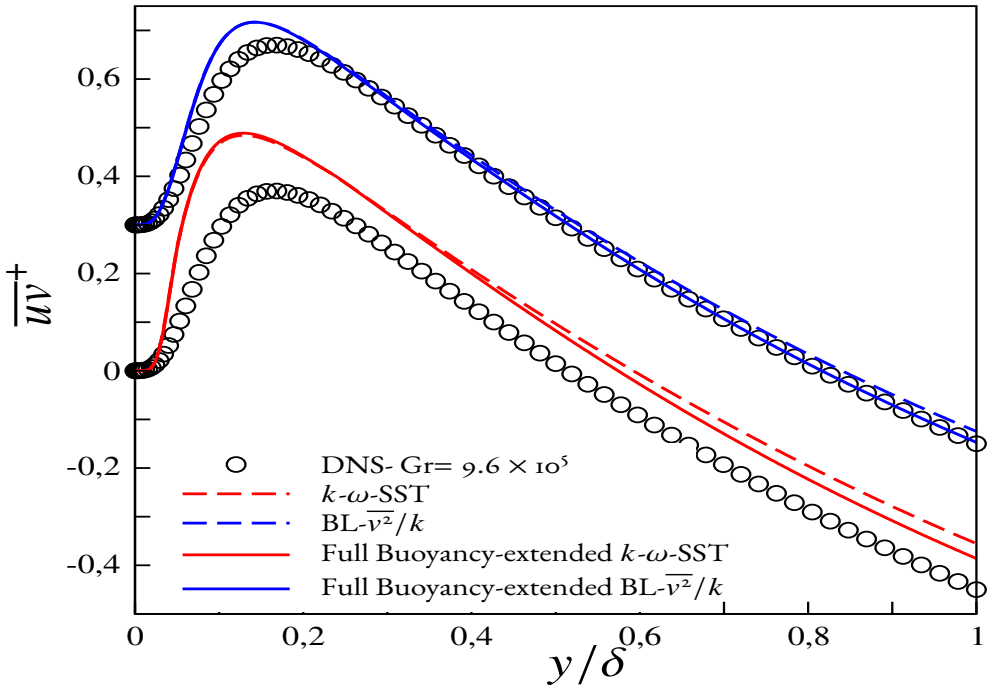

Figure 4.11 – Shear stress for the aiding side at Gr $= 9.6 \times 10^5$ [Kasagi and Nishimura, 1997] [Plots are shifted for clarity]

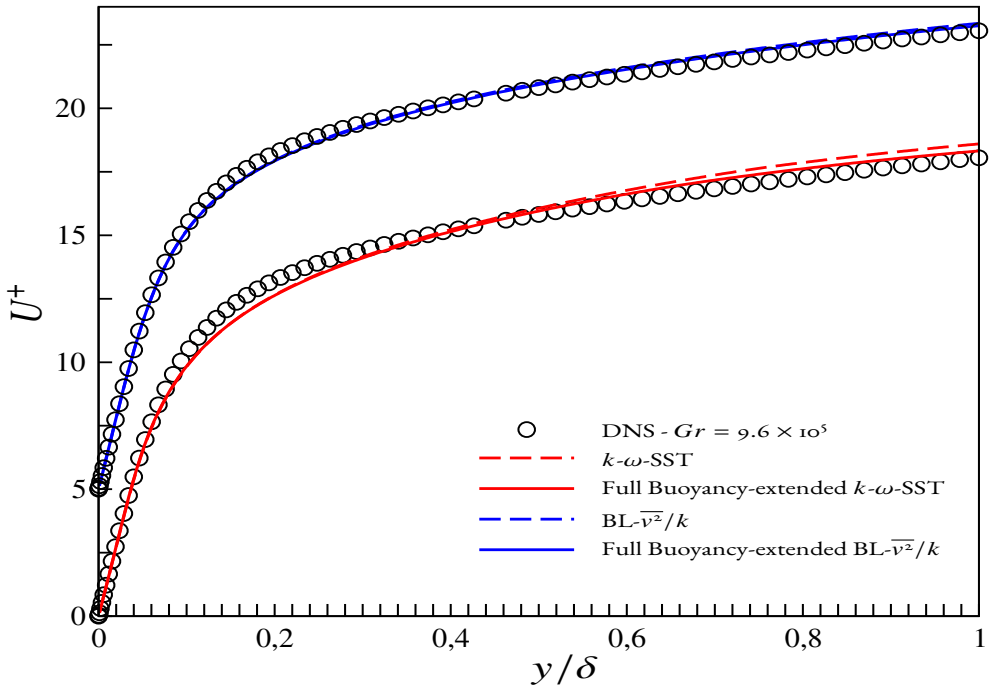

Figure 4.12 – Mean velocity for the opposing side at Gr$= 9.6 \times 10^5$ [Kasagi and Nishimura, 1997] [Plots are shifted for clarity]

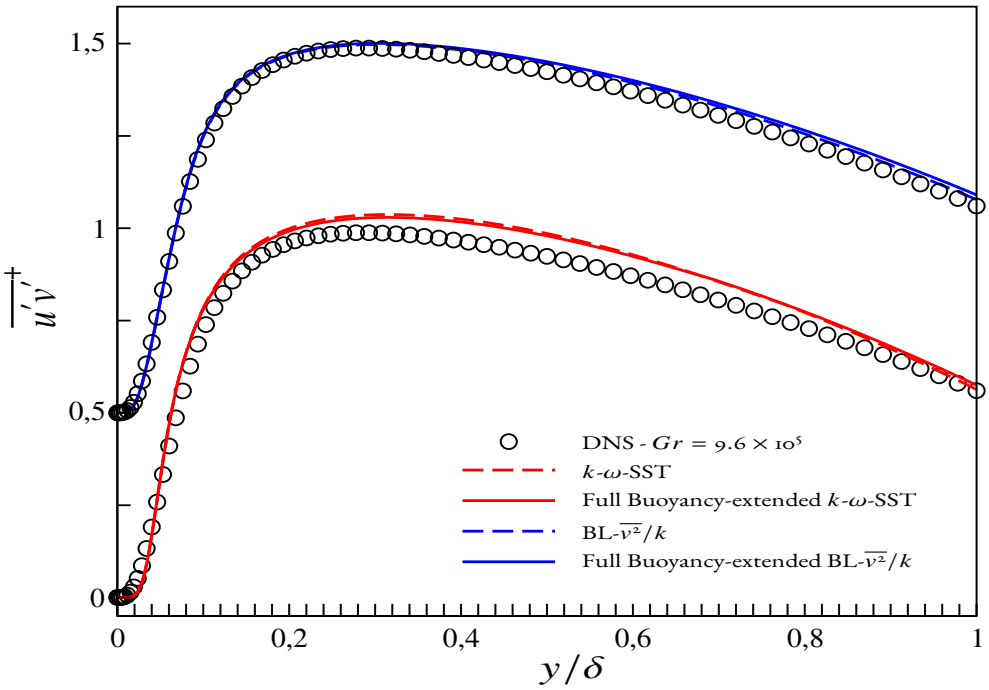

Figure 4.13 – Shear stress for the opposing side at Gr= 9.6×10^5 [Kasagi and Nishimura, 1997] [Plots are shifted for clarity]

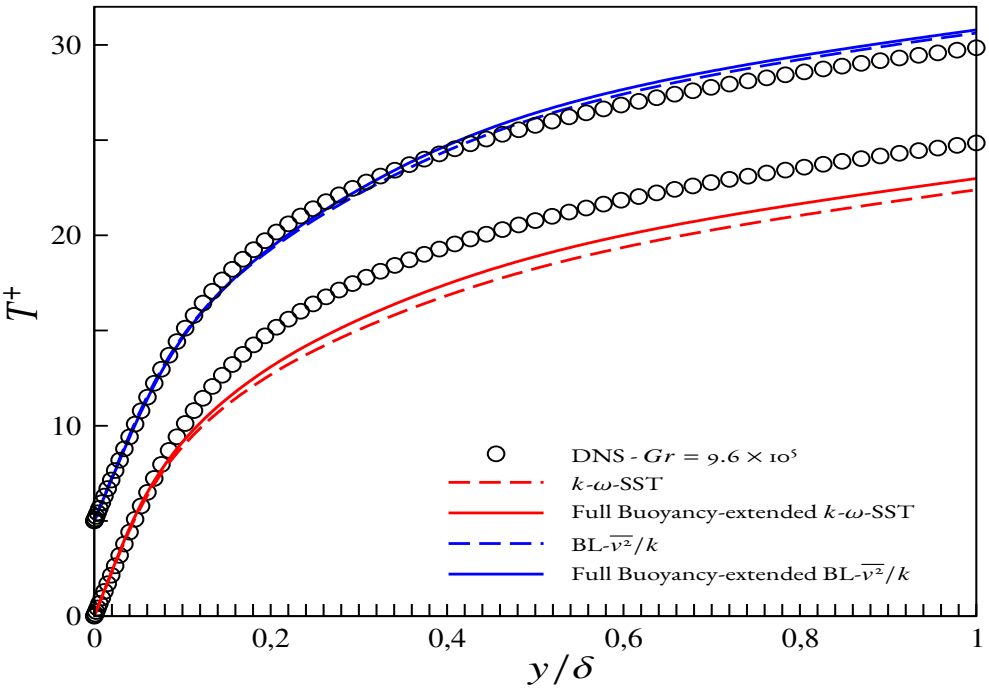

Figure 4.14 – Mean temperature for the aiding side at Gr= 9.6×10^5 [Kasagi and Nishimura, 1997] [Plots are shifted for clarity]

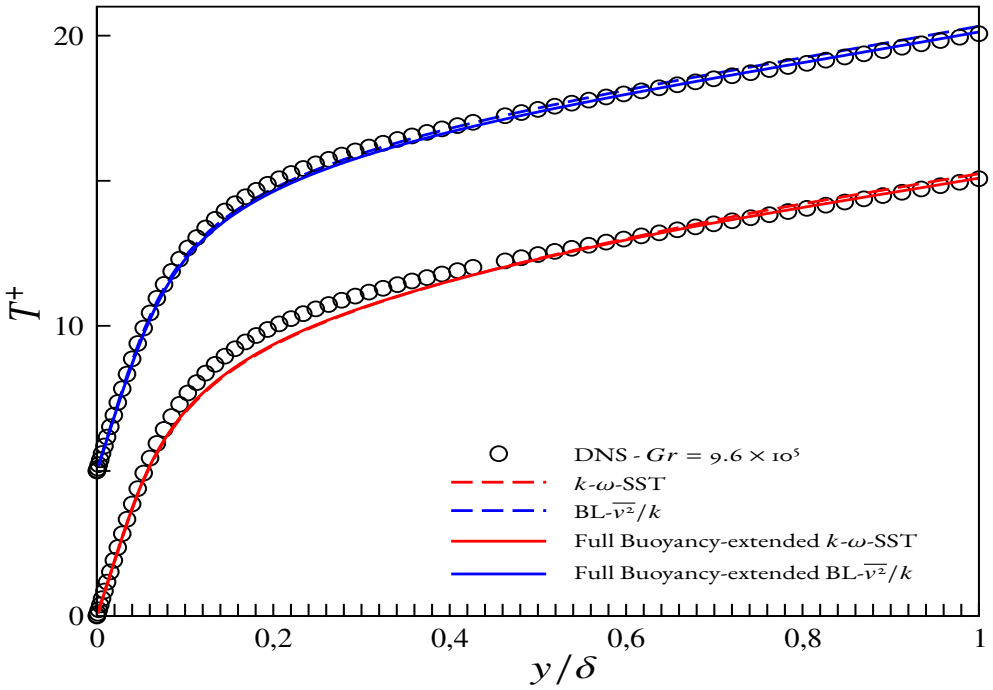

Figure 4.15 – Mean temperature for the opposing side at Gr= 9.6×10^5 [Kasagi and Nishimura, 1997] [Plots are shifted for clarity]

For the analysis of the effect of the buoyancy extension on thermal characteristics, the mean temperature distribution (T^+) is plotted in Fig. 4.14 and Fig. 4.15. On the aiding side, it is observed that there is improvement in mean temperature prediction particularly with buoyancy-extended k-ω-SST model. To understand about this prediction it is required to observe the effect of buoyancy extended heat flux on the energy balance such that energy equation is integrated from the wall to some distance y. In wall units, we have

$$1 = \frac{1}{Re_\tau Pr}\frac{d\widetilde{T}^+}{d\widetilde{y}}\bigg|_0 - \widetilde{\overline{v'\theta}}^+ \tag{4.38}$$

In Eq. (4.38), it can be seen that the turbulent heat flux is tending towards the value of 1.0 far from the wall, owing to negligible molecular heat flux. However, it is crucial to predict the turbulent heat flux close to the wall which is marginally improved as shown in Fig. 4.16, which explains the marginal improvement in the mean temperature on the aiding side which is underestimated with the original k-ω-SST model. Moreover, the prediction of the mean temperature on the aiding side with the BL-$\overline{v^2}/k$ model is satisfactory. On the opposing side, the prediction of heat flux with original models is satisfactory as can be seen in Fig. 4.17 and this explains the better prediction of mean temperature as can be seen in Fig. 4.15.

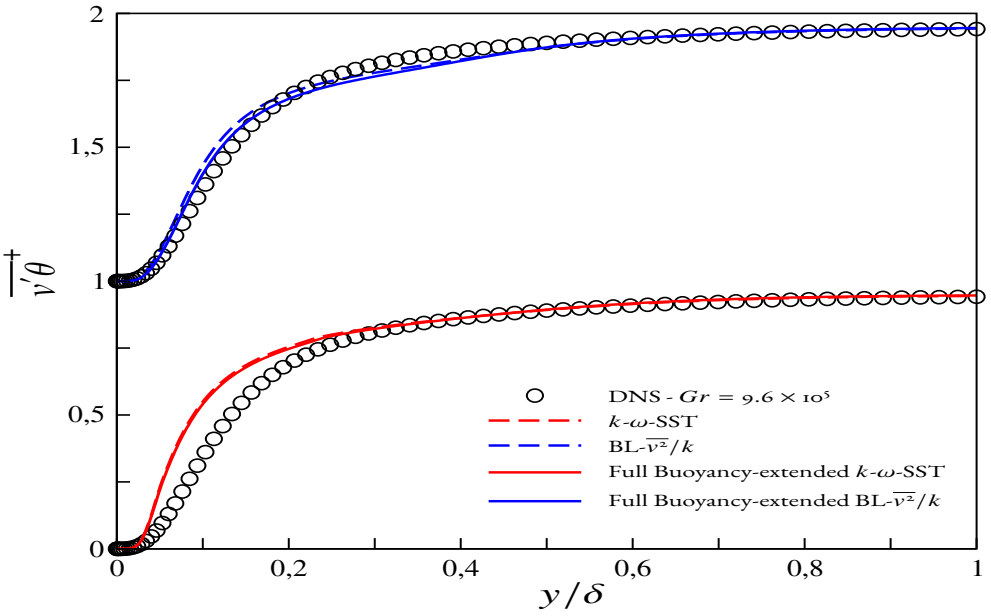

Figure 4.16 – Wall normal heat flux for the aiding side at Gr= 9.6×10^5 [Kasagi and Nishimura, 1997] [Plots are shifted for clarity]

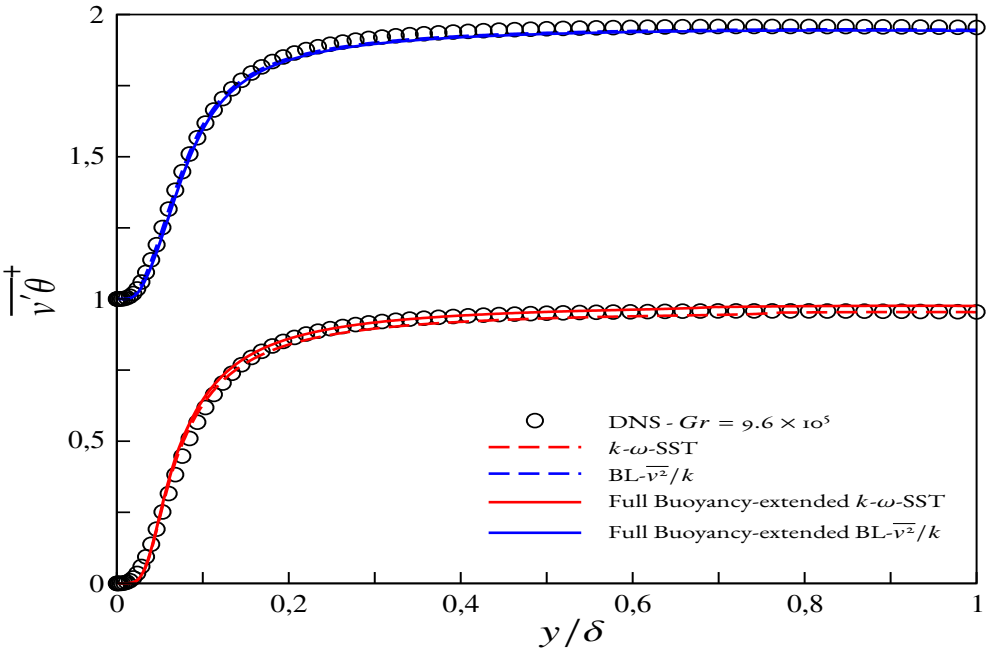

Figure 4.17 – Wall normal heat flux for opposing side at Gr= 9.6×10^5 Kasagi and Nishimura, 1997

4.2.9 Conclusion

In order to avoid ad hoc modifications, Buoyancy extended k-ω-SST and BL-$\overline{v^2}/k$ models have been developed by extending the constitutive relations using the buoyant

term derived from the Reynolds stress model under the weak-equilibrium hypothesis. The approach thus introduces a physically relevant term without sacrificing the linearity of the models. The extended constitutive relation for the Reynolds stress accounts for the influence of buoyancy on the turbulent anisotropy in association with the generalized gradient diffusion hypothesis (GGDH), which in turn involves the influence of the buoyancy extension on the turbulent heat flux.
By simulating two different regimes namely mixed and natural convection flows in a differentially heated vertical channel, it is noticed that the buoyancy extended k-ω-SST and BL-$\overline{v^2}/k$ model are able to predict the mean velocity and turbulent quantities quite well and certainly the discrepancy of the results obtained with the original k-ω-SST and BL-$\overline{v^2}/k$ model with respect to DNS data is due to the absence of the contribution of buoyancy in the turbulent shear stress and normal heat flux in the momentum and energy balance. These encouraging results pave the way for this model to be validated in natural convection configurations encountered in the industry. In the next section of this work, a simplified form of buoyancy sensitized model is presented.

4.3 Simplified form of buoyancy sensisitized models

4.3.1 Simple buoyancy extended models

The motivation for the development of this model comes from the fact that the modeling of tensorial diffusivity (GGDH) for the heat flux is not possible in Ansys Fluent which is used by PSA group for the designing of the underhood space of automobiles. So, simple version of buoyancy extended models are developed in the context of the k-ω-SST and BL-$\overline{v^2}/k$ models.
The approach is analogous to the model developed by Davidson [1990]. Davidson [1990] used a low-Reynolds number k-ε model which is similar to the models of Jones and Launder [1972] and Lam and Bremhorst [1981]. In his model, generalized gradient diffusion hypothesis (GGDH) was used to model heat fluxes in the energy equation but he used the simple gradient diffusion hypothesis (SGDH) approach to model heat fluxes in the buoyancy extension part of Reynolds stresses and also to model the buoyancy production terms of the k and ε equations, respectively.
In the present, simple buoyancy-extended models are developed in such a way that, simple gradient diffusion hypothesis (SGDH) is used to model heat fluxes everywhere and additional buoyant contribution is added in the Boussinesq relation of Reynolds stress in a linear way without changing the coefficients. Validation of this model is performed on the natural convection flow in a differentially heated vertical channel at available highest Rayleigh number ($Ra = 1.7 \times 10^7$) DNS data [Kiš and Herwig, 2014]. In these simple

models, Eq. (4.21) is still used which reads:

$$\overline{u_i'u_j'} = \underbrace{\frac{2}{3}k\delta_{ij} - \nu_t\left(\frac{\partial U_i}{\partial x_j} + \frac{\partial U_j}{\partial x_i}\right)}_{Boussinesq} + \underbrace{C_\theta{}^*\tau(G_{ij} - \frac{1}{3}\delta_{ij}G_{kk})}_{Buoyancy-extension} \tag{4.39}$$

where $G_{ij} = -\beta(g_j\overline{u_i'\theta} + g_i\overline{u_j'\theta})$ and in this simple buoyancy extended models, the optimal value of C_θ^* is 0.2.
The difference with the models developed in the previous section is that the heat fluxes are modeled using simple gradient diffusion hypothesis (SGDH) which reads:

$$\overline{u_i'\theta} = -\frac{\nu_t}{Pr_t}\frac{\partial T}{\partial x_i} \tag{4.40}$$

where Pr_t is the turbulent Prandtl number taken as 1.0.
The buoyancy extension is also considered in the dynamic production terms of turbulent kinetic energy (k) and dissipation (ε) or specific dissipation (ω) equations respectively:

$$P_k = -\Bigg(\underbrace{\overline{u_i'u_j'}}_{Boussinesq} + \underbrace{\overline{u_i'u_j'}}_{Buoyancy-extension}\Bigg)\frac{\partial U_i}{\partial x_j} \tag{4.41}$$

An intriguing feature of this model is that the buoyancy contribution coming from the buoyancy production terms in the transport equation of turbulent kinetic energy (G_k) and dissipation (G_ε) is negligible in the weakly stratified flows (in channel flows) as simple gradient diffusion hypothesis (SGDH) is used to model heat fluxes. since in this case, the temperature gradient is perpendicular to the direction of gravity, such that

$$\left.\begin{aligned} G_k &= \beta g_i\frac{\nu_t}{Pr_t}\frac{\partial T}{\partial x_i} \simeq 0 \ (weakly\ stratified\ flows) \\ G_\varepsilon &= C_{\varepsilon 3}\frac{1}{T}G_k \simeq 0; \qquad G_\omega = \frac{\gamma}{\nu_t}G_k \simeq 0 \end{aligned}\right\} \tag{4.42}$$

The fact that the these terms are zero is the reason why the coefficient of the buoyancy extension, C_θ^* must be recalibrated.

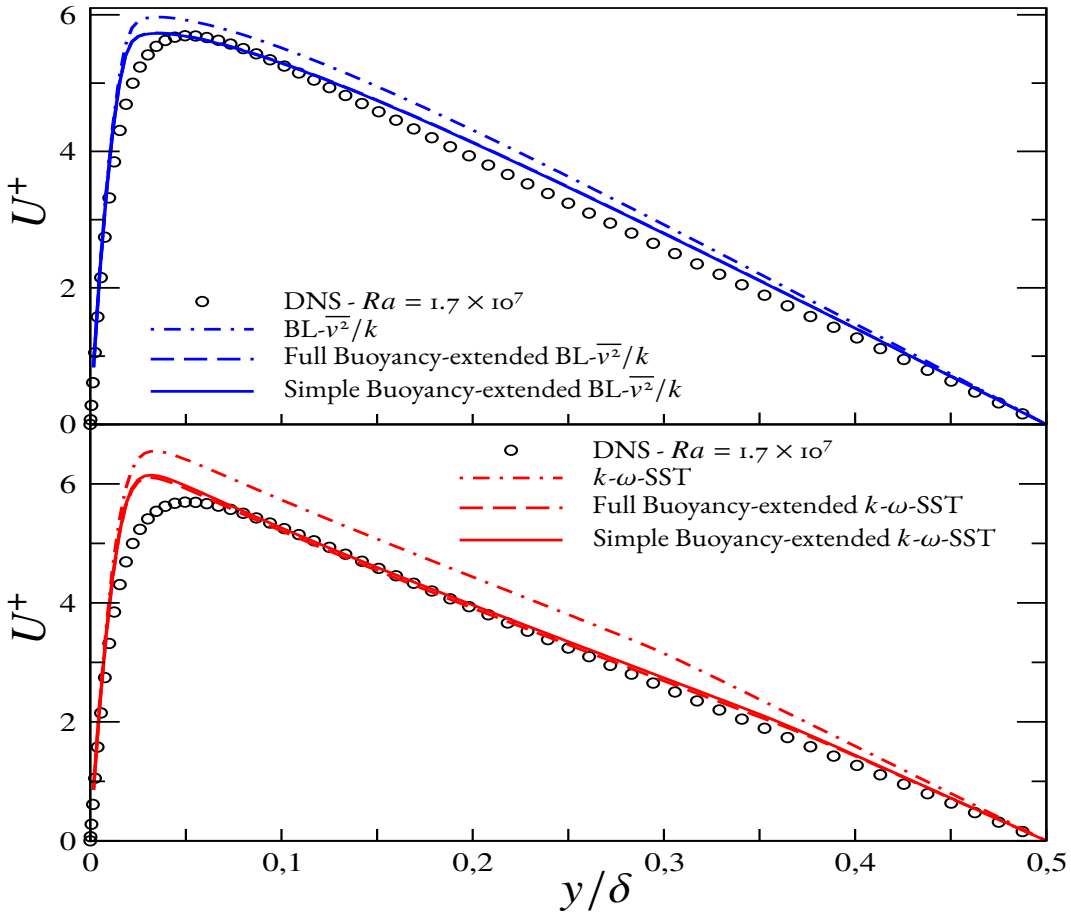

Figure 4.18 – Effect of simple buoyancy-extended on mean velocity profile at Ra = 1.7×10^7 [Kiš and Herwig, 2014]

In this model the optimal coefficient (C^*_θ) come out to be 0.2, which is 0.1 in the full buoyancy-extended model presented in the previous section.

From Fig. 4.18, it is observed that the buoyancy extension leads to the improvement of the mean velocity predictions which are severely overestimated by the original k-ω-SST and BL-$\overline{v^2}/k$ models. As we have discussed in the Section 4.2.5 and Section 4.2.6, the buoyancy extension modifies the turbulent shear stress (See Eq. 4.32) in such a way that it provides the contribution due to buoyancy in turbulent shear stress which is missing in the Boussinesq constitutive relation used in the original models (see Section 4.2.7). To complete the comparison, the prediction with full-buoyancy extended version of models is also compared. It is observed that the results are virtually identical between full buoyancy-extended and simple buoyancy-extended models, which shows that the lack of buoyancy contribution in the production terms can be somewhat artificially compensated by an increase of the coefficient C^*_θ, i.e., an increase of the contribution of buoyancy in the momentum balance.

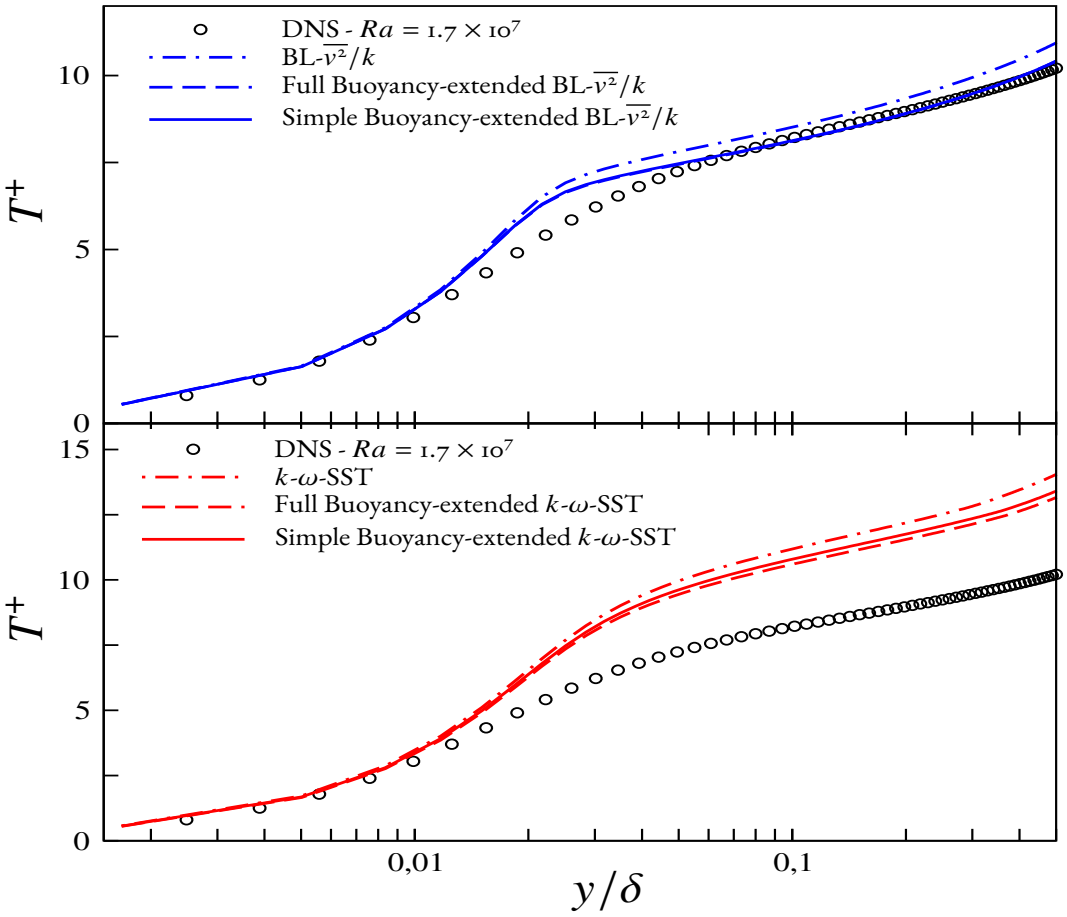

Figure 4.19 – Effect of simple buoyancy extended on mean temperature profile at Ra = 1.7×10^7 [Kiš and Herwig, 2014]

By looking into the mean temperature distribution as shown in Fig. 4.19, it is realized that the buoyancy extension is modifying the solution in such a way that there is an improvement in mean temperature prediction which is relatively overestimated with the original models. In the energy balance, the heat flux must be balanced by the sum of molecular and turbulent heat fluxes. Hence, the underprediction of $\overline{v'\theta}$ by the original k-ω-SST and BL-$\overline{v^2}/k$ models lead to the misprediction of temperature. However, there is an improvement in the mean temperature prediction with the simple versions of buoyancy-extended models. Again, it is observed that with the increased coefficient C^*_θ, the simple models are able to provide results very close to those given by the full buoyancy-extended models.

4.3.2 Effect of only adding buoyancy production terms

As seen in the previous sections, introducing the buoyancy extension in the Boussinesq relation modifies the momentum balance, the energy balance and the production terms of the transported turbulent variables. The results obtained with the simplified models

have shown that the buoyancy production terms have a significant effect, such that their absence must be compensated by an increase of C_θ^*. Thus, a question naturally emerges: whether the inclusion of buoyancy in the production terms be sufficient to improve the results, thereby avoiding the need of a buoyancy extension in the Boussinesq relation.
This part of the chapter is dedicated to the influence of adding buoyancy source terms in the transport equation of turbulent kinetic energy (k) and its dissipation rate (ε) or specific dissipation rate (ω) without modifying the original Boussinesq relation. The inclusion of the effect of buoyancy is generally made by introducing additional source terms in the transport equations of k and ε. Several authors applied the simple gradient diffusion hypothesis (SGDH) as expressed in Eq. (4.43) to model buoyancy production terms [Annarumma et al., 1991, Cox and Kumar, 1987, Fletcher et al., 1994, Nam and Bill Jr, 1993, Sinai and Owens, 1995],

$$\overline{u_i'\theta} = -\frac{\nu_t}{Pr_t}\frac{\partial T}{\partial x_i} \tag{4.43}$$

However, as shown above, with the simple gradient diffusion hypothesis (SGDH) approach, the effect of buoyancy on turbulence can be severely underestimated, since only the component of the temperature gradient aligned with the gravity vector is taken into account and in weakly stratified flows it becomes negligible [Ince and Launder, 1989]. Moreover, in simple shear flows, with the use of an eddy-diffusivity model, the streamwise flux is severely underpredicted and this behaviour has an impact on the prediction of the mean flow owing to the absence of buoyancy effects. To overcome this limitation, authors listed in Table. 4.2 consider the generalized gradient diffusion hypothesis (GGDH) of Daly and Harlow [1970] as mentioned in Eq. (4.44) for modeling the buoyancy source terms in the $k-\varepsilon$ turbulence models.

$$\overline{u_i'\theta} = -C_\theta \frac{k}{\varepsilon}\overline{u_i'u_j'}\frac{\partial T}{\partial x_j} \tag{4.44}$$

For the ε or ω equations, the formulation (mentioned in the Table. 4.2) of the buoyancy source terms have been tried in this study and detailed sensitivity analysis of the coefficient $C_{\varepsilon 3}$ have been performed for the k-ω-SST and BL-$\overline{v^2}/k$ models.

References	$C_{\varepsilon 3}$
$S_\varepsilon = C_{\varepsilon 1}\frac{\varepsilon}{k}[P_k + C_{\varepsilon 3} max(G_k, 0)] - C_{\varepsilon 2}\rho\frac{\varepsilon^2}{k}$	–
Novozhilov [2001]	1.0
Fletcher et al. [1994]	1.0
Hara and Kato [2004]	1.0
Sinai and Owens [1995]	1.0

Table 4.2 – Value of the constant for the definitions of S_ε source terms in ε equation

Buoyancy production terms in k-ω-SST model

In this section, more classical approaches of using the same Boussinesq relation for Reynolds stresses but introducing buoyancy production terms (definition of these types of source terms are reported in Table. 4.2) in the transport equation of turbulent kinetic energy (k) and specific dissipation (ω) are analyzed. Moreover, the sensitivity of the coefficient C_3 (in the present study $C_{\varepsilon 3}$ is denoted by C_3) is also examined.
The modified transport equation of turbulent kinetic energy (k) and specific dissipation (ω) equations are expressed as follows:

$$\frac{\partial k}{\partial t} + U_k \frac{\partial k}{\partial x_k} = P_k + G_k - \beta^* k\omega + \frac{\partial}{\partial x_k}\left[\left(\nu + \sigma_k \nu_t\right)\frac{\partial k}{\partial x_k}\right] \tag{4.45}$$

$$\begin{aligned}\frac{\partial \omega}{\partial t} + U_k \frac{\partial \omega}{\partial x_k} = \frac{\gamma}{\nu_t} P_k + \underbrace{max\left(\frac{C_3}{\nu_t} G_k, 0\right)}_{G_\omega} - \beta\omega^2 + \frac{\partial}{\partial x_k}\left[\left(\nu + \sigma_\omega \nu_t\right)\frac{\partial \omega}{\partial x_k}\right] \\ +2(1-F_1)\sigma_{\omega 2}\frac{1}{\omega}\frac{\partial k}{\partial x_k}\frac{\partial \omega}{\partial x_k}\end{aligned} \tag{4.46}$$

Where constants and blending functions are as per standard of k-ω-SST by Menter [1994], G_k is modeled based on the GGDH approach which writes:

$$G_k = -\beta g_i \overline{u_i' \theta}; \qquad \overline{u_i{}' \theta} = -C_\theta \frac{1}{C_\mu \omega}\left(\overline{u_i' u_j'}\frac{\partial T}{\partial x_j}\right) \tag{4.47}$$

Buoyancy production terms in BL-$\overline{v^2}/k$ model

The modified transport equations of turbulent kinetic energy (k) and its dissipation rate (ε) are expressed as follows:

$$\frac{Dk}{Dt} = P_k + G_k - \varepsilon - 2C_{\varepsilon 3}\nu\nu_t(1-\alpha)^3\frac{k}{\varepsilon}\left(\frac{\partial^2 U_i}{\partial x_k \partial x_j}\right)^2 + \frac{\partial}{\partial x_j}\left[\left(\frac{\nu}{2} + \frac{\nu_t}{\sigma_k}\right)\frac{\partial k}{\partial x_j}\right] \tag{4.48}$$

$$\frac{D\varepsilon}{Dt} = \frac{C_{\varepsilon 1} P_k - C_{\varepsilon 2}{}^* \varepsilon}{T} + \underbrace{max\left(C_3 \frac{G_k}{T}, 0\right)}_{G_\varepsilon} + \frac{\partial}{\partial x_j}\left[\left(\frac{\nu}{2} + \frac{\nu_t}{\sigma_\varepsilon}\right)\frac{\partial \varepsilon}{\partial x_j}\right] \tag{4.49}$$

where constants, other functions and equations for φ and f are as per BL-$\overline{v^2}/k$ model [Billard and Laurence, 2012], G_k is modeled based on the GGDH approach, as follows:

$$G_k = -\beta g_i \overline{u_i' \theta}; \qquad \overline{u_i' \theta} = -C_\theta T\left(\overline{u_i' u_j'}\frac{\partial T}{\partial x_j}\right); \quad T = \sqrt{\left(\frac{k}{\varepsilon}\right)^2 + {C_T}^2\left(\frac{k}{\varepsilon}\right)} \tag{4.50}$$

In this study, the Reynolds stresses in the averaged momentum equation are modeled using the standard Boussinesq constitutive relation:

$$\overline{u_i' u_j'} = \frac{2}{3} k \delta_{ij} - \nu_t \left(\frac{\partial U_i}{\partial x_j} + \frac{\partial U_j}{\partial x_i} \right) \tag{4.51}$$

The turbulent heat fluxes in the mean temperature equation are modeled using the simple gradient diffusion hypothesis (SGDH) as mentioned in Eq. (4.52) which writes:

$$\overline{u_i' \theta} = -\frac{\nu_t}{Pr_t} \frac{\partial T}{\partial x_i} \tag{4.52}$$

The max in the definition of G_ω (in Eq. 4.46) or G_ε (in Eq. 4.49) is considered owing to the fact that in a stably stratified flow, buoyancy has a tendency to damp the turbulence such that G_k is negative and due to the max in the relation, the influence of buoyancy on the transport equation for ε or ω is 0 [Fletcher et al., 1994, Hara and Kato, 2004, Novozhilov, 2001, Sinai and Owens, 1995]. For unstably stratified flows, the expression for buoyancy production in ω or ε reduces to

$$\begin{aligned} G_\omega &= \frac{C_3}{\nu_t} G_k \\ G_\varepsilon &= C_3 \frac{\varepsilon}{k} G_k \end{aligned} \tag{4.53}$$

In this part of the chapter, the effect of adding additional buoyancy source terms, G_k and G_ω or G_ε is analyzed for k-ω-SST and BL-$\overline{v^2}/k$ model. Moreover, the other aim of this section is to perform the sensitivity analysis of coefficient, $C_{\varepsilon 3}$. The challenging natural convection regime in a vertical channel at Rayleigh number, $Ra = 1.7 \times 10^7$ is selected and results are compared to the DNS data of Kiš and Herwig [2014].

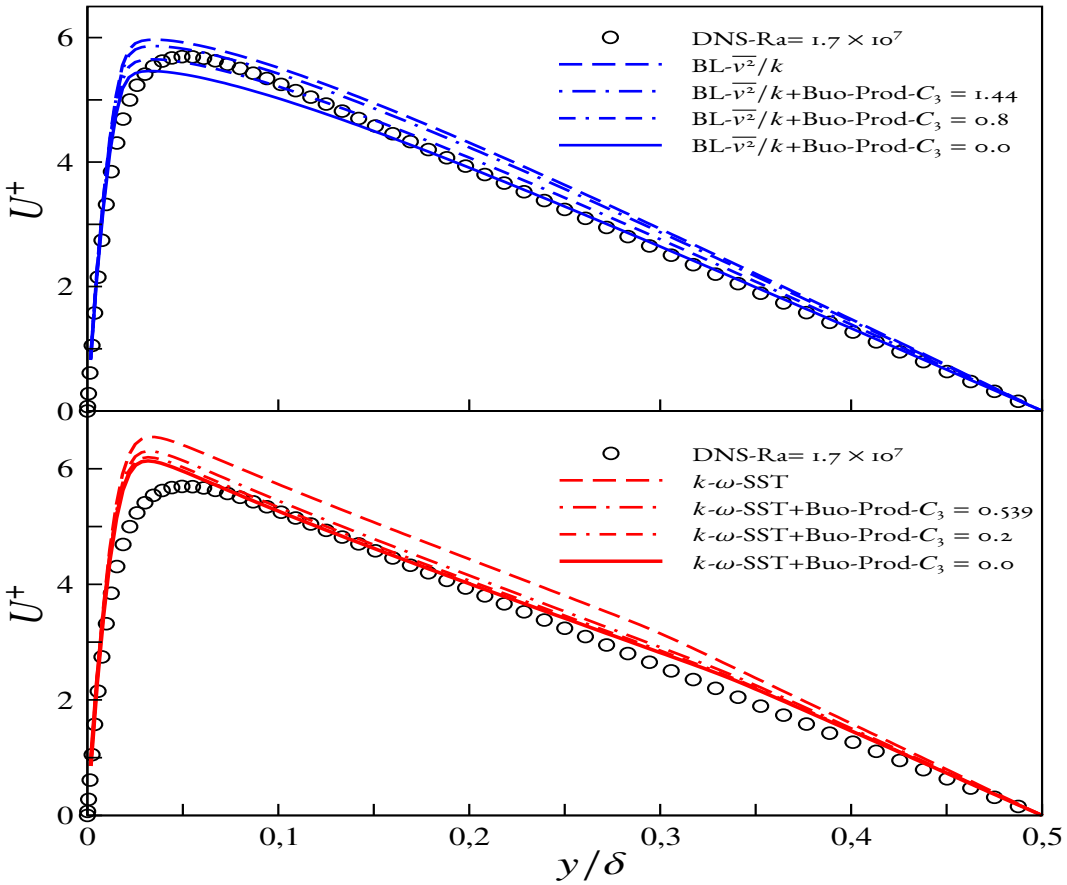

Figure 4.20 – Mean velocity profile [Plots are shifted for clarity]

For the mean velocity profile as shown in Fig. 4.20, it is observed that there is a competition between the influence of G_k and the influence of G_ω or G_ε. The case with $C_3 = 0$ shows that the G_k term has a tendency to reduce the mean velocity, which is overestimated with the original models, but can possibly reduce it too much (for the BL-$\overline{v^2}/k$ model). The G_ω or G_ε term plays in the opposite direction, with an intensity driven by the coefficient C_3 and there is an optimal value of C_3, This behaviour is observed with both the models. Further, by looking into the turbulent viscosity profile as shown in Fig. 4.21, it is observed that the original models are underpredicting the turbulent viscosity in a major portion of the channel. By introducing the buoyancy source terms, this underprediction is avoided and results are improved. Again it is realized that adding only G_k ($C_3 = 0$) leads to significantly improve the prediction of turbulent viscosity. Now looking into the sensitivity to the coefficient (C_3), it is realized that if the value of C_3 is increased to some large value, the results gradually revert back to the original model.

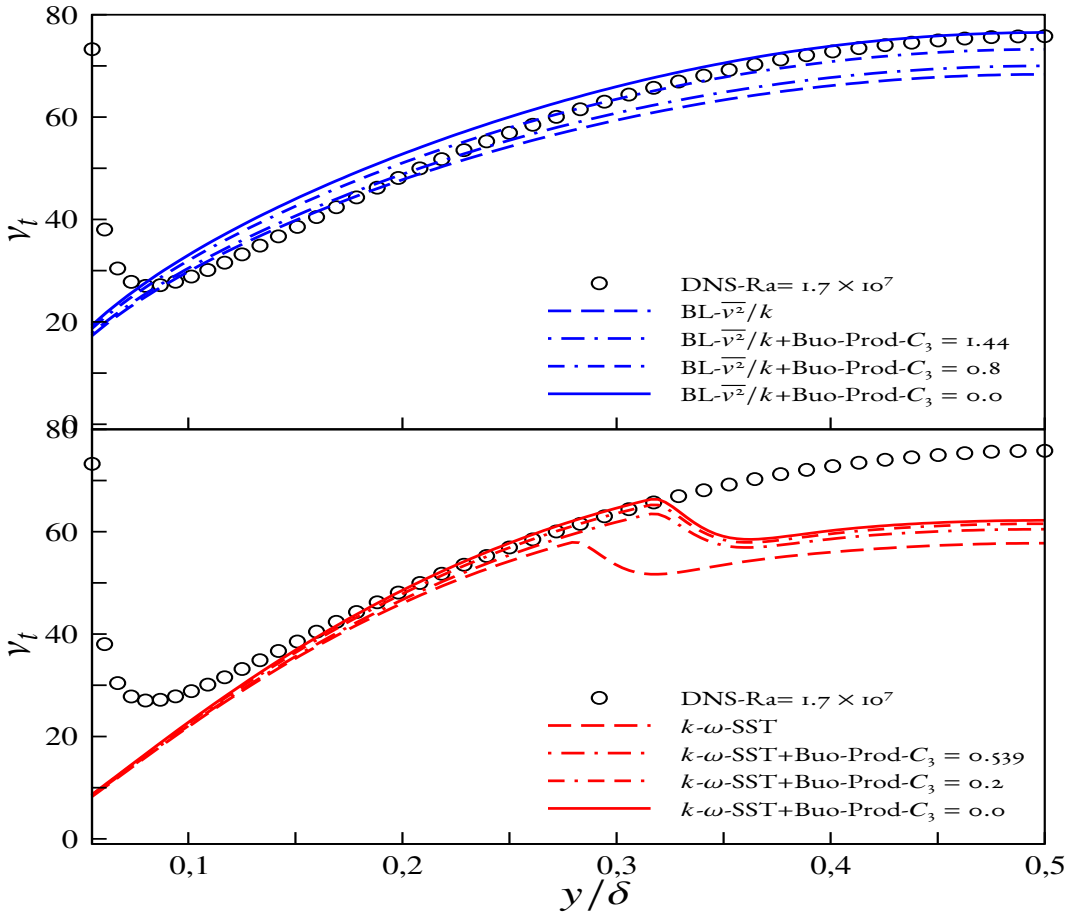

Figure 4.21 – Turbulent viscosity profile [Plots are shifted for clarity]

For instance in the case k-ω-SST model, it is observed that if the value of $C_3 = 0.539$ (which is the same coefficient used for dynamic production of ω), the results are not as improved as corresponding to $C_3 = 0.2$ and it becomes better at $C_3 = 0$ as shown in Fig. 4.21. Similar behaviour is observed with BL-$\overline{v^2}/k$ model, when we change the value of C_3 from 1.44 to 0.0. This signifies that the inclusion of only G_k modifies the turbulent viscosity significantly. This prediction of the turbulent viscosity leads to modify the Reynolds shear stress (as the Boussinesq constitutive relation is used to model the Reynolds stresses) which directly affects the momentum balance. To probe more deeply, total production of turbulent kinetic energy and dissipation (or specific dissipation) budget are shown in Fig. 4.22 and Fig. 4.23. In the near-wall region, the addition of G_k and G_ε or G_ω reduce the total production $(P_k + G_k)$ marginally from $0.01 < y < 0.05$ owing to the negative production of (G_k) as shown in Fig. 4.22. Moreover, it is realized that the addition of only G_k $(C_3 = 0.0)$ has significantly reduced the total production of turbulent kinetic energy near the wall. In the central region, it is observed that the introduction of buoyancy source terms G_k and G_ε or G_ω leads to the enhancement of $P_k + G_k$ in the range $0.05 < y < 0.35$ as can be seen in Fig. 4.22 for both the models.

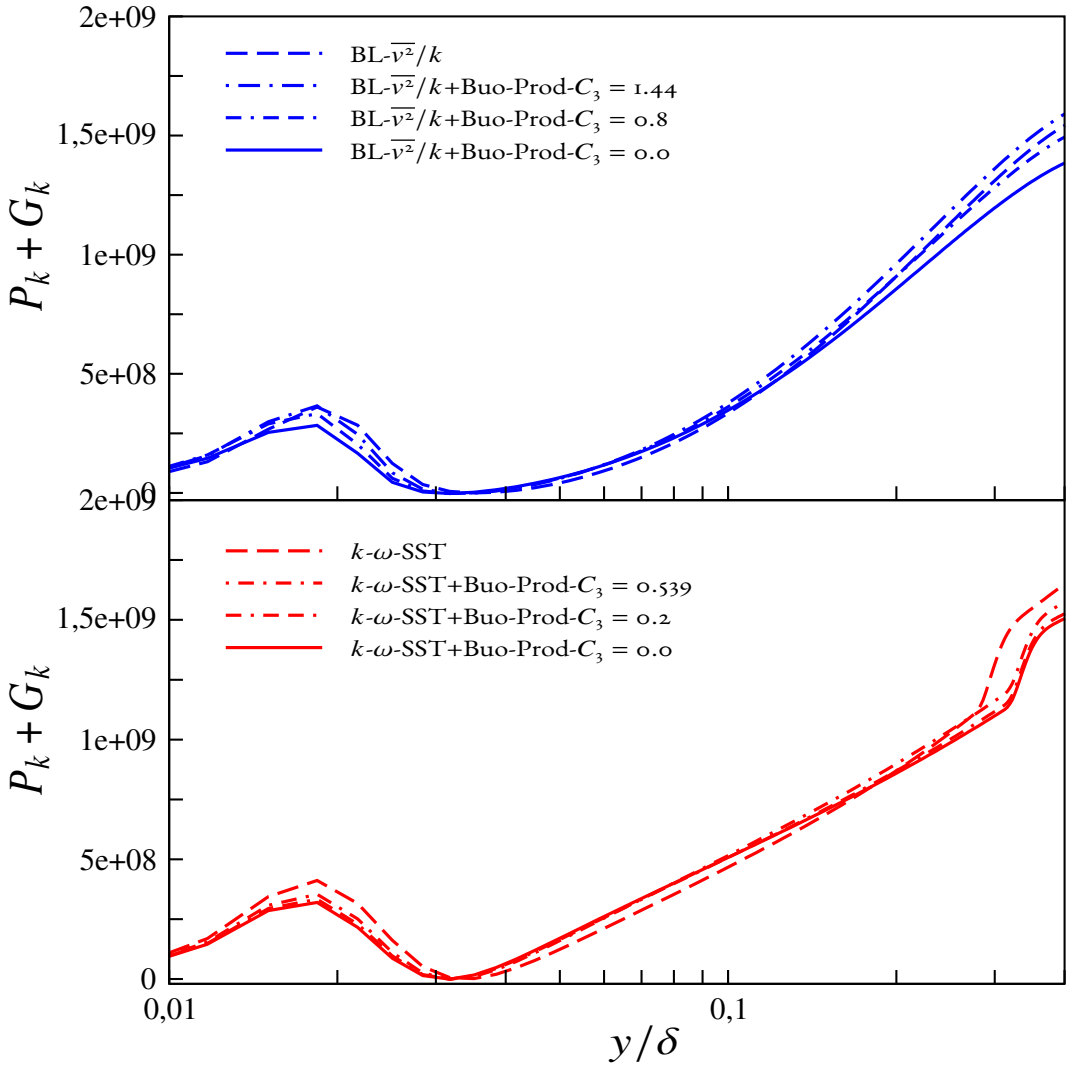

Figure 4.22 – Profiles of production of turbulent kinetic energy [Plots are shifted for clarity]

Predictions of $P_\omega + G_\omega$ or $P_\varepsilon + G_\varepsilon$ are shown in Fig. 4.23. Not introducing the term G_ε or G_ω corresponds to $C_3 = 0$. However, adding it corresponds to using a non-zero coefficient and it is observed that the addition of G_ε or G_ω leads to increase the total production in the dissipation (or specific) equation compared to the case with G_k only ($C_3 = 0$). This tendency is of course enhanced when we increase the coefficient C_3.
These predictions contribute to the improvement of the turbulent viscosity which is underpredicted by the original models as can be seen in Fig. 4.21. From the analysis of the production of turbulent kinetic energy, it has been observed that the inclusion of buoyancy source terms has a significant effect on the budget of turbulent kinetic energy and its dissipation rate. Moreover, the coefficient C_3 has a monotonic influence on the predictions.

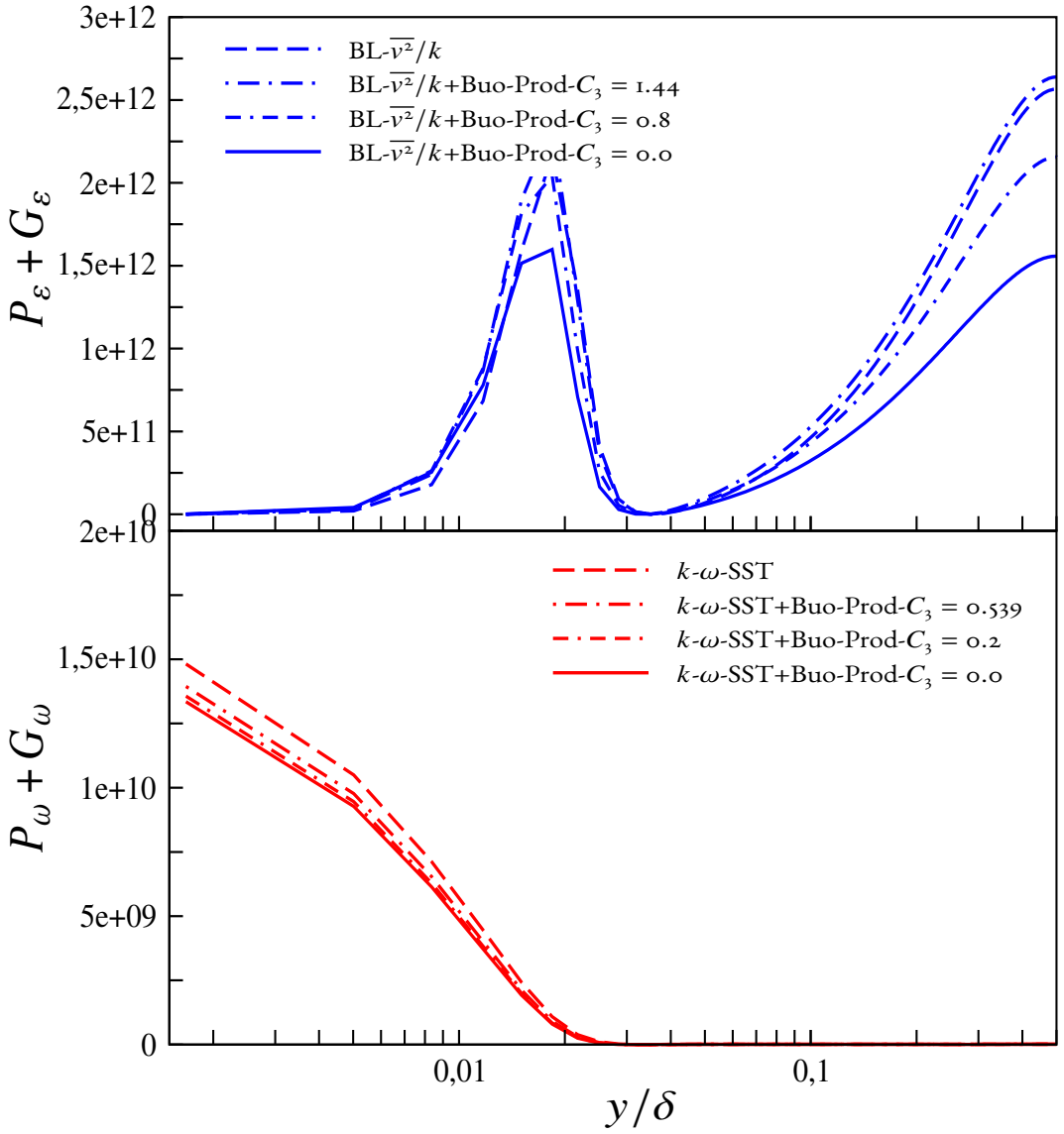

Figure 4.23 – Total production of dissipation equation of turbulent kinetic energy profiles [Plots are shifted for clarity]

By looking into the prediction of mean temperature as shown in Fig. 4.24, it is observed that the inclusion of buoyancy source terms acts as a positive contributor in such a way that it improves the prediction of mean temperature for both the models. It can be seen that the addition of the G_k term alone ($C_3 = 0$) significantly reduces the value of T^+, while the inclusion of G_ε or G_ω plays in the other direction. This prediction of mean temperature is related to the prediction of wall-normal heat flux by the models. For instance, in the case of original BL-$\overline{v^2}/k$, there is a better prediction of mean temperature (as seen in Fig. 4.24) owing to the better prediction of wall-normal heat flux.

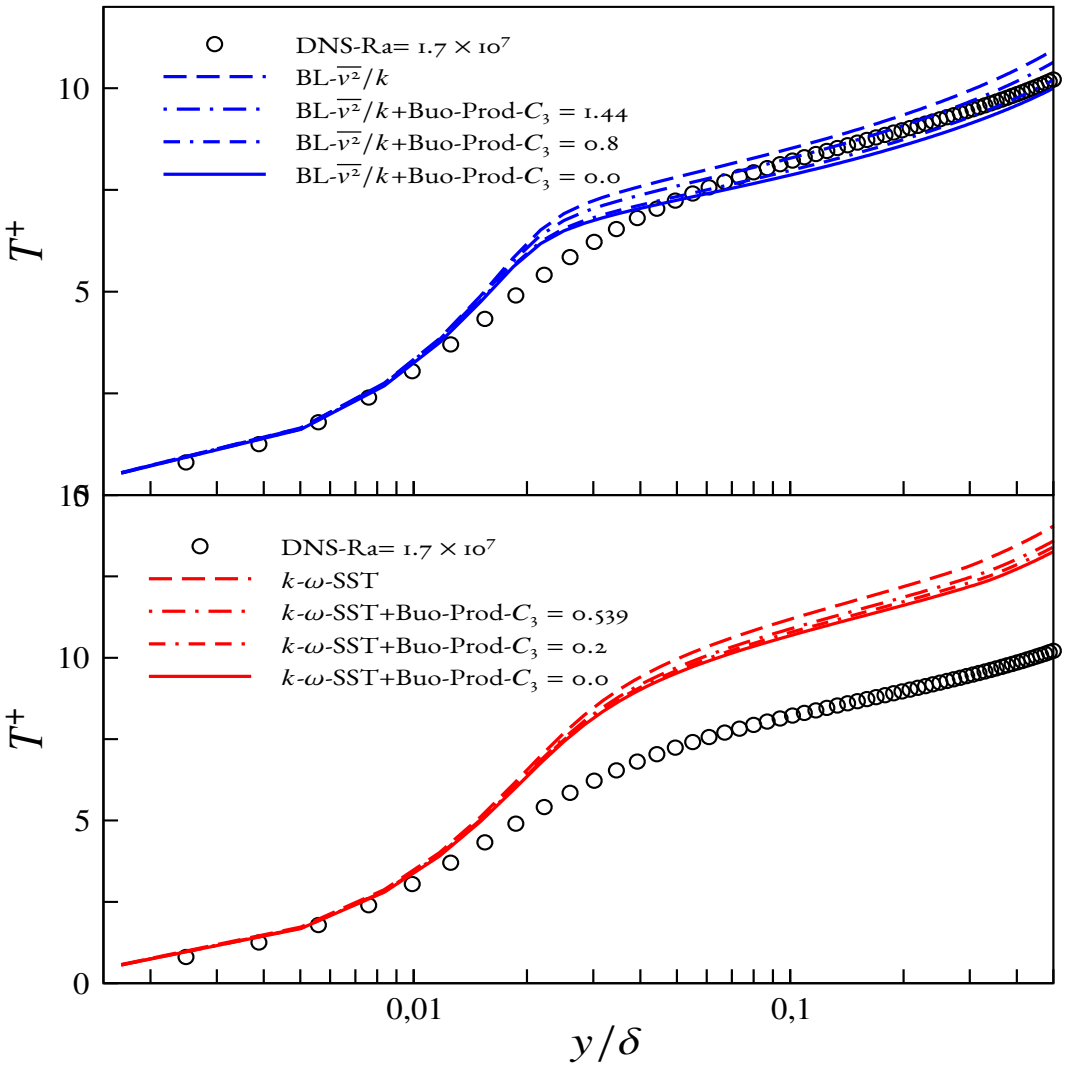

Figure 4.24 – Mean temperature profile [Plots are shifted for clarity]

This fact is reinforced by the fact that there is an underprediction of the wall-normal heat flux close to the wall by the original models (as seen in Fig. 4.25) which explain the overprediction of the mean temperature and the inclusion of the buoyancy source term also affects the solution of the energy equation in such a way that the tendency of underprediction of heat flux is avoided to a certain extent. Furthermore for the BL-$\overline{v^2}/k$ model, it is realized that the inclusion of only G_k has a significant influence (actually too strong) on the prediction of wall-normal heat flux and thus the necessity to introduce also G_ε (with $C_3 = 0.8$) is to moderate it. Authors (Hara and Kato [2004], Novozhilov [2001], Sinai and Owens [1995]) have used the value of the coefficient (C_3) to be 1.0 for different variants of buoyancy modified k-ε models. However, in the present study, it is observed that the value of this coefficient depends mainly on the type of turbulence model chosen for the study. Moreover, the optimal value of the coefficient (C_3) is 0.0 (introducing only G_k term) for the k-ω-SST model and 0.8 for the BL-$\overline{v^2}/k$ model respectively. An interesting

conclusion is that with such a simple model, we can correct the predictions, although it is less "rich" than the complete buoyancy-extended models.

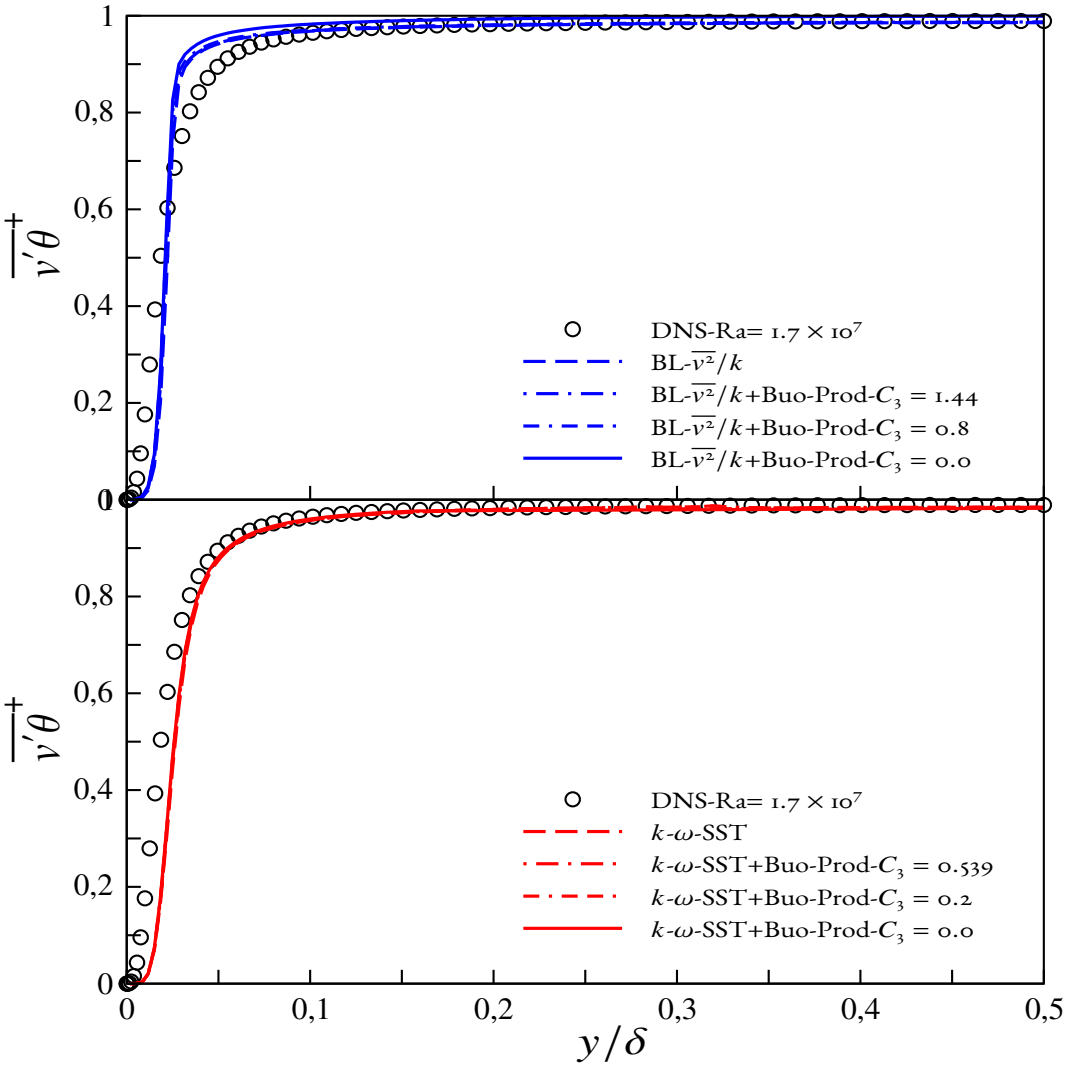

Figure 4.25 – Wall normal heat flux profile [Plots are shifted for clarity]

In the next section of this chapter, the effect of including flux Richardson number in the definition of G_ω or G_ε is discussed in the context of k-ω-SST and BL-$\overline{v^2}/k$ models.

Effect of flux Richardson number

Several authors (mentioned in Table. 4.3) included the flux Richardson number in the definition of G_ε, and we want to see that if it has some interest in improving the results. The conventional definition of flux Richardson is expressed as:

$$R_f = -\frac{G_k}{P_k} \tag{4.54}$$

However, some authors Markatos et al. [1982], Worthy et al. [2001], Xue et al. [2001] used other definition of flux Richardson number which is expressed as below:

$$R_f = -\frac{G_k}{P_k + G_k} \tag{4.55}$$

The details of the buoyancy source term are listed in Table. 4.3 respectively.

References	$C_{\varepsilon 3}$	R_f
$S_\varepsilon = C_{\varepsilon 1}\frac{\varepsilon}{k}(P+G)(1+C_{\varepsilon 3}R_f) - C_{\varepsilon 2}\rho\frac{\varepsilon^2}{k}$	–	–
Worthy et al. [2001]	Different value	$R_f = \frac{-G}{(P+G)}$
Markatos et al. [1982]	0.9	$R_f = \frac{-G}{(P+G)}$
Yan and Holmstedt [1999]	0.6	R_f not given
Xue et al. [2001]	0.8	R_f not given

Table 4.3 – Value of the constant for the definitions of S_ε source terms in ε equation

However, this definition does not distinguish between the horizontal and vertical buoyant flows. Rodi [1984], proposed a definition of flux Richardson to distinguish between horizontal and vertical buoyant flows and the definition of such modified flux Richardson number is expressed as follows:

$$R_f = -\frac{1}{2}\frac{G_{\overline{v^2}}}{P_k + G_k} \tag{4.56}$$

where $G_{\overline{v^2}}$ is the buoyancy production or destruction of the transverse fluctuating component. However, such a definition is only applicable to 2D flows, since the notion of transverse component is not well-defined in 3D flows. In the present study, the effect of adding buoyancy production terms which consider flux Richardson number in its definition (Eq. 4.55) is analyzed in the context of the k-ω-SST and BL-$\overline{v^2}/k$ models respectively.

Inclusion of the flux Richardson number in the k-ω-SST model

Considering the flux Richardson number in the k-ω-SST model, the transport equations of k and ω write:

$$\frac{\partial k}{\partial t} + U_k\frac{\partial k}{\partial x_k} = P_k + G_k - \beta^* k\omega + \frac{\partial}{\partial x_k}\left[\left(\nu + \sigma_k\nu_t\right)\frac{\partial k}{\partial x_k}\right] \tag{4.57}$$

$$\frac{\partial \omega}{\partial t} + U_k \frac{\partial \omega}{\partial x_k} = \underbrace{\frac{\gamma}{\nu_t} P_k (1 + C_3 R_f)}_{P_\omega} + \underbrace{\frac{\gamma}{\nu_t} G_k (1 + C_3 R_f)}_{G_\omega} - \beta \omega^2 + \frac{\partial}{\partial x_k}\left[\left(\nu + \sigma_\omega \nu_t\right)\frac{\partial \omega}{\partial x_k}\right] + 2(1 - F_1)\sigma_{\omega 2}\frac{1}{\omega}\frac{\partial k}{\partial x_k}\frac{\partial \omega}{\partial x_k} \tag{4.58}$$

The buoyancy production terms are modeled using generalized gradient diffusion hypothesis (GGDH) such that

$$G_k = -\beta g_i \overline{u_i' \theta};\ \ \overline{u_i' \theta} = -C_\theta \frac{1}{C_\mu \omega}\overline{u_i' u_j'}\frac{\partial T}{\partial x_j};\ \ R_f = -\frac{G_k}{P_k + G_k} \tag{4.59}$$

Inclusion of the flux richardson number in the BL-$\overline{v^2}/k$ model

Considering the flux Richardson number in the BL-$\overline{v^2}/k$ model, the transport equations of k, ε and φ write:

$$\frac{Dk}{Dt} = P_k + G_k - \varepsilon - 2C_{\varepsilon 3}\nu\nu_t(1-\alpha)^3\frac{k}{\varepsilon}\left(\frac{\partial^2 U_i}{\partial x_k \partial x_j}\right)^2 + \frac{\partial}{\partial x_j}\left[\left(\frac{\nu}{2} + \frac{\nu_t}{\sigma_k}\right)\frac{\partial k}{\partial x_j}\right] \tag{4.60}$$

$$\frac{D\varepsilon}{Dt} = \underbrace{\frac{C_{\varepsilon 1}}{T} P_k (1 + C_3 R_f)}_{P_\varepsilon} + \underbrace{\frac{C_{\varepsilon 1}}{T} G_k (1 + C_3 R_f)}_{G_\varepsilon} - \frac{{C_{\varepsilon 2}}^* \varepsilon}{T} + \frac{\partial}{\partial x_j}\left[\left(\frac{\nu}{2} + \frac{\nu_t}{\sigma_\varepsilon}\right)\frac{\partial \varepsilon}{\partial x_j}\right] \tag{4.61}$$

$$\frac{D\varphi}{Dt} = -(1-\alpha^3)\frac{\varepsilon}{2}\frac{\varphi}{k} + \alpha^3 f_h - (P_k + G_k)\frac{\varphi}{k} + \frac{2}{k}\frac{\nu_t}{\sigma_k}\frac{\partial k}{\partial x_j}\frac{\partial \varphi}{\partial x_j} + \frac{\partial}{\partial x_j}\left[\left(\frac{\nu}{2} + \frac{\nu_t}{\sigma_\varphi}\right)\frac{\partial \varphi}{\partial x_j}\right] \tag{4.62}$$

$$f_h = -\frac{1}{T}\left(C_1 - 1 + C_2\frac{(P_k + G_k)}{\varepsilon}\right)\left(\varphi - \frac{2}{3}\right) \tag{4.63}$$

The buoyancy production term is modeled using the generalised gradient diffusion hypothesis (GGDH) such that

$$G_k = -\beta g_i \overline{u_i' \theta};\ \ \overline{u_i' \theta} = -C_\theta \frac{1}{T}\left(\overline{u_i' u_j'}\frac{\partial T}{\partial x_j}\right);\ \ T = \sqrt{\left(\frac{k}{\varepsilon}\right)^2 + {C_T}^2\left(\frac{k}{\varepsilon}\right)} \tag{4.64}$$

The natural convection case in a differentially heated vertical channel is considered for this study. By looking into the mean velocity distribution as shown in Fig. 4.26: it is observed that the inclusion of the flux Richardson number leads to an improvement in the predictions, and by increasing the value of coefficient C_3, mean velocity prediction is further improved.

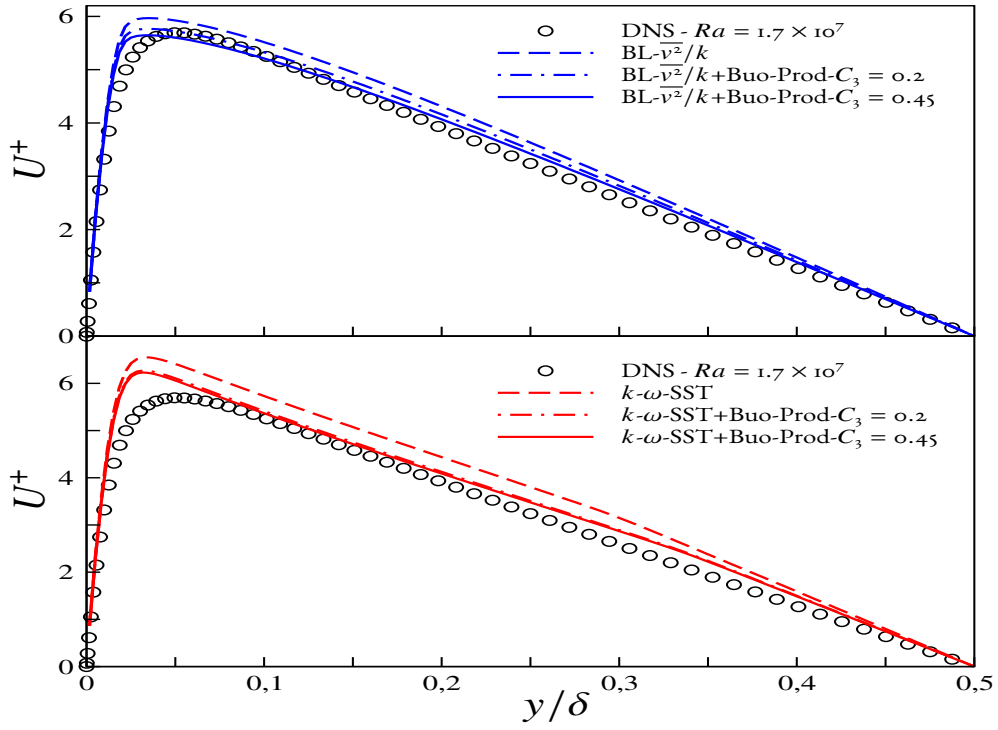

Figure 4.26 – Effect of the flux Richardson number on the mean velocity profile at $Ra = 1.7 \times 10^7$ and $Pr = 0.71$

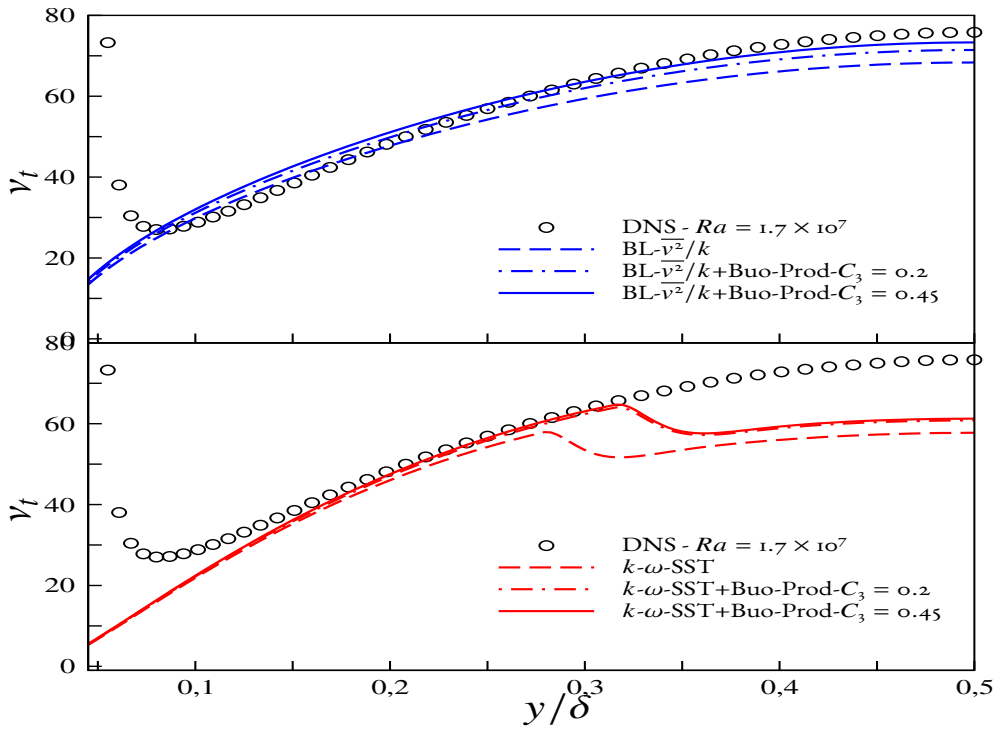

Figure 4.27 – Effect of the flux Richardson number on the turbulent viscosity (ν_t) profile at $Ra = 1.7 \times 10^7$ and $Pr = 0.71$

In order to probe how buoyancy source terms are modifying the turbulent quantities, turbulent viscosity is shown in Fig. 4.27, where it is seen again that there is an under-prediction of turbulent viscosity with original k-ω-SST and BL-$\overline{v^2}/k$ models respectively. However, the inclusion of the R_f leads to the improvement of the prediction of turbulent viscosity particularly corresponding to the value of coefficient C_3 that is 0.45, this prediction of turbulent viscosity modifies the Reynolds shear stress (as Boussinesq relation is considered to model Reynolds stresses) and owing to this there is an improvement in the prediction of mean velocity distribution. Now to understand the modification of turbulent viscosity by the inclusion of buoyancy source terms, total production of turbulent kinetic energy ($P_k + G_k$) and total production of dissipation ($P_\varepsilon + G_\varepsilon$) or specific dissipation ($P_\omega + G_\omega$) are plotted in Fig. 4.28 and Fig. 4.30 respectively.

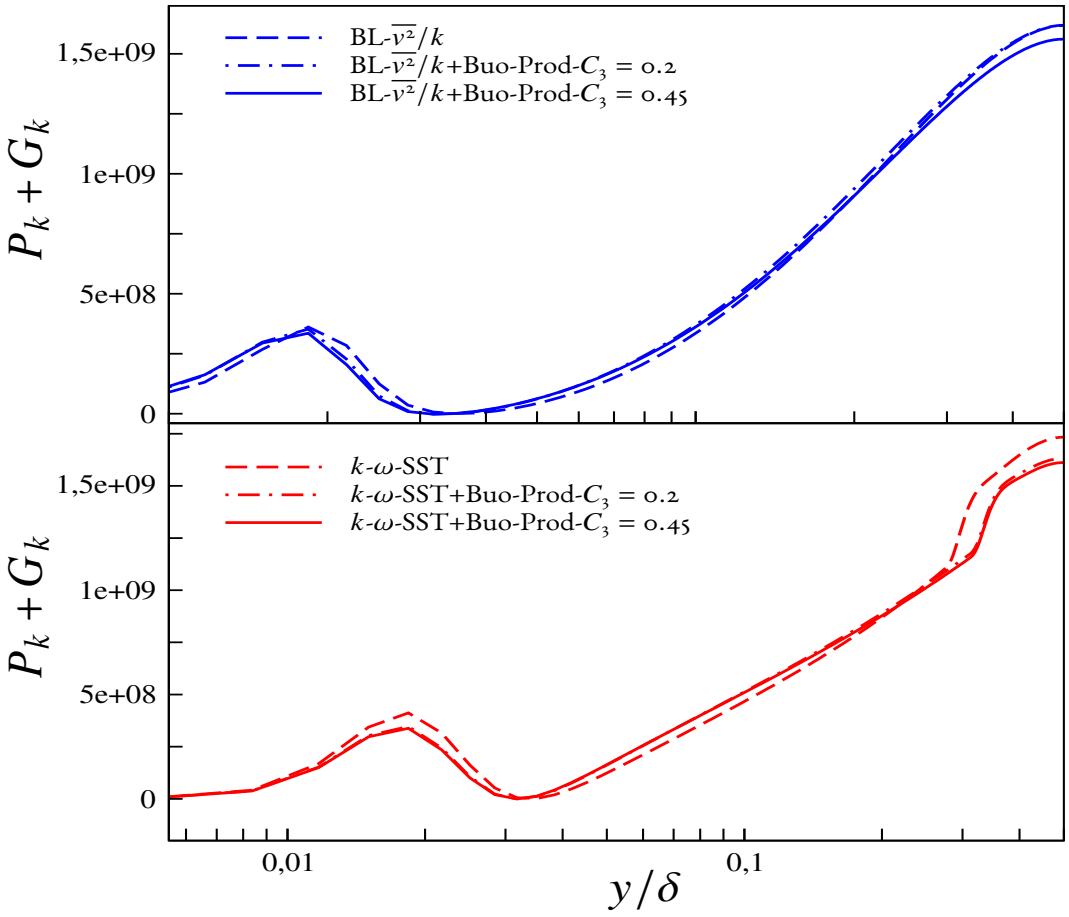

Figure 4.28 – Production of turbulent kinetic energy profile at $Ra = 1.7 \times 10^7$ and $Pr = 0.71$

From Fig. 4.28, it is observed that there is an increase in the production ($P_k + G_k$) in the major portion of the channel, and with the increase of the coefficient (C_3) from 0.2 to 0.45, this increment in production is further enhanced. This is further reinforced by the fact that the inclusion of buoyancy source terms reduce the production of dissipation (P_ε

$+ G_\varepsilon$) or specific dissipation ($P_\omega + G_\omega$) terms as can be seen in Fig. 4.30. This explains the improvement in the prediction of turbulent viscosity as shown in Fig. 4.27.

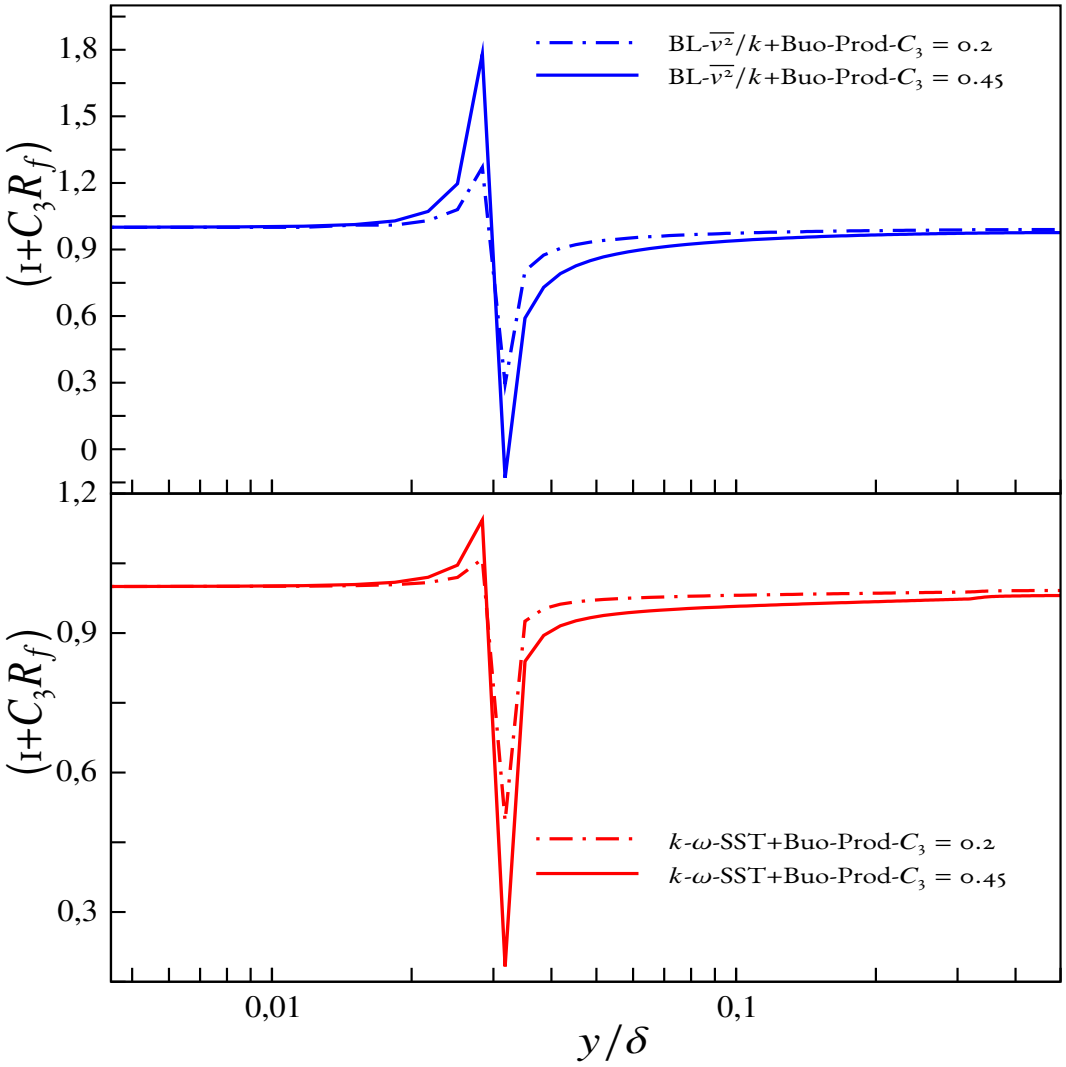

Figure 4.29 – Flux Richardson number factor profile at $Ra = 1.7 \times 10^7$ and $Pr = 0.71$

To probe further in this context, flux Richardson number factor $(1 + C_3 R_f)$ is plotted in Fig. 4.29, it is realized that this factor is increased close to the wall and decreased in the rest of the channel. Moreover, this behavior is enhanced with the increase of the coefficient (C_3), so it is concluded that the role of increasing flux Richardson number factor (by increasing the value of C_3) is to reduce the $P_\omega + G_\omega$ or $P_\varepsilon + G_\varepsilon$ (as shown in Fig. 4.30) and thereby the production $(P_k + G_k)$ of turbulent kinetic energy is enhanced which explain the improvement of turbulent viscosity profile.

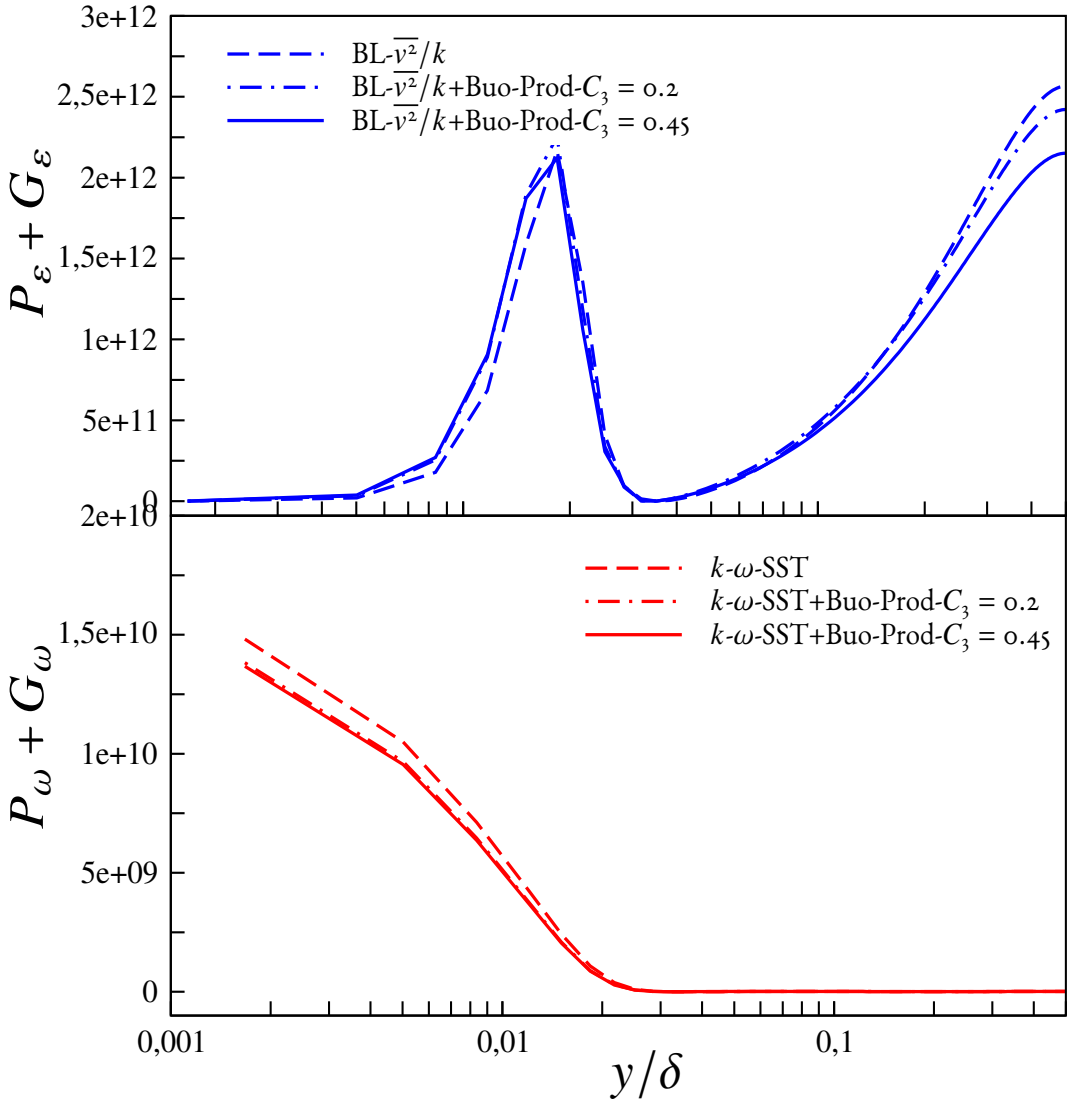

Figure 4.30 – Total production of dissipation or specific dissipation profile at $Ra = 1.7\times10^7$ and $Pr = 0.71$

Mean temperature distribution is shown in Fig. 4.31 and it is noticed that the additional buoyancy source terms improve the prediction of mean temperature. It is noticed that the optimal value of the coefficient (C_3) for both the models is 0.45. In order to overcome the limitation of providing different values of the coefficient C_3 as observed in the previous section, a formulation based on the flux Richardson number has been formulated and tested for the k-ω-SST and BL-v^2/k models. Selecting the optimal value of 0.45 for the two models, it is observed that the inclusion of the flux Richardson number did improve the prediction of mean and turbulent quantities.

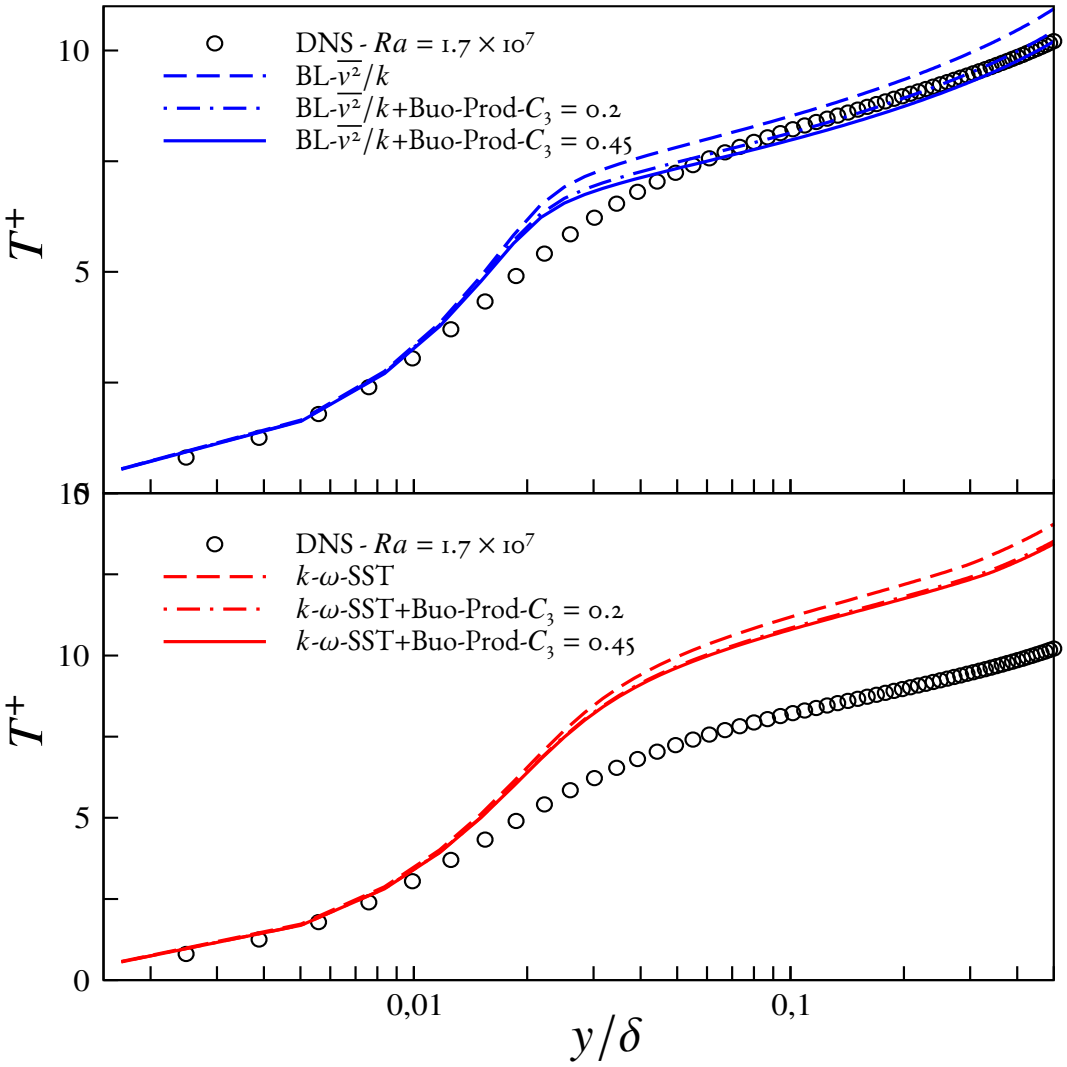

Figure 4.31 – Effect of the flux Richardson number on the mean temperature (T^+) profile at $Ra = 1.7 \times 10^7$ and $Pr = 0.71$

4.3.3 Conclusion

In the first part of this section, simple buoyancy-extended k-ω-SST and BL-$\overline{v^2}/k$ models are formulated and their performances are analyzed in differentially heated vertical channel. It is realized that the simplified buoyancy-extended models are able to better predict the mean and turbulent quantities than the original models which shows that, even with a very simple model for the turbulent heat flux (SGDH), the introduction of a buoyancy extension in the Boussinesq relation is favourable. Secondly, the effect of only adding buoyancy source terms (without the buoyancy-extension in the Boussinesq relation) in the transport equations of turbulent kinetic energy (k) and its dissipation rate (ε or ω) is examined and in addition to that, the sensitivity analysis of the coefficient C_3 is also performed. Two very different turbulence models namely k-ω-SST and BL-$\overline{v^2}/k$

are sensitized to the buoyancy effects. It has been observed that the consideration of the buoyancy source term certainly improves the prediction of mean and turbulent quantities. However, it is noticed that the effect of the inclusion of G_k is strong in improving the results and the addition of G_ε or G_ω is to moderate this effect. As far as the role played by these additional buoyancy source terms in the context of k-ω-SST and BL-$\overline{v^2}/k$ model is concerned, it is increasing the eddy-viscosity which is severely underpredicted by the original version of these models.
As far as the interest of including Flux Richardson number R_f is concerned, it is realised that the effect is the same as with a constant buoyancy coefficient, but the fact that the coefficient C_3 is the same for the two models show an indication of the fact that this modification is less arbitrary.

4.4 Buoyancy sensitized Launder-Sharma model

In this part of the chapter, buoyancy-sensitized Launder-Sharma models is formulated and validated in a challenging natural convection regime in a differentially heated vertical channel corresponding to the highest available Rayleigh number, $Ra = 1.7 \times 10^7$ and results are compared with the DNS data [Kiš and Herwig, 2014].

4.4.1 Buoyancy-extended Launder-Sharma model

As for the others models, the buoyancy-extended Reynolds stress relation for Launder-Sharma model is formulated from the weak equilibrium hypothesis and expressed as follows:

$$\overline{u_i'u_j'} = \underbrace{\frac{2}{3}k\delta_{ij} - \nu_t\left(\frac{\partial U_i}{\partial x_j} + \frac{\partial U_j}{\partial x_i}\right)}_{Boussinesq} + \underbrace{C_\theta^*\frac{k}{\varepsilon}(G_{ij} - \frac{1}{3}\delta_{ij}G_{kk})}_{Buoyancy-extension} \tag{4.65}$$

where $C_\theta^* = 0.1$ and $G_{ij} = -\beta(g_i\overline{u_j'\theta} + g_j\overline{u_i'\theta})$.
The buoyancy-extended heat flux relation is described as follows:

$$\overline{u_i'\theta} = -C_\theta\frac{k}{\varepsilon}\left[(\overline{u_i'u_j'})_{Boussinesq} + (\overline{u_i'u_j'})_{Buoyancy-extension}\right]\frac{\partial T}{\partial x_j} \tag{4.66}$$

C_θ is formulated in such a manner that buoyancy-extended model must revert back to original Launder-Sharma model if the influence of buoyancy is negligible and expressed as follow:

$$\overline{v'\theta} = \underbrace{-\frac{\nu_t}{Pr_t}\frac{\partial T}{\partial y}}_{SGDH} = \underbrace{-C_\theta\frac{k}{\varepsilon}\overline{v'^2}\frac{\partial T}{\partial y}}_{GGDH}$$
$$C_\theta = \frac{3}{2}\frac{C_\mu}{Pr_t}f_\mu \tag{4.67}$$

This buoyancy modified Reynolds stress and heat flux relations are used in the momentum and energy equations. The effect of the buoyancy extension is considered in the dynamic production of turbulent kinetic energy and expressed in the following equation :

$$P_k = -\left[(\overline{u_i'u_j'})_{Boussinesq} + (\overline{u_i'u_j'})_{Buoyancy-extension}\right]\frac{\partial U_i}{\partial x_j} \tag{4.68}$$

The buoyancy production terms in the transport equation of turbulent kinetic energy and dissipation equation are modeled using the generalized gradient diffusion hypothesis (GGDH) and expressed as follows:

$$\begin{aligned} G_k &= -\beta g_i \overline{u_i'\theta} \\ G_\varepsilon &= C_{\varepsilon 3}\frac{\varepsilon}{k} max(G_k, 0) \end{aligned} \tag{4.69}$$

The modified transport equations of k and ε are:

$$\frac{Dk}{Dt} = P_k + G_k + \frac{\partial}{\partial x_j}\left[\left(\nu + \frac{\nu_t}{\sigma_k}\right)\frac{\partial k}{\partial x_j}\right] - \left[\widetilde{\varepsilon} + \underbrace{2\frac{\mu}{\rho}\left(\frac{\partial\sqrt{k}}{\partial x_j}\right)^2}_{D}\right] \tag{4.70}$$

$$\frac{D\widetilde{\varepsilon}}{Dt} = C_{\varepsilon 1} f_1 \frac{\widetilde{\varepsilon}}{k} P_k + \underbrace{C_{\varepsilon 3} f_1 \frac{\widetilde{\varepsilon}}{k} max\left(G_k, 0\right)}_{G_\varepsilon} + \frac{\partial}{\partial x_j}\left[\left(\nu + \frac{\nu_t}{\sigma_\varepsilon}\right)\frac{\partial \widetilde{\varepsilon}}{\partial x_j}\right] - C_{\varepsilon 2} f_2 \frac{\widetilde{\varepsilon}}{k} + 2\nu\nu_t\left[\left(\frac{\partial U_i}{\partial x_j}\right)^2\right] + \underbrace{0.83\left(\frac{k^{3/2}}{c_l\widetilde{\varepsilon}y} - 1\right)\left(\frac{k^{3/2}}{c_l\widetilde{\varepsilon}y}\right)^2\frac{\widetilde{\varepsilon}^2}{k}}_{Yap-term} \tag{4.71}$$

where $C_{\varepsilon 3} = 2.6$ and other functions are as per standard Launder-Sharma model [Launder and Sharma, 1974]. As we have seen in Chapter-2, the introduction of Yap term leads to the improvement of the results to some extent, but there are discrepancies in the mean flow profiles particularly in mean temperature profile. So the goal of this section is to analyse the effect of the buoyancy-extended Launder-Sharma model which is associated with the Yap term.

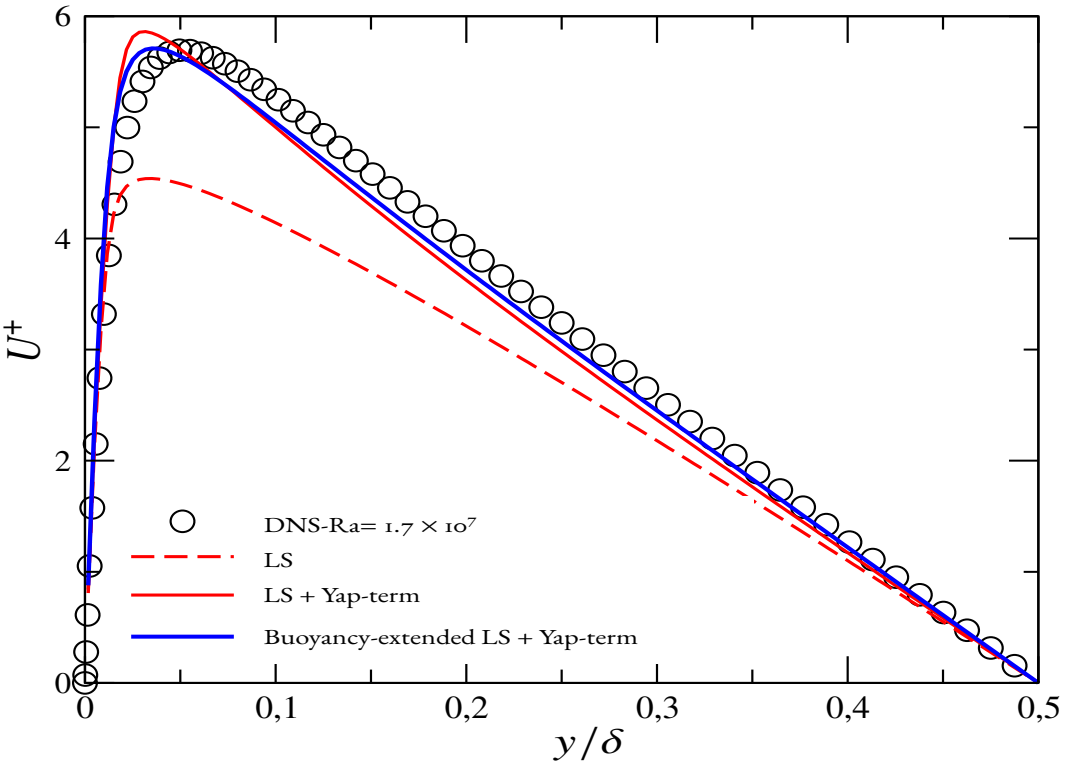

Figure 4.32 – Mean velocity profile at $Ra = 1.7 \times 10^7$ and $Pr = 0.71$

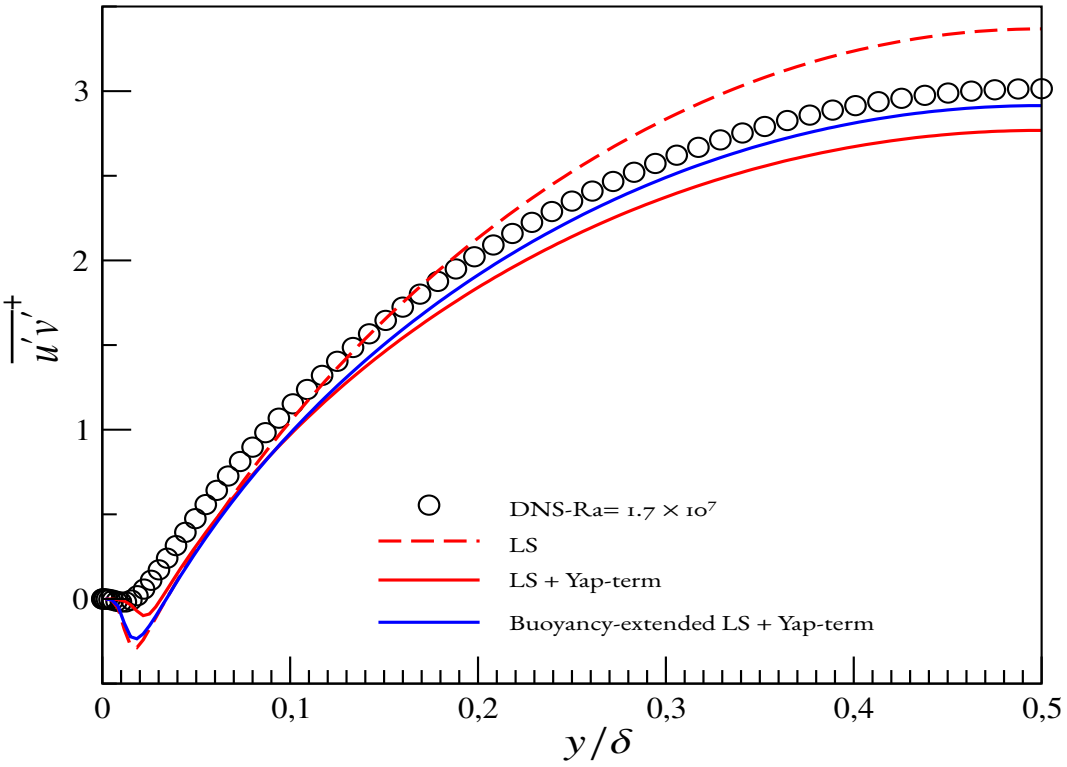

Figure 4.33 – Turbulent shear stress profile at $Ra = 1.7 \times 10^7$ and $Pr = 0.71$

Looking into the Fig. 4.32, it is observed that there is a significant improvement in the mean velocity with the inclusion of the Yap term as compared to the prediction of the original Launder-Sharma model which severely underpredicts it. However, mean velocity remains slightly underestimated even with the inclusion of Yap term. The inclusion of buoyancy-extension in the Launder-Sharma model, leads to slightly improve the mean velocity. Again, this improvement in prediction of mean velocity is linked to the better prediction of turbulent shear stress which is underestimated even with the addition of the Yap term. Due to the inclusion of buoyancy-extension in the standard Boussinesq relation of Reynolds stress, the discrepancy in the prediction of shear stress is avoided as shown in Fig. 4.33, and this leads to the better prediction of mean velocity.

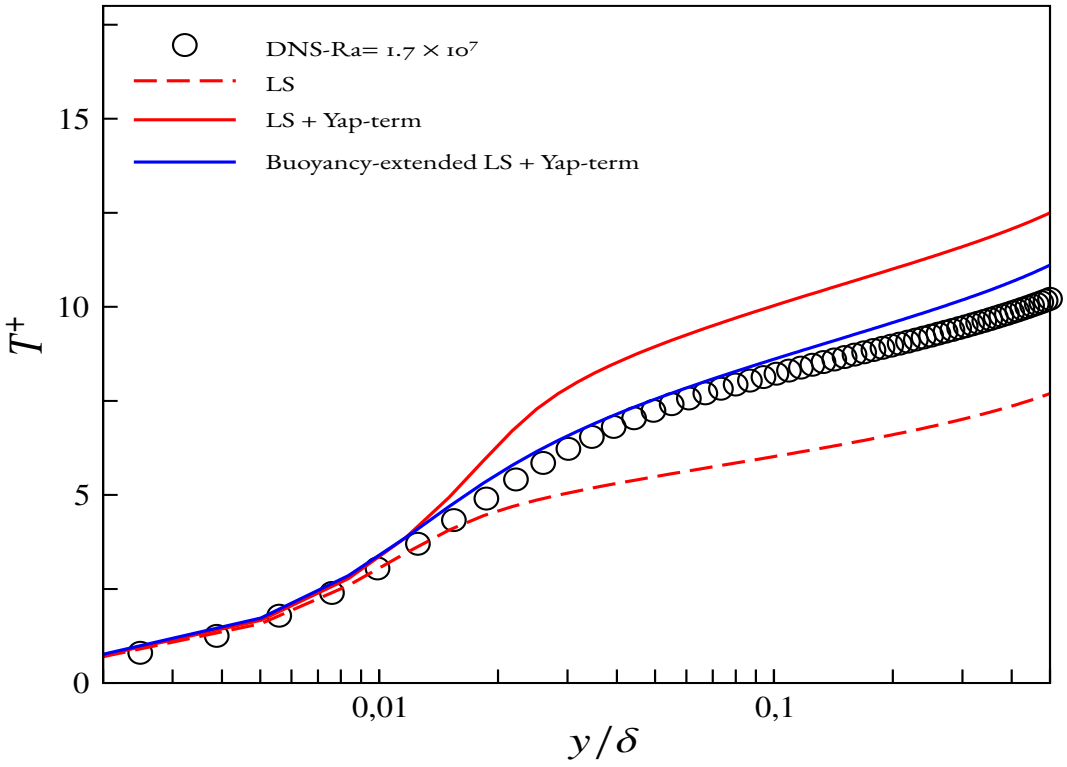

Figure 4.34 – Mean temperature profile at $Ra = 1.7 \times 10^7$ and $Pr = 0.71$

Mean temperature distribution is shown in Fig. 4.34 and it is realized that the inclusion of the Yap term in the Launder-Sharma model does not lead to a correct prediction of the mean temperature. However, there is a drastic improvement in the mean temperature prediction with the buoyancy-extended model, and the misprediction of mean temperature is avoided to a great extent. This prediction of mean temperature is directly linked to the prediction of the wall-normal heat flux, which is improved with the buoyancy-extended model as shown in Fig. 4.35 and the better prediction of the wall-normal heat flux is the root cause for the improved prediction of mean temperature. So it is noticed that the inclusion of buoyancy extension in association with the Yap term improves the prediction of

mean and turbulent quantities, which signify that this buoyancy extension is the physically relevant term which is missing in the original model.

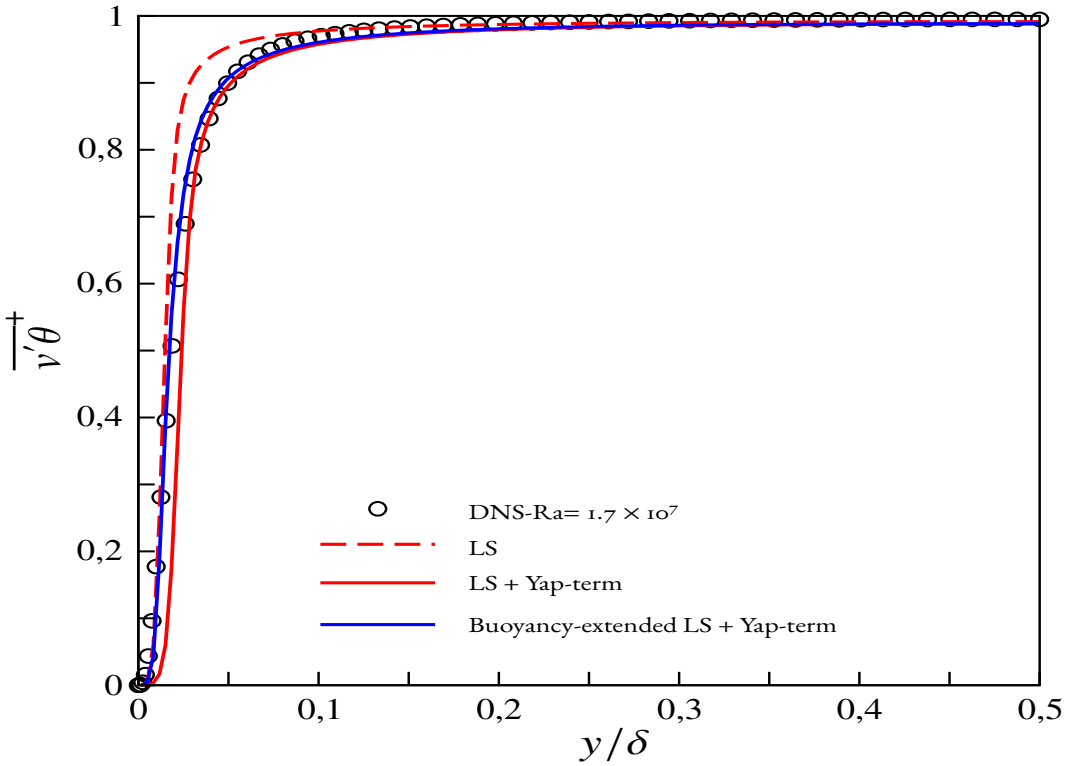

Figure 4.35 – Wall normal heat flux profile at $Ra = 1.7 \times 10^7$ and $Pr = 0.71$

In the next section, a detailed analysis of adding only buoyancy source terms in the Launder-Sharma model is performed.

4.4.2 Effect of adding only buoyancy source terms in the Launder-Sharma model

Similar to the other models, we have investigated the influence of adding the buoyant source terms associated with the original Boussinesq relation. After adding the buoyant source terms, the transport equations of the turbulent kinetic energy and the turbulent dissipation rate for Launder and Sharma [1974] model is given below:

$$\frac{\partial k}{\partial t} + U_k \frac{\partial k}{\partial x_k} = P_k + G_k + \frac{\partial}{\partial x_j}\left[\left(\nu + \frac{\nu_t}{\sigma_k}\right)\frac{\partial k}{\partial x_j}\right] - \left[\widetilde{\varepsilon} + \underbrace{2\frac{\mu}{\rho}\left(\frac{\partial \sqrt{k}}{\partial x_j}\right)^2}_{D}\right] \tag{4.72}$$

$$\frac{\partial \widetilde{\varepsilon}}{\partial t} + U_k \frac{\partial \widetilde{\varepsilon}}{\partial x_k} = C_{\varepsilon 1} f_1 \frac{\widetilde{\varepsilon}}{k} P_k + \underbrace{C_3 f_1 \frac{\widetilde{\varepsilon}}{k} max\left(G_k, 0\right)}_{G_\varepsilon} + \frac{\partial}{\partial x_j}\left[\left(\nu + \frac{\nu_t}{\sigma_\varepsilon}\right)\frac{\partial \widetilde{\varepsilon}}{\partial x_j}\right] - C_{\varepsilon 2} f_2 \frac{\widetilde{\varepsilon}}{k} + 2\nu\nu_t\left[\left(\frac{\partial U_i}{\partial x_j}\right)^2\right] \tag{4.73}$$

where constants and other functions are as per Launder and Sharma [1974] model. Note that the Yap term is not introduced here. Moreover, the max in the definition of G_ε in Eq. 4.73 is included to distinguish between the stably and unstably stratified flows (as discussed in Section 4.3.2). G_k is modeled based on the GGDH approach:

$$G_k = -\beta g_i \overline{u_i{}'\theta}; \quad \overline{u_i{}'\theta} = -C_\theta \frac{k}{\varepsilon}\left(\overline{u_i{}'u_j{}'}\frac{\partial T}{\partial x_j}\right) \tag{4.74}$$

However, the Reynolds stresses in the momentum equation and the turbulent heat fluxes in the energy equation are modeled using the original Boussinesq relation and the simple gradient diffusion hypothesis (SGDH) respectively. Different values of the coefficient C_3 are considered to analyse the sensitivity of this coefficient. Moreover, $C_3 = 0.0$ represents the effect of only adding G_k.

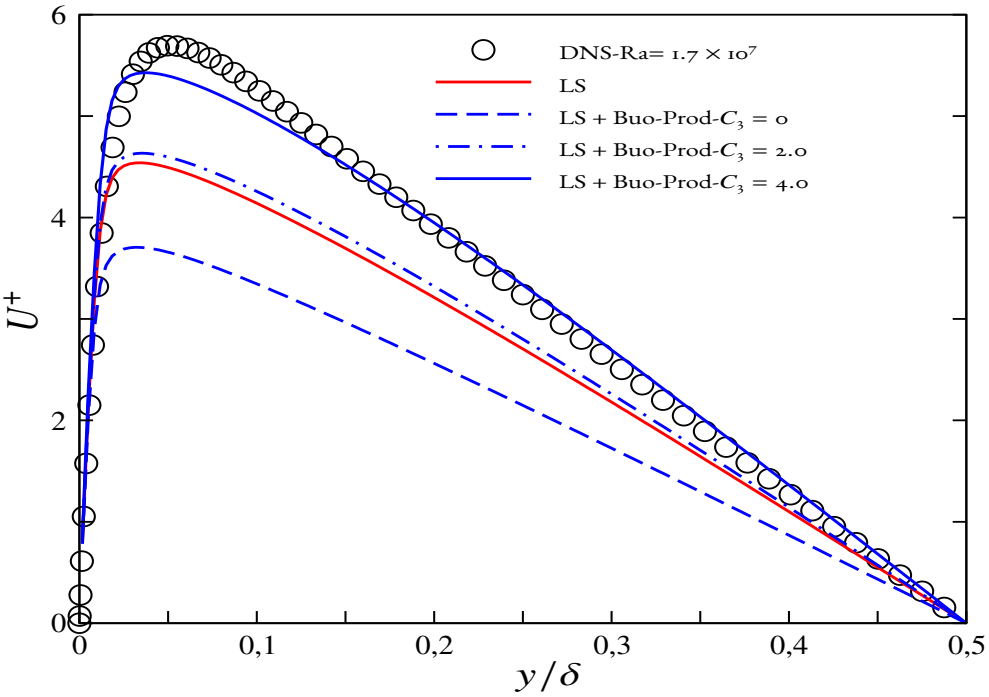

Figure 4.36 – Mean velocity profile at $Ra = 1.7 \times 10^7$ and $Pr = 0.71$

In this part of the section, the effect of adding buoyancy source terms in the transport equation of turbulent kinetic energy and its dissipation rate is analyzed by simulating differentially heated vertical channel at the available highest Rayleigh number that is Ra $= 1.7 \times 10^7$. Looking into Fig. 4.36, it can be seen that there is a severe underestimation of the mean velocity with the original Launder-Sharma model. As discussed previously, the addition of only G_k brings drastic improvement in the case of k-ω-SST and BL-$\overline{v^2}/k$ models, since it reduces the mean velocity which is initially overestimated. On the contrary, in the case of the Launder-Sharma model, adding only G_k term make the prediction of mean velocity worse, as the mean velocity is initially underestimated.

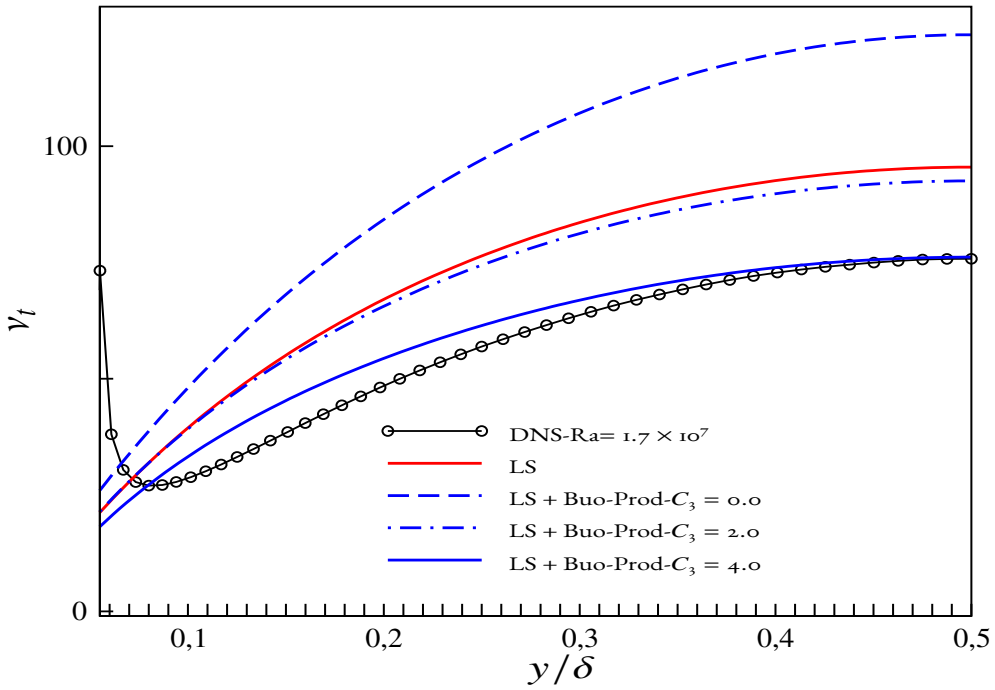

Figure 4.37 – Turbulent viscosity profile at $Ra = 1.7 \times 10^7$ and $Pr = 0.71$

Moreover, it is noticed that by increasing the value of the coefficient C_3 (in G_ε term), there is an improvement in the prediction as can be seen in Fig. 4.36.

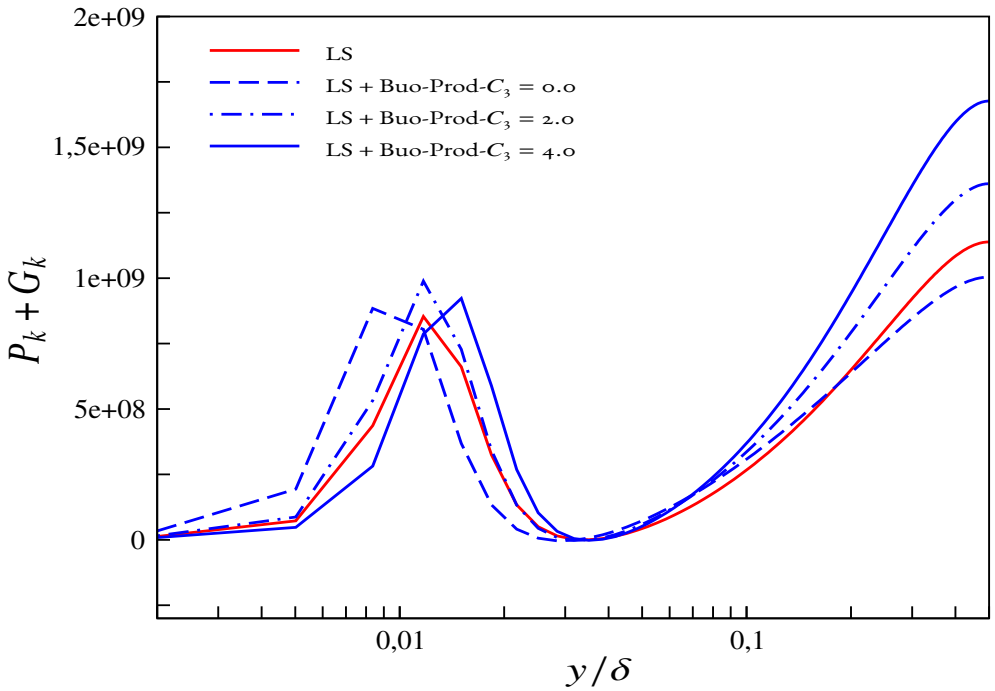

Figure 4.38 – Total production of turbulent kinetic energy at $Ra = 1.7 \times 10^7$ and $Pr = 0.71$

Furthermore, it is realized that the inclusion of the G_ε term is vital in the case of

the Launder-Sharma model. In order to better understand the role of these additional buoyant source terms, the distribution of turbulent viscosity is analyzed. From Fig. 4.37, it is observed that there is a severe overestimation of the turbulent viscosity by the original Launder-Sharma model. This discrepancy in turbulent viscosity is further enhanced with the addition of the G_k ($C_3 = 0.0$) term only. However, with the inclusion of the G_ε term, there is an improvement in the prediction and corresponding to the value of coefficient $C_3 = 4.0$, the turbulent viscosity is greatly improved. This recovery in the prediction of turbulent viscosity affects the momentum balance through turbulent shear stress (as Boussinesq relation is used to model Reynolds stresses) which avoid the misprediction of the mean velocity gradient and hence there is an improvement in the prediction of mean velocity. In order to investigate further, analysis of the effect of buoyancy source terms on the production ($P_k + G_k$) of the turbulent kinetic energy, and production of dissipation ($P_\varepsilon + G_\varepsilon$) terms is done. Looking into Fig. 4.38, it is noticed that with the addition of the G_ε term, there is an increase in total production ($P_k + G_k$) in a major portion of the channel (except in the near-wall region). However, the total production of dissipation ($P_\varepsilon + G_\varepsilon$) is greatly enhanced in magnitude (as shown in Fig. 4.39) as compare to $P_k + G_k$ term, which shows that the role of adding the G_ε term in the Launder-Sharma model is to damp the turbulent viscosity greatly as shown in Fig. 4.37.

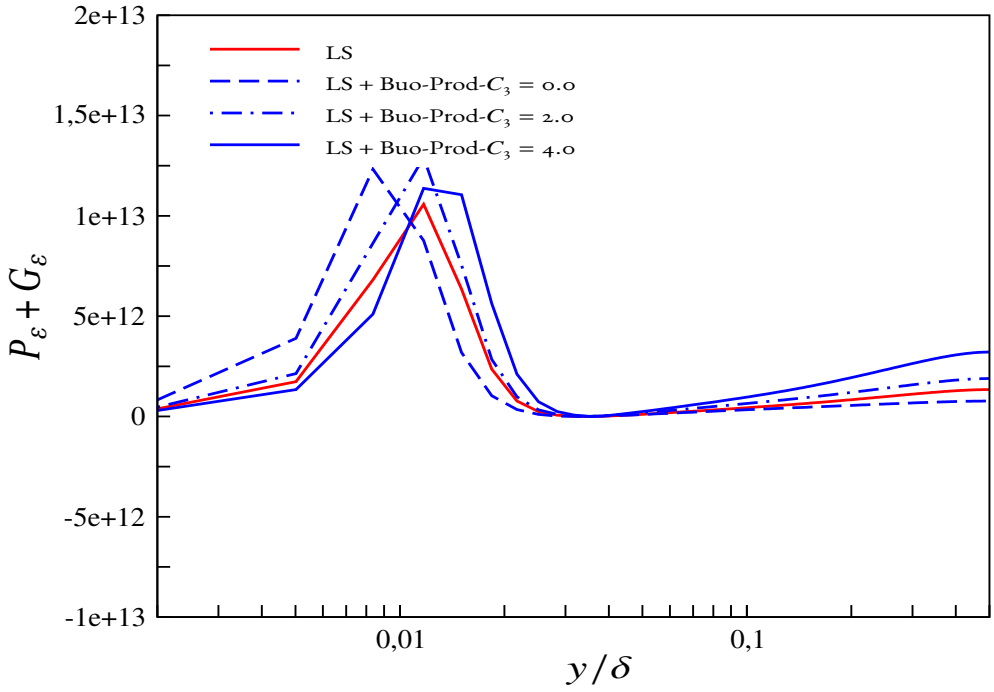

Figure 4.39 – Total production of dissipation rate of turbulent kinetic energy at $Ra = 1.7 \times 10^7$ and $Pr = 0.71$

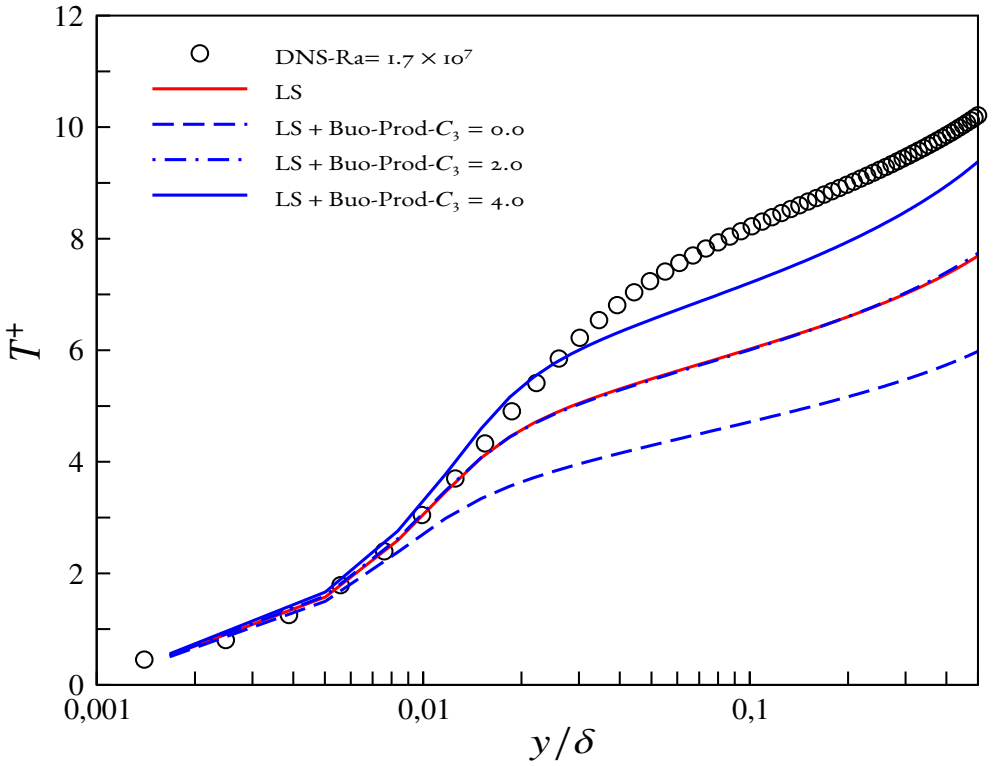

Figure 4.40 – Mean temperature profile at $Ra = 1.7 \times 10^7$ and $Pr = 0.71$

The mean temperature distribution is shown in Fig. 4.40. It is observed that the original Launder-Sharma model severely underestimates the mean temperature. Moreover, the addition of only G_k leads to further underestimates the mean temperature and worsen the results. However, the inclusion of the G_ε term leads to the improvement in the mean temperature and corresponding to the value of coefficient $C_3 = 4.0$, there is a drastic improvement in mean temperature profile. Again it is confirmed that the addition of G_ε in Launder-Sharma model is necessary.

4.4.3 Conclusion for the Launder-Sharma model

Firstly, the buoyancy-extended Launder-Sharma model in association with the Yap term is formulated and its performance is analyzed in differentially heated channel cases. It is interesting to observe that the buoyancy extension applied to Launder-Sharma model has a strong effect on the mean temperature profile and also corrects the misprediction of velocity profile. In contrast, for the buoyant source terms alone, the velocity profile is very well corrected but the temperature profile is not accurate. Moreover, the addition of the G_ε term is necessary in the Launder-Sharma model and the results are improved by increasing the value of C_3 from 0.0 to 4.0.

4.5 Conclusion

Buoyancy driven flows are observed in many heat transfer applications which is also a major concern for the industry, in particular for the application that has motivated this work, the heat transfer in the underhood space of automobiles.
For the thermal under hood design of cars, eddy-viscosity based turbulence models available in commercial codes are not sufficiently sensitive to buoyancy effects. In Ansys Fluent used by the PSA group for the designing of the engine compartment, there is a provision of activating the buoyancy production terms. However, these terms are based on simple gradient diffusion hypothesis (SGDH) and this will lead to underestimate the influence of buoyancy on turbulence. On the other hand, these models are able to give good results in the cruising stages of the vehicle, but for the situation when the buoyancy is playing a dominant role in modifying turbulence, these models are insufficient to reproduce the physics and characteristics of the flow. The goal of the present chapter was to develop a range of buoyancy modified eddy-viscosity models which can provide satisfactory results in the design of the real underhood compartment of automobiles.
In the pursuit of this objective, three very different turbulence models are sensitized to the buoyancy effects with the determination that these sensitized models are able to reproduce the anisotropy of turbulence due to buoyancy which is absent in the original models. The investigation of turbulent phenomena is most conveniently made in the flow configurations where the influence of other physical processes can be isolated. In the context of the design of underhood-space of the automobiles, differentially heated vertical channel flow at high Rayleigh number is selected to develop and to validate the buoyancy modified turbulence models namely k-ω-SST, BL-$\overline{v^2}/k$ and Launder-Sharma model respectively. The other major concern of the work is to sensitize the turbulence models in such a manner that the physically relevant terms need to be provided in the eddy-viscosity models so that the anisotropy of turbulence due to buoyancy can be reproduced and the models revert back to the original version of the model, when it is used to compute flows where buoyancy is negligible.
In the pursuit of this objective, different versions of buoyancy extended models are developed based on the complexity and capability of reproducing the characteristics of flow. In these buoyancy-extended models, the modeling of the buoyancy extension is performed in such a way that the buoyancy contribution is taken directly from the Reynolds stress equation in association with the generalized gradient diffusion hypothesis (GGDH) to model heat fluxes and this buoyancy extension preserves the linearity of the Reynolds stress relation.
Motivated by the limitation to model tensorial diffusivity in the commercial codes, in particular for Ansys Fluent, simple versions of buoyancy extended models are developed and validated. It is observed that the buoyancy extension is indeed required for capturing the effect of buoyancy on turbulence. For instance, original versions of k-ω-SST and BL-$\overline{v^2}/k$

model lead to the severe overprediction of the mean velocity and underprediction of turbulent viscosity. By providing this buoyancy extension in the constitutive relation of the Reynolds stress and heat flux, the results are drastically improved which confirms that the misprediction of the mean and turbulent quantities by the original models is due to the lack of this buoyancy contribution.

Further, a simpler approach without the buoyancy extension is considered by adding only buoyant source terms (in k and ε or ω equations) which is modeled using GGDH approach. Moreover, the necessity of including the buoyant source term G_ε or G_ω in the dissipation equation is also analyzed. It has been observed that the choice of the coefficient C_3 (in G_ε or G_ω) is dependent on the selected model. For instance, in the case of k-ω-SST and BL-$\overline{v^2}/k$ model, the results are better by reducing the value of this coefficient and the addition of only the G_k term ($C_3 = 0.0$) has a strong effect on results and the inclusion of G_ε or G_ω moderates the results. On the other hand, for the Launder-Sharma model, it is noticed that the addition of only G_k ($C_3 = 0.0$) worsens the results and it is necessary to include the G_ε term and the results are better by increasing the value of coefficient C_3 from 0.0 to 4.0.

Moreover, the effect of including the flux Richardson number in G_ω or G_ε is also analysed in association with the k-ω-SST and BL-$\overline{v^2}/k$ model. It is noticed that the prediction of mean velocity and mean temperature profiles are improved and strikingly the optimal value of the coefficient $C_3 = 0.45$ is same for the both the models.

Chapter 5

Rectangular cavity

Contents

5.1 Description of the test case

This test case is based on the DNS data by Trias et al. [2010] in a differentially heated rectangular cavity with the aspect ratio of 4 : 1 in the natural convection regime. The Rayleigh number based on the height of the cavity is 10^{11}. This DNS simulation [Trias et al., 2010] is the continuation of the work by Trias et al. [2007] where a lower Rayleigh number was considered. In this DNS, kinematic viscosity (ν) and thermal diffusivity (κ) are considered to be constant. For the variation of density, the Boussinesq approximation is used with the linear variation of density with temperature. The testing of the buoyancy-extended models is performed for this configuration. In addition to that, the analysis of adding only buoyant source terms in the transport equations of k and ω or ε is made, where these source terms are modeled using two different approaches, namely the simple gradient diffusion hypothesis (SGDH) and the generalized gradient diffusion hypothesis (GGDH), respectively.

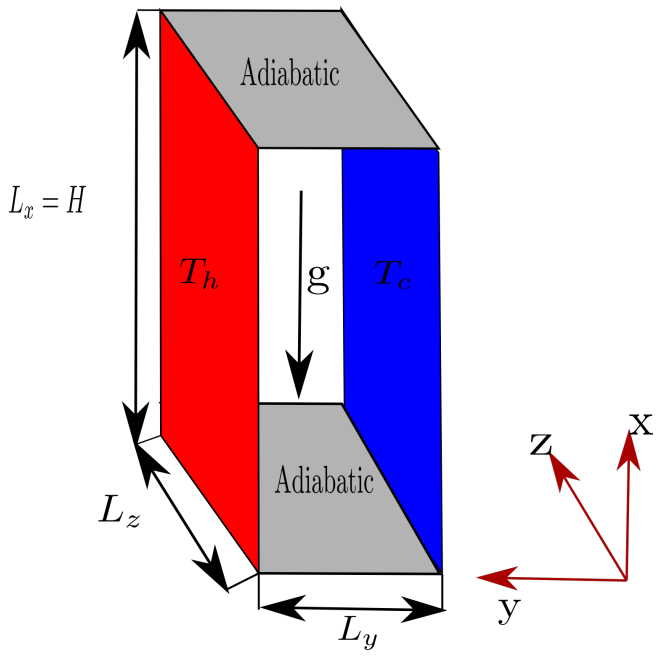

Figure 5.1 – Schematic diagram of the rectangular cavity of aspect ratio 4 : 1 [Trias et al., 2010]

Fig. 5.1 shows the schematic diagram of the flow configuration of the cavity, where $L_x = H$ and $L_y = L_z = 0.25H$. The cavity is subjected to a uniform temperature difference (ΔT) between the hot wall at $y = L$ and the cold wall at $y = 0$. The bottom and top walls are considered to be adiabatic. DNS data of Trias et al. [2007] provide the mean and turbulent quantities to compare the performance of eddy-viscosity models. No radiation is taken into account, and the momentum and energy equations are non-

dimensionalized by the Rayleigh number which writes

$$Ra = \frac{g\beta\Delta T H^3}{\nu\kappa} \tag{5.1}$$

which is based on the height of the cavity, and the Prandtl number is defined as

$$Pr = \frac{\nu}{\kappa} \tag{5.2}$$

The scales used for non-dimensionalization are H for the length scale, $\frac{H^2}{\kappa}\sqrt{Ra}$ for the time scale, ΔT for the temperature scale, and for the dynamic pressure $\rho\frac{\kappa^2}{H^2}Ra$, respectively. The non-dimensionalized momentum and energy equations become:

$$\frac{D\widetilde{U_i}}{D\widetilde{t}} = \frac{Pr}{\sqrt{Ra}}\nabla^2\widetilde{U_i} - \nabla\widetilde{P} + \widetilde{f_i} \tag{5.3}$$

$$\frac{D\widetilde{T}}{D\widetilde{t}} = \frac{1}{\sqrt{Ra}}\nabla^2\widetilde{T} \tag{5.4}$$

where $f_i = (Pr\widetilde{T}, 0, 0)$

From the point of view of understanding the physics of this cavity of aspect ratio 4 : 1, this flow configuration is quite different from the infinite cavity discussed in the previous chapter. The cavity is characterized by laminar, transitional and turbulent regions, and it is very different from the fully developed case used before (vertical channel) for the development of buoyancy sensitized models and it is a challenge for the assessment of these models, as the models are used in the off-design condition. Moreover, in this type of cavity flow, boundary layers on the two vertical walls have very marginal interactions and thereby the level of turbulence is low in the central region.

Saury et al. [2011] performed the experimental investigation of natural convection in an air-filled rectangular cavity. It has been reported in his study that the stratification parameter was not significantly modified when the Rayleigh number is changed, and it is the aspect ratio of 4 : 1 which played an important role in the stratification mechanism. Moreover, wall radiation modifies wall temperature and it reduces the vertical temperature gradient and thereby the stratification parameter is lower. As far as the general behavior in the cavity is concerned, it is reported that there is a recirculation area in the upper part of the cavity and with the increase of Rayleigh number, downward airflow intensifies on the outer edge of the hot boundary layer. Based on the velocity vectors, two kinds of airflow behavior are categorized, namely Case-1 and Case-2. In Case-1, the cold boundary layer is fed by the downward flow and in Case-2, the hot boundary layer is fed by downward airflow.

Trias et al. [2010] used the same dimensions of the cavity as used in Saury et al. [2011] but periodicity is applied in the z-direction, which makes this cavity less costly and easier for testing models. In view of this context, the distribution of turbulent kinetic energy

is shown in the third line of Fig. 5.2 for the three selected models, namely the k-ω-SST, BL-$\overline{v^2}/k$, and low Reynolds Launder-Sharma models. It is observed that the flow is almost laminar in all the cavity except for two zones in the near-wall region of the upper part on the side of the hot wall and the lower part on the side of the cold wall (there is a central symmetry in this flow). Furthermore, it is noticed that the prediction of the transition from laminar to turbulent is very different for each model. For instance, the k-ω-SST and Launder-Sharma models predict early transition as compared to the BL-$\overline{v^2}/k$ model. Fig. 5.2 also shows the distribution of the magnitude of the velocity on the first line and temperature on the second line: it is observed that the velocity and temperature are almost uniform and constant in y, in the center of the cavity, and the boundary layers are very thin. A stratification is clearly visible on the temperature fields.

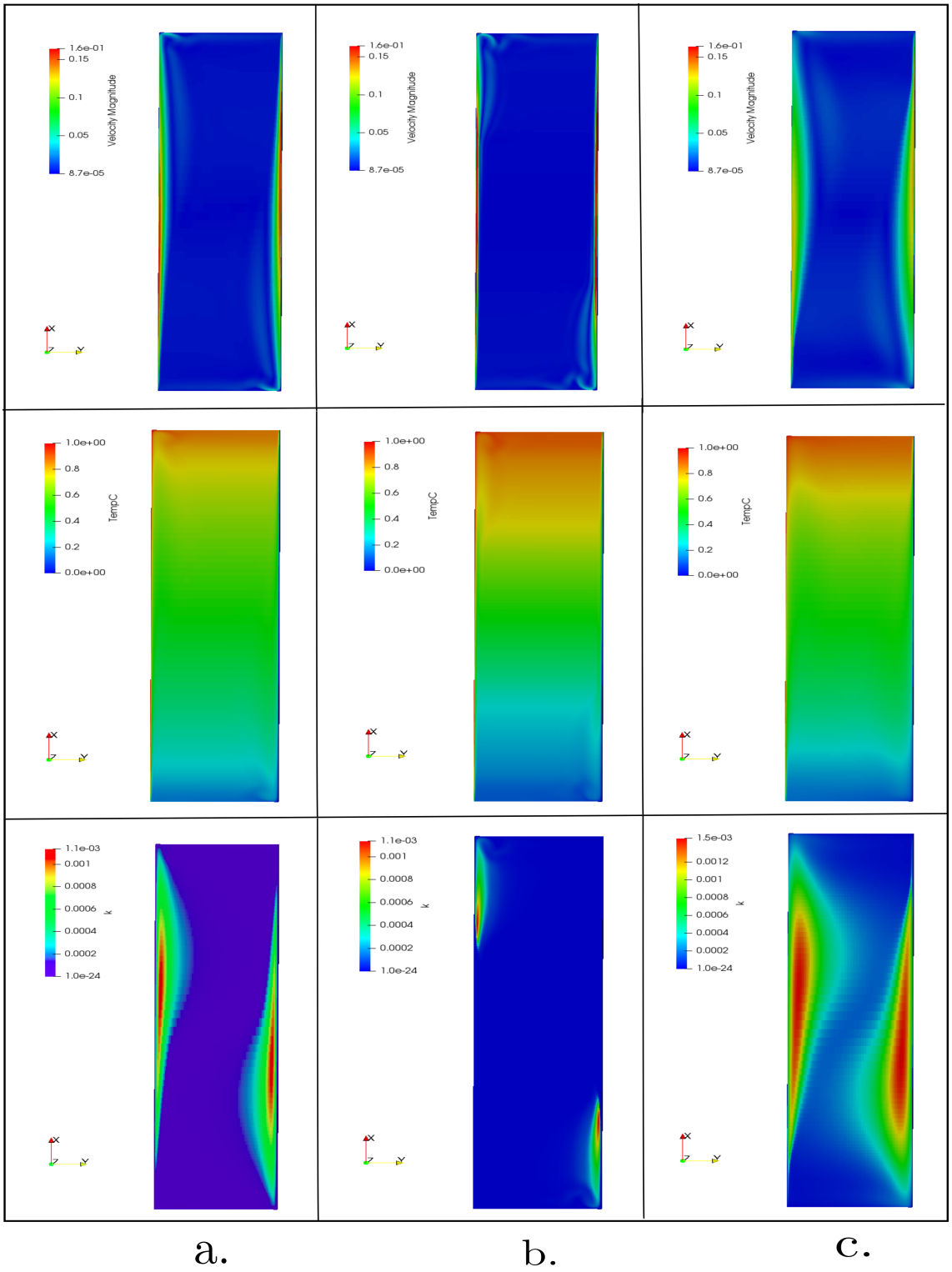

Figure 5.2 – Distribution of velocity (first line), temperature (second line), turbulent kinetic energy (third line) in $4:1$ cavity [Trias et al., 2010] for three models:
(a.) k-ω-SST; (b.) BL-$\overline{v^2}/k$; (c.) Launder-Sharma

In the next section, the performance of the buoyancy modified models are evaluated against the DNS of Trias et al. [2010].

5.2 Performance of the buoyancy sensitised models

5.2.1 Buoyancy-extended models

A brief recall of the full buoyancy-extended model is discussed, where the buoyancy-extension is derived from the transport equation of the Reynolds stress by considering the weak equilibrium hypothesis.
The buoyancy-extended Reynolds stress relation writes as follows:

$$\overline{u_i' u_j'} = \underbrace{\frac{2}{3}k\delta_{ij} - \nu_t\left(\frac{\partial U_i}{\partial x_j} + \frac{\partial U_j}{\partial x_i}\right)}_{Boussinesq} + \underbrace{C_\theta^* \tau (G_{ij} - \frac{1}{3}\delta_{ij}G_{kk})}_{Buo-extension} \tag{5.5}$$

where $C_\theta^* = 0.1$ and $G_{ij} = -\beta(g_j\overline{u_i'\theta} + g_i\overline{u_j'\theta})$.
Heat fluxes in buoyancy production terms is modeled using GGDH approach which reads:

$$G_k = -\beta g_i \overline{u_i'\theta} \tag{5.6}$$

The performance of the buoyancy-extended k-ω-SST and buoyancy-extended BL-$\overline{v^2}/k$ models are examined by plotting the mean and turbulent quantities at different heights of the cavity. Due to central symmetry, the following figures only show the hot side of the wall.
The wall shear stress on the hot side is plotted in Fig. 5.3 and it is observed from the DNS of Trias et al. [2010] that the flow remains laminar up to the height $x = 0.4$, the flow transitions in the region between $0.4 < x/L < 0.6$ and finally it is fully turbulent in the region between $0.6 < x/L < 0.9$. Fig. 5.4 shows that this transition does not significantly affect the Nusselt number up to the end of the transition region, at $x/L = 0.6$, where a kink is observed, leading to a higher level of the Nusselt number in the fully turbulent region.
In Fig. 5.4, it can be seen that the k-ω-SST model experiences an abrupt transition to turbulence before $x/L = 0.2$, since the Nusselt number rapidly reaches a turbulent value. The buoyancy extension significantly delays the transition and also leads to a less abrupt transition. In contrast, Figs. 5.3 and 5.4 show that the BL-$\overline{v^2}/k$ starts transitioning around $x/L = 0.3$, but the transition is very slow and a fully turbulent state is reached only at $x/L = 0.8$. Fig. 5.5(a) and Fig. 5.5(d) in the laminar region shows that the original k-ω-SST model predicts a much too early transition, whereas original BL-$\overline{v^2}/k$ remains laminar. The transition phenomena by the k-ω-SST model is improved by the buoyancy-extended version (Fig. 5.5 (d) at $x = 0.2$). From Fig. 5.5 (b) and Fig. 5.5 (e), since the k-ω-SST model is already transitioned, the results are acceptable. In contrast,

the BL-$\overline{v^2}/k$ model predicts too slow a transition, but this is improved by the buoyancy-extended version (Fig. 5.5 (e) at $x = 0.7$). This improvement by the buoyancy-extended models is important as it improves the location and rapidity of transition. Moreover, there is an improvement in the prediction of the mean velocity by the buoyancy-extended models in the turbulence zone as shown in Fig. 5.5 (c) and Fig. 5.5 (f), and this improvement is the consequence of the improvement of results in the transition zone shown in Fig. 5.5 (b) and Fig. 5.5 (e).

To observe the effect of the buoyancy extension on thermal characteristics, mean temperature profiles are plotted at different heights of the cavity. It is observed in Fig. 5.6 (a) and Fig. 5.6 (d) that the prediction of mean temperature profile by the k-ω-SST model show much too early a transition. However, the BL-$\overline{v^2}/k$ model remains laminar and results are in good agreement with the mean temperature profile of DNS. Fig. 5.6 (b) and Fig. 5.6 (e) show that the k-ω-SST model is already transitioned as can be seen in the prediction of wall-normal heat flux and BL-$\overline{v^2}/k$ model predicts too slow a transition, but this is improved by the buoyancy-extended BL-$\overline{v^2}/k$ model (Fig. 5.6 (e) at $x = 0.7$). Further, it is observed that there is an improvement in the prediction of mean temperature by the buoyancy-extended models as can be seen in Fig. 5.6 (c) which is the consequence of the prediction in the transitioning zone. The misprediction of the mean temperature and wall-normal heat flux by the BL-$\overline{v^2}/k$ model particularly at $x = 0.8$ is just due to the very slow transition.

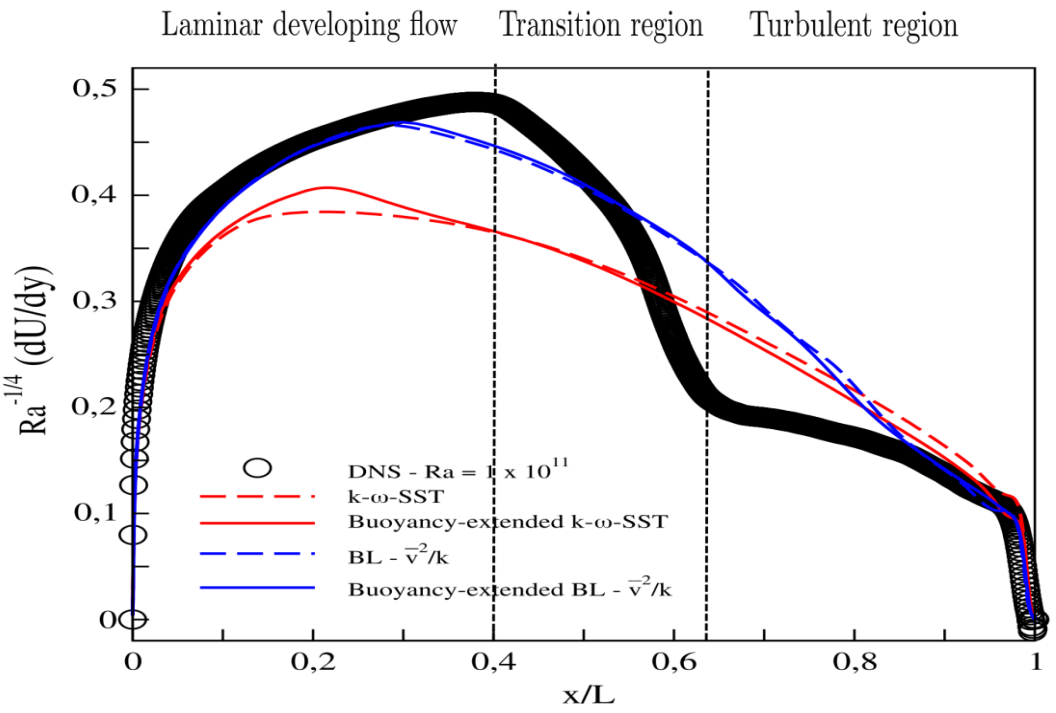

Figure 5.3 – Comparison of vertical wall shear stress scaled by $Ra^{-1/4}$ with DNS data [Trias et al., 2010] at $Ra = 1.0 \times 10^{11}$ and $Pr = 0.71$

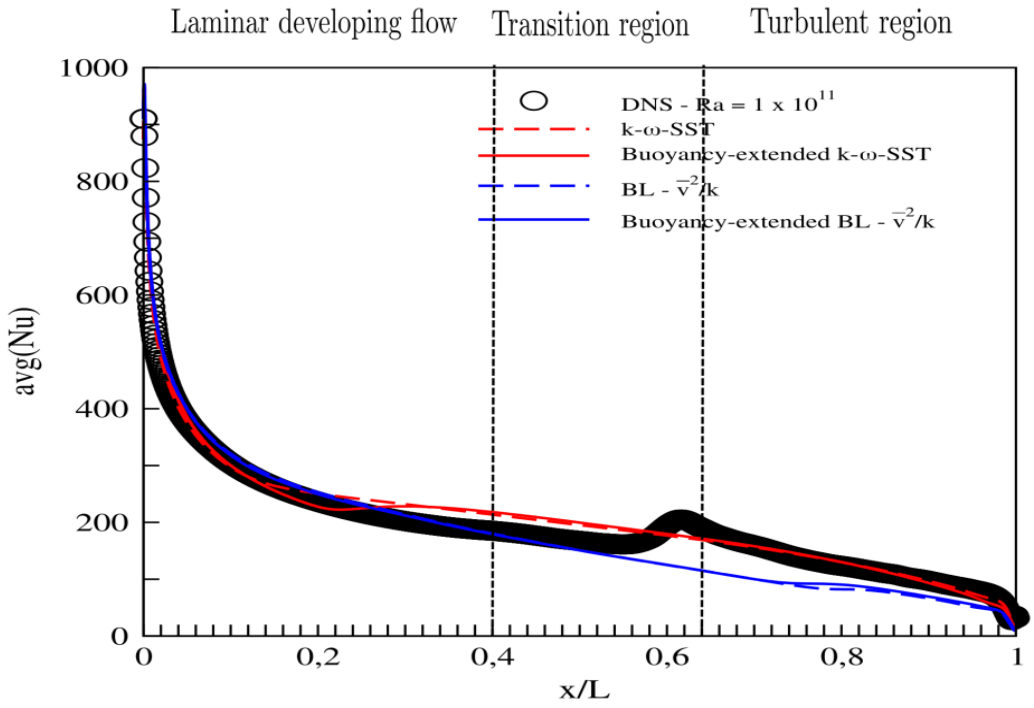

Figure 5.4 – Comparison of local Nusselt number distribution with DNS data [Trias et al., 2010] at $Ra = 1.0 \times 10^{11}$ and $Pr = 0.71$

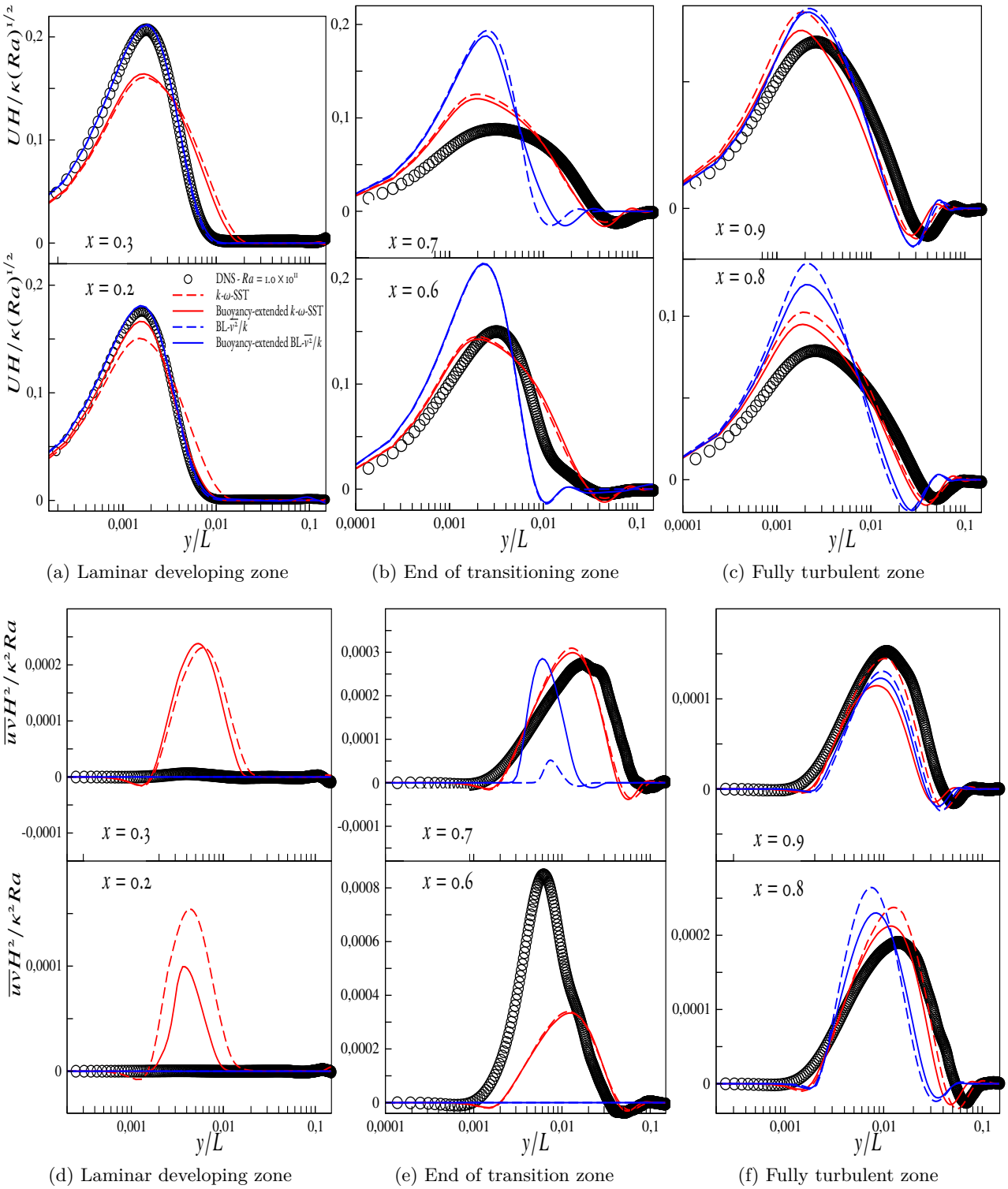

(a) Laminar developing zone (b) End of transitioning zone (c) Fully turbulent zone

(d) Laminar developing zone (e) End of transition zone (f) Fully turbulent zone

Figure 5.5 – Comparison of the mean velocity $[UH/\kappa(Ra)^{1/2}]$ (first line) and turbulence shear stress $[\overline{uv}H^2/\kappa^2 Ra]$ (second line) predictions of the buoyancy-extended k-ω-SST (red color) and buoyancy extended BL-$\overline{v^2}/k$ (blue color) models with DNS data [Trias et al., 2010] at $Ra = 1.0 \times 10^{11}$ and $Pr = 0.71$

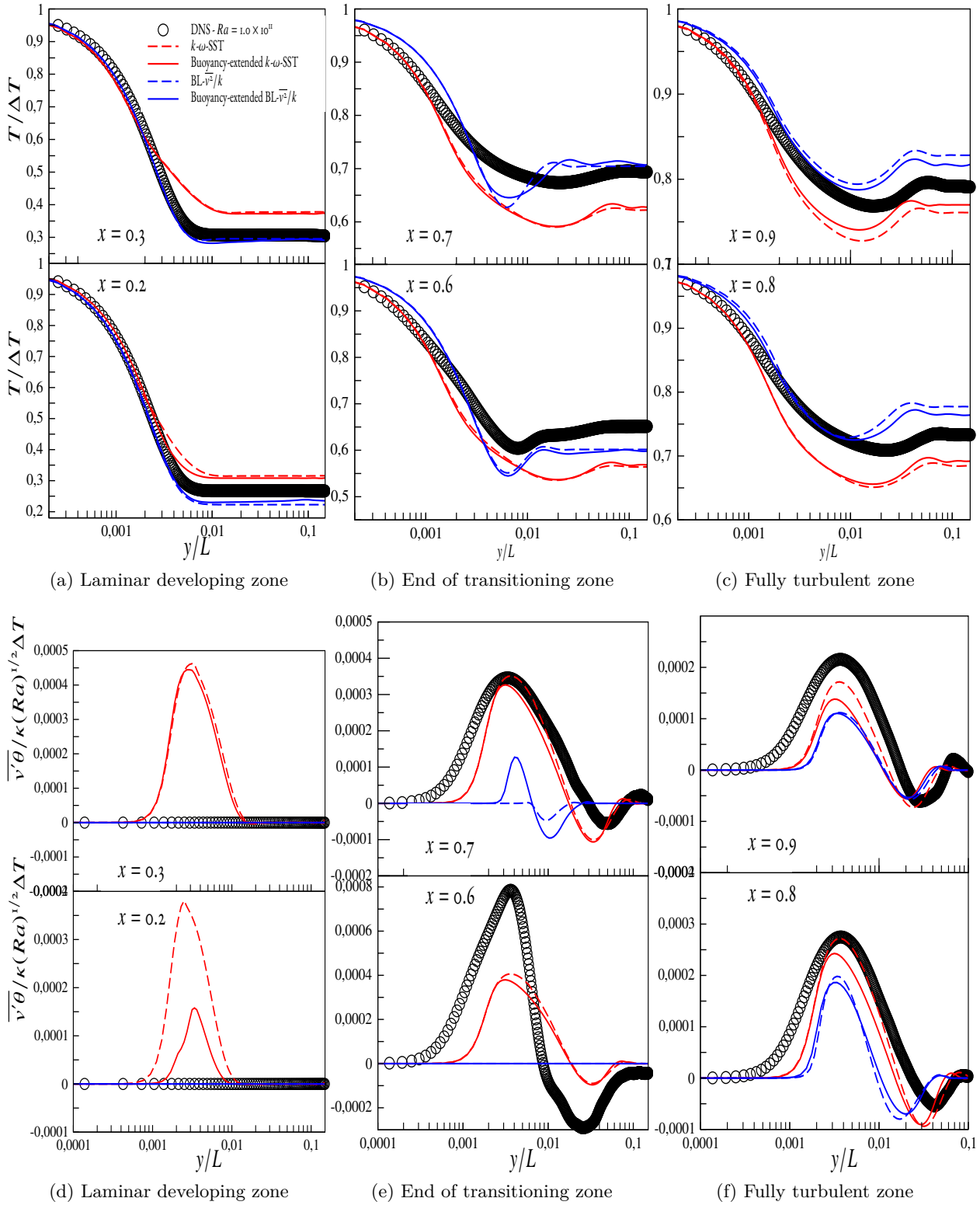

(a) Laminar developing zone (b) End of transitioning zone (c) Fully turbulent zone

(d) Laminar developing zone (e) End of transitioning zone (f) Fully turbulent zone

Figure 5.6 – Comparison of mean temperature $[T/\Delta T]$ (first line) and wall normal heat flux $[\overline{v'\theta}H/\kappa(Ra)^{1/2}\Delta T]$ (second line) predictions of buoyancy-extended k-ω-SST (red color) and buoyancy extended BL-$\overline{v^2}/k$ (blue color) models with DNS data [Trias et al., 2010] at $Ra = 1.0 \times 10^{11}$ and $Pr = 0.71$

5.2.2 Effect of adding buoyancy production terms

In this part of the section, the effect of only adding buoyancy production terms in the transport equation of turbulent kinetic energy (k) and dissipation (ε) or specific dissipation (ω) is discussed.

Buoyancy sensitised k-ω-SST model

It is recalled here that the transport equations of turbulent kinetic energy and specific dissipation are expressed as follow:

$$\frac{Dk}{Dt} = P_k + G_k - \beta^* k\omega + \frac{\partial}{\partial x_k}\left[\left(\nu + \sigma_k \nu_t\right)\frac{\partial k}{\partial x_k}\right] \tag{5.7}$$

$$\begin{aligned}\frac{D\omega}{Dt} = \frac{\gamma}{\nu_t}P_k + max\left(\frac{\gamma}{\nu_t}G_k, 0\right) - \beta\omega^2 + \frac{\partial}{\partial x_k}\left[\left(\nu + \sigma_\omega \nu_t\right)\frac{\partial \omega}{\partial x_k}\right] \\ +2(1-F_1)\sigma_{\omega 2}\frac{1}{\omega}\frac{\partial k}{\partial x_k}\frac{\partial \omega}{\partial x_k}\end{aligned} \tag{5.8}$$

Where constants and blending functions are as per the standard k-ω-SST model [Menter, 1994].

Buoyancy sensitised BL-$\overline{v^2}/k$ model

The transport equations of turbulent kinetic energy and its dissipation rate are expressed as follows:

$$\frac{Dk}{Dt} = P_k + G_k - \varepsilon - 2C_{\varepsilon 3}\nu\nu_t(1-\alpha)^3\frac{k}{\varepsilon}\left(\frac{\partial^2 U_i}{\partial x_k \partial x_j}\right)^2 + \frac{\partial}{\partial x_j}\left[\left(\frac{\nu}{2} + \frac{\nu_t}{\sigma_k}\right)\frac{\partial k}{\partial x_j}\right] \tag{5.9}$$

$$\frac{D\varepsilon}{Dt} = \frac{C_{\varepsilon 1}P_k - C^*_{\varepsilon 2}\varepsilon}{T} + max\left(C_{\varepsilon 1}\frac{G_k}{T}, 0\right) + \frac{\partial}{\partial x_j}\left[\left(\frac{\nu}{2} + \frac{\nu_t}{\sigma_\varepsilon}\right)\frac{\partial \varepsilon}{\partial x_j}\right] \tag{5.10}$$

where the constants and other functions are as per the BL-$\overline{v^2}/k$ model [Billard and Laurence, 2012].

$$G_k = -\beta g_i \overline{u_i' \theta} \tag{5.11}$$

The Reynolds stresses in the averaged momentum equation is modeled using the standard Boussinesq constitutive relation (Eq. 5.12) which writes:

$$\overline{u_i' u_j'} = \frac{2}{3}k\delta_{ij} - \nu_t\left(\frac{\partial U_i}{\partial x_j} + \frac{\partial U_j}{\partial x_i}\right) \tag{5.12}$$

The turbulent heat fluxes in the mean temperature equation are modeled using simple gradient diffusion hypothesis (SGDH) approach (Eq. 5.13) which writes:

$$\overline{u_i'\theta} = -\frac{\nu_t}{Pr_t}\frac{\partial T}{\partial x_i} \tag{5.13}$$

In an infinite cavity (vertical channel), the vertical temperature gradient is zero due to the absence of stratification and the use of SGDH approach to model buoyancy production terms is inappropriate as it will not introduce any influence of the buoyancy on turbulence ($G_k = -\beta g_i \overline{u_i'\theta}$), such that the GGDH approach has been used for this buoyancy production terms in Chapter 4. However, in this type of rectangular cavity where the stratification is present, the SGDH approach is also considered to model the buoyancy source terms in comparison with the GGDH approach.

The Wall shear stress is shown in Fig. 5.7 and it is observed that the addition of buoyancy production terms tends to delay the transition (early transition point is shifted) and the SGDH and GGDH approaches give a similar effect as previously observed with the buoyancy-extended k-ω-SST model. However, the inverse effect is observed with the original BL-$\overline{v^2}/k$ model where the delayed transition is observed and the inclusion of buoyancy source terms worsen the predictions. In the turbulent region, the tendency of adding buoyancy production terms in k-ω-SST model is to slightly improve the predictions. However, the inverse effect is observed by adding buoyancy source term in BL-$\overline{v^2}/k$ model.

Looking into the distribution of Nusselt number in Fig. 5.8 (plotted for the hot wall), it is realized that the inclusion of buoyancy production in the k-ω-SST model, using SGDH and GGDH, has the same effect as previously observed with the buoyancy-extended version in delaying the transition. In contrast, the buoyancy production terms have virtually no effect on the Nusselt number prediction of the BL-$\overline{v^2}/k$ model.

From the plots of mean velocity and turbulent shear stress shown in Fig. 5.9 (a) and Fig. 5.9 (d), it is confirmed that the transition is delayed by adding buoyancy production terms (see Fig. 5.9 (d)), whereas BL-$\overline{v^2}/k$ model remains laminar. Fig. 5.9 (b) and Fig. 5.9 (e) shows the prediction at the end of the transition zone and it is observed that the effect of the production terms is weak in this region. However, the BL-$\overline{v^2}/k$ predicts very late transitioning and with the inclusion of buoyancy production terms, the transition is further delayed (see Fig. 5.9 (e) at $x/L = 0.7$) At locations $x/L = 0.8$ and $x/L = 0.9$ in the fully turbulent zone, it is observed that there is an improvement in the predictions of mean velocity with the addition of buoyancy production terms in the k-ω-SST and this effect is the consequence of the improvement in the transition zone (see Fig. 5.9 (b) and Fig. 5.9 (e)). Moreover, the effect of adding buoyancy production terms in the BL-$\overline{v^2}/k$ model is to further delay the transitioning and the speed to achieve a fully turbulent state is slower (see Fig. 5.9 (c) and Fig. 5.9 (f)) as compared to the original BL-$\overline{v^2}/k$ model.

From the mean temperature distribution in the laminar developing zone, it is realized that the addition of buoyancy source term in k-ω-SST model partly corrects the early transition

phenomenon as can be seen in Fig. 5.10 (a) and Fig. 5.10 (d) and the effect is rather strong (see Fig. 5.10 (d) at $x/L = 0.2$). In contrast, the buoyancy production terms have virtually no effect on the BL-$\overline{v^2}/k$ model in this region. At the end of the transitioning zone shown in Fig. 5.10 (b) and Fig. 5.10 (e), the addition of buoyancy source terms in k-ω-SST and BL-$\overline{v^2}/k$ model have virtually no effect on the prediction of the transitioning phenomena.

In the fully turbulent zone, the inclusion of buoyancy production terms in k-ω-SST model leads to the improvement in the prediction of mean temperature. However, for the BL-$\overline{v^2}/k$ model, there are no substantial effect with the addition of buoyancy source terms.

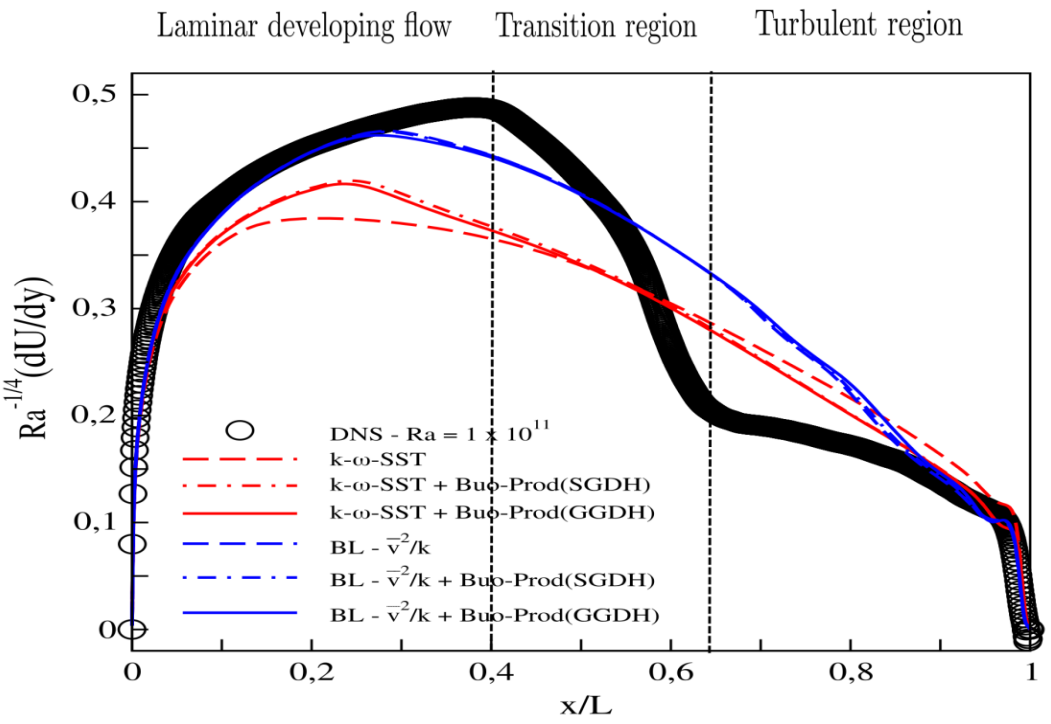

Figure 5.7 – Comparison of vertical wall shear stress scaled by $Ra^{-1/4}$ with DNS data [Trias et al., 2010] at $Ra = 1.0 \times 10^{11}$ and $Pr = 0.71$

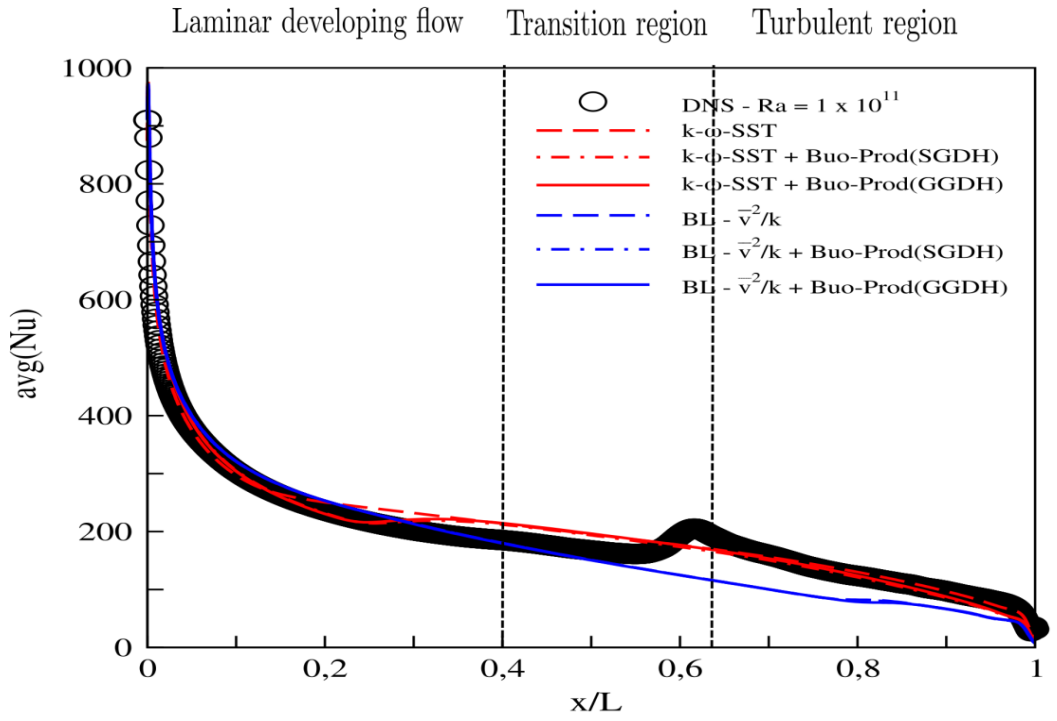

Figure 5.8 – Comparison of local Nusselt number distribution with DNS data [Trias et al., 2010] at $Ra = 1.0 \times 10^{11}$ and $Pr = 0.71$

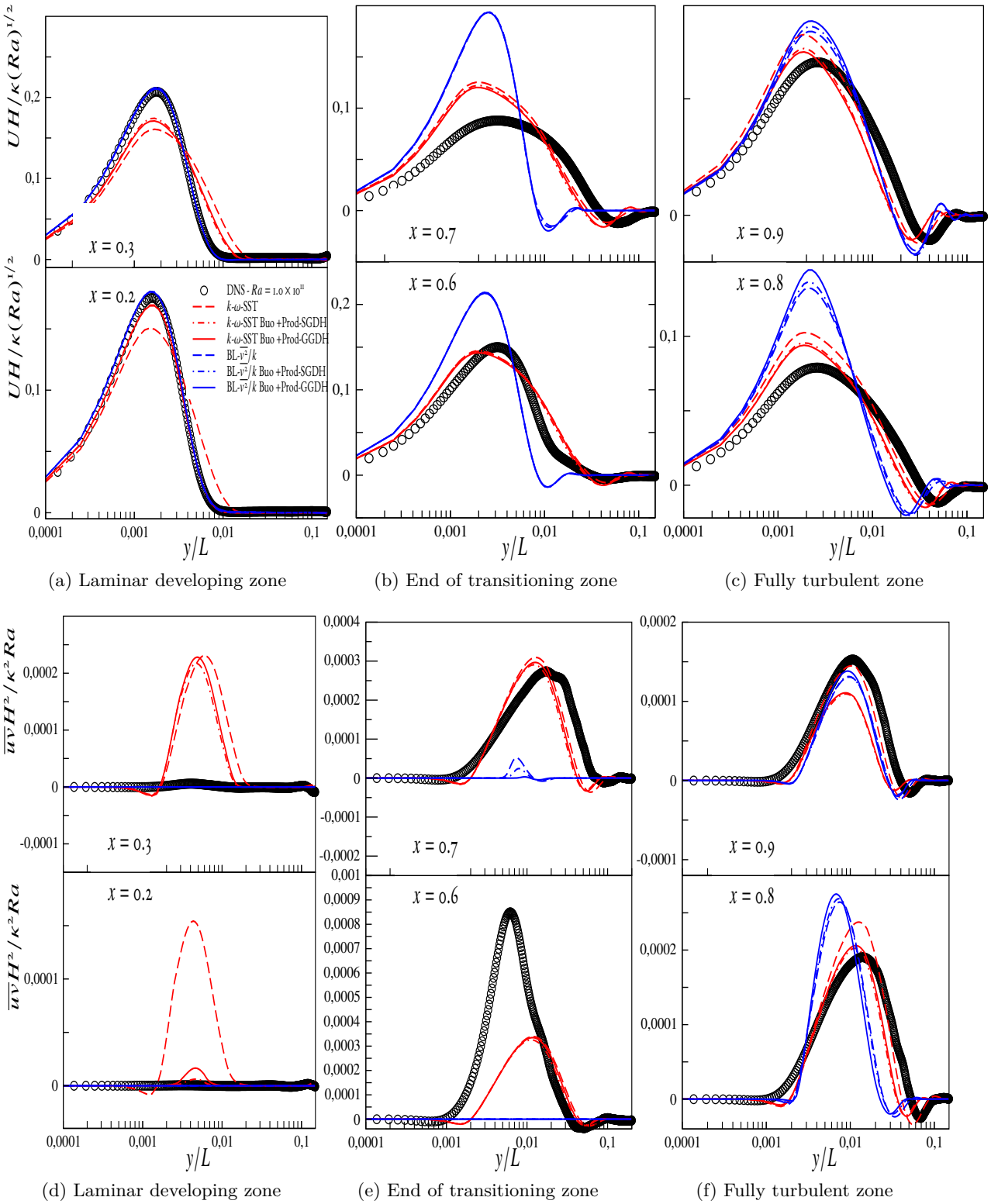

(a) Laminar developing zone (b) End of transitioning zone (c) Fully turbulent zone

(d) Laminar developing zone (e) End of transitioning zone (f) Fully turbulent zone

Figure 5.9 – Comparison of mean velocity $[\overline{U}H/\kappa(Ra)^{1/2}]$ (first line) and turbulence shear stress $[\overline{uv}H^2/\kappa^2 Ra]$ (second line) predictions of buoyancy sensitised k-ω-SST and BL-$\overline{v^2}/k$ models with DNS data [Trias et al., 2010] at $Ra = 1 \times 10^{11}$ and $Pr = 0.71$

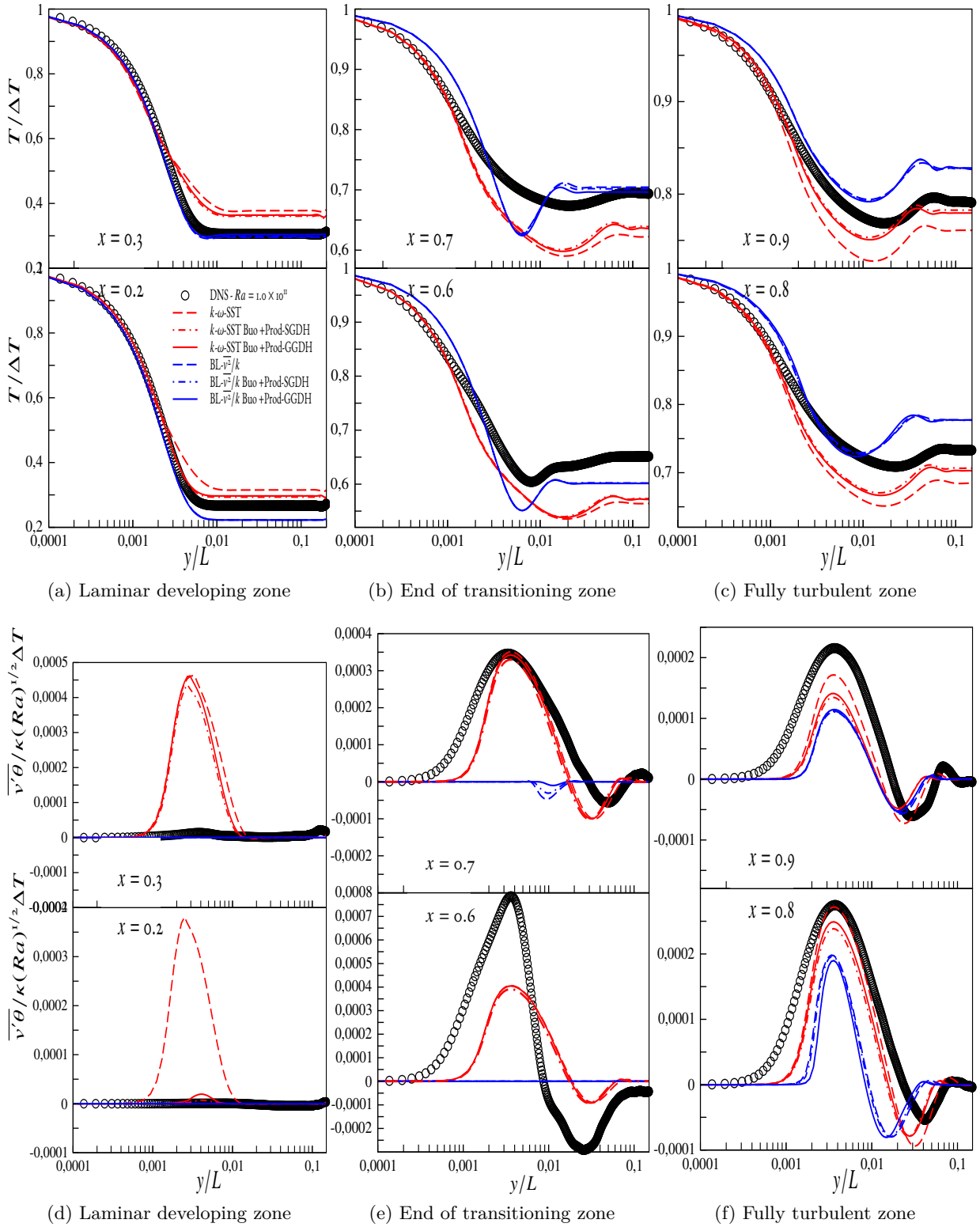

(a) Laminar developing zone (b) End of transitioning zone (c) Fully turbulent zone

(d) Laminar developing zone (e) End of transitioning zone (f) Fully turbulent zone

Figure 5.10 – Comparison of mean temperature$[T/\Delta T]$ (first line) and wall normal heat flux$[\overline{v'\theta}H/\kappa\sqrt{Ra}\Delta\theta]$ (second line) predictions of buoyancy sensitized k-ω-SST and BL-$\overline{v^2}/k$ models with DNS data [Trias et al., 2010] at $Ra = 1 \times 10^{11}$ and $Pr = 0.71$

5.3 Effect of Yap term in Launder-Sharma model

We have seen in chapter 3 that the inclusion of the Yap term in the Launder-Sharma model leads to an improvement in the predictions of dynamic and thermal characteristics in an infinite cavity, so motivated by this fact the Yap term is introduced in the low-Reynolds Launder-Sharma model and simulation is performed in the rectangular cavity. The Yap term (S_ε) is expressed as follows:

$$S_\varepsilon = max\left[0.83\left(\frac{k^{3/2}}{c_l \varepsilon y} - 1\right)\left(\frac{k^{3/2}}{c_l \varepsilon y}\right)^2 \frac{\varepsilon^2}{k}, 0\right] \tag{5.14}$$

where y is the wall normal distance and c_l is the slope of the turbulent length scale ($k^{3/2}/\varepsilon$) in the near-wall region in constant-stress shear flow.
The distributions of the wall shear stress and the Nusselt number are shown in Fig. 5.11 and Fig. 5.12, respectively. It is realized that the original Launder-Sharma model predicts an early and rapid transition and the inclusion of Yap term removes this limitation to a certain extent in such a way that the transition point is shifted towards the DNS profile. In the turbulent region, the tendency of the original Launder-Sharma model to reach fully turbulent state is too early and with the inclusion of Yap term, there is a drastic improvement and fully turbulent state is reached later.
From the plots of mean velocity and turbulent shear stress profiles in laminar zone as shown in Fig. 5.13 (a) and Fig. 5.14 (a), it is confirmed that the original Launder-Sharma model predict early transitioning, and this limitation is avoided by introducing Yap term, which lead to significant improvement in the mean velocity profile. Fig. 5.13 (b) and Fig. 5.14 (b) show that the predictions at the end of transitioning zone are significantly improved by the Yap term. At the locations $x/L = 0.8$ and $x/L = 0.9$, in fully turbulent zone, it is also observed that there is an improvement in the prediction of mean velocity with Yap term (as can be seen in Fig. 5.13 (c)), owing to the better prediction of turbulent shear stress as can be seen in Fig. 5.14 (c).
From the mean temperature distribution in the laminar zone showed in Fig. 5.15 (a), it is observed that the early transition leads to a severe misprediction of the temperature profile. The inclusion of Yap term brings in a drastic improvement in the prediction of mean temperature owing to the better representation of turbulent heat flux as shown in Fig. 5.16 (a). In the end of transitioning zone, the original Launder-Sharma model severely overestimates the turbulent heat flux and this limitation is avoided by the inclusion of Yap term as shown in Fig. 5.16 (b) and the consequence of this improvement in turbulent heat flux leads to the better prediction of mean temperature as shown in Fig. 5.15 (b). In the fully turbulent zone, the inclusion of Yap term also brings in a drastic improvement in the prediction of turbulent heat flux by improving the speed to transition as shown in Fig. 5.16 (c) and this provides the better prediction of mean temperature as can be seen

in Fig. 5.15 (c).

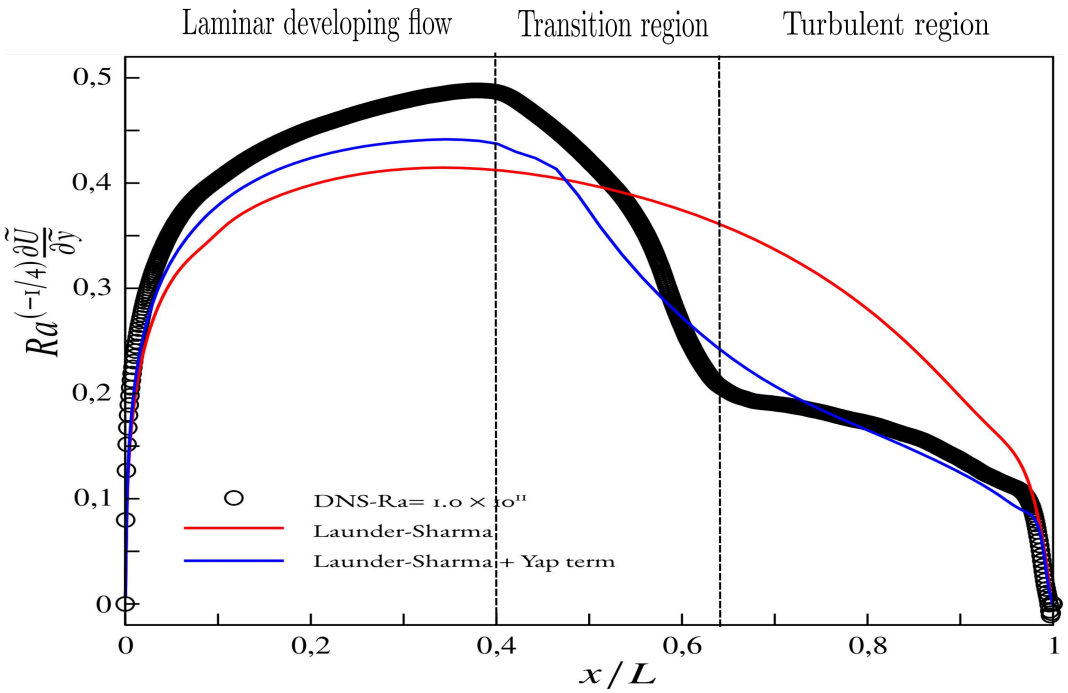

Figure 5.11 – Comparison of vertical wall shear stress scaled by $Ra^{-1/4}$ with DNS data [Trias et al., 2010] at $Ra = 1.0 \times 10^{11}$ and $Pr = 0.71$

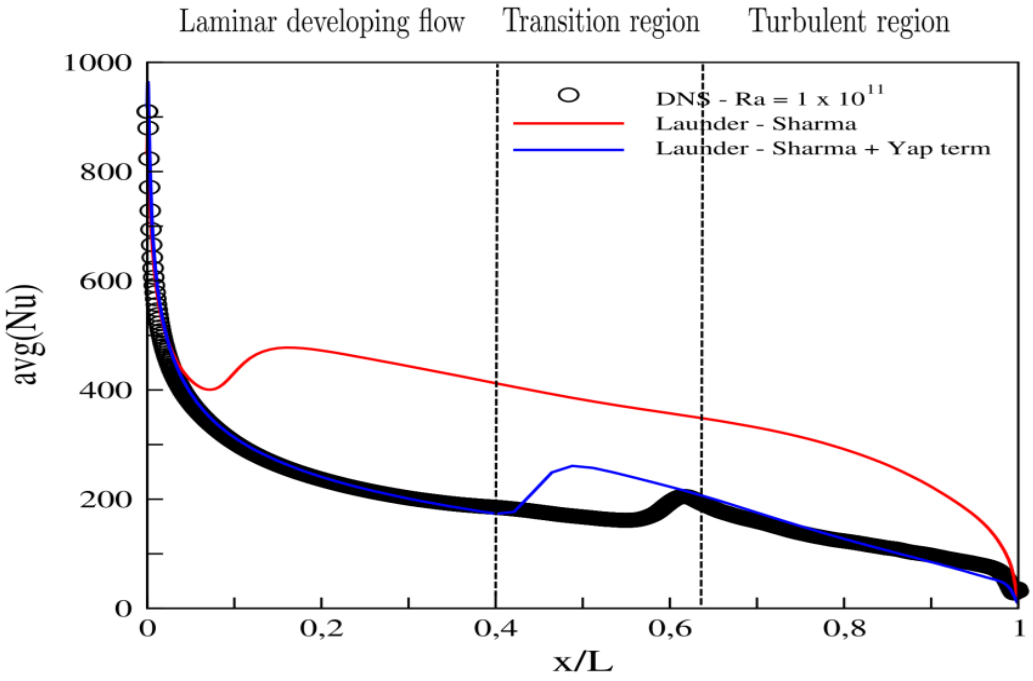

Figure 5.12 – Comparison of local Nusselt number distribution with DNS data [Trias et al., 2010] at $Ra = 1.0 \times 10^{11}$ and $Pr = 0.71$

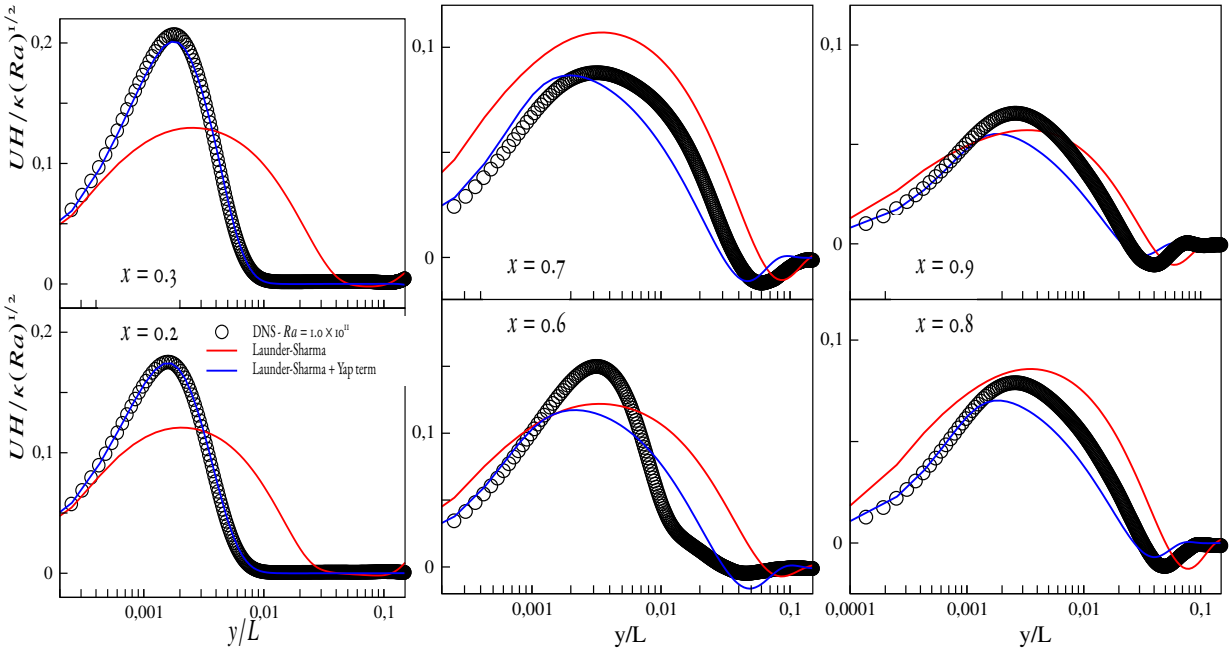

(a) Laminar developing zone (b) End of transitioning zone (c) Fully turbulent zone

Figure 5.13 – Comparison of mean velocity $[\overline{U}H/\kappa(Ra)^{1/2}]$ with DNS data [Trias et al., 2010] at $Ra = 1.0 \times 10^{11}$ and $Pr = 0.71$

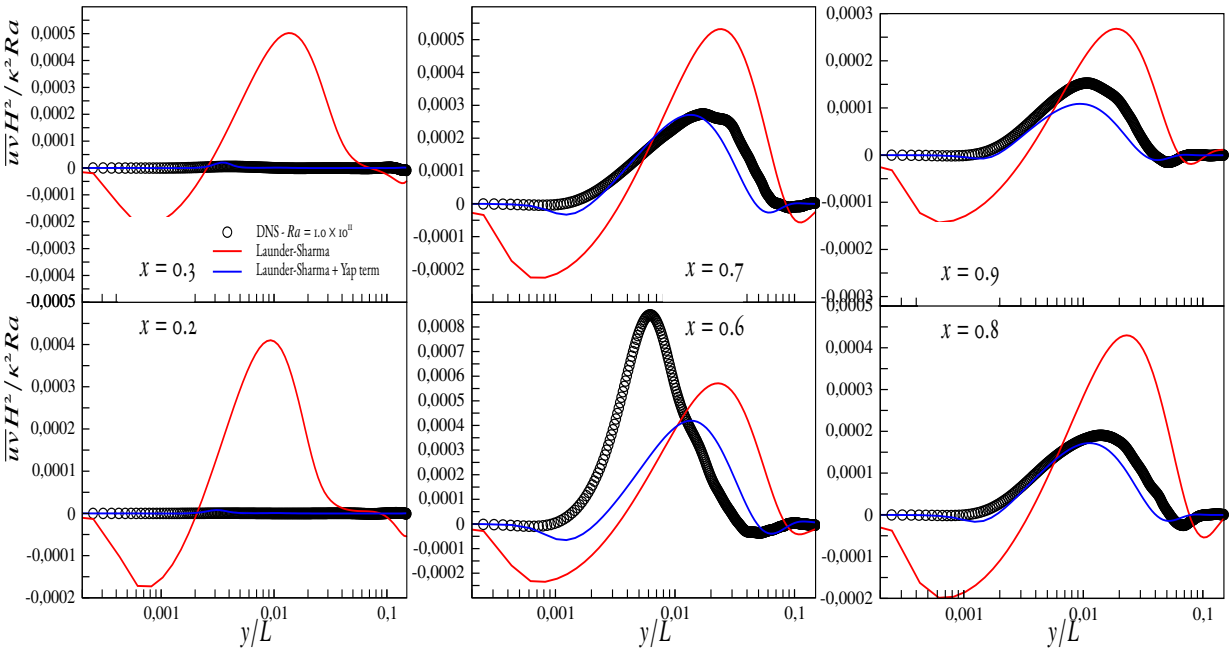

(a) Laminar developing zone (b) End of transitioning zone (c) Fully turbulent zone

Figure 5.14 – Comparison of turbulence shear stress $[\overline{uv}H^2/\kappa^2 Ra]$ with DNS data [Trias et al., 2010] at $Ra = 1.0 \times 10^{11}$ and $Pr = 0.71$

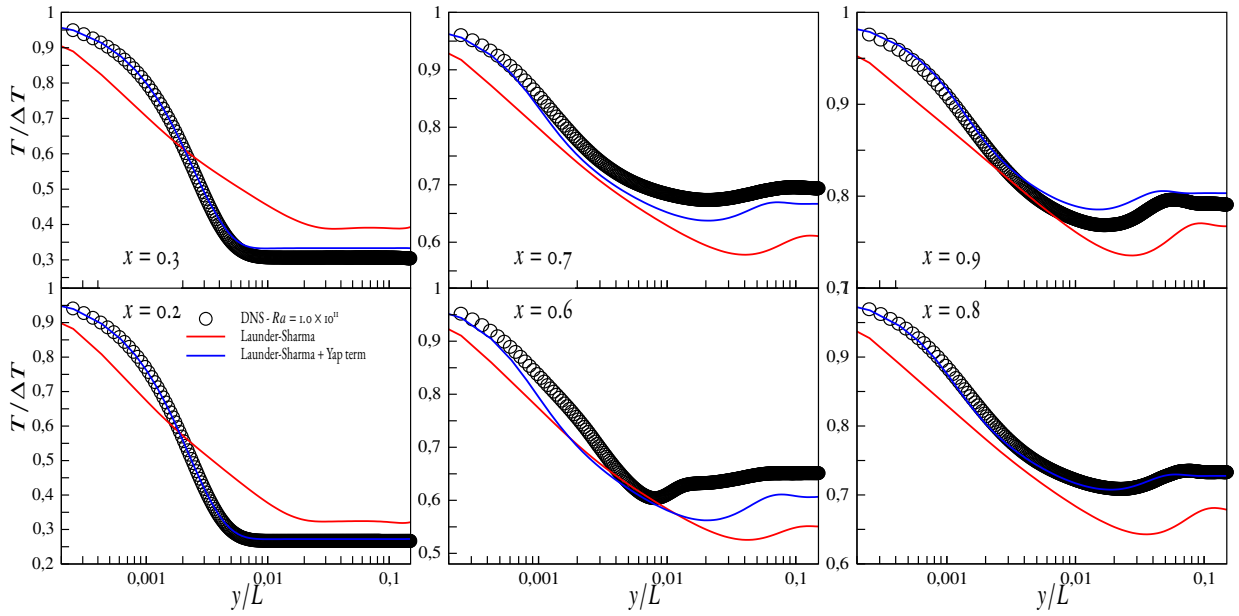

(a) Laminar developing zone (b) End of transitioning zone (c) Fully turbulent zone

Figure 5.15 – Comparison of mean temperature $[T/\Delta T]$ with DNS data [Trias et al., 2010] at $Ra = 1.0 \times 10^{11}$ and $Pr = 0.71$

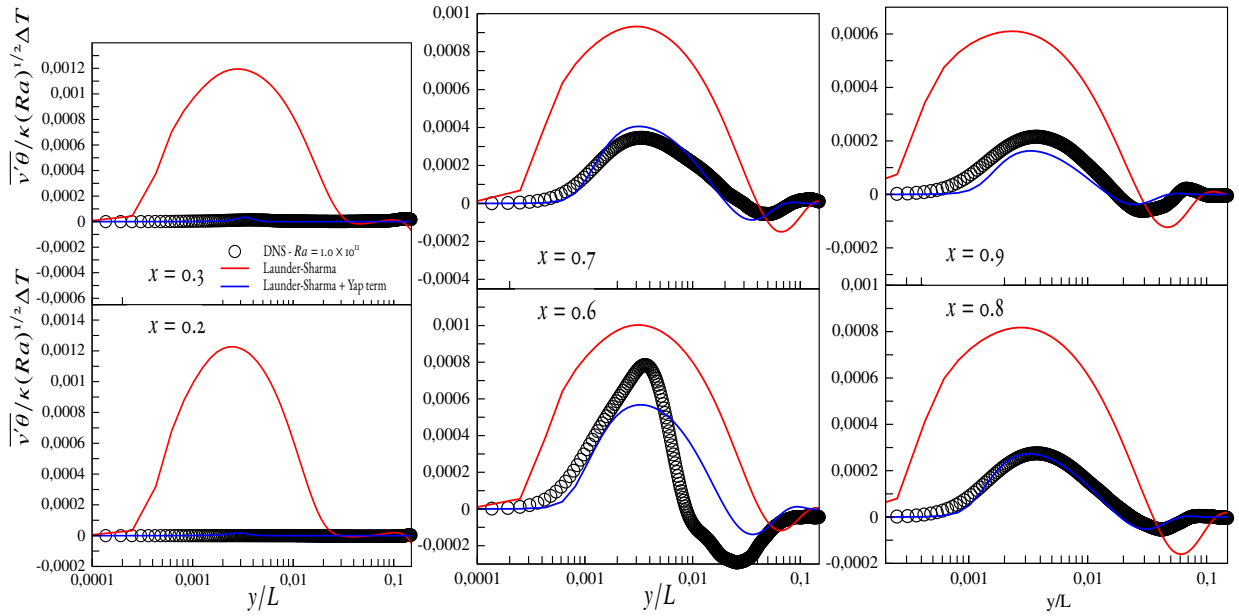

(a) Laminar developing zone (b) End of transitioning zone (c) Fully turbulent zone

Figure 5.16 – Comparison of wall normal heat flux $[\overline{v'\theta}H/\kappa\sqrt{Ra}\Delta\theta]$ with DNS data [Trias et al., 2010] at $Ra = 1.0 \times 10^{11}$ and $Pr = 0.71$

5.4 Conclusion

The performance of buoyancy sensitized models has been examined by computing a more challenging rectangular cavity where stratification is playing an important role. Firstly, the performance of the buoyancy-extended k-ω-SST and BL-$\overline{v^2}/k$ models are examined by computing rectangular cavity of aspect ratio 4 : 1 with adiabatic horizontal walls corresponding to the highest Rayleigh number, $Ra = 1.0 \times 10^{11}$ which is based on the height of the cavity.

It is observed that the original k-ω-SST model predicts very early transition to the turbulent state leading to the early increase of the wall shear stress and for the BL-$\overline{v^2}/k$ model, transition is too late. The buoyancy-extended k-ω-SST model leads to moderate the early transition. Moreover, the tendency of buoyancy-extended BL-$\overline{v^2}/k$ model is to trigger the transition which is delayed as predicted by the original BL-$\overline{v^2}/k$ model. It is observed that both the original and buoyancy-extended versions of the models show an early effect of the transition on the Nusselt number distribution which is contrary to the prediction of DNS data in which there is a formation of the kink at the end of the transition. Attempts were made to investigate the performance of the buoyancy-extended Launder-Sharma model in this rectangular cavity, but there are convergence issues and so the results are not presented in this study.

Secondly, the effect of introducing only buoyancy source terms in the transport equations of turbulent kinetic energy (k) and dissipation (ε) or (ω) is examined. These buoyant source terms are modeled using SGDH and GGDH approaches, respectively. It is observed that there is improvement in the prediction of mean velocity and mean temperature when buoyancy source terms are added to the k-ω-SST model as well as the prediction of wall shear stress is improved and the early transition to turbulence by original k-ω-SST is corrected to a certain extent. However, there are no substantial changes in the predictions when the buoyancy source terms are added to the BL-v^2/k model. The analysis of adding only buoyancy source terms explain the superiority of buoyancy-extended models in sensitizing the original k-ω-SST and BL-$\overline{v^2}/k$ model to buoyancy effects by providing the physically relevant terms which are missing in the original models.

Chapter 6

Conclusions and future work

Contents

6.1 General Conclusion

This thesis proposes modifications into eddy-viscosity based models that take into account of the buoyancy effects. The selection of the eddy-viscosity models is based on the ability of models to be integrated down to the wall. This is the primary requirement for natural convection flows, since the wall function approach is not very established for natural convection flows and also to isolate the effect of other physical phenomena that complicate the problem while introducing buoyancy effects into models.
The selected models come from three very different families in order to investigate how the proposed modifications work independent of the model specificities. From the k-ω family, the k-ω-SST model, from the $\overline{v^2}$-f family, the BL-$\overline{v^2}/k$ model, and from the low-Reynolds number family the Launder-Sharma are selected, respectively. Three different turbulent convective regimes namely forced, mixed and natural convection are studied and considered for the model development. Model development is performed based on channel flow configurations and the models are also tested in cavity flows. The analysis started from the forced convection flows which are considered while developing most of the eddy-viscosity models: it has been observed that all the three selected models are able to predict the mean velocity well in agreement to the DNS data close to the wall. However, there were discrepancies in the prediction of the logarithmic region particularly with k-ω-SST model. Moreover, there is a severe underprediction of turbulent kinetic energy by the original models particularly with the k-ω-SST and Launder-Sharma models whereas the BL-$\overline{v^2}/k$ model comes out to be the better model in predicting mean flow and turbulent quantities. Further, it is observed that the predictions of mean temperature by the models are satisfactory. Overall behavior of the models is in good agreement with DNS data.
For eddy-viscosity models, the standard approach to model the Reynolds stresses is the Boussinesq constitutive relation and the simple gradient diffusion hypothesis (SGDH) for modeling turbulent heat fluxes, but we know that using these standard approaches is not reliable for buoyancy-driven flows. So the objective of the work is to incorporate the buoyancy contribution into the selected eddy-viscosity models and in the pursuit of this goal, buoyancy-extended Reynolds stress and heat flux models are developed using the weak equilibrium approach. One of the constraints to formulate the buoyancy-extended model is to take into account of the fact that the modified models do not change the predictions of forced convection flows which were found to be reliable particularly in the Underhood space simulation performed at PSA Group. So keeping in view this constraint, models are modified in such a manner that in the absence of buoyancy, the modified model will go back to original models.
The development phase of buoyancy sensitized model is started by checking the robustness of the models in three convective regimes, particularly for the natural convection regime where buoyancy has a decisive impact on the mean flow and turbulent quantities.
The buoyancy extension approach has been proposed in association with the three selected

models. It has been observed that the buoyancy-extended models bring a significant improvement in the prediction of mean and turbulent quantities compared to the original models which confirm that the missing contribution of buoyancy is indeed required in Reynolds stress and heat flux relations. Another favourable aspect of buoyancy-extended models is that it preserve the linearity in the Reynolds stress and turbulent heat flux relations. The open-source code *Code_Saturne* is used for the development of buoyancy-extended models due to the flexibility and availability of this open source code.

The goal of the work is to propose a span of buoyancy sensitized model that can be implemented in ANSYS Fluent. So in this context another constraint of the work is the modeling of tensorial diffusivity (considered in GGDH approach to model the heat flux) which is not possible in ANSYS Fluent [Fluent]. In view of this, simple versions of buoyancy-extended models are proposed in association with the k-ω-SST and BL-$\overline{v^2}/k$ models. The differentially heated vertical channel case of Kiš and Herwig [2014] is considered for the development and validation of these simple buoyancy-extended models. In these versions of the models, simple gradient diffusion hypothesis (SGDH) is considered for modeling turbulent heat fluxes. However, with this approach, the buoyancy contribution coming from the buoyancy production terms is negligible in weakly stratified flows and becomes zero for differentially heated vertical channel flow. However, it has been observed that there is a significant improvement in the prediction of the mean and turbulent quantities with these simplified buoyancy-extended models.

A simple way of taking into account of buoyancy contribution in the eddy-viscosity models is to only add buoyancy source terms in the transport equation of turbulent kinetic energy and its dissipation or specific dissipation rate. However, if these buoyancy source terms are modeled using the SGDH approach it will underestimate the effect of buoyancy on turbulence. So in view of this fact, buoyancy source terms were modeled using the GGDH approach and the sensitivity analysis of the coefficient C_3 is done in association with three models namely k-ω-SST, BL-$\overline{v^2}/k$ and Launder-Sharma model respectively. The most challenging natural convection case of Kiš and Herwig [2014] is considered for this analysis. It has been observed that the effect of only adding G_k is strong in k-ω-SST and BL-$\overline{v^2}/k$ model and bring in significant improvement in the mean velocity and mean temperature profile. Moreover, it is noticed that, as the value of the coefficient C_3 (in G_ε or G_ω) is reduced, the results are better. On the contrary, in the case of Launder-Sharma model, addition of only G_k worsen the results and the addition of G_ε is necessary. This study suggested that the need of buoyancy extension can be avoided by the addition of only buoyant source terms. However, the buoyancy-extended models are physically richer. Another analysis of taking into account of the flux Richardson number in association with the k-ω-SST and BL-$\overline{v^2}/k$ models is performed. It is noticed that the results are improved and the optimal value of the coefficient C_3 is 0.45 for both the models. To complete the study, the effect of adding the Yap [1987] term in the dissipation rate equation of Launder-

Sharma model is analyzed. It is observed that the inclusion of only the Yap term improved the prediction of the mean velocity. However, there is a misprediction of the temperature profile. This misprediction is greatly reduced by the buoyancy-extended Launder-Sharma model in association with the Yap term.
Another natural convection case, the rectangular cavity of Trias et al. [2007, 2010] at the highest Rayleigh number, $Ra = 1.0 \times 10^{11}$ is considered for analyzing the performance of buoyancy sensitized models. It is observed that the buoyancy-extended models lead to an improvement in the prediction of transition which is crucial for this cavity. To complete the study, the effects of only adding buoyancy production terms in the k-ω-SST and BL-$\overline{v^2}/k$ models is also examined in association with the simple gradient diffusion hypothesis (SGDH) and the generalized gradient diffusion hypothesis (GGDH). It has been observed that the inclusion of these additional source terms for the k-ω-SST model brings improvement in the mean velocity and mean temperature. However, there are virtually no effect of adding these source terms on BL-$\overline{v^2}/k$ model.
So it has been concluded that more advanced modeling in terms of buoyancy extension provided to Reynolds stresses and turbulent heat fluxes is more appropriate as this approach is more physical, consistent and brings in drastic improvement of results.
Further, the effect of introducing the Yap term in the Launder-Sharma model is also examined in this cavity flow and it has been realised that the inclusion of this additional term leads to the improvement not only in the prediction of mean velocity and mean temperature but also in the turbulent variables. Also the discrepancy of early transition to turbulence by the original Launder-Sharma model is significantly delayed which made the improvement in the wall shear stress and Nusselt number. So the consideration of Yap term in Launder-Sharma model is further reinforced by the prediction in this rectangular cavity flow and it has been inferred that the Yap term is indeed required for the Launder-Sharma model which is in accordance to the available literature.

6.2 Prospects

The detailed analysis of several modifications in the context of three very different eddy-viscosity models provide significant insight into the flows affected or driven by thermal buoyancy. Validation of these buoyancy modified models needs to be done in the other buoyancy affected cavity flows such as square cavity of Sebilleau et al. [2018] and rectangular cavity of Saury et al. [2011] at highest Rayleigh numbers. The other important objective of the future work is the testing and validation of these buoyancy modified models in several other buoyancy dominated flow configurations using Ansys Fluent (used by PSA Group). In particular the buoyancy modified model will be tested in the simplified real underhood space of cars at PSA group. Furthermore, this work is the part of ANR Monaco project, and one of the goals of the project is to predict the buoyancy induced transient phenomena which pose a barrier that must be overcome. A particular effort

needs to be given in the future on the extension of the present work to the development of hybrid RANS/LES methods and to analyze the potential of these methods for buoyancy driven flows. In the framework of this goal, a particular attention will be given to the RANS zones while developing Hybrid RANS/LES methods.

This work is motivated by the problem faced by the PSA group in reproducing the different buoyancy influenced phases. Moreover, during the thermal designing of the underhood space of cars, there are certain important factors that needs particular attention, such as the dimensioning of the car which imposes constraints on the compactness of several parts of underhood space and this makes the flow to become complex in the cavity between engine and its auxillary parts. The other important requirement is the reduction of the weight of the car by using plastic instead of metal for which thermal management in the underhood space is crucial. These two requirements are directly linked to the overheating of the underhood components during different phases of vehicle motion. During the cruising phases, the simulation results are reliable and able to predict high temperature levels. However, when the vehicle is suddenly stopped, the heat soak phase arises in which there is a sudden rise of surface temperature of some underhood components and this might lead to the risk of auto-ignition of fluids in the underhood components. The computation of this thermal soak phase (where the natural convection phenomena is dominant) is not possible with the available turbulence model in Ansys Fluent. The present work paves the way towards the use of CFD to study this problems and to dimension the elements present in the underhood space.

Moreover, buoyancy plays a crucial role in several heat transfer applications of other industrial flows like in the nuclear industry, thermal management in buildings, solar power plants, aeronautics, chemical industies and others. Owing to the complicated geometry, constraint on the size of the equipments and different temperature levels, the flow becomes turbulent. The eddy-viscosity models are still the mainstay of the industrial computations, this work pave the way to compute industrial flows satisfactorily and allows better understanding of the natural convection flows in several flow configurations.

Bibliography

AM Abdelmeguid and DB Spalding. Turbulent flow and heat transfer in pipes with buoyancy effects. *Journal of Fluid Mechanics*, 94(2):383–400, 1979.

Hiroyuki Abe, Hiroshi Kawamura, and Yuichi Matsuo. Surface heat-flux fluctuations in a turbulent channel flow up to reτ= 1020 with pr= 0.025 and 0.71. *International Journal of Heat and Fluid Flow*, 25(3):404–419, 2004.

K Abe, Y Nagano, and T Kondoh. Numerical prediction of separating and reattaching flows with a modified low-reynolds-number k- model. *Journal of Wind Engineering and Industrial Aerodynamics*, 46:85–94, 1993.

Ales Alajbegovic, Raja Sengupta, and Wilko Jansen. Cooling airflow simulation for passenger cars using detailed underhood geometry. Technical report, SAE Technical Paper, 2006.

MO Annarumma, JM Most, and P Joulain. On the numerical modeling of buoyancy-dominated turbulent vertical diffusion flames. *Combustion and Flame*, 85(3-4):403–415, 1991.

Frédéric Archambeau, Namane Méchitoua, and Marc Sakiz. Code saturne: A finite volume code for the computation of turbulent incompressible flows-industrial applications. 2004.

Brian P Axcell and WB Hall. Mixed convection to air in a vertical pipe. In *International Heat Transfer Conference Digital Library*. Begel House Inc., 1978.

Ed Bendell. Investigation of a coupled cfd and thermal modelling methodology for prediction of vehicle underbody temperatures. Technical report, SAE Technical Paper, 2005.

RW Bilger. Computational field models in fire research and engineering. *Fire Safety Science*, 4:95–110, 1994.

F Billard and D Laurence. A robust k- ε- v2/k elliptic blending turbulence model applied to near-wall, separated and buoyant flows. *International Journal of Heat and Fluid Flow*, 33(1):45–58, 2012.

WG Bos, T van Den Elsen, and CJ Hoogendoorn. Comments on 'numerical study of stratification of a smoke layer in a corridor'. *Combust. Sci. Technol*, 46:333, 1986.

P Bradshaw. The strategy of calculation methods for complex turbulent flows. ic aero rep. 73-05, aeronaut. dep. *Imperial Coll. Sci. & Technol*, 1973.

CP Brescianini and MA Delichatsios. New evaluation of the k-ε turbulence model forfree buoyant plumes. *Numerical Heat Transfer: Part A: Applications*, 43(7):731–751, 2003.

JA Businger. A note on the businger-dyer profiles. In *Topics in Micrometeorology. A Festschrift for Arch Dyer*, pages 145–151. Springer, 1988.

AD Carr, MA Connor, and HO Buhr. Velocity, temperature, and turbulence measurements in air for pipe flow with combined free and forced convection. 1973.

Kuo-Huey Chen, Jim Johnson, P Merati, NJ Cooper, and CH Leong. Investigation of the buoyancy driven flow in a simplified underhood-part ii, numerical study. Technical report, SAE Technical Paper, 2006.

Kuei-Yuan Chien. Predictions of channel and boundary-layer flows with a low-reynolds-number turbulence model. *AIAA journal*, 20(1):33–38, 1982.

Seok-Ki Choi and Seong-O Kim. Treatment of turbulent heat fluxes with the elliptic-blending second-moment closure for turbulent natural convection flows. *International Journal of Heat and Mass Transfer*, 51(9-10):2377–2388, 2008.

Seok-Ki Choi, Ji-Woong Han, Seong-O Kim, and Tae-Ho Lee. Computation of turbulent natural convection with the elliptic-blending differential and algebraic flux models. *Numerical Heat Transfer, Part B: Fundamentals*, 71(1):37–49, 2017.

W Chung and CB Devaud. Buoyancy-corrected k–ε models and large eddy simulation applied to a large axisymmetric helium plume. *International journal for numerical methods in fluids*, 58(1):57–89, 2008.

MA Cotton and JO Ismael. A strain parameter turbulence model and its application to homogeneous and thin shear flows. *International journal of heat and fluid flow*, 19(4): 326–337, 1998.

MA Cotton and JD Jackson. Vertical tube air flows in the turbulent mixed convection regime calculated using a low-reynolds-number k˜ model. *International journal of heat and mass transfer*, 33(2):275–286, 1990.

MA Cotton and PJ Kirwin. A comparative study of two-equation turbulence models applied to turbulent mixed convection in vertical pipes. In *Proc. 5th Int. Symp. on Refined Flow Modelling and Turbulence Measurements. Paris, France*, 1993.

G Cox and S Kumar. Field modelling of fire in forced ventilated enclosures. *Combustion Science and Technology*, 52(1-3):7–23, 1987.

Geoffrey Cox. *Combustion fundamentals of fire*. Acad. press London etc, 1995.

TJ Craft. Second-moment modelling of turbulent scalar transport. 1991.

TJ Craft, BE Launder, and K Suga. Development and application of a cubic eddy-viscosity model of turbulence. *International Journal of Heat and Fluid Flow*, 17(2):108–115, 1996.

NL Crauford, SK Liew, and JB Moss. Experimental and numerical simulation of a buoyant fire. *Combustion and flame*, 61(1):63–77, 1985.

Bart J Daly and Francis H Harlow. Transport equations in turbulence. *The Physics of Fluids*, 13(11):2634–2649, 1970.

Lars Davidson. Second-order corrections of the k-ε model to account for non-isotropic effects due to buoyancy. *International Journal of Heat and Mass Transfer*, 33(12): 2599–2608, 1990.

F Dehoux, Sofiane Benhamadouche, and Remi Manceau. An elliptic blending differential flux model for natural, mixed and forced convection. *International Journal of Heat and Fluid Flow*, 63:190–204, 2017.

Frederic Dehoux, Yannick Lecocq, Sofiane Benhamadouche, Remi Manceau, and Laurent-Emmanuel Brizzi. Algebraic modeling of the turbulent heat fluxes using the elliptic blending approach—application to forced and mixed convection regimes. *Flow, turbulence and combustion*, 88(1-2):77–100, 2012.

Ayodeji O Demuren and Wolfgang Rodi. Calculation of turbulence-driven secondary motion in non-circular ducts. *Journal of Fluid Mechanics*, 140:189–222, 1984.

HS Dol and K Hanjalić. Computational study of turbulent natural convection in a side-heated near-cubic enclosure at a high rayleigh number. *International Journal of Heat and Mass Transfer*, 44(12):2323–2344, 2001.

HS Dol, K Hanjalić, and S Kenjereš. A comparative assessment of the second-moment differential and algebraic models in turbulent natural convection. *International journal of heat and fluid flow*, 18(1):4–14, 1997.

HS Dol, K Hanjalić, and TAM Versteegh. A dns-based thermal second-moment closure for buoyant convection at vertical walls. *Journal of Fluid Mechanics*, 391:211–247, 1999.

Coleman DuP Donaldson, Roger D Sullivan, and Harold Rosenbaum. A theoretical study of the generation of atmospheric-clear air turbulence. *AIAA Journal*, 10(2):162–170, 1972.

PA Durbin. A reynolds stress model for near-wall turbulence. *Journal of Fluid Mechanics*, 249:465–498, 1993.

Paul A Durbin. Near-wall turbulence closure modeling without "damping functions". *Theoretical and Computational Fluid Dynamics*, 3(1):1–13, 1991.

Hans Ertel. Ein neuer hydrodynamischer wirbelsatz. *Met. Z.*, 59:277–281, 1942.

Sixin Fan, Budugur Lakshminarayana, and Mark Barnett. Low-reynolds-number k-epsilon model for unsteady turbulent boundary-layer flows. *AIAA journal*, 31(10):1777–1784, 1993.

DF Fletcher, JH Kent, VB Apte, and AR Green. Numerical simulations of smoke movement from a pool fire in a ventilated tunnel. *Fire Safety Journal*, 23(3):305–325, 1994.

ANSYS Fluent. 15.0 user's manual, ansys documentation n fluent n user's guide & theory guide—release 15.0. *ANSYS Inc.*

E Fournier and Tim Bayne. Under hood temperature measurements. Technical report, SAE Technical Paper, 2007.

Ed Fournier and T Bayne. Underhood temperature measurements of four vehicles. *Motor Vehicle Fire Research Institute, Biokinetics and Associates, Ltd., Report R04-13*, page 20, 2004.

Ed Fournier and Tim Bayne. Assessment of thermocouple attachment methods for measuring vehicle exhaust temperature. *Motor Vehicle Fire Research Institute, Biokinetics and Associates, Ltd., Report R06-23b for MVFRI*, 2006.

Matteo Franchetta, KO Suen, Paul A Williams, and TG Bancroft. Investigation into natural convection in an underhood model under heat soak condition. Technical report, SAE Technical Paper, 2005.

Matteo Franchetta, Thomas G Bancroft, and KO Suen. Fast transient simulation of vehicle underhood in heat soak. *SAE Transactions*, pages 1526–1538, 2006.

Manuel Garcia-Villalba and Juan C Del Alamo. Turbulence modification by stable stratification in channel flow. *Physics of Fluids*, 23(4):045104, 2011.

Thomas B Gatski and Charles G Speziale. On explicit algebraic stress models for complex turbulent flows. *Journal of fluid Mechanics*, 254:59–78, 1993.

MM Gibson and BE Launder. On the calculation of horizontal, turbulent, free shear flows under gravitational influence. *ASME Transactions Journal of Heat Transfer*, 98:81–87, 1976.

MM Gibson and BE Launder. Ground effects on pressure fluctuations in the atmospheric boundary layer. *Journal of Fluid Mechanics*, 86(3):491–511, 1978.

Sharath S Girimaji. Fully explicit and self-consistent algebraic reynolds stress model. *Theoretical and Computational Fluid Dynamics*, 8(6):387–402, 1996.

Olof Grundestam, Stefan Wallin, and Arne V Johansson. Techniques for deriving explicit algebraic reynolds stress models based on incomplete sets of basis tensors and predictions of fully developed rotating pipe flow. *Physics of fluids*, 17(11):115103, 2005.

J Gu, M Ouyang, D Lu, J Li, and L Lu. Energy efficiency optimization of electric vehicle driven by in-wheel motors. *International Journal of Automotive Technology*, 14(5):763–772, 2013.

K Hanjalic. Achievements and limitations in modelllng and computation of buoyant turbulent flows and heat transfer. In *International Heat Transfer Conference Digital Library*. Begel House Inc., 1994.

K Hanjalić. One-point closure models for buoyancy-driven turbulent flows. *Annual review of fluid mechanics*, 34(1):321–347, 2002.

K Hanjalić, S Kenjereš, and F Durst. Natural convection in partitioned two-dimensional enclosures at higher rayleigh numbers. *International journal of heat and mass transfer*, 39(7):1407–1427, 1996.

Kemal Hanjalić and Brian Launder. *Modelling turbulence in engineering and the environment: second-moment routes to closure*. Cambridge university press, 2011.

Kemal Hanjalić and Brian E Launder. A reynolds stress model of turbulence and its application to thin shear flows. *Journal of fluid Mechanics*, 52(4):609–638, 1972.

Tetsuo Hara and Shinsuke Kato. Numerical simulation of thermal plumes in free space using the standard k–ε model. *Fire Safety Journal*, 39(2):105–129, 2004.

Samuel Hassid and Michael Poreh. A turbulent energy dissipation model for flows with drag reduction. 1978.

TJ Heindel, S Ramadhyani, and FP Incropera. Assessment of turbulence models for natural convection in an enclosure. *Numerical Heat Transfer*, 26(2):147–172, 1994.

RAWM Henkes and CJ Hoogendoorn. Comparison of turbulence models for the natural convection boundary layer along a heated vertical plate. *International journal of heat and mass transfer*, 32(1):157–169, 1989.

Gunnar Heskestad. Engineering relations for fire plumes. *Fire Safety Journal*, 7(1):25–32, 1984.

Gilbert H Hoffman. Improved form of the low reynolds number k- ε turbulence model. *The Physics of Fluids*, 18(3):309–312, 1975.

MS Hossain. Mathematical modelling of vertical mixing in stratified channel flow. In *Proc. 2nd Int. Symp. on Stratified Flows, Trondheim, Norway, 1980*, 1980.

NZ Ince and BE Launder. On the computation of buoyancy-driven turbulent flows in rectangular enclosures. *International Journal of Heat and Fluid Flow*, 10(2):110–117, 1989.

JD Jackson and DP Mikielewicz. Computational studies of buoyancy-influenced flow of air in a vertical pipe. In *Engineering Turbulence Modelling and Experiments*, pages 349–358. Elsevier, 1996.

WP Jones and Brian Edward Launder. The prediction of laminarization with a two-equation model of turbulence. *International journal of heat and mass transfer*, 15(2): 301–314, 1972.

WP Jones and BrnE Launder. The calculation of low-reynolds-number phenomena with a two-equation model of turbulence. *International Journal of Heat and Mass Transfer*, 16(6):1119–1130, 1973.

Tim Juan. Investigation and assessment of factors affecting the underhood cooling air flow using cfd. Technical report, SAE Technical Paper, 2008.

BA Kader. Temperature and concentration profiles in fully turbulent boundary layers. *International journal of heat and mass transfer*, 24(9):1541–1544, 1981.

Nobuhide Kasagi and Mitsugu Nishimura. Direct numerical simulation of combined forced and natural turbulent convection in a vertical plane channel. *International Journal of Heat and Fluid Flow*, 18(1):88–99, 1997.

Shailendra Kaushik. Thermal management of a vehicle's underhood and underbody using appropriate math-based analytical tools and methodologies. Technical report, SAE Technical Paper, 2007.

Wiliam M Kays. Turbulent prandtl number. where are we? *ASME Transactions Journal of Heat Transfer*, 116:284–295, 1994.

WM Kays and ME Crawford. Convective heat and mass transfer. chapter 10. *Heat transfer: The laminar external boundary layer. McGraw-Hill*, pages 159–191, 1993.

S Kenjereš and K Hanjalić. Convective rolls and heat transfer in finite-length rayleigh-bénard convection: A two-dimensional numerical study. *Physical Review E*, 62(6):7987, 2000.

S Kenjereš, SB Gunarjo, and K Hanjalić. Contribution to elliptic relaxation modelling of turbulent natural and mixed convection. *International Journal of Heat and Fluid Flow*, 26(4):569–586, 2005.

Sasa Kenjeres. Numerical modelling of complex buoyancy-driven flows. *PhD Thesis Delft University of Technology*, 1998.

Amir Keshmiri, Yacine Addad, Mark A Cotton, Dominique R Laurence, and Flavien Billard. Refined eddy viscosity schemes and large eddy simulations for ascending mixed convection flows. In *ICHMT DIGITAL LIBRARY ONLINE*. Begel House Inc., 2008.

Mahmoud Khaled, Fabien Harambat, and Hassan Peerhossaini. Effects of car inclination on air flow and aerothermal behavior in the underhood compartment. In *ASME 2008 Fluids Engineering Division Summer Meeting collocated with the Heat Transfer, Energy Sustainability, and 3rd Energy Nanotechnology Conferences*, pages 517–522. American Society of Mechanical Engineers Digital Collection, 2008.

Mahmoud Khaled, Fabien Harambat, and Hassan Peerhossaini. A quantitative method for assessment of car inclination effects on thermal management of the underhood compartment. *Journal of Thermal Science and Engineering Applications*, 1(1), 2009.

Mahmoud Khaled, MG Elrab, C Habchi, A Al Shaer, Ahmed Elmarakbi, F Harambat, and H Peerhossaini. Analysis and modeling of the thermal soak phase of a vehicle—temperature and heat flux measurements. *International Journal of Automotive Technology*, 16(2):221–229, 2015.

WS Kim, John Derek Jackson, and S He. Computational investigation into buoyancy-aided turbulent flow and heat transfer to air in a vertical tube. In *ICHMT DIGITAL LIBRARY ONLINE*. Begel House Inc., 2006.

Santosh Kini and Richard Thoms. Multi-domain meshes for automobile underhood applications. Technical report, SAE Technical Paper, 2009.

Peter James Kirwin. *Investigation and development of two-equation turbulence closures with reference to mixed convection in vertical pipes*. PhD thesis, The University of Manchester, 1995.

P Kiš and H Herwig. Natural convection in a vertical plane channel: Dns results for high grashof numbers. *Heat and Mass Transfer*, 50(7):957–972, 2014.

Andrey Nikolaevich Kolmogorov. The local structure of turbulence in incompressible viscous fluid for very large reynolds numbers. *Cr Acad. Sci. URSS*, 30:301–305, 1941.

Rajesh Kumar and Anupam Dewan. Assessment of buoyancy-corrected turbulence models for thermal plumes. *Engineering Applications of Computational Fluid Mechanics*, 7(2): 239–249, 2013.

Vivek Kumar, Sangeet Kapoor, Gyan Arora, Sandip K Saha, and Pradip Dutta. A combined cfd and flow network modeling approach for vehicle underhood air flow and thermal analysis. Technical report, SAE Technical Paper, 2009.

YG Lai and RMC So. On near-wall turbulent flow modelling. *Journal of Fluid Mechanics*, 221:641–673, 1990.

CKG Lam and K Bremhorst. A modified form of the k-ε model for predicting wall turbulence. 1981.

BE Launder. On the effects of a gravitational field on the turbulent transport of heat and momentum. *Journal of Fluid Mechanics*, 67(3):569–581, 1975.

BE Launder. Heat and mass transport. turbulence-topics in applied physics/ed. bradshaw p, 1976.

Brian Edward Launder. On the computation of convective heat transfer in complex turbulent flows. 1988.

Brian Edward Launder and BI Sharma. Application of the energy-dissipation model of turbulence to the calculation of flow near a spinning disc. *Letters in heat and mass transfer*, 1(2):131–137, 1974.

Brian Edward Launder, G Jr Reece, and W Rodi. Progress in the development of a reynolds-stress turbulence closure. *Journal of fluid mechanics*, 68(3):537–566, 1975.

Fue-Sang Lien and Georgi Kalitzin. Computations of transonic flow with the v2–f turbulence model. *International Journal of Heat and Fluid Flow*, 22(1):53–61, 2001.

F Liu and JX Wen. Development and validation of an advanced turbulence model for buoyancy driven flows in enclosures. *International Journal of Heat and Mass Transfer*, 42(21):3967–3981, 1999.

F Liu and JX Wen. The effect of turbulence modelling on the cfd simulation of buoyant diffusion flames. *Fire safety journal*, 37(2):125–150, 2002.

JL Lumley. A model for computation of stratified turbulent flows. In *International Symposium on Stratified Flows, Novosibirsk*, 1972.

Mingchun Luo and Vaughan Beck. The fire environment in a multi-room building—comparison of predicted and experimental results. *Fire safety journal*, 23(4):413–438, 1994.

Remi Manceau. Recent progress in the development of the elliptic blending reynolds-stress model. *International Journal of Heat and Fluid Flow*, 51:195–220, 2015.

Rémi Manceau and Kemal Hanjalić. Elliptic blending model: A new near-wall reynolds-stress turbulence closure. *Physics of Fluids*, 14(2):744–754, 2002.

Shuhaimi Mansor and Martin A Passmore. Effect of rear slant angle on vehicle cross-wind stability simulation on a simplified car model. *International journal of automotive technology*, 14(5):701–706, 2013.

NC Markatos, MR Malin, and G Cox. Mathematical modelling of buoyancy-induced smoke flow in enclosures. *International Journal of Heat and Mass Transfer*, 25(1):63–75, 1982.

George L Mellor and Tetsuji Yamada. Development of a turbulence closure model for geophysical fluid problems. *Reviews of Geophysics*, 20(4):851–875, 1982.

Florian R Menter. Two-equation eddy-viscosity turbulence models for engineering applications. *AIAA journal*, 32(8):1598–1605, 1994.

Vittorio Michelassi, Wolfgang Rodi, and J Zhu. Testing a low-reynolds number k-epsilon turbulence model based on direct simulation data. *AIAA journal*, 31(9):1720–1723, 1993.

Dariusz Przemysław Mikielewicz. Comparative studies of turbulence models under conditions of mixed convection with variable properties in heated vertical tubes. *Ph. D. Thesis, Univ. of Manchester*, 1994.

AS Monin. On the symmetry properties of turbulence in the surface layer of air. *Isv. Atmos. Ocean. Phys.*, 1:45–54, 1965.

S Murakami, N Ohira, and S Kato. Cfd analysis of a thermal plume and the indoor air flow using k-ε models with buoyancy effects. *Flow, turbulence and combustion*, 63(1-4): 113, 2000.

Shuzo Murakami, Shinsuke Kato, Tomoyuki Chikamoto, D Laurence, and D Blay. New low-reynolds-number k-ε model including damping effect due to buoyancy in a stratified flow field. *International journal of heat and mass transfer*, 39(16):3483–3496, 1996.

Soonil Nam and Robert G Bill Jr. Numerical simulation of thermal plumes. *Fire Safety Journal*, 21(3):231–256, 1993.

D Naot. Interactions between components of the turbulent velocity correlation tensor. *Isr. J. Technol.*, 8:259–269, 1970.

V Novozhilov. Computational fluid dynamics modeling of compartment fires. *Progress in Energy and Combustion science*, 27(6):611–666, 2001.

Roger Guy Owen. An analytical turbulent transport model applied to nonisothermal fully-developed duct flows. 1974.

Virendra C Patel, Wolfgang Rodi, and Georg Scheuerer. Turbulence models for near-wall and low reynolds number flows-a review. *AIAA journal*, 23(9):1308–1319, 1985.

TWJ Peeters and RAWM Henkes. The reynolds-stress model of turbulence applied to the natural-convection boundary layer along a heated vertical plate. *International journal of heat and mass transfer*, 35(2):403–420, 1992.

AF Polyakov and SA Shindin. Development of turbulent heat transfer over the length of vertical tubes in the presence of mixed air convection. *International journal of heat and mass transfer*, 31(5):987–992, 1988.

SB Pope. A more general effective-viscosity hypothesis. *Journal of Fluid Mechanics*, 72 (2):331–340, 1975.

Charles Henry Brian Priestley and WC Swinbank. Vertical transport of heat by turbulence in the atmosphere. *Proceedings of the Royal Society of London. Series A. Mathematical and Physical Sciences*, 189(1019):543–561, 1947.

H Reister and M Maihöfer. Underhood component temperature analysis for passenger cars. In *VTMS 6 SAE Conference, 2003. C599/028*, 2003.

JS Rho and HS Ryou. A numerical study of atrium fires using deterministic models. *Fire Safety Journal*, 33(3):213–229, 1999.

Adam H Richards, Robert E Spall, and Donald M McEligot. An assessment of turbulence models forstrongly-heated internal gas flows. In *Proc. 15 th IASTED int. Conf., Modeling and Simulation, Marina Del Rey, California, USA*, 2004.

W Rodi. Influence of buoyancy and rotation on equations for the turbulent length scale. In *2nd Symposium on Turbulent Shear Flows*, pages 10–37, 1979.

W Rodi and NN Mansour. Low reynolds number k—ε modelling with the aid of direct simulation data. *Journal of Fluid Mechanics*, 250:509–529, 1993.

W Rodi and G Scheuerer. Scrutinizing the k-epsilon-model under adverse pressure gradient conditions. *stsf*, pages 2–8, 1984.

Wolfgang Rodi. The prediction of free turbulent boundary layers by use of a two equation model of turbulence. 1972.

Wolfgang Rodi. Turbulence models and their applications in hydraulics-a state-of-the-art review. *IAHR monograph*, 1984.

JC Rotta. Statistische theorie nichthomogener turbulenz. *Zeitschrift für Physik*, 129(6): 547–572, 1951.

Christopher L Rumsey, Thomas B Gatski, and Joseph H Morrison. Turbulence model predictions of strongly curved flow in a u-duct. *AIAA journal*, 38(8):1394–1402, 2000.

Didier Saury, Nicolas Rouger, Francis Djanna, and François Penot. Natural convection in an air-filled cavity: Experimental results at large rayleigh numbers. *International Communications in Heat and Mass Transfer*, 38(6):679–687, 2011.

M Schuster. Application of cfd as an efficient analysis tool supporting the experimental investigation of underhood and underbody airflows. In *VTMS 6 SAE Conference, 2003. C599/056*, 2003.

Frederic Sebilleau, Raad Issa, Sylvain Lardeau, and Simon P Walker. Direct numerical simulation of an air-filled differentially heated square cavity with rayleigh numbers up to 1011. *International Journal of Heat and Mass Transfer*, 123:297–319, 2018.

A Shabbir and DB Taulbee. Evaluation of turbulence models for predicting buoyant flows. 1990.

A Mohsen Shehata and Donald M McEligot. Mean structure in the viscous layer of strongly-heated internal gas flows. measurements. *International journal of heat and mass transfer*, 41(24):4297–4313, 1998.

Jong Keun Shin, Jeong Soo An, and Young Don Choi. Elliptic relaxation second moment closure for turbulent heat flux. In *TSFP DIGITAL LIBRARY ONLINE*. Begel House Inc., 2005.

Jong Keun Shin, Jeong Soo An, Young Don Choi, Young Chan Kim, and Min Soo Kim. Elliptic relaxation second moment closure for the turbulent heat fluxes. *Journal of Turbulence*, (9):N3, 2008.

YL Sinai and Matthew P Owens. Validation of cfd modelling of unconfined pool fires with cross-wind: flame geometry. *Fire Safety Journal*, 24(1):1–34, 1995.

RMC So, HS Zhang, and CG Speziale. Near-wall modeling of the dissipation rate equation. *AIAA journal*, 29(12):2069–2076, 1991.

RMC So, LH Jin, and TB Gatski. An explicit algebraic reynolds stress and heat flux model for incompressible turbulence: Part ii buoyant flow. *Theoretical and Computational Fluid Dynamics*, 17(5-6):377–406, 2004.

Alejandro Steiner. On the reverse transition of a turbulent flow under the action of buoyancy forces. *Journal of Fluid Mechanics*, 47(3):503–512, 1971.

Geoffrey Ingram Taylor. I. eddy motion in the atmosphere. *Philosophical Transactions of the Royal Society of London. Series A, Containing Papers of a Mathematical or Physical Character*, 215(523-537):1–26, 1915.

Yongsheng Tian. *Low turbulence natural convection in an air filled square cavity.* PhD thesis, South Bank University, 1997.

Yongsheng Tian, Tassos G Karayiannis, Richard D Matthews, and Jennifer X Wen. Reynolds stress in low turbulence natural convection in an air filled square cavity. In *International Heat Transfer Conference Digital Library*. Begel House Inc., 1998.

FX Trias, M Soria, A Oliva, and CD Pérez-Segarra. Direct numerical simulations of two-and three-dimensional turbulent natural convection flows in a differentially heated cavity of aspect ratio 4. *Journal of Fluid Mechanics*, 586:259–293, 2007.

FX Trias, Andrei Gorobets, M Soria, and A Oliva. Direct numerical simulation of a differentially heated cavity of aspect ratio 4 with rayleigh numbers up to 1011–part i: Numerical methods and time-averaged flow. *International Journal of Heat and Mass Transfer*, 53(4):665–673, 2010.

Karim Van Maele and Bart Merci. Application of two buoyancy-modified k–ε turbulence models to different types of buoyant plumes. *Fire Safety Journal*, 41(2):122–138, 2006.

D Vanpouille, B Aupoix, and E Laroche. Development of an explicit algebraic turbulence model for buoyant flows–part 2: Model development and validation. *International Journal of Heat and Fluid Flow*, 53:195–209, 2015.

TAM Versteegh and FTM Nieuwstadt. Scaling of free convection between two differentially heated infinite vertical plates. *Turbulent Shear Flow*, 11, 1996.

TAM Versteegh and FTM Nieuwstadt. Turbulent budgets of natural convection in an infinite, differentially heated, vertical channel. *International Journal of Heat and Fluid Flow*, 19(2):135–149, 1998.

JV Vilemas, PS Poškas, and VE Kaupas. Local heat transfer in a vertical gas-cooled tube with turbulent mixed convection and different heat fluxes. *International journal of heat and mass transfer*, 35(10):2421–2428, 1992.

PJ Walklate. *A comparative study of theoretical models of turbulence for the numerical prediction of boundary-layer flows.* PhD thesis, University of Manchester Institute of Science and Technology, 1976.

Ernst Peter Weidmann, Jochen Wiedemann, Thomas Binner, and Heinrich Reister. Underhood temperature analysis in case of natural convection. Technical report, SAE Technical Paper, 2005.

Ernst Peter Weidmann, Thomas Binner, and Heinrich Reister. Experimental and numerical investigations of thermal soak. *SAE International Journal of Materials and Manufacturing*, 1(1):145–153, 2009.

David C Wilcox. Comparison of two-equation turbulence models for boundary layers with pressure gradient. *AIAA journal*, 31(8):1414–1421, 1993.

Martin Wörner. *Direkte Simulation turbulenter Rayleigh-Bénard-Konvektion in flüssigem Natrium*. PhD thesis, Kernforschungszentrum, 1994.

Jude Worthy, V Sanderson, and P Rubini. Comparison of modified k-? turbulence models for buoyant plumes. *Numerical Heat Transfer: Part B: Fundamentals*, 39(2):151–165, 2001.

John C Wyngaard and OR Coté. The evolution of a convective planetary boundary layer—a higher-order-closure model study. *Boundary-Layer Meteorology*, 7(3):289–308, 1974.

H Xue, JC Ho, and YM Cheng. Comparison of different combustion models in enclosure fire simulation. *Fire Safety Journal*, 36(1):37–54, 2001.

Zhenghua Yan and Göran Holmstedt. A two-equation turbulence model and its application to a buoyant diffusion flame. *International Journal of Heat and Mass Transfer*, 42(7): 1305–1315, 1999.

Z Yang and Tsan-Hsing Shih. New time scale based k-epsilon model for near-wall turbulence. *AIAA journal*, 31(7):1191–1198, 1993.

CHRISTOPHERR Yap. Turbulent heat and momentum transfer in recirculating and impinging flows(ph. d. thesis). 1987.

Jongwoo You, Jung Y Yoo, and Haecheon Choi. Direct numerical simulation of heated vertical air flows in fully developed turbulent mixed convection. *International Journal of Heat and Mass Transfer*, 46(9):1613–1627, 2003.

LSL Yu. *A computational study of turbulent mixed convection in vertical tubes*. PhD thesis, University of Manchester, 1991.

SS Zilitinkevich, T Elperin, N Kleeorin, and I Rogachevskii. Energy-and flux-budget (efb) turbulence closure model for stably stratified flows. part i: steady-state, homogeneous regimes. In *Atmospheric Boundary Layers*, pages 11–35. Springer, 2007.

Appendix A

Implementation of the buoyancy sensitized models in Ansys Fluent

A.1 Introduction

For the thermal designing of the underhood space of vehicules, PSA group uses Ansys Fluent, but due to the unavailability of the sources of this code, it is not flexible enough to modify and analyze the effects of modifications done in turbulence models. Keeping in view this fact, the open source code "Code-Saturne" has been used to develop buoyancy sensitized models.
Two version of buoyancy sensitized k-ω-SST models are now implemented in Ansys Fluent using user-defined functions and the main objective of this chapter is to compare the results given by the two codes. A Comparison of only buoyancy sensitized k-ω-SST models is performed as the BL-$\overline{v^2}/k$ model is not available in Ansys Fluent.
In the last part of this chapter, attempts are made to analyze the effect of varying turbulent Prandtl number in association with the Reynolds analogy.

A.2 Comparison of buoyancy sensitised k-ω-SST model

Attempts are made to investigate the performance of buoyancy sensitized k-ω-SST models by simulating the differentially heated vertical channel case corresponding to the highest Rayleigh number, $Ra = 1.7 \times 10^7$ and the results are compared to the DNS data of Kiš and Herwig [2014]. The flow configurtion is shown in Fig. A.1.

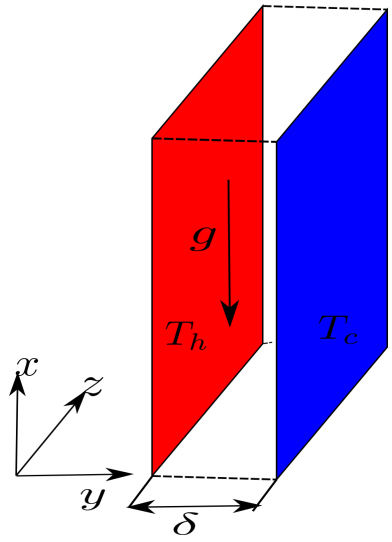

Figure A.1 – Flow configuration for the differentially heated vertical channel

The standard approach to model Reynolds stresses is to use the Boussinesq constitutive relation (linear stress-strain relation) which is expressed as follows:

$$\overline{u_i' u_j'} = \frac{2}{3} k \delta_{ij} - \nu_t \left(\frac{\partial U_i}{\partial x_j} + \frac{\partial U_j}{\partial x_i} \right) \tag{A.1}$$

The standard approach to model the heat fluxes is the simple gradient diffusion hypothesis (SGDH).

$$\overline{u_i' \theta} = -\frac{\nu_t}{Pr_t} \frac{\partial T}{\partial x_i} \tag{A.2}$$

However, these standard approaches are insufficient to predict the thermal buoyancy-driven flows [Hanjalić, 2002]. In view of this context, k-ω-SST model is sensitized by using two sensitization methods and the performance of these buoyancy-sensitized k-ω-SST model is examined in the following section.

A.2.1 Buoyancy-extended k-ω-SST models

The first method of sensitization involves the inclusion of the buoyancy extension into the Boussinesq relation. The buoyancy-extended model is developed in such a way that the buoyancy extension is derived from exact Reynolds stress equation using the weak equilibrium hypothesis and associated with k-ω-SST model. One of the constraints in developing buoyancy-extended heat flux model is that the modeling of tensorial diffusivity (GGDH) is not possible in ANSYS Fluent and owing to this, the simple version of the buoyancy-extended k-ω-SST model is used, where the heat flux is modeled using simple gradient diffusion hypothesis (SGDH) approach and this simplified buoyancy-extended k-ω-SST model is implemented in Ansys Fluent using User-defined functions. Under the weak equilibrium hypothesis, the buoyancy-extended Reynolds stress relation is expressed

as follows:

$$\overline{u_i^{'}u_j^{'}} = \underbrace{\frac{2}{3}k\delta_{ij} - \nu_t\left(\frac{\partial U_i}{\partial x_j} + \frac{\partial U_j}{\partial x_i}\right)}_{Boussinesq} + \underbrace{{C_\theta}^* \frac{1}{C_\mu \omega}(G_{ij} - \frac{1}{3}\delta_{ij}G_{kk})}_{Buoyancy-extension} \tag{A.3}$$

where $G_{ij} = -\beta(g_j\overline{u_j^{'}\theta} + g_i\overline{u_i^{'}\theta})$ and $C_\theta^* = 0.2$

The turbulent heat flux is modeled using a simple gradient diffusion hypothesis (SGDH) approach which writes:

$$\overline{u_i^{'}\theta} = -\frac{\nu_t}{Pr_t}\frac{\partial T}{\partial x_i} \tag{A.4}$$

The buoyancy extension of the Reynolds stresses is also incorporated in the dynamic production of turbulent kinetic energy and in specific dissipation rate equations which write:

$$P_k = -\left[(\overline{u_i^{'}u_i^{'}})_{Boussinesq} + (\overline{u_i^{'}u_i^{'}})_{Buoyancy-extension}\right]\frac{\partial U_i}{\partial x_j} \tag{A.5}$$

Buoyancy production terms in the transport equation of the turbulent kinetic energy become:

$$G_k = \beta g_i \frac{\nu_t}{Pr_t}\frac{\partial T}{\partial x_i} \tag{A.6}$$

From Fig. A.2, it is observed that there is a severe overestimation of mean velocity by the original k-ω-SST model as predicted by both the codes. Moreover, there are differences in the prediction of mean velocity between the original models available in Ansys Fluent and Code Saturne respectively. These differences in predictions by the original k-ω-SST model in two codes might be linked to a different way of implementation of the boundary condition on ω. The boundary condition proposed by Menter [1994] is expressed as follows:

$$\omega_w = 10\frac{6\nu}{\beta_1 \Delta y_1^2} \quad at \quad y = 0 \tag{A.7}$$

where ω_w and Δy_1 are the value of ω at the wall and the distance to the next point away from the wall, respectively. This boundary condition in its true form is implemented in Code Saturne. However, in Ansys Fluent, this boundary condition is implemented with a formulation in a manner expressed as follows:

$$\omega_w = \frac{\rho(u_\tau)^2}{\mu}\omega^+ \tag{A.8}$$

where ω^+ for laminar sublayer is defined as follows:

$$\omega^+ = \frac{6}{\beta_1(y^+)^2} \tag{A.9}$$

For the logarithmic region, a wall function is used in such a way that the ω^+ becomes:

$$\omega^+ = \frac{1}{\sqrt{{\beta_\infty}^*}}\frac{d{u_{turb}}^+}{dy^+} \tag{A.10}$$

where ${\beta_\infty}^* = 0.09$.
However, it is not clear from the theory guide of Fluent, whether this value is applied at the wall or imposed at the center of the first cell. This different formulation might be linked to the differences in the prediction by the original and modified models in the two codes.

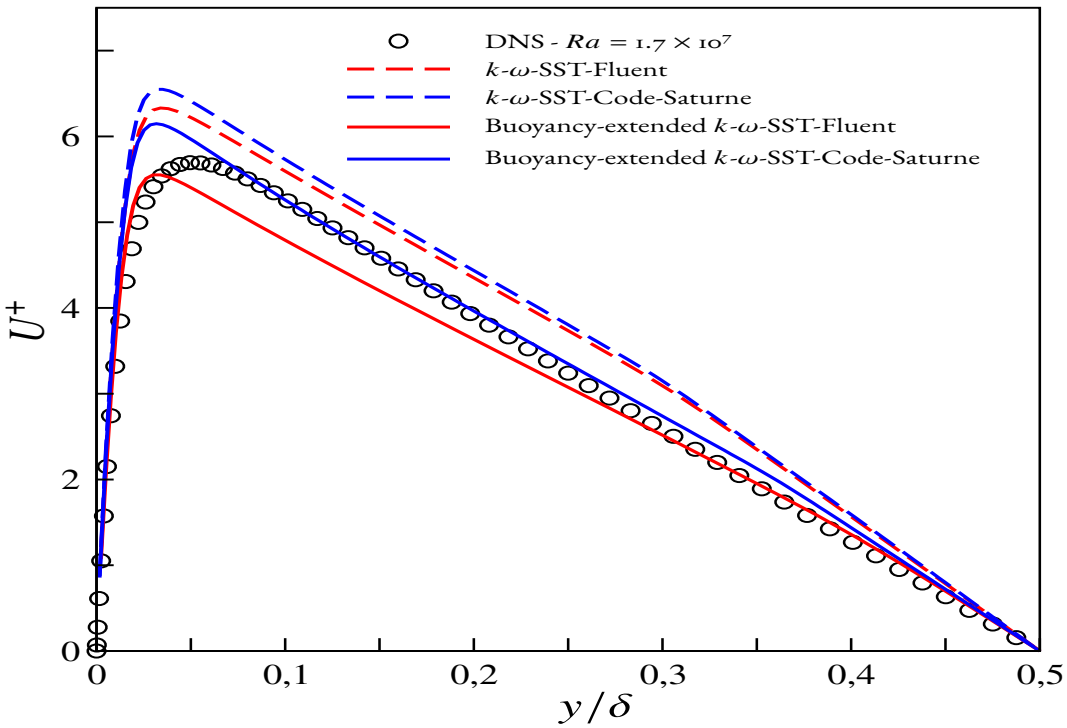

Figure A.2 – Comparison of mean velocity (U^+) profiles for buoyancy extended k-ω-SST model in Fluent (red color) and in Code Saturne (blue color) with the DNS data Kiš and Herwig [2014] at $Ra = 1.7 \times 10^7$ and $Pr = 0.71$

As far as the effect of buoyancy extension on the prediction of mean velocity (see Fig. A.2) is concerned, it is noticed that the inclusion of the buoyancy extension in the Boussinesq relation indeed improves the prediction of mean velocity and this improvement is observed with both the codes. However, with Ansys Fluent with buoyancy extension, there is an underestimation of mean velocity as compared with the prediction by Code Saturne which is in good agreement with DNS data. To probe further into this, turbulent shear stress is plotted in Fig. A.3: it is realized that the inclusion of the buoyancy extension leads to the improvement in the turbulent shear stress, although the prediction of Code Saturne seems to be in better agreement with DNS data as compared to the prediction by Ansys Fluent in which turbulent shear stress is marginally increased. If we analyze the momentum balance which is integrated from the wall to some arbitrary distance y away

from the wall, which writes:

$$0 = \int_0^y \nu \frac{\partial^2 \widetilde{U}}{\partial \widetilde{y}^2} dy - \int_0^y \frac{\partial \widetilde{\overline{u'v'}}}{\partial \widetilde{y}} d\widetilde{y} + \int_0^y \beta g(\widetilde{T} - \widetilde{T_{ref}}) d\widetilde{y} \tag{A.11}$$

It is observed that in the range between the peak of mean velocity and center of a channel, the contribution of buoyancy force must be balanced by viscous friction at the wall and the sum of viscous friction and turbulent shear stress in y, which is directed downwards such that

$$\int_0^y \widetilde{\beta} g(\widetilde{T} - \widetilde{T}_{ref}) d\widetilde{y} = \rho u_\tau^2 - \nu \frac{\partial \widetilde{U}}{\partial \widetilde{y}} + \widetilde{\overline{u'v'}} \tag{A.12}$$

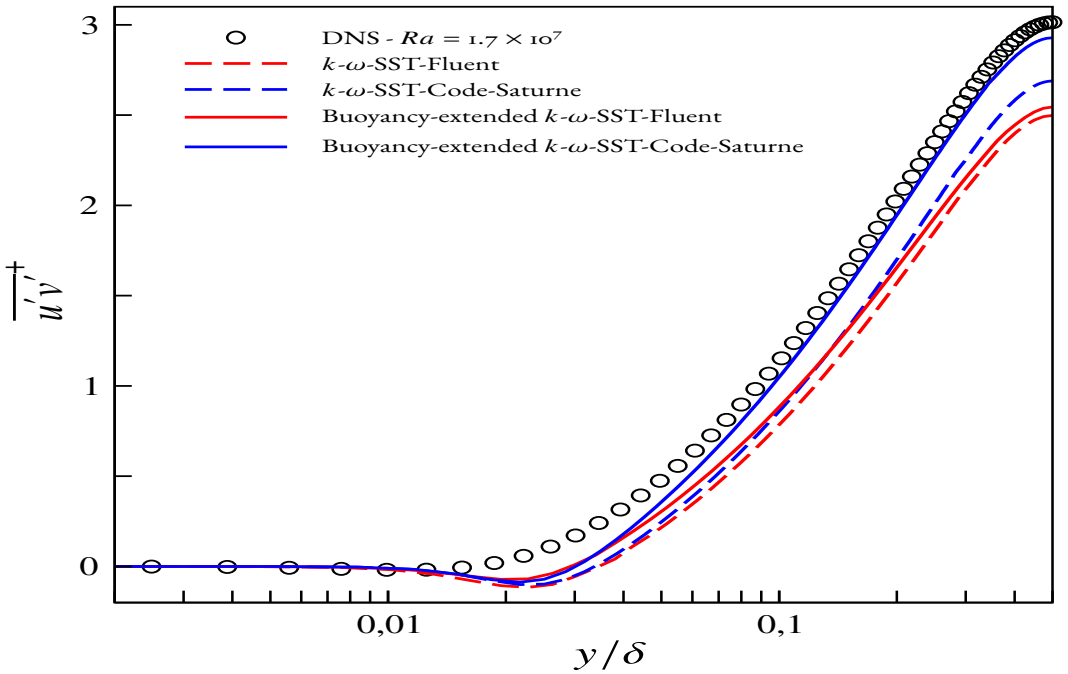

Figure A.3 – Comparison of the turbulent shear stress ($\overline{uv}^+$) for the buoyancy extended k-ω-SST model in Fluent (red color) and in Code Saturne (blue color) with DNS data of Kiš and Herwig [2014] at $Ra = 1.7 \times 10^7$ and $Pr = 0.71$

It is observed from Fig. A.3 that the original k-ω-SST model severely underestimated the turbulent shear stress and this must be recompensated by the viscous stresses in such a manner that a negative slope of mean velocity and friction velocity is increased. The role played by the buoyancy extension in the turbulent shear stress is to provide a positive contribution to the Boussinesq constitutive relation for the Reynolds stresses expressed as follows:

$$\widetilde{\overline{u'v'}} = -\nu_t \frac{\partial \widetilde{U}}{\partial \widetilde{y}} + \frac{{C_\theta}^*}{C_\mu \omega} \widetilde{\beta} g \widetilde{\overline{v'\theta}} \tag{A.13}$$

From Eq. A.13, it can be seen that the positive contribution of $\overline{v'\theta}$ enhances the turbulent shear stress such that mean velocity prediction is improved.

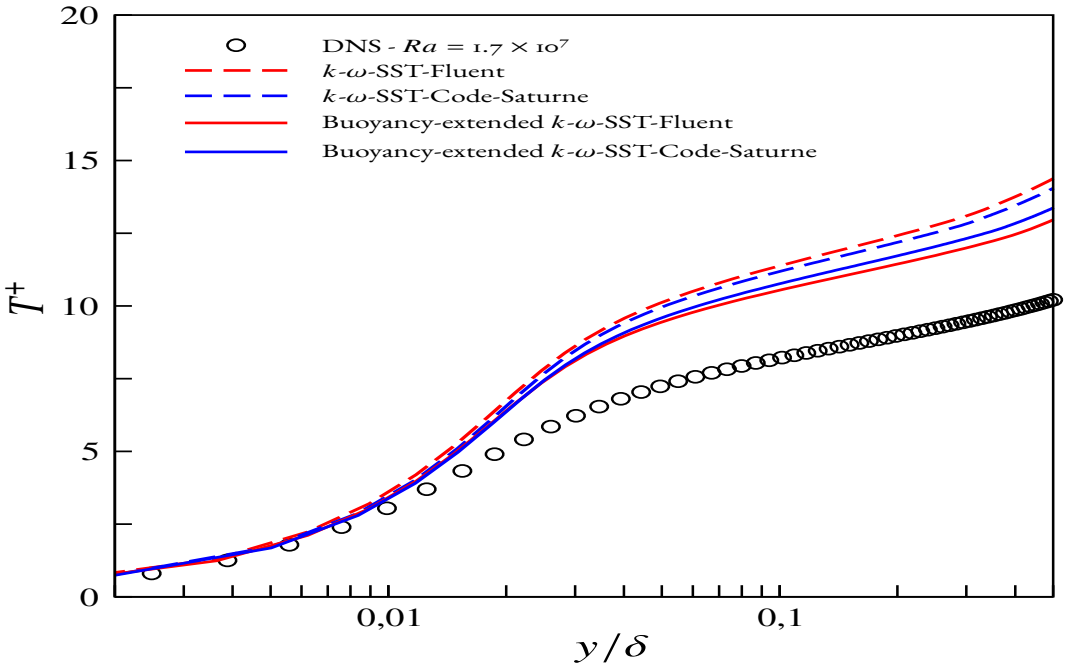

Figure A.4 – Comparison of the mean temperature (T^+) for the buoyancy extended k-ω-SST model in Fluent (red color) and in Code Saturne (blue color) with DNS data of Kiš and Herwig [2014] at $Ra = 1.7 \times 10^7$ and $Pr = 0.71$

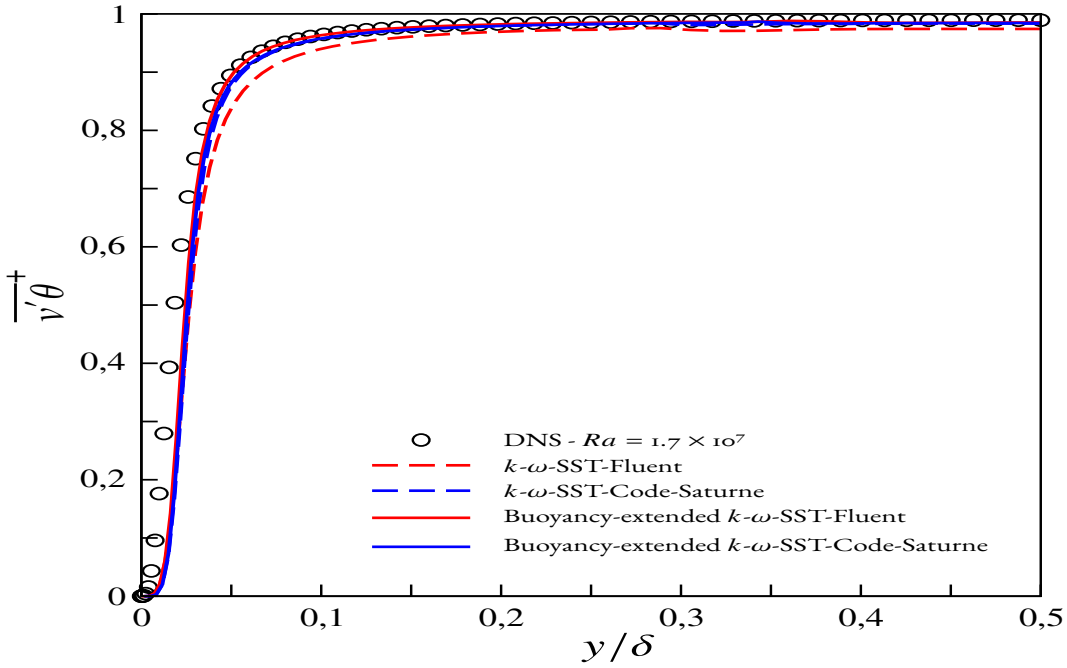

Figure A.5 – Comparison of wall normal heat flux ($\overline{v'\theta}^+$) for buoyancy extended k-ω-SST model in Fluent (red color) and in Code Saturne (blue color) with DNS data of Kiš and Herwig [2014] at $Ra = 1.7 \times 10^7$ and $Pr = 0.71$

From Fig. A.4 showing the mean temperature predictions, it is observed that the inclusion of the buoyancy extension improves the prediction of mean temperature. However, there are differences in the predictions by both the original and buoyancy-extended k-ω-SST models of the two codes probably due to the difference in the implementation as discussed above. It is important to have correct prediction of wall-normal heat flux component (active component in energy balance) and it is observed from Fig. A.5 that the heat flux far from the wall tends to 1.0 and this is independent of the heat flux model. With the buoyancy extension, there is an improvement in the prediction of the wall-normal heat flux close to the wall and this behavior is observed with both the codes, although there are differences in prediction between the codes. This prediction of the wall-normal heat flux corrects the misprediction of mean temperature (although it is insufficient) as can be seen in Fig. A.4.

A.2.2 Effect of adding only buoyancy production terms in the k-ω-SST model

A simpler way of taking into consideration of buoyancy effect is to add the buoyancy source terms in the transport equation for the turbulent kinetic energy (k) and the specific dissipation (ω), respectively. In the context of k-ε models, several researchers applied the simple gradient diffusion hypothesis (SGDH) approach to model these buoyancy source terms [Annarumma et al., 1991, Cox and Kumar, 1987, Fletcher et al., 1994, Luo and Beck, 1994, Markatos et al., 1982, Nam and Bill Jr, 1993, Rho and Ryou, 1999, Sinai and Owens, 1995, Xue et al., 2001]. However, with this approach, the effect of buoyancy on turbulence is severely underestimated and in order to overcome this limitation, Other authors Brescianini and Delichatsios [2003], Worthy et al. [2001], Yan and Holmstedt [1999] have applied the generalized gradient diffusion hypothesis (GGDH) of Daly and Harlow [1970] to model the buoyancy source terms.

In this part of the chapter, the effect of only adding buoyancy production terms in the transport equation of k and ω equation in the k-ω-SST model is analyzed by the simulating differentially heated vertical channel case of Kiš and Herwig [2014] corresponding to the highest available Rayleigh number, $Ra = 1.7 \times 10^7$.

The transport equations of the modified k-ω-SST model can be expressed as follows:

$$\frac{\partial k}{\partial t} + U_k \frac{\partial k}{\partial x_k} = P_k + G_k - \beta^* k\omega + \frac{\partial}{\partial x_k}\left[\left(\nu + \sigma_k \nu_t\right)\frac{\partial k}{\partial x_k}\right] \tag{A.14}$$

$$\frac{\partial \omega}{\partial t} + U_k \frac{\partial \omega}{\partial x_k} = \frac{\gamma}{\nu_t} P_k + \underbrace{max\left(\frac{C_3}{\nu_t} G_k, 0\right)}_{G_\omega} - \beta\omega^2 + \frac{\partial}{\partial x_k}\left[\left(\nu + \sigma_\omega \nu_t\right)\frac{\partial \omega}{\partial x_k}\right] + 2(1 - F_1)\sigma_{\omega 2}\frac{1}{\omega}\frac{\partial k}{\partial x_k}\frac{\partial \omega}{\partial x_k} \tag{A.15}$$

Where constants and blending functions are as per standard k-ω-SST model of Menter [1994], except constant C_3 in the buoyancy source term (G_ω) which is most of the time considered to be equal to the coefficient (γ) applied to the dynamic production term (P_ω). G_k is modeled using the generalized gradient diffusion hypothesis (GGDH) approach expressed as follows:

$$G_k = -\beta g_i \overline{u_i' \theta}; \qquad G_\omega = max\left(\frac{C_3}{\nu_t} G_k, 0\right); \qquad \overline{u_i' \theta} = -C_\theta \frac{1}{C_\mu \omega}\left(\overline{u_i' u_j'}\right)\frac{\partial T}{\partial x_j} \tag{A.16}$$

Where $C_3 = 0.2$.
The Boussinesq constitutive relation for the modeling of Reynolds stresses is used, which writes:

$$\overline{u_i' u_j'} = \frac{2}{3} k \delta_{ij} - \nu_t \left(\frac{\partial U_i}{\partial x_j} + \frac{\partial U_j}{\partial x_i}\right) \tag{A.17}$$

The simple gradient diffusion hypothesis (SGDH) is used to model the turbulent heat fluxes in the temperature equation as mentioned below:

$$\overline{u_i' \theta} = -\frac{\nu_t}{Pr_t}\frac{\partial T}{\partial x_i}; \qquad Pr_t = 1.0 \tag{A.18}$$

The mean velocity distribution is shown in Fig. A.6. It is observed that the inclusion of the buoyancy source terms leads to the improvement in the mean velocity which is severely overestimated by the original k-ω-SST model. This improvement in mean velocity is observed with both codes. However, it has been observed that the modified models through buoyancy source terms give a larger difference of improvement in the case of Ansys Fluent which is probably linked to the way the boundary conditions on ω is imposed on the original k-ω-SST model.

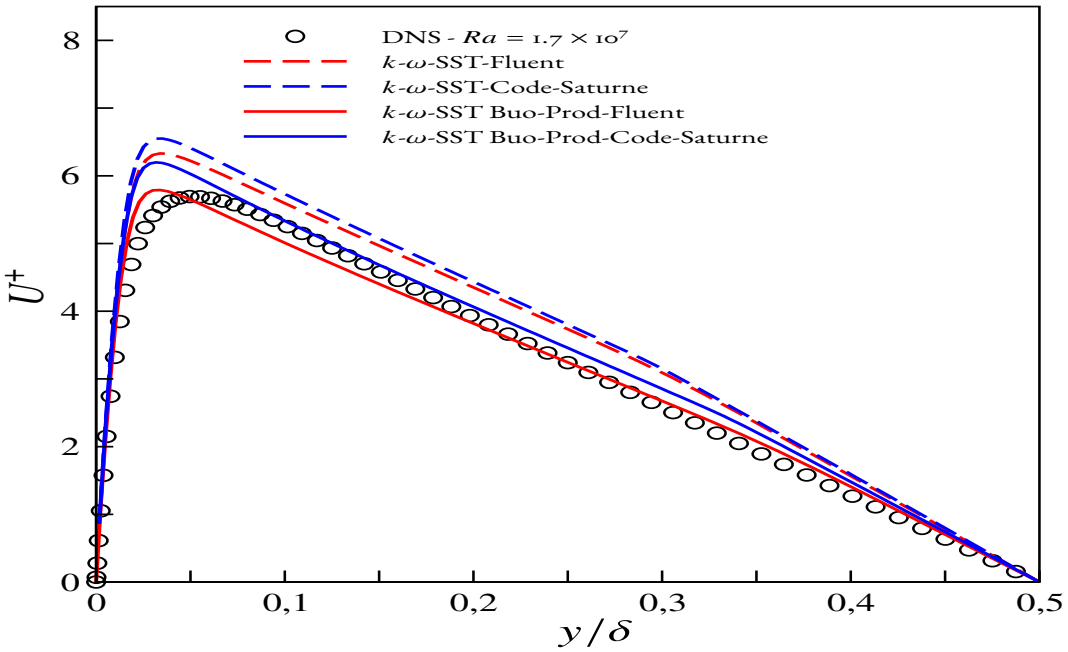

Figure A.6 – Comparison of mean velocity (U^+) profiles for buoyancy sensitized k-ω-SST model in Fluent (red color) and in Code Saturne (blue color) with DNS data Kiš and Herwig [2014] at $Ra = 1.7 \times 10^7$ and $Pr = 0.71$

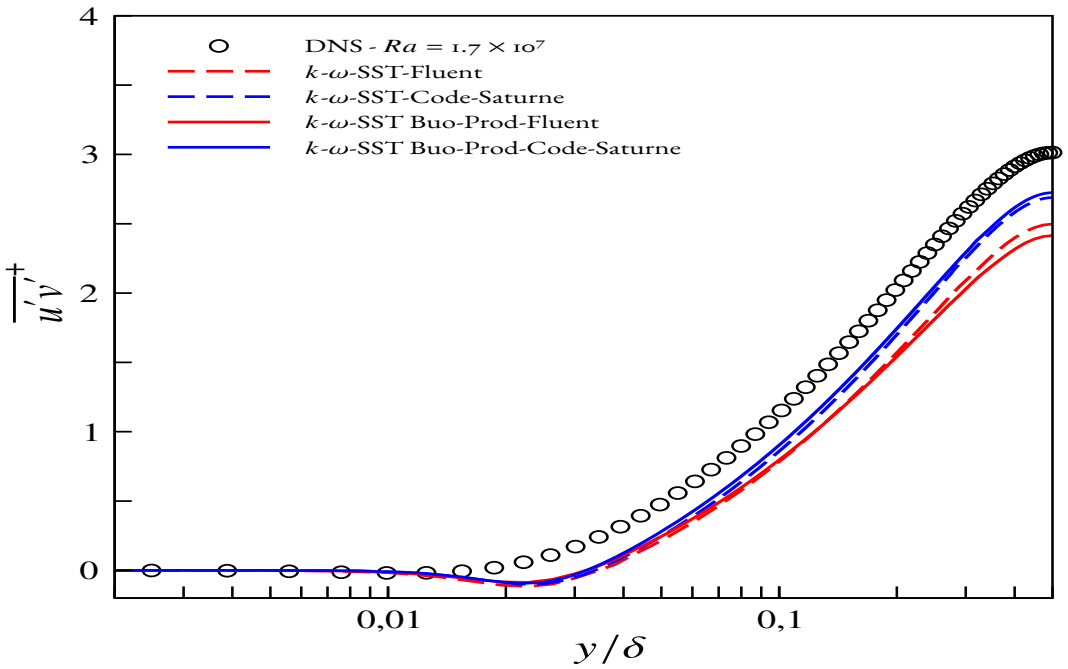

Figure A.7 – Comparison of turbulent shear stress ($\overline{uv}^+$) profiles for buoyancy sensitized k-ω-SST model in Fluent (red color) and in Code Saturne (blue color) with DNS data Kiš and Herwig [2014] at $Ra = 1.7 \times 10^7$ and $Pr = 0.71$

In order to probe the effect of buoyancy source terms on turbulent statistics, the

turbulent shear stress distribution is shown in Fig. A.7. It is realized that there is a marginal change of $\overline{u'v'}$ as compared to the original k-ω-SST model.
From Fig. A.8, it is realized that the effect of adding these buoyancy source terms is to improve the prediction of mean temperature which is mispredicted by the original k-ω-SST model in both codes. Nevertheless, it is intriguing to see that the effect of introducing G_k and G_ω in Ansys Fluent have a larger influence on temperature prediction such that there are differences in improvement in mean temperature corresponding to the same value of coefficient C_3 which is utilized in Code Saturne.

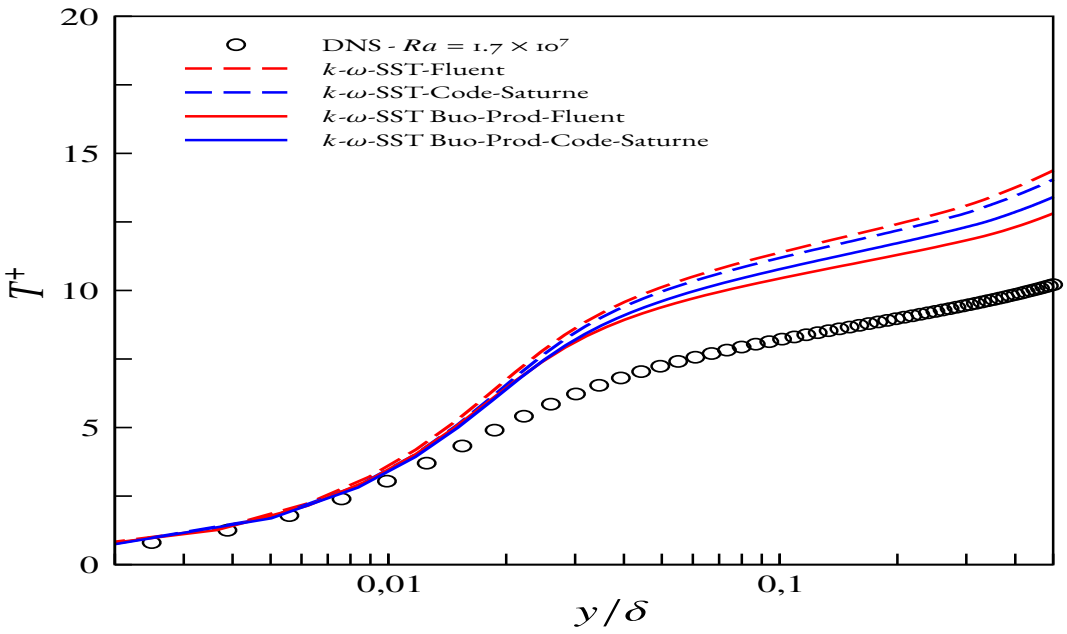

Figure A.8 – Comparison of mean temperature (T^+) profiles for buoyancy sensitised k-ω-SST model in Fluent (red color) and in Code Saturne (blue color) with DNS data Kiš and Herwig [2014] at $Ra = 1.7 \times 10^7$ and $Pr = 0.71$

This prediction of mean temperature is linked to the prediction of turbulent heat flux which is underestimated by the original k-ω-SST model as observed in both codes and the inclusion of the buoyancy source terms make an improvement in the wall normal component of the turbulent heat flux, and this explains the improvement of the mean temperature. By analyzing the influence of these buoyancy source terms in predicting the dynamics and thermal characteristics in the context of comparing two codes, it is observed that the inclusion of these buoyancy source terms is indeed favorable for taking into account the buoyancy effects.

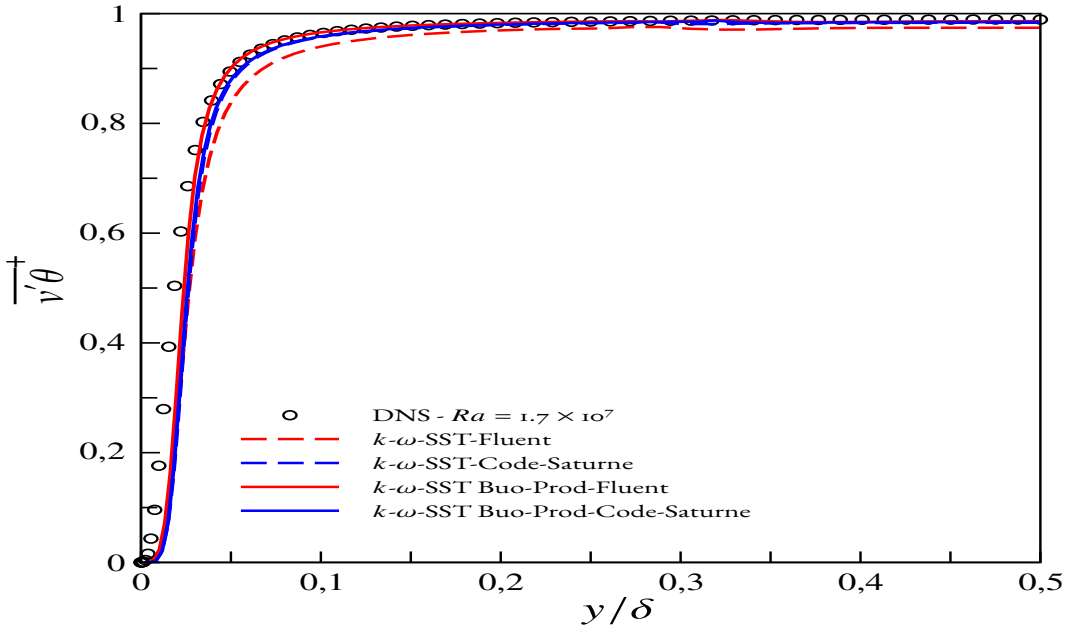

Figure A.9 – Comparison of wall normal heat flux ($\overline{vT}^+$) profiles for buoyancy sensitised k-ω-SST model in Fluent (red color) and in Code Saturne (blue color) with DNS data Kiš and Herwig [2014] at $Ra = 1.7 \times 10^7$ and $Pr = 0.71$

A.3 Influence of the turbulent Prandtl number

Precise computation of the turbulent heat fluxes plays a major role in buoyancy-driven flows. In industrial simulations where the RANS approach is the most considered approach, first moment turbulence closures are still the mainstay of the engineers, where Pr_t can be viewed as a key input that links the eddy diffusivity for heat to the eddy viscosity for momentum. The origin of the turbulent Prandtl number concept dates back from the early twentieth century when Taylor [1915] proposed the concept of eddy-diffusivity. More precisely, the turbulent Prandtl number is a pertinent concept for turbulent heat transfer. The turbulent Prandtl number is mainly an indication of the dissimilarity between turbulent transports of momentum and heat and can be expressed as follows:

$$Pr_t = \frac{\nu_t}{\alpha_t} \tag{A.19}$$

Where ν_t and α_t are the eddy viscosity and eddy diffusivity for heat, respectively. According to the Reynolds analogy, heat is transported in a similar way as momentum in turbulent flows such that $Pr_t = 1.0$. This analogy continues to find its way in engineering applications.

From the atmospheric modeling point of view, precise predictions of the turbulent Prandtl number leads to better predictions of heat transfer for weather and climate. Moreover it will have an impact on the measurement of air quality, ecosystem and agriculture manage-

ment. The scientific community for atmospheric flows has a different point of view for the role of the turbulent Prandtl number and researchers have discovered the role of thermal stratification in inducing the dissimilarity between turbulent transport of momentum and heat [Ertel, 1942, Priestley and Swinbank, 1947]. Thermal stratification has a significant role in the atmospheric boundary layer and there are several models proposed by the authors [Businger, 1988, Mellor and Yamada, 1982, Zilitinkevich et al., 2007] to take into account the dissimilarity of turbulent transport of momentum and heat. A Discussion of these proposals have been made in the bibliography chapter. Moreover, the span of the atmospheric boundary layer is several orders of the magnitude as compared to the boundary layer developed in industrial flows and it is not known whether the models developed for the estimation of turbulent Prandtl number for atmospheric flows is going to work for industrial flows.

Keeping in view this aspect, the goal of this section is to analyze the effect of different constant values of turbulent Prandtl number in the permissible range. The differentially heated vertical channel case is computed corresponding to the highest Rayleigh number, $Ra = 1.7 \times 10^7$ available and the results are compared to the DNS data of Kiš and Herwig [2014].

Looking into Fig. A.10, it is observed that by reducing the value of the turbulent Prandtl number from 1.0 to 0.85, there is a marginal improvement in the prediction of mean velocity in such a way that the peak value of mean velocity reduces by 1% and this reduction is observed with both the codes. Nevertheless there are differences in the prediction of mean velocity by the two codes. Another undesirable feature of changing the turbulent Prandtl number to a lower value (from 1.0 to 0.85) is that the turbulent shear stress is underestimated far from the wall as compared to the value observed with $Pr_t = 1.0$ and this phenomenon is predicted by the two codes as shown in Fig. A.11. From the distribution of mean temperature as shown in Fig. A.12, it is observed that there is an improvement in the prediction of mean temperature by changing the value of Pr_t from 1.0 to 0.85. To probe into this prediction further, the prediction of the wall-normal heat flux component is examined in Fig. A.13. It is observed that corresponding to the lower value of turbulent Prandtl number that is 0.85, the heat flux is increased by 17% which is affecting the energy balance in such a way that the misprediction of temperature is avoided to a certain extent although in an insufficient manner.

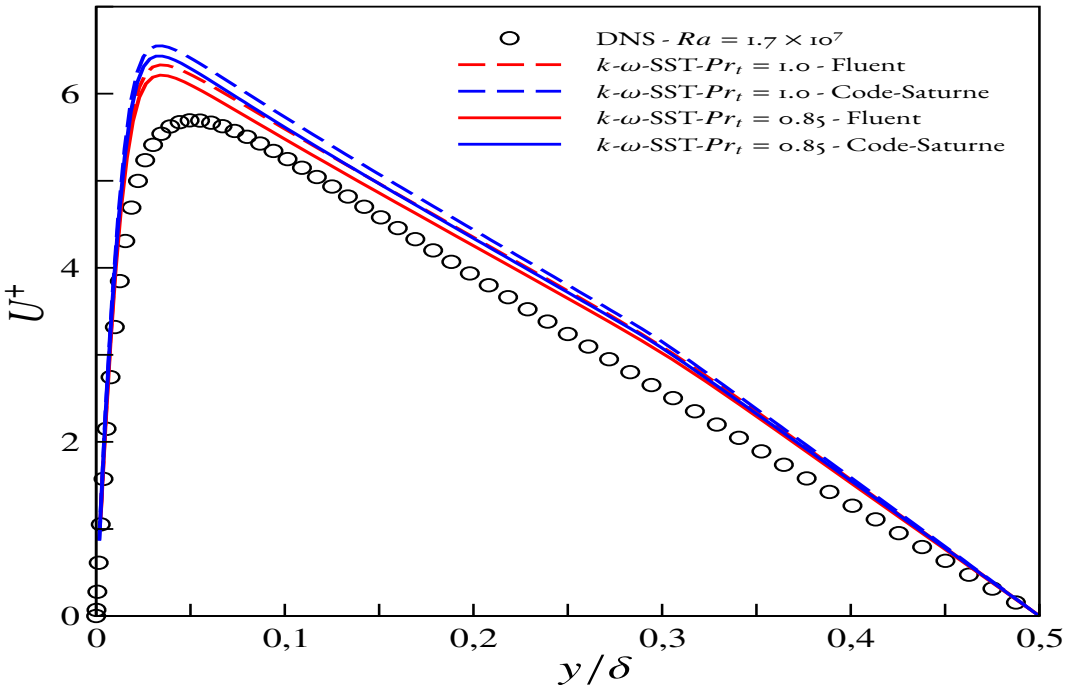

Figure A.10 – Comparison of mean velocity (U^+) profiles for different Prandtl number in the k-ω-SST model in Fluent (red color) and in Code Saturne (blue color) with DNS data Kiš and Herwig [2014] at $Ra = 1.7 \times 10^7$ and $Pr = 0.71$

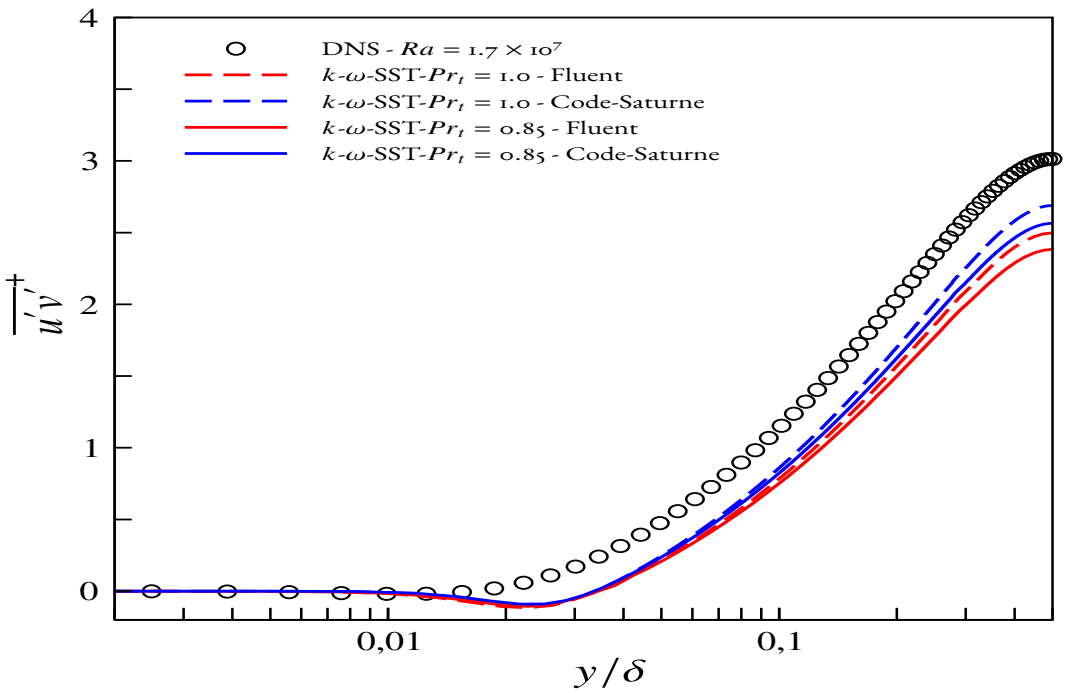

Figure A.11 – Comparison of turbulent shear stress ($\overline{uv}^+$) profiles for for different Prandtl number in the k-ω-SST model in Fluent (red color) and in Code Saturne (blue color) with DNS data Kiš and Herwig [2014] at $Ra = 1.7 \times 10^7$ and $Pr = 0.71$

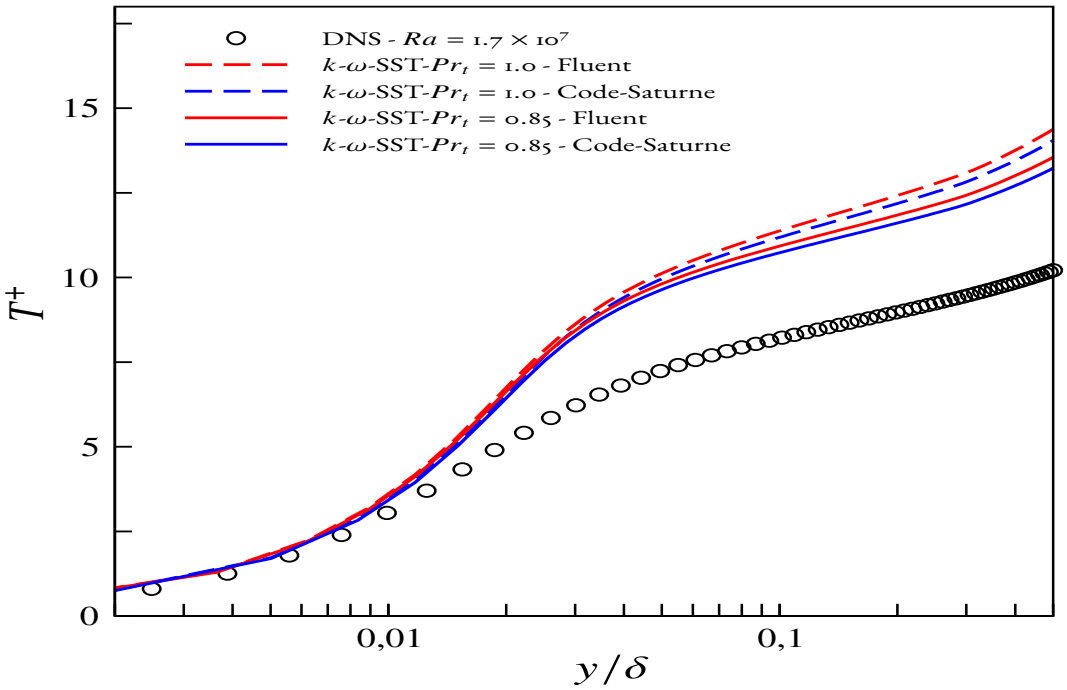

Figure A.12 – Comparison of mean temperature (T^+) profiles for different prandtl number in k-ω-SST model in Fluent (red color) and in Code Saturne (blue color) with DNS data Kiš and Herwig [2014] at $Ra = 1.7 \times 10^7$ and $Pr = 0.71$

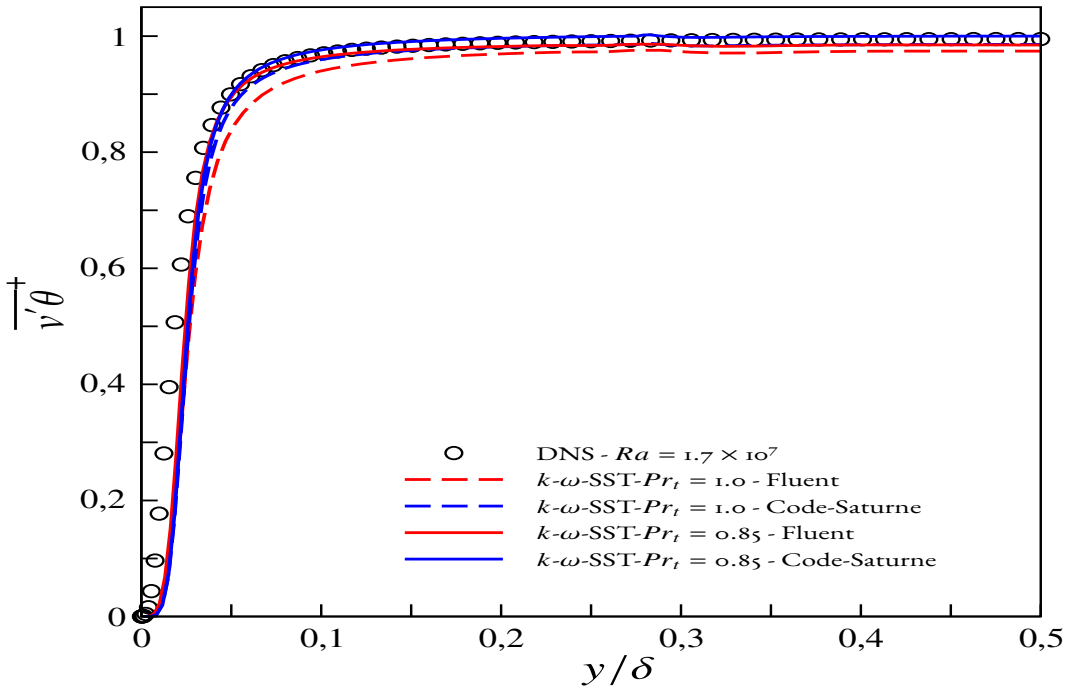

Figure A.13 – Comparison of wall normal heat flux ($\overline{vT}^+$) profiles for different Prandtl number in k-ω-SST model in Fluent (red color) and in Code Saturne (blue color) with DNS data Kiš and Herwig [2014] at $Ra = 1.7 \times 10^7$ and $Pr = 0.71$

Conclusion and Future prospects

An analysis of the comparison between Ansys Fluent and Code Saturne codes is made in reproducing the dynamics and turbulent quantities in a differentially heated vertical channel. The first part of this appendix is dedicated to the comparison of simple buoyancy-extended k-ω-SST model in Ansys Fluent and Code Saturne. A simple buoyancy-extended k-ω-SST model is developed in such a way that the buoyancy contribution is taken from Reynolds stress equation and added explicitly to the Boussinesq constitutive relation. Another favorable aspect of this buoyancy-extended model is its simplicity in a way that it does not require the modeling of tensorial diffusivity which is not possible in Ansys Fluent. It is realized that there is a drastic improvement in the prediction of mean and turbulent quantities by this simple buoyancy-extended k-ω-SST model and also it is observed that this modification is not an adhoc modification rather it provides a better momentum balance which is missing in the original k-ω-SST model.
In the second part of this appendix, attempts are made to analyze the effects of adding only buoyancy source terms which are modeled using generalized gradient diffusion hypothesis (GGDH) approach. However, the Reynolds stresses and turbulent heat fluxes are modeled using the Boussinesq constitutive relation and the SGDH approach respectively, which is the standard way of modeling in most of the commercial codes, particularly Ansys Fluent. It is noticed that the inclusion of the additional buoyancy source terms made it possible to take into account the buoyancy mechanism to a certain extent in such a way that it improves the prediction of mean velocity and mean temperature. However, this buoyancy sensitized k-ω-SST model is sensitive to the choice of the coefficient (as can be seen in Chapter 4) and this limits the generality of this type of modification.
Finally, the effects of changing the turbulent Prandtl number in the context of Reynolds analogy is estimated. It has been observed that the mean velocity and mean temperature is improved in an insufficient manner corresponding to the value of turbulent Prandtl number, $Pr_t = 0.85$, which is the default value in Ansys Fluent. This work is the part of ANR Monaco project, and the long term goal of the project is to predict the buoyancy induced transient phenomena which poses a barrier that must be overcome by the extension of this work to the development of hybrid RANS/LES methods for buoyancy driven flows. Moreover, during the development of Hybrid RANS/LES methods, special attention will be given to the RANS zones.
During the thermal designing of the underhood space of cars, reducing the weight of the car by using plastic instead of metal is of paramount importance, which is crucial in thermal management in the underhood space. This is directly linked to the overheating of the underhood components during different phases of vehicle motion. During the thermal underhood managment, the simulation results are reliable during cruising phases and able to predict high temperature levels. However, during the heat soak phase, there is a sudden rise of surface temperature of some underhood components and this might lead to the risk

of auto-ignition of fluids in the underhood components. The computation of this thermal soak phase (when the natural convection is a dominant phenomenon) is a challenge that the buoyancy sensitized models developed in the present work will help to tackle.

Appendix B

HEFAT Conference paper

SENSITIZATION OF EDDY-VISCOSITY MODELS TO BUOYANCY EFFECTS FOR PREDICTING NATURAL CONVECTION FLOWS

S.M. Saad Jameel*[1,2], Rémi Manceau[2] and Vincent Herbert[1]
[1]PSA Group, Centre technique, 2 route de Gisy, 78943 Velizy Villacoublay, France
[2]CNRS / Univ Pau & Pays Adour / E2S UPPA, Laboratoire de mathématiques et de leurs applications de Pau - Fédération IPRA, UMR5142, 64000, Pau, France and Inria Bordeaux-Sud-Ouest, project-team CAGIRE,
E-mail: syed-mohd-saad.jameel@etud.univ-pau.fr

ABSTRACT

Eddy-viscosity turbulence models are sensitized to the effects of buoyancy, in order to improve the prediction in natural convection flows. The approach extends in a linear way the constitutive relations for the Reynolds stress and the turbulent heat flux, in order to account for the anisotropic influence of buoyancy. The novelty of this work involves the buoyancy extension applied to two very different eddy-viscosity models, which leads to encouraging results for the highly challenging case of the differentially heated vertical channel.

INTRODUCTION

Turbulent flows influenced by thermal buoyancy are present in many technological applications, in particular in the automotive industry. For instance, CFD is consistently used in the design cycle in order to avoid the recourse to costly wind-tunnel experiments, for dimensioning the underhood compartment. Although this methodology reproduces the flow and heat transfer correctly at cruising speed, it is not reliable in phases where natural convection dominates, i.e., when the car stops, mainly because turbulence-buoyancy interactions are not accounted for in a comprehensive manner. Such computations are performed using commercial softwares and linear eddy-viscosity turbulence models, such that the objective of the present work is to introduce the mechanisms involved in the turbulence-buoyancy interaction in such models.

In linear eddy-viscosity models, the Reynolds-stress tensor is proportional to the mean strain tensor, such that the influence of complex phenomena on the turbulence anisotropy cannot be directly taken into account. In particular, for flows driven by thermal buoyancy, such models lead to inaccurate prediction of turbulent dynamics and mean flow properties [1]. In contrast, second moment closures, based on the resolution of transport equations for the Reynolds stress and the turbulent heat fluxes, naturally contain source terms originating from the volume force appearing in the Navier-Stokes equations [2], such that buoyancy effects on turbulence can be accounted for without the need for *ad hoc* modifications. Certainly, Reynolds stress and turbulent heat flux transport equations require the modelling of unknown correlations, such as pressure-strain ϕ_{ij} and pressure-temperature-gradient $\phi_{\theta i}$ terms which are of decisive importance. In this context, it can be shown [3] that there are buoyant contributions which needs to be incorporated and, with term by term modelling, it is possible to correctly treat the turbulence-buoyancy interactions [3; 4]. Significant progress was recently achieved by using the elliptic blending concept to model the Reynolds stresses [5] extended to the turbulent heat flux to take into account near-wall effects [6; 7]. However, as mentioned above, second moment closure is not used for design in the car industry, such that the objective of the present work is to sensitize eddy-viscosity models to buoyancy, by incorporating physically-based terms derived from second-moment closure.

In the literature, inclusion of buoyancy effects has mainly been considered in the context of strongly stratified flows, by adding buoyancy source terms to the transport equations for k and ε or ω. However, since the turbulent heat fluxes are generally modelled using the simple gradient diffusion hypothesis (SGDH) the influence of buoyancy on turbulence is considerably underestimated [8] and exactly zero for unstratified flows. However, in the engine compartement of a vehicule, the most critical region, at the origin of the natural convection motion observed, is the volume between the engine and the radiator. This region is similar to a tall vertical differentially-heated cavity, i.e., a weakly stratified configuration. Since introducing buoyancy source terms based on the generalized gradient diffusion hypothesis (GGDH) is not sufficient [8; 9], it is necessary to extend the constitutive relations for the Reynolds stress and turbulent heat flux [10; 11]. In particular, Davidson [10] sensitized the low-Reynolds-number k-ε model by the inclusion of a buoyancy extension for the Reynolds stress derived from a second-moment closure. The present study aims at extending this work to two very different eddy-viscosity models, namely the k-ω-SST [12] and BL-$\overline{v^2}/k$ models [13], respectively, in order to demonstrate that this approach is physically sound and not limited to a particular type of models, with the short-term objective of its application to real underhood configuration.

GOVERNING EQUATIONS

Using the Boussinesq approximation, the Reynolds-averaged conservation equations for mass, momentum and energy reduce

to

$$\frac{\partial U_i}{\partial x_i} = 0, \tag{1}$$

$$\frac{DU_i}{Dt} = -\frac{1}{\rho}\frac{\partial P}{\partial x_i} + \frac{\partial}{\partial x_j}\left(\nu\frac{\partial U_i}{\partial x_j} - \overline{u_i u_j}\right) - \beta g_i (T - T_{\text{ref}}), \tag{2}$$

$$\frac{DT}{Dt} = \frac{\partial}{\partial x_i}\left(\frac{\nu}{Pr}\frac{\partial T}{\partial x_i} - \overline{\theta u_i}\right), \tag{3}$$

where, β, g_i, ν and Pr are thermal expansion coefficient, gravitational vector, kinematic viscosity and Prandtl number, respectively. In the two standard turbulence models used herein, the Reynolds stress is modelled using the Boussinesq relation

$$\overline{u_i u_j} = \frac{2}{3}k\delta_{ij} - \nu_t\left(\frac{\partial U_i}{\partial x_j} + \frac{\partial U_j}{\partial x_i}\right) \tag{4}$$

and the turbulent heat flux using the SGDH

$$\overline{\theta u_i} = -\frac{\nu_t}{Pr_t}\frac{\partial T}{\partial x_i}. \tag{5}$$

where, ν_t and Pr_t, are turbulent viscosity and turbulent Prandtl number, respectively. In the BL-$\overline{v^2}/k$ model [13], similar to other eddy-viscosity models using ε, buoyancy appears in the k on ε equations through the buoyancy production terms

$$G = -\beta g_i \overline{\theta u_i} \tag{6}$$

and G_ε. The latter is modelled as a function of the former, $G_\varepsilon = C_{\varepsilon 1} G/\tau$, where τ is the turbulent time scale, in a way similar to the production term due to velocity gradients, such that the equations write as follows [13]

$$\frac{Dk}{Dt} = P + G - \varepsilon - 2C_{\varepsilon 3}\nu\nu_t(1-\alpha^p)\frac{k}{\varepsilon}\left(\frac{\partial^2 \overline{U_i}}{\partial x_k \partial x_j}\right)^2 + D_k \tag{7}$$

$$\frac{D\varepsilon}{Dt} = \frac{C_{\varepsilon 1}(P+G) - C_{\varepsilon 2}{}^*\varepsilon}{\tau} + D_\varepsilon \tag{8}$$

$$\text{where} \quad \tau = \sqrt{\left(\frac{k}{\varepsilon}\right)^2 + C_T^2\left(\frac{\nu}{\varepsilon}\right)^2}, \tag{9}$$

with $C_T = 4$, and D_k and D_ε stand for diffusion terms, which do not need to be explicited here. The specificity of the BL-$\overline{v^2}/k$ model compared to other k-ε models is that, in order to account for the wall-blockage effect on turbulence, which is crucial for heat transfer [5], the eddy-viscosity is computed as

$$\nu_t = C_\mu \varphi k \tau, \tag{10}$$

where φ is the ratio of the energy of the wall-normal fluctuations to the turbulent energy k. This ratio is solution of the transport equation as follows [13]

$$\frac{D\varphi}{Dt} = -(1-\alpha^p)\frac{\varepsilon}{2}\frac{\varphi}{k} + \alpha^p f_h - (P+G)\frac{\varphi}{k} + \frac{2}{k}\frac{\nu_t}{\sigma_k}\frac{\partial k}{\partial x_j}\frac{\partial \varphi}{\partial x_j} + D_\varphi, \tag{11}$$

where

$$f_h = -\frac{1}{\tau}\left(C_1 - 1 + C_2\frac{(P+G)}{\varepsilon}\right)\left(\varphi - \frac{2}{3}\right). \tag{12}$$

In constrast, in the k-ω-SST model [12], the eddy-viscosity is modelled as

$$\nu_t = \frac{a_1 k}{max(a_1\omega, SF_2)}, \tag{13}$$

where $\omega = \varepsilon/(\beta^* k)$, and the k- and ω-equations also involve buoyancy-production terms G and G_ω, respectively, where G_ω is again modelled as a function of G, since $G_\omega = G_\varepsilon/(\beta^* k) = G/\nu_t$, which yields

$$\frac{Dk}{Dt} = P + G - \beta^* k\omega + D_k \tag{14}$$

$$\frac{D\omega}{Dt} = \alpha\frac{(P+G)}{\nu_t} - \beta\omega^2 + D_\omega + 2(1-F_1)\sigma_{\omega 2}\frac{1}{\omega}\frac{\partial k}{\partial x_i}\frac{\partial \omega}{\partial x_i} \tag{15}$$

However, with the SGDH model (5) for the turbulent heat flux $\overline{\theta u_i}$, the buoyancy-production terms in the above equations for k and ε or ω are negligible for weakly stratified flows, such a way that buoyancy as virtually no influence on turbulence, which contradicts the observations [14]. Indeed, in the absence of stratification, the temperature gradient and the gravity vector are orthogonal, such that, Eqs. (5) and (6) yield $G = 0$.

BUOYANCY-EXTENDED EDDY-VISCOSITY MODELS

Buoyancy effects can be taken into account by extending the constitutive relation (4) for the Reynolds stress $\overline{u_i u_j}$ and the rationale for this buoyancy extension comes from the weak equilibrium hypothesis applied to the Reynolds stress transport equation

$$\frac{D\overline{u_i u_j}}{Dt} = P_{ij} + G_{ij} + \phi_{ij} - \varepsilon_{ij} + D_{ij}, \tag{16}$$

where P_{ij}, ε_{ij} and D_{ij} stand for the production, dissipation and diffusion tensors, respectively. The buoyancy production term writes

$$G_{ij} = -\beta(g_i\overline{\theta u_j} + g_j\overline{\theta u_i}) \tag{17}$$

and the model for the pressure-strain correlation includes buoyancy effects [3]. Assuming that turbulence is in *weak equilibrium*, i.e., that the anisotropy of turbulence is in local equilibrium, an implicit algebraic relation is obtained for the Reynolds stress that involves buoyancy production,

$$\begin{aligned}\overline{u_i u_j} = \frac{2}{3}k\delta_{ij} &+ \frac{k}{\varepsilon}\frac{1-C_2}{C_1 + \frac{P+G}{\varepsilon} - 1}\left(P_{ij} - \frac{2}{3}P\delta_{ij}\right) \\ &+ \frac{k}{\varepsilon}\frac{1-C_3}{C_1 + \frac{P+G}{\varepsilon} - 1}\left(G_{ij} - \frac{2}{3}G\delta_{ij}\right),\end{aligned} \tag{18}$$

where C_1, C_2 and C_3 are coefficients of the model for ϕ_{ij} used in Eq. (16), for the slow, rapid and buoyant parts, respectively. As mentioned in the introduction, our purpose is not to use such

an algebraic Reynolds-stress model, but to extend standard linear eddy-viscosity models to buoyancy effects. Therefore, the second term of Eq. (18), which is the part related to the mean velocity gradient, is kept unchanged, i.e., is modelled by the linear Boussinesq relation (4). However, Eq. (18) suggests that the Boussinesq relation can be extended by introducing the influence of buoyancy production [10; 11]. Assuming that turbulence is close to equilibrium, i.e., $P+G=\varepsilon$, the buoyancy-extended constitutive relation reads

$$\overline{u_i u_j} = \underbrace{\frac{2}{3}k\delta_{ij} - \nu_t\left(\frac{\partial U_i}{\partial x_j}+\frac{\partial U_j}{\partial x_i}\right)}_{\overline{u_i u_j}_{\text{Bouss}}} + \underbrace{C^*_\theta \tau\left(G_{ij}-\frac{2}{3}G\delta_{ij}\right)}_{\overline{u_i u_j}_{\text{Buo}}}, \qquad (19)$$

where $C^*_\theta = 0.1$; $G=\frac{1}{2}G_{kk}$. This extension directly influences momentum conservation (2), but also the transport equations for the turbulent variables via the modification of the production term

$$P = -\overline{u_i u_j}\frac{\partial U_i}{\partial x_j} = -\left(\overline{u_i u_j}_{\text{Bouss}} + \overline{u_i u_j}_{\text{Buo}}\right)\frac{\partial U_i}{\partial x_j}. \qquad (20)$$

This extended constitutive relation can be associated to any eddy-viscosity model, in particular to the BL-$\overline{v^2}/k$ and k-ω-SST models used herein. It can be seen as a linear algebraic correction to the eddy-viscosity based turbulence model.

TURBULENT HEAT FLUX MODEL

A correct representation of turbulent heat flux is of uttermost importance for accurate prediction of heat transfer for natural convection flows. In particular, since Eq. (19) aims at representing the influence of buoyancy on the anisotropy of turbulence, using the SGDH (5) is inadequate, such that a more general heat flux model must be considered. Such a relation can be obtained from the full transport equation for the turbulent heat flux, using the same algebraic methodology as for the Reynolds stress used above [1], leading to the Algebraic Flux Model (AFM)

$$\overline{\theta u_i} = -C_\theta \tau\left[\overline{u_i u_k}\frac{\partial T}{\partial x_k} + (1-C_{2\theta})\overline{\theta u_k}\frac{\partial U_i}{\partial x_k} + (1-C_{3\theta})\beta g_i \overline{\theta^2}\right], \qquad (21)$$

where τ is the turbulent time scale and coefficients come from the model for the scrambling term in the original model. Although this relation can be useful in the future, in the present work the Generalized Gradient Diffusion Hypothesis (GGDH) is used, which corresponds to the first term in Eq. (21),

$$\begin{aligned}\overline{\theta u_i} &= \overline{\theta u_i}_{\text{Bouss}} + \overline{\theta u_i}_{\text{Buo}} \\ &= -C_\theta \tau \overline{u_i u_j}_{\text{Bouss}}\frac{\partial T}{\partial x_j} - C_\theta \tau \overline{u_i u_j}_{\text{Buo}}\frac{\partial T}{\partial x_j},\end{aligned} \qquad (22)$$

in which the decomposition into two terms highlights the contribution of the Boussinesq part and the extension in Eq. (19). It is thus to be noted that this extension has an influence, via Eq. (22), on the mean temperature equation (3), as well as in the equations of the turbulence models (7)-(8) or (14)-(15), via the buoyancy-production term

$$G = -\beta g_i\left(\overline{\theta u_i}_{\text{Bouss}} + \overline{\theta u_i}_{\text{Buo}}\right). \qquad (23)$$

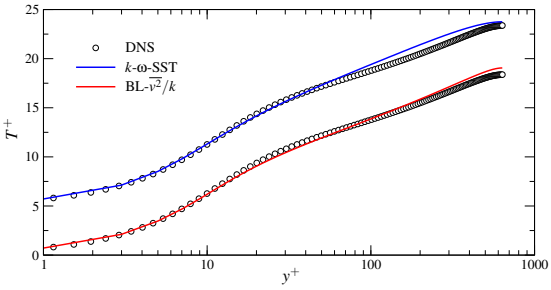

Figure 1. Forced convection case at $Re_\tau = 640$ [15]. Mean temperature. Profiles are shifted for clarity.

As mentioned in the introduction, our purpose is not to modify the turbulence models used in the industry, but rather to extend their validity to buoyant flows. Therefore, a particular constraint to take into account is that the buoyancy-extended model must not spoil the satisfactory results obtained in forced convection. In such a situation, the influence of buoyancy is negligible, such that Eq. (19) reduces to the Boussinesq relation, but the use of the GGDH (22) instead of the SGDH (5) imposes the value of the coefficient C_θ. Indeed, in order to avoid a modification of the predictions in a thermal boundary layer in the forced convection regime, in which the mean temperature profile is driven by the wall-normal turbulent heat flux, say $\overline{\theta v}$, the model must revert to the original model, such that

$$\overline{\theta v} = \underbrace{-\frac{\nu_t}{Pr_t}\frac{\partial T}{\partial y}}_{SGDH} = \underbrace{-C_\theta \tau \overline{v^2}\frac{\partial T}{\partial y}}_{GGDH}, \qquad (24)$$

in which $\overline{v^2} = \overline{v^2}_{\text{Bouss}} = \frac{2}{3}k$, which imposes

$$C_\theta = \frac{3}{2k\tau}\frac{\nu_t}{Pr_t}. \qquad (25)$$

In the k-ω-SST model, this constraint yields

$$C_\theta = \frac{3}{2}\frac{C_\mu}{Pr_t}\frac{a_1\omega}{max(a_1\omega, SF_2)}, \qquad (26)$$

and in the BL-$\overline{v^2}/k$ model,

$$C_\theta = \frac{3}{2}\frac{C_\mu}{Pr_t}\varphi. \qquad (27)$$

With this particular value of the coefficient C_θ, the buoyancy extension does not modify the predictions of the models in forced convection, such that the k-ω-SST and BL-$\overline{v^2}/k$ models still satisfactorily reproduce the friction temperature $T^+ = (T_w - T)/T_\tau$, as shown in Fig. 1 for the case at $Re_\tau = 640$ [15].

VALIDATION

The computations are carried out using EDF in-house open source code (www.code-saturne.org). , a collocated finite volume solver based on the SIMPLEC algorithm and the Rhie and Chow interpolation, with second order accuracy in space. Details can be found in Archambeau et al. [16]. For all the computations, a grid-convergence study was performed.

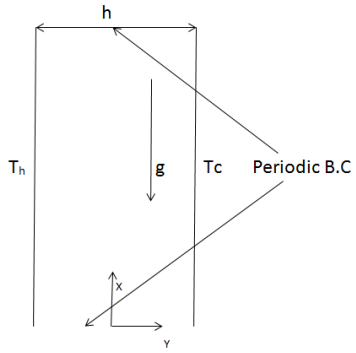

Figure 2. Natural and mixed convection configurations.

Case	u_τ/U_{ref}	Error	$T_\tau/\Delta T$	Error
DNS	322	-	0.049	-
k-ω-SST	343.05	+6 %	0.036	-26%
k-ω-SST + Buoyancy extension	334.43	+4%	0.038	-22%
BL-$\overline{v^2}/k$	328.98	+2%	0.045	-8%
BL-$\overline{v^2}/k$ + Buoyancy extension	326.04	+1%	0.048	-2%

Table 1. Friction velocity and friction temperature

As mentioned in the introduction, one of the most critical situation for flows in the underhood compartment of vehicules is the generation by buoyancy of a vertical flow due to the differential heating between the radiator and the engine. In order to investigate the performance of the extended models proposed in the previous sections in such a situation, the well-documented academic configuration of the flow in a differentially heated vertical channel is selected. Flows in tall or infinite vertical cavities are known for being extremely challenging for modelling [6; 7], since the flow is entirely driven by buoyancy, which induces subtle couplings between the dynamic and thermal turbulent fields. The recent DNS database of Kiš and Herwig [14] is particularly relevant due to the realistic values of the Rayleigh number. The configuration is described in Fig. 2. The highest Rayleigh number available, $Ra = \beta g \Delta T h^3/(\nu\kappa)$, based on the width h of the channel, is 1.7×10^7. The flow is periodic in the vertical x-direction. For the computation, physical quantities are made non-dimensional using the width h of the channel, the temperature difference ΔT, the reference density ρ and the reference velocity $U_{\text{ref}} = \sqrt{\beta g \Delta T h}$, such that the molecular viscosity is $Ra^{-1/2}$ and the molecular diffusivity $Pr^{-1}Ra^{-1/2}$, with $Pr = 0.71$.

Results are presented in Figs. 3 to 4. Due to the antisymmetry of the configuration, only the flow on the hot side is plotted. In order to better evaluate the predictions of the models against DNS data, results are plotted in wall units, i.e., units based on the friction velocity u_τ, the friction temperature T_τ and the viscosity ν. The values of u_τ and T_τ are compared with the DNS in Tab. 1. Turbulence models in general, including Reynolds-stress

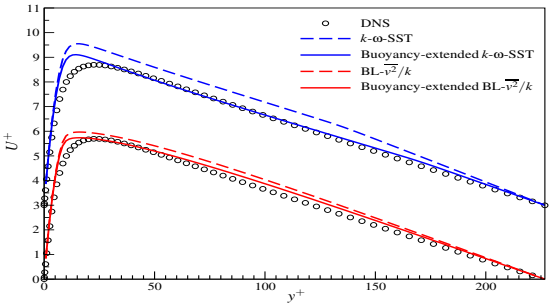

Figure 3. Mean velocity. Profiles are shifted for clarity.

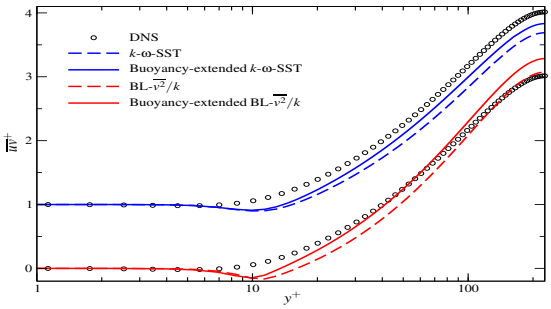

Figure 4. Turbulent shear stress. Profiles are shifted for clarity.

models [7], have a tendency to overestimate the mean velocity peak. Fig. 3 shows that this is the case with the original versions of the two models, in wall-units, and this is reinforced by the fact that the friction velocity is overstimated, in particular with the k-ω-SST model (Tab. 1). This weakness is directly related to a misprediction of the turbulent shear stress $\overline{uv}$ by the Boussinesq relation (4). Indeed, integrating the x-momentum balance between the wall and an arbitrary point y yields

$$0 = \int_0^y \nu \frac{\partial^2 U}{\partial y^2}\,\mathrm{d}Y - \int_0^y \frac{\partial \overline{uv}}{\partial y}\,\mathrm{d}Y + \int_0^y \beta g (T - T_{ref})\,\mathrm{d}Y. \qquad (28)$$

For a point y located between the mean-velocity peak and the centre of the channel, the driving force, the contribution of buoyancy, must be balanced by the viscous friction at the wall and the sum of the viscous friction and the turbulent shear stress in y, which are directed downwards, such that

$$\int_0^y \beta g (T - T_{ref})\mathrm{d}Y = \rho {u_\tau}^2 - \nu \frac{\partial U}{\partial y} + \overline{uv}. \qquad (29)$$

It is observed in Fig. 4 that the turbulent stress is severely underestimated in the region between the velocity peak and the centre, and this must be compensated by the viscous stresses, such that the negative slope of the velocity profile and the friction velocity are both overestimated, as seen in Fig. 3 and Tab. 1. This limitation of the Boussinesq relation is corrected by the buoyancy extension in Eq. (19), which yields

$$\overline{uv} = -\nu_t \frac{\partial U}{\partial y} + C_\theta^* \tau \beta g \overline{\theta v} \qquad (30)$$

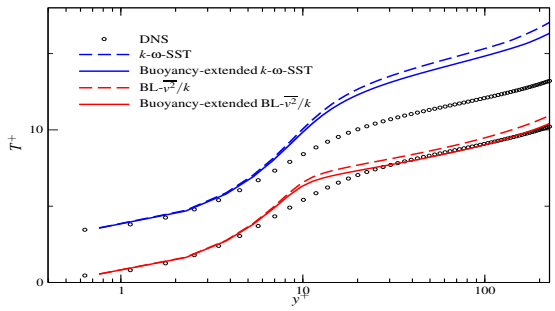

Figure 5. Mean temperature. Profiles are shifted for clarity.

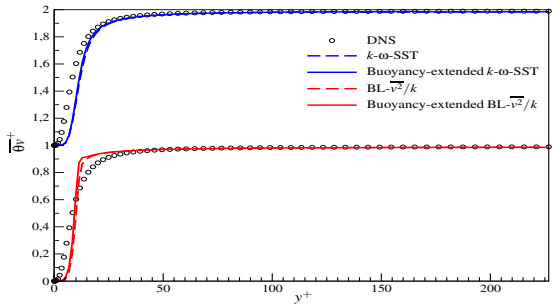

Figure 6. Wall-normal turbulent heat flux. Profiles are shifted for clarity.

As seen in Fig. 6, $\overline{\theta v}$ is positive, such that the buoyancy extension increases the turbulent shear stress, as can be seen in Fig. 4. Consequently, the balance (29) is improved, such that the viscous friction does not need to be overestimated to compensate for the lack of turbulent stress, and eventually the velocity gradient is corrected. This mechanism is beneficial for both turbulence models. It is worth pointing out that, despite the fact that the buoyancy extension is the same for the two models, with *the same coefficient* C^*_θ, the correction for the BL-$\overline{v^2}/k$ model is moderate compared to the k-ω-SST model, in accordance with the fact that the prediction by the original model is less discrepant. This results confirms that the buoyancy extension is not an *ad hoc* correction, but rather a physically sound mechanism, which favours the correct balance of the terms in the momentum equations. While the mean velocity profile is significantly improved with both models, the friction velocity remains overestimated, as seen in Tab. 1. In particular, with the k-ω-SST model, although the error is reduced by a factor of 1.5, it remains as large as 4%.

Now, integrating the temperature equation (3) between the wall and an arbitrary point y yields

$$0 = \int_0^y \alpha \frac{\partial^2 T}{\partial y^2} \mathrm{d}Y - \int_0^y \frac{\partial \overline{\theta v}}{\partial y} \mathrm{d}Y, \tag{31}$$

such that the heat flux from the wall to the fluid must be balanced by the sum of the viscous and the turbulent heat fluxes. Since in wall units, the heat flux at the wall is unity, the balance reduces

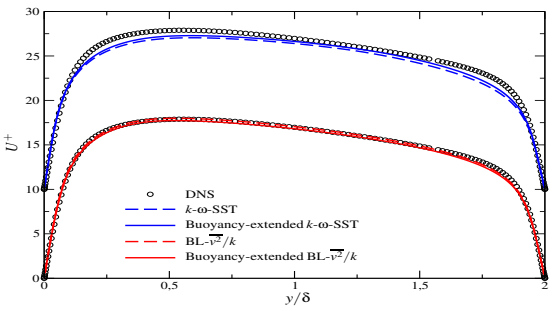

Figure 7. Mixed convection case. Mean velocity. Profiles are shifted for clarity.

to

$$1 = -\frac{1}{Pr}\frac{\partial T^+}{\partial y^+} + \overline{\theta v}^+, \tag{32}$$

such that, whatever the model, $\overline{\theta v}^+$ goes to one far from the wall, where molecular diffusivity is negligible, as seen in Fig. 6. Integrating Eq. (32) between the wall and an arbitray value of y^+ leads to

$$\frac{T^+}{Pr} = y^+ - \int_0^{y^+} \overline{\theta v}^+ \mathrm{d}Y^+, \tag{33}$$

which shows that the departure from the linear, laminar profile of mean temperature is due to the integral of the turbulent heat flux. The misprediction of the temperature profiles seen in Fig. 5, which is particularly large for the k-ω-SST model, is uniquely related to the fact that $\overline{\theta v}^+$ is underestimated in the near-wall region (Fig. 6). However, with the BL-$\overline{v^2}/k$ model, it can be observed that the much better prediction of the temperature profile is due to a compensation of errors in the integral of $\overline{\theta v}^+$. Substituting Eq. (30) into Eq. (22) shows that the contribution of the buoyancy extension is

$$\overline{\theta v}_{\mathrm{Buo}} = \frac{1}{3} C^*_\theta \tau \beta g \overline{\theta u}, \tag{34}$$

which is positive. Therefore, via its contribution to $\overline{\theta v}$, the buoyancy extension improves the temperature profile, although the correction is not sufficient for the k-ω-SST model. As seen in Tab. 1, the friction temperature at the wall, which is related to the Nusselt number, is significantly underestimated by the original models, in particular the k-ω-SST model. The introduction of the buoyancy extension helps reducing the error, in an insufficient way for the k-ω-SST model. For the buoyancy-extended BL-$\overline{v^2}/k$ model, the error is acceptable, which is rather satisfactory owing to the difficulty of predicting such a flow and the simplicity of the eddy-viscosity formulation.

Finally, although this test case is much less difficult to reproduce, the mixed convection case of Kasagi and Nishimura [17] is computed in order to confirm that the buoyancy extended models perform in a satisfactory way for this regime. The configuration, depicted in Fig. 2, is identical to the natural convection case,

except for the presence of an imposed pressure gradient, which generates a flow directed upwards. The flow is characterized by three non-dimensional numbers, $Re_\tau = 150$, $Gr = 9.6 \times 10^5$ and $Pr = 0.71$. Fig. 7 confirms the conclusions drawn for the natural convection case: mean velocity predictions are improved by the introduction of the buoyancy extension, and the correction is stronger for the k-ω-SST model which is exhibiting less accurate results. However, in this case, the contribution of buoyancy to the momentum balance is small, such that the influence of the buoyancy extension remains modest.

CONCLUSION

In the present work, eddy-viscosity turbulence models are sensitized to the effects of buoyancy, with the short-term objective of an application to industrial flows encountered in the automotive industry, in particular in the engine compartment. In order to avoid *ad hoc* modifications, the models are modified by extending the constitutive relations using the buoyant term derived from a Reynolds-stress model under the weak-equilibrium assumption. The approach thus introduces a physically relevant term without sacrificing the linearity of the models. The constitutive relation for the Reynolds stress accounts for the influence of buoyancy on the turbulent anisotropy, in association with the GGDH, which in turn involves the influence of the buoyancy extension on the turbulent heat flux. Using the proper constraint for the coefficient for the GGDH model, it is shown that the extension does not modify the original models in the case of forced convection flows.

In order to evaluate the validity of the assumptions and the improvement of the predictions, the buoyancy extension is applied to two very different eddy-viscosity models, the k-ω-SST and the BL-$\overline{v^2}/k$. The challenging test case of the differentially heated vertical channel flow of Kiš and Herwig [14], which is purely driven by buoyancy, is selected. Computation performed with the open-source solver Code_Saturne show that the predictions are significantly improved by the buoyancy extension. It is worth noting that the amplitude of the correction depends of the initial error, which supports the statement that the buoyancy extension is not only an *ad hoc* correction, but is a physically relevant term. Indeed, it can be shown that the discrepancy of the results obtained with the original models with respect to DNS is due to the absence of the contribution of buoyancy in the turbulent shear stress and normal heat flux in the momentum balance and the energy balance, respectively, which is corrected by the buoyancy extension. These encouraging results call for a broader validation of this approach in cavity flows representative of natural convection configurations encountered in the automotive industry.

ACKNOWLEDGMENT

This work was jointly conducted by PSA Group and the Université de Pau et des Pays de l'Adour (UPPA) with the support of ANRT (CIFRE contract 2016/1162) and the ANR project MONACO_2025 (ANR-17-CE06-0005-01_ACT). This work was granted access to the computing facilities of the MCIA (Mésocentre de Calcul Intensif Aquitain) of the University of Bordeaux and the UPPA. The authors are indebted to Prof. Herwig for providing the DNS database [14].

REFERENCES

[1] K. Hanjalić. One-point closure models for buoyancy-driven turbulent flows. *Annu. Rev. Fluid Mech.*, 34:321–347, 2002.

[2] A. S. Monin. On the symmetry of turbulence in the surface layer of air. *IZV Atm. Oceanic Phys.*, 1:45–54, 1965.

[3] M. M. Gibson and B. E. Launder. Ground effects on pressure fluctuations in the atmospheric boundary layer. *J. Fluid Mech.*, 86(3):491–511, 1978.

[4] H.S. Dol, K Hanjalić, and S. Kenjereš. A comparative assessment of the second-moment differential and algebraic models in turbulent natural convection. *Int. J. Heat Fluid Fl.*, 18(1):4–14, 1997.

[5] R. Manceau. Recent progress in the development of the Elliptic Blending Reynolds-stress model. *Int. J. Heat Fluid Fl.*, 51:195–220, 2015.

[6] S.-K. Choi, J.-W. Han, S.-O. Kim, and T.-H. Lee. Computation of turbulent natural convection with the elliptic-blending differential and algebraic flux models. *Numer. Heat Tr. B-Fund.*, 71(1):37–49, 2017.

[7] F. Dehoux, S. Benhamadouche, and R. Manceau. An elliptic blending differential flux model for natural, mixed and forced convection. *Int. J. Heat Fluid Fl.*, 63:190–204, 2017.

[8] K. van Maele and B. Merci. Application of two buoyancy-modified k-ε turbulence models to different types of buoyant plumes. *Fire Safety Journal*, 41(2):122–138, 2006.

[9] N.Z. Ince and B.E. Launder. On the computation of buoyancy-driven turbulent flows in rectangular enclosures. *Int. J. Heat Fluid Fl.*, 10(2):110–117, 1989.

[10] L. Davidson. Second-order corrections of the k-ε model to account for non-isotropic effects due to buoyancy. *Int. J. Heat Mass Tran.*, 33(12):2599–2608, 1990.

[11] S. Kenjereš, S.B. Gunarjo, and K. Hanjalić. Contribution to elliptic relaxation modelling of turbulent natural and mixed convection. *Int. J. Heat Fluid Fl.*, 26(4):569–586, 2005.

[12] F. R. Menter. Two-equation eddy-viscosity turbulence models for engineering applications. *AIAA J.*, 32(8):1598–1605, 1994.

[13] F. Billard and D. Laurence. A robust k-ε-v^2/k elliptic blending turbulence model applied to near-wall, separated and buoyant flows. *Int. J. Heat Fluid Fl.*, 33(1):45–58, 2012.

[14] P. Kiš and H. Herwig. Natural convection in a vertical plane channel: DNS results for high Grashof numbers. *Heat Mass Transfer*, 50(7):957–972, 2014.

[15] H. Kawamura, H. Abe, and Y. Matsuo. DNS of turbulent heat transfer in channel flow with respect to Reynolds and Prandtl number effects. *Int. J. Heat Fluid Fl.*, 20:196–207, 1999.

[16] F. Archambeau, N. Méchitoua, and M. Sakiz. Code Saturne: A Finite Volume Code for the Computation of Turbulent Incompressible flows - Industrial Applications. *Int. J. on Finite Volume, Electronical edition: http://averoes.math.univ-paris13.fr/html*, ISSN 1634(0655), 2004.

[17] N. Kasagi and M. Nishimura. Direct Numerical Simulation of Combined Forced and Natural Turbulent Convection in a Vertical Plane Channel. *Int. J. Heat Fluid Fl.*, 18(1):88–99, 1997.